UNIVERSITY OF SOUTHAMPTON

FACULTY OF NATURAL AND ENVIRONMENTAL SCIENCES

Ocean and Earth Science

Particulate Trace Metals, Carbon and Nitrogen in the Mesopelagic

by

Christopher Matthew Marsay

Thesis for the degree of Doctor of Philosophy

September 2012

UNIVERSITY OF SOUTHAMPTON

ABSTRACT

FACULTY OF NATURAL AND ENVIRONMENTAL SCIENCES

Ocean and Earth Sciences

Doctor of Philosophy

PARTICULATE TRACE METALS, CARBON AND NITROGEN IN THE MESOPELAGIC

by Christopher Matthew Marsay

The biological carbon pump (BCP) is an important part of the global carbon cycle, providing a route for carbon dioxide to be removed from the atmosphere and transported as particulate organic carbon (POC) to the ocean interior. This process affects the water column distributions of macronutrients and trace elements that are essential materials for marine ecosystems. This thesis addresses two areas that affect the strength and efficiency of the BCP: factors influencing the attenuation of POC flux as it sinks through mesopelagic depths (from the base of the euphotic zone to ~1000 m depth) and the role of particulate material in the biogeochemical cycle of iron, an important micronutrient known to limit the rate of primary production in extensive areas of the ocean.

A neutrally buoyant sediment trap, PELAGRA, was used to measure POC fluxes at multiple mesopelagic depths at the Porcupine Abyssal Plain (PAP) site (49 °N 16.5 °W) and in the Irminger and Iceland Basins in the high latitude North Atlantic (HLNA). From the resulting data, the coefficient of attenuation, *b*, was calculated for POC flux at each site, with values ranging from 0.72 to 1.00. Combined with *b* values for sites in the North Pacific, the data were compared to numerous parameters to investigate the controlling factor for mesopelagic POC flux attenuation, with upper water column temperature determined to be the most important of those considered.

The same trap deployments were used to measure particulate organic nitrogen and biomineral fluxes, and to make particulate iron (pFe) flux measurements; the first time that PELAGRA has been successfully used to measure fluxes of trace metals. Fluxes of 0.3 – 2.2 μmol pFe m^{-2} d^{-1} were measured at the PAP site (50 – 670 m depth) and 0.6 – 9.9 μmol m^{-2} d^{-1} in the HLNA (80 – 400 m depth).

In-situ pumps (SAPS) were used during three cruises in 2010 to measure spatial and seasonal changes in POC, PON and trace metal concentrations across the HLNA region. Two of the cruises coincided with the eruption of the volcano, Eyjafjallajökull, in southern Iceland, with the result that pFe concentrations in the northern Iceland Basin reached ~40 times those measured in the Irminger Basin (~0.7 nmol L^{-1}). Summer concentrations were also enhanced in the Iceland Basin, relative to the Irminger Basin (median ~0.7 nmol L^{-1} *cf.* ~0.2 nmol L^{-1}), though this was probably a result of greater influence of relatively Fe-rich shelf-derived waters, rather than continuing effects of volcanic ash deposition. While pFe concentrations generally changed little or increased with depth, biogenic pFe (estimated from Fe/Al ratios) decreased from ~31 % of the total pFe inventory in the mixed layer to ~13 % in the upper mesopelagic.

PELAGRA and SAPS data were combined, along with measurements of atmospheric inputs, to synthesise budgets for pFe in the HLNA, both with and without volcanic ash influence, which were then compared to budgets for other regions. A discrepancy of a factor of 6 – 10 was found between low inputs and greater export, suggesting that an additional Fe source, such as lateral advection may be extant. The volcanic ash input was found to pass through the upper ocean rather quickly (<1 – 3 days).

Contents

ABSTRACT ..... *i*

Contents ..... *iii*

List of figures ..... *vii*

List of tables ..... *xi*

Declaration of authorship ..... *xiii*

Acknowledgements ..... *xv*

Chapter 1: Introduction **1**

1.1 Overview 1
1.2 The role of the oceans in the global carbon cycle 1
1.3 The biological carbon pump 3
1.3.1 Chemical composition of particulate material 6
1.3.1.1 Particulate organic material (POM) 7
1.3.1.2 Particulate Inorganic Carbon (PIC) 8
1.3.1.3 Biogenic silica (bSi) 9
1.3.1.4 Lithogenic material 10
1.3.2 Measuring sinking particle flux 11
1.3.2.1 Traditional sediment traps 11
1.3.2.2 Radionuclide disequilibria 13
1.3.2.3 Other methods 14
1.3.3 Predicting POC flux 15
1.4 The marine biogeochemistry of iron 17
1.4.1 Sources and sinks of iron in the surface ocean 18
1.4.2 The speciation of iron in seawater 20
1.4.3 Iron cycling in the upper ocean 21
1.4.4 Iron limitation 23
1.5 Thesis objectives 24
1.6 Thesis structure 25

Chapter 2: Sampling methods and analytical techniques **27**

2.1 Overview 27
2.2 Precautions for trace metal work 27
2.2.1 Cleaning of plastic ware 28
2.2.2 Choice of reagents 29
2.3 Sampling of sinking particulate material 29
2.3.1 The PELAGRA sediment trap 30
2.3.2 Processing of sample splits 31
2.4 Bulk collection of marine particulate material 31
2.5 Analysis of the major fractions of particulate material 33
2.5.1 Mass 33
2.5.2 Particulate organic carbon and nitrogen 34
2.5.3 Particulate inorganic carbon 36
2.5.4 Biogenic silica 38
2.6 Analysis of trace metals in particulate material 39
2.6.1 Overview of methods used in previous studies 39
2.6.2 Protocol for leach and digest of particulate material 41
2.6.2.1 Preparations and sample filtration 42
2.6.2.2 Leach procedure 42
2.6.2.3 Total digest procedure 43

2.6.3 Analysis by ICP-MS 43
2.6.3.1 Reagent and filter blanks for Fe and Al 44
2.6.3.2 Sample precision 44
2.6.3.3 Digest method verification 45

Chapter 3: Mesopelagic particle flux in the North Atlantic Ocean 47

3.1 Overview 47
3.2 Introduction 47
3.2.1 The "Martin" curve 48
3.2.2 The VERTIGO programme 50
3.2.3 Iron in sinking particles 51
3.2.4 Aims and hypotheses 52
3.3 Overview of the two research cruises 52
3.3.1 Cruise D341: PAP site, summer 2009 53
3.3.2 Cruise D354: Irminger and Iceland Basins, summer 2010 55
3.4 Results 57
3.4.1 Process blanks 57
3.4.2 D341 results 58
3.4.2.1 Seasonal context and hydrography 58
3.4.2.2 Geographical coverage of the traps 59
3.4.2.3 PELAGRA fluxes 61
3.4.3 D354 results 65
3.4.3.1 Seasonal and hydrographical context 65
3.4.3.2 PELAGRA trap geographical coverage 66
3.4.3.3 Measured fluxes 67
3.5 Discussion 72
3.5.1 Comparison to previous data 72
3.5.2 Trends in organic material and biominerals 73
3.5.3 Attenuation of POC flux 75
3.5.3.1 Calculation of *"b"* values for the PAP site and HLNA 76
3.5.3.2 Implications of the calculated *"b"* values 83
3.5.4 Measurements of particulate iron flux 85
3.5.4.1 PAP site Fe data 86
3.5.4.2 High latitude North Atlantic iron data 89
3.6 Summary 92

Chapter 4: Particulate trace metals in high latitude North Atlantic surface waters 95

4.1 Overview 95
4.2 Introduction 95
4.2.1 Concentrations of suspended particulate trace metals: previous studies 96
4.2.2 Labile versus refractory particulate metals 99
4.2.3 Molar ratios of particulate trace metals 100
4.2.4 Aims and hypotheses 101
4.3 Overview of the research cruises and sampling strategy 102
4.4 Results and discussion 104
4.4.1 Hydrographic context 104
4.4.2 Methods critique 106
4.4.2.1 Mass measurements: significance for estimates of SPM concentrations 106
4.4.2.2 POC and PON measurements: comparison to Th-SAPS results 107
4.4.2.3 Consideration of the rinse filtrate 110
4.4.3 Variations in SPM, POC and PON concentrations 111
4.4.4 Trace metal, POC and PON concentrations within SPM 114
4.4.4.1 Spatial variation of pFe, pAl and organic material 116
4.4.4.2 Size fractionation of pFe, pAl and organic material 118

4.4.4.3 Leachable pFe and pAl 121
4.4.4.4 Consideration of elemental ratios 123
4.4.5 Estimating the biogenic contribution to pFe 127
4.4.6 Is there evidence of influence from the Eyjafjallajökull eruption during D350, D351 and D354? 132
4.4.7 A SAPS-derived estimate of sinking pFe flux 134
4.5 Summary 136

Chapter 5: Towards the synthesis of iron budgets for the high latitude North Atlantic 139

5.1 Overview 139
5.2 Previous iron budgets 139
5.3 Iron measurements in the HLNA 142
5.3.1 Suspended pFe concentrations 142
5.3.1.1 Lithogenic versus biogenic pFe in the surface mixed layer 143
5.3.2 Mixed layer dFe concentrations 143
5.3.3 Sinking flux of pFe 144
5.3.4 Aerosol Fe inputs 145
5.3.5 Vertical turbulent diffusivity 146
5.4 Discussion 146
5.4.1 Reasons for observed differences in D354 pFe flux estimates 146
5.4.2 High latitude North Atlantic iron budgets 148
5.4.2.1 D354 budgets 148
5.4.2.2 D350 iron budget: volcanic influence on the HLNA Fe cycle 150
5.4.3 Comparison to previous budgets 151
5.5 Summary and conclusions 155

Chapter 6: Conclusions and future work 157

6.1 Conclusions and major findings 157
6.1.1 Fluxes of POC, PON and biominerals 157
6.1.2 PELAGRA measurements of particulate trace metal fluxes 159
6.1.3 SAPS findings and conclusions 159
6.1.4 Synthesis of iron budgets for the HLNA 161
6.2 Future directions 161

Appendix A: Collection of sinking particulate material using the PELAGRA sediment trap 165

A.1 PELAGRA trap components 165
A.2 Operation of PELAGRA 166
A.3 Brine preparation 168
A.4 Process blanks 169
A.5 Initial sample processing 170
A.5.1 Sample splitting 170
A.6 Calculation of fluxes 172

Appendix B: Sampling using Stand Alone Pumping Systems (SAPS) 173

B.1 Overview of SAPS 173
B.2 Preparation 173
B.3 Deployment 174
B.4 Sample processing 174

Appendix C: Analytical method for the determination of trace metals in particulate material 177

C.1 Sample collection and processing 177
C.2 Leach and digest procedures 178

C.2.1 Acetic acid leach 178
C.2.2 Mixed acid total digest 179
C.3 Sample analysis 179
C.3.1 Internal standards 180
C.3.2 ICP-MS run details 181
C.3.3 Measured blank values 182

Appendix D: PELAGRA sampling details 185

Appendix E: SAPS sampling details 197

References 203

List of figures

Figure 1.1: A simplified representation of the Holocene carbon cycle, showing only the major reservoirs thought to be important for glacial/interglacial variations in atmospheric carbon dioxide levels (values are in Pg = 1 x 10^{15} g). Also shown are some of the (pre-industrial) fluxes into and out of the surface ocean. Reproduced from Sigman and Boyle (2000). 2

Figure 1.2: Schematic of the biological carbon pump, showing the main transport pathways of carbon (named in red), from photosynthetic uptake to sedimentation and burial. Adapted from a figure in "A New Wave of Ocean Science" (U.S.JGOFS, 2001). Estimated magnitudes of carbon transfer are given for the numbered processes. *References: (1)* Falkowski *et al.* (1998), *(2)* De La Rocha and Passow (2007), *(3)* Henson *et al.* (2011). 4

Figure 1.3: Schematic showing the main inputs (black arrows) and sink (shaded arrow) of iron in the ocean. Flux estimates are given for inputs in Tg Fe yr^{-1} (1 Tg = 1 x 10^{12} g) Red arrows summarise processes important in the redistribution of iron in the ocean: *(a)* remobilisation of Fe in margin and deep sea sediments, *(b)* lateral advection, *(c,d)* biological uptake and remineralisation, *(e)* transport and release by sea ice and icebergs, *(f – h)* supply to the surface ocean by upwelling, vertical diffusion and seasonal convective overturning, *(i)* transport by eddies. Flux estimates are from Jickells *et al.* (2005). 19

Figure 1.4: Summary of Fe biogeochemical cycling in the surface ocean. Thick arrows show inputs of new Fe. Numbered transfer paths are *(1)* passive adsorption and complexation of Fe to surface ligands of phytoplankton cells, *(2)* desorption from phytoplankton cell surfaces, *(3)* assimilation of cell surface-bound Fe, *(4)* transfer of Fe to zooplankton by grazing, *(5)* remineralisation through action of grazers, *(6)* phytoplankton death, producing detrital Fe, *(7)* zooplankton contribution to detrital Fe through faecal pellet production, death, cell break-up *etc.*, *(8)* solubilisation of minerals, desorption from and remineralisation of detrital Fe, and photoreduction of pFe, *(9)* scavenging of dFe through adsorption, precipitation and colloidal aggregation, *(10)* export of pFe from the surface ocean. Reproduced from Hutchins *et al.* (1993). 22

Figure 2.1: A PELAGRA trap, complete with sample pots 30

Figure 3.1: Open ocean composite of POC fluxes measured during the VERTEX programme, overlaid with the best-fit "Martin curve", $F = 1.53(z/100)^{-0.868}$. Reproduced from Martin *et al.* (1987). 49

Figure 3.2: Locations of the study areas for research cruises D341 (PAP site, 49 °N 16.5 °W) and D354, to the high latitude North Atlantic (HLNA). In the black box, *a* represents the Irminger Basin and *b*, the Iceland Basin, defined by the Reykjanes Ridge separating these regions. 53

Figure 3.3: Depth and temporal coverage of PELAGRA traps during D341. Asterisks denote traps that were not stable for the entire deployment 55

Figure 3.4: Depth and temporal coverage of PELAGRA traps during D354, along with (inset) deployment locations. 57

Figure 3.5: MODIS satellite-derived chlorophyll concentrations for 2009 at the PAP site, based on the mean values of 8-day time intervals. Timing of research cruise D341 is shown by the shaded box (days 194 – 221). 59

Figure 3.6: Deployment positions of traps for PAP1 (red square), PAP2 (blue triangle), PAP3 (green inverted triangle) and PAP4 (black diamond) and approximate locations of traps upon surfacing. Dashed/dotted lines depict straight-line transit of each trap while submerged. 60

Figure 3.7: Fluxes of *(a)* mass, *(b)* POC, *(c)* PON, *(d)* PIC, *(e)* bSi, *(f)* aluminium, *(g)* iron, *(h)* phosphorus and *(i)* manganese during D341. Measurements from PAP1 - PAP3 are shown in blue; those from PAP4 in red. All values are corrected for process blanks. 64

Figure 3.8: MODIS satellite-derived chlorophyll concentrations for 2010 in the Irminger and Iceland Basins and the Reykjanes Ridge region between the two. The timing of cruise D354 is shown by the shaded area between days 190 - 219. 66

Figure 3.9: Locations of PELAGRA deployments during D354, and the first recorded locations of the traps upon resurfacing. For IB3 P4 see comments in text. .. 67

Figure 3.10: Fluxes of *(a)* mass, *(b)* POC, *(c)* PON, *(d)* PIC, *(e)* bSi, *(f)* aluminium, *(g)* iron, *(h)* phosphorus and *(i)* manganese during D354. Measurements from IB1 and IB2 are shown in black, those from IB3 in blue, and those from IB4 in red. All values are corrected for process blanks. 68

Figure 3.11: Observed POC flux profiles from PAP4 during D341 and from IB3 and IB4 during D354. 76

Figure 3.12: Composition of material collected in PAP4, IB3 and IB4 traps, by proportion of total mass flux. 79

Figure 3.13: Selected plots of *b* versus various properties of the water column/sinking particulate material, with details of any correlation found (using Pearson product-moment correlation; $P < 0.05$ is considered significant). For all plots, $n = 7$. Parameters are: *(a)* mean calcite contribution to mass in traps over upper 500 m, *(b)* opal contribution to mass in 150 m trap, *(c)* biomineral contribution to mass in 150 m trap, *(d)* mean PIC:POC ratio of trap material, *(e)* surface water phosphate concentration, *(f)* mean temperature over upper 100 m, *(g)* mean temperature over upper 500 m, *(h)* mean O_2 concentration over upper 100 m. 81

Figure 3.14: Comparison of POC flux attenuation for Pacific and Atlantic Ocean sites, using calculated *b* values and flux normalised to 100 m. 83

Figure 3.15: Plots for D341 data of *(a)* Fe/Al molar ratio against depth, and *(b)* "biogenic" Fe against depth. Biogenic pFe is calculated by assuming an average crustal Fe/Al of 0.19 (Wedepohl, 1995) and applying this to the measured pAl flux to estimate lithogenic pFe flux, then subtracting this from the total pFe flux. The dashed line is included to highlight that some of the calculated biogenic pFe fluxes are < 0 μmol m^{-2} d^{-1}. 88

Figure 3.16: *(a)* correlation between Fe and Al fluxes during D354, with Spearman's rank-order correlation coefficient, $r_s = 0.952$ ($P < 0.001$, $n = 8$). *(b)* Fe/Al molar ratio of D354 sinking particles plotted against depth. Dashed lines represent estimates of global crustal average Fe/Al ratio: long-dashes = 0.19 (Wedepohl, 1995), short-dashes = 0.33 (Taylor, 1964). 90

Figure 4.1: Locations of SAPS sampling stations during cruises *(a)* D350 and D351, and *(b)* D354. Red outlines surround stations in >1500 m deep water in the Irminger or Iceland Basins (as labelled). Stations D350-4, D354-12 and D354-14 were in water <1500 m deep above the Reykjanes Ridge, while D350-8 was in <1500 m deep water over the continental slope south of Iceland. 103

Figure 4.2: High latitude North Atlantic data for *(a)* chlorophyll, and *(b)* primary productivity in 2010. Data is derived from MODIS satellite images, with regions defined by a southerly limit of 58 °N and with water depths of >1500 m for the Irminger and Iceland Basins. 104

Figure 4.3: Comparison of POC concentrations determined from Th-SAPS and TM-SAPS, where *(a)* 53 μm Nitex filters have been used for both, *(b)* 1 μm Nitex filters have been used for both, and *(c)* 1 μm Nitex filters have been used for Th-SAPS and 1 μm polycarbonate filters have been used for TM-SAPS. 108

Figure 4.4: Depth-related comparisons of *(a)* mean POC, and *(b)* mean PON concentrations in the Irminger and Iceland Basins during D350 and D354. Error bars represent one standard deviation. 114

Figure 4.5: Iron concentrations in SPM during D350 and D351, in μmol g^{-1}, with (inset) absolute concentrations, in nmol L^{-1}, for comparison. Values are shown for 50 m and 150 m depth. Circled data point (D351-1) was collected at 62.0 °N 20.1 °W and has been displaced so that the data point for D350-7 can also be seen. Value for 50 m depth at D350-7 was 353 μmol g^{-1}. 117

Figure 4.6: Iron concentrations in SPM during research cruise D354, in μmol g^{-1}, with (inset) absolute concentrations, in nmol L^{-1}, for comparison. Values are shown for 20 m, 50 m and 150 m depth. Colour bars are the same scale as those in Figure 4.5. 119

Figure 4.7: *Per gram* concentration results by size fraction for pFe and POC during D354. Plots show POC concentrations in SPM in *(a)* >53 μm and *(b)* 1 – 53 μm size fractions, and pFe concentrations in SPM in *(c)* >53 μm and *(d)* 1 – 53 μm size fractions. 120

Figure 4.8: Average values, by element and by cruise, for the fraction of particulate metals present that was HAc-leachable. Error bars represent one standard deviation. 121

Figure 4.9: The percentage of total pFe present in leachable forms, as a function of depth, for three stations during D354. Error bars represent propagated errors from analytical uncertainties. 122

Figure 4.10: POC content of SPM against pFe content of SPM for cruises D350, D351 and D354. Note the change in scale for values of pFe above 200 μmol g^{-1}. 124

Figure 4.11: Scatter plots for D350 (black dots) and D351 (red dots) of concentrations in SPM of (a) pAl and pFe, (b) pTi and pFe, (c) pAl and pTi. Each includes the calculated regression line (solid black line) with 95 % confidence intervals (dashed blue lines), regression equation, correlation coefficient and P-value. 125

Figure 4.12: Scatter plots for D354 of concentrations in SPM of (a) pAl and pFe, (b) pTi and pFe, (c) pAl and pTi. Each includes the calculated regression line (solid black line) with 95 % confidence intervals (dashed blue lines), regression equation, correlation coefficient and P-value. 125

Figure 4.13: Absolute concentrations of POC plotted against those of pFe for *(a)* all samples from D350, D351 and D354, and *(b)* D354 mixed layer samples only, with regression line. Regression does not include sample D354-2, which had a much higher pFe concentration than any of the other stations. 126

Figure 4.14: Box plots of measured Fe/Al molar ratios in total particulate material, showing variations between *(a)* cruises, *(b)* size fractions and *(c)* depth. Boxes represent interquartile range (left-hand and right-hand edges of box), divided by the median value; whiskers span values within 1.5 interquartile ranges of the quartiles and any values outside that range are represented as dots. For *(b)* and *(c)*, only data from D354 is used. 130

Figure 5.1: Iron budget for the surface mixed layer during FeCycle, reproduced from Boyd *et al.* (2005). All fluxes are in nmol Fe m^{-2} d^{-1}. Term "(a)" is the literature-derived atmospheric deposition rate, pools "(b)" and "(c)" are the calculated dFe and pFe inventories respectively, "(d)" is lateral advection of dFe, "(e)" and "(f)" are biological uptake and regeneration rates, "(g)" is vertical diffusive supply, "(h)" is measured pFe export and "(i)" is the estimated biogenic and lithogenic contribution to pFe export flux. Full details of measurements and construction of the budget are outlined in Boyd *et al.* (2005). 140

Figure 5.2: Partial biogeochemical iron budgets for *(a)* the Irminger Basin and *(b)* the Iceland Basin during D354, with pools in μmol m^{-2} and fluxes in nmol m^{-2} d^{-1}. Atmospheric Fe input (shown as mean and standard deviation) is averaged over both basins during the entire cruise period, as is vertical diffusion of dFe. Inventory values for pFe are mean and standard deviation of multiple stations, while dFe values are provisional estimates. Export values are sinking pFe flux measured for each basin by one PELAGRA trap at 80 m depth (with propagated uncertainty). Biogenic pFe export (in red) is calculated by applying Fe/Al ratios of *(i)* 0.43 and *(ii)* 0.19 to pAl fluxes measured by the same trap. 149

Figure 5.3: Partial biogeochemical iron budget for the region of the Iceland Basin influenced by heavy volcanic ash deposition. Fluxes shown are in nmol pFe m^{-2} d^{-1} and inventories in μmol m^{-2}. Values shown were measured as described in the text. 150

Figure A.1: Schematic of the PELAGRA sediment trap. 166

Figure A.2: Set-up used to split PELAGRA samples, showing the 4 L bottle into which cups were combined (inverted in photo) and the rotary splitter, loaded with 500 mL bottles. 171

Figure D.1: PAP1 deployment profiles for *(a)* P2, *(b)* P4, *(c)* P5, *(d)* P6 and *(e)* P7. Blue vertical dotted lines represent pot opening/closing times; red horizontal dashed line represents average trap depth over entire sampling period (shown in bottom corner). Note that vertical axis scales differ between plots. 188

Figure D.2: PAP2 deployment profiles for *(a)* P2, *(b)* P4, *(c)* P5, *(d)* P6 and *(e)* P7. Details are as for Figure D.1. 189

Figure D.3: PAP3 deployment profiles for *(a)* P2, *(b)* P4, *(c)* P5, *(d)* P6 and *(e)* P7. Details are as for Figure D.1. 190

Figure D.4: PAP4 deployment profiles for *(a)* P2, *(b)* P4, *(c)* P5, *(d)* P6 and *(e)* P7. Details are as for Figure D.1. 191

Figure D.5: IB1 deployment profiles for *(a)* P4 and *(b)* P6. Blue, vertical dotted lines represent pot opening/closing times; red horizontal dashed line represents average trap depth during sampling period (shown in bottom corner). 194

Figure D.6: IB2 deployment profiles for *(a)* P4 and *(b)* P6. Details are as for Figure D.5. 194

Figure D.7: IB3 deployment profiles for *(a)* P4, *(b)* P6 and *(c)* P7. Details are as for Figure D.5. Note change to vertical axis scale in *(c)*. 195

Figure D.8: IB4 deployment profiles for *(a)* P4, *(b)* P6 and *(c)* P7. Details are as for Figure D.5. Note change to vertical axis scale in *(c)*. 196

List of tables

Table 2.1: Filter blank means and standard deviations, and the resulting limit of detection values for filter blank-corrected POC and PON. All values are in µg. 35

Table 2.2: Filter blank means and standard deviations, and the resulting limit of detection values of filter blank-corrected Ca analyses for D341 and D354 PELAGRA samples (all values are in µg). 37

Table 2.3: Filter blank means and standard deviations, and the resulting limit of detection values of filter blank-corrected bSi analyses for D341 and D354 PELAGRA samples (all values are in µg). 38

Table 2.4: Mean ($\pm 1\sigma$) reagent blank and filter blank values for Fe and Al from ICP-MS analyses of leach samples, along with corresponding method limit of detection values (3σ). All values are in ng. 44

Table 2.5: Mean ($\pm$ 1σ) reagent blank and filter blank values for Fe and Al from ICP-MS analyses of digest samples, along with corresponding method limit of detection values (3σ). All values are in ng. 45

Table 2.6: Certified concentrations (in bold red) of Fe and Al in reference materials, compared to results obtained using the described digest protocol. All concentrations are in ppm. Also shown (in brackets) is the number of replicates analysed in each case. Values in italics represent mean percentage recovery. 46

Table 3.1: Flux summaries for mass and biogenic components of particulate material during D341 (corrected for process blanks). DL = detection limit, based on 3σ of process blank. Samples in italics had not stabilised before sample cups opened, while PAP3 P4 (highlighted in red) spent a significant time at a shallower depth than the stable depth shown (see text and Appendix D). 62

Table 3.2: Flux summaries for Al, Fe, P and Mn during D341 (corrected for process blanks). Values shown are total values (leach + digest). DL = detection limit, based on 3σ of process blank. Samples in italics had not stabilised before sample cups opened, while PAP3 P4 (highlighted in red) spent a significant time at a shallower depth than the stable depth shown (see text and Appendix D). 63

Table 3.3: Flux summaries for mass and biogenic components of particulate material during D354 (corrected for process blanks). 70

Table 3.4: Flux summaries for Al, Fe, P and Mn during D354 (corrected for process blanks). Values shown are total values (leach + digest). DL for Al D354 blank = detection limit, based on 3σ of filter blank. 71

Table 3.5: A comparison of mesopelagic measurements of "*b*" at a range of locations. 77

Table 3.6: Relative contributions (by weight) of the four main flux components to material collected during PAP4, IB3, IB4 and at the VERTIGO stations. 79

Table 3.7: Particulate iron (pFe) fluxes measured by neutrally buoyant, free-drifting or moored sediment traps between 50 - 800 m depth. 87

Table 4.1: Summary of literature values for *per gram* concentrations of selected metals in suspended particulate material. All concentrations are in µmol g^{-1}. n/a = details not available. 97

Table 4.2: Summary of literature values for *per volume* concentrations of selected particulate metals in the upper 500 m of the water column. Data shown are either ranges (References 1 – 8) or calculated mean values (References 9 – 11). Fe and Al data are in nmol L^{-1}; all other metals are in pmol L^{-1} 98

Table 4.3: Surface nutrients and chlorophyll data from underway measurements made during D350 and D354. Data shown is the range of values in each region, with the median value in brackets. 105

Table 4.4: Amount of each element measured in deionised water rinse as a percentage of the total measured in the rinse, leach and digest fractions. Values shown are the mean value and standard deviation for the number of samples (*n*) from which the rinse was analysed. 111

Table 4.5: Size-fractionated and total suspended particulate material concentrations for D350, D351 and D354. For each depth, the range, mean and standard deviation are shown. 112

Table 4.6: Summary of POC, PON, P and total trace metal (leach + digest) concentrations in SPM collected during cruises D350, D351 and D354. POC and PON values are in mmol g^{-1}, Co and Pb in nmol g^{-1}, and all others in μmol g^{-1}. 115

Table 4.7: Effect of the choice of Fe/Al ratio upon calculated values for the percentage of particulate Fe present in the lithogenic fraction and upon the calculated biogenic pFe concentrations. For each cruise and ratio, the ranges of calculated values are shown, based on pFe and pAl measurements. In each case the median value is shown in brackets. 131

Table 5.1: Summary of measurements made for iron budgets in this and previous studies 152

Table C.1: Operating parameters used during ICP-MS analysis. 180

Table C.2: Range of standard concentrations used for ICP-MS analysis. All concentrations are in ppb 182

Table C.3: Mean reagent blank and filter blank values for 25 % HAc leaches (±1σ). All values are in ng. 183

Table C.4: Mean reagent blank and filter blank values for total acid digestions (±1σ). All values are in ng. 184

Table D.1: Deployment details for D341 (depths in brackets represent average depth during stable period if not stable for entire sampling time). 186

Table D.2: Deployment details for D354 (depth in brackets represents average depth during stable period, as trap was not stable for entire sampling time). 192

Table E.1: Sample details for D350 SAPS deployments. 197

Table E.2: Sample details for D351 SAPS deployments. 198

Table E.3: Sample details for D354 SAPS deployments. 199

Declaration of authorship

I, Christopher Matthew Marsay declare that the thesis entitled **'Particulate Trace Metals, Carbon and Nitrogen in the Mesopelagic'** and the work presented in the thesis are both my own, and have been generated by me as the result of my own original research. I confirm that:

- this work was done wholly or mainly while in candidature for a research degree at this University;
- where any part of this thesis has previously been submitted for a degree or any other qualification at this University or any other institution, this has been clearly stated;
- where I have consulted the published work of others, this is always clearly attributed;
- where I have quoted from the work of others, the source is always given. With the exception of such quotations, this thesis is entirely my own work;
- I have acknowledged all main sources of help;
- where the thesis is based on work done by myself jointly with others, I have made clear exactly what was done by others and what I have contributed myself;
- none of this work has been published before submission.

Signed: ……

Date:……

Acknowledgements

Three and a half years after starting my PhD, the end is in sight. My sincere thanks go to Eric Achterberg for taking time out from chasing dust storms in the tropical Atlantic to respond to my initial enquiry about starting a project, and for helping to secure the NOCS studentship that set me on my way to this research. My thanks also, to Eric and to Richard Sanders and Peter Statham: for the discussions, the guidance, the cruise opportunities, the reassurances and the enthusiasm. And thank you to Richard Lampitt for the early discussions about PELAGRA and about measuring sinking particle flux.

Five research cruises on the RRS *Discovery* have contributed to this research. Many thanks to all the crew and officers that made the voyages possible, and also to the science crews of PAP site cruise D341 and the Ellett Line and Iceland/Irminger Basin cruises in which I participated. Particular gratitude is due to Kev Saw and Sam Ward for their support with the PELAGRA traps and to Peter for his help getting to grips with processing my first sediment trap samples. Thanks also to Fred Le Moigne, Maria Villa and Kostas Kiriakoulakis for the teamwork in deploying SAPS.

Many people have helped in collecting the data for this thesis. The long hours in the lab were made easier by the shared POC, PIC and bSi work with Fred and Jen Riley and SAPS processing with Sebastian Steigenberger, while the assistance from Darryl Green in running PIC samples, Matt Cooper for letting me take over his hotplate for several months and Andy Milton for time on the ICP-MS was all invaluable. Thanks also to Bob Head in Plymouth for running POC samples. Additional data included in these pages is here courtesy of Stephanie Henson (satellite-derived measurements), Fred Le Moigne (^{234}Th-derived data) and Alex Baker (aerosol data).

I would never have been able to start, or complete, my PhD without the support and encouragement that I have received from my family in everything that I have done, for which I am profoundly grateful.

Finally, thank you to Liz, for making the past two years easier and more enjoyable. Thanks for understanding the weekends spent working, thanks for listening, and thanks for distracting me when I've needed it.

Chapter 1: Introduction

1.1 Overview

The biogeochemical cycles of carbon, the major nutrients and trace elements in the ocean are intrinsically linked. Biological uptake and photosynthetic fixation of carbon (C), nitrogen (N) and phosphorus (P) by phytoplankton takes place in the surface ocean in average molar proportions of 106:16:1 (Redfield *et al.*, 1963), though in any volume of water, numerous physical, chemical and biological factors, including the phycological requirements of plankton species present, result in deviations from this stoichiometry (Arrigo, 2005). Other elements are also required by phytoplankton for biochemical (*e.g.* iron, manganese, zinc) or structural (*e.g.* silicon, calcium) purposes, resulting in attempts to expand the traditional Redfield stoichiometry to reflect average requirements for these other elements (*e.g.* Ho *et al.*, 2003).

As a result of such requirements, the availability (or lack) of certain elements may promote or restrict growth of one type of phytoplankton over another, or even limit the total rate of primary production. The distribution of biologically important elements can therefore play a major role in the biological assimilation of carbon in the ocean, and thus the uptake of carbon dioxide (CO_2) by the ocean from the atmosphere. In turn, the fate of this biological material will influence the distribution of the elements associated with it.

This chapter begins with an overview of the biological carbon pump – the biologically mediated transfer of carbon from the euphotic zone to the deep ocean – with a focus on the major components of the sinking flux. This is followed by an overview of the tools and techniques used to quantify or predict this flux. There is then an introduction to the importance of iron (Fe) to marine primary production, and an overview of its inputs, speciation, cycling and fate in the marine environment.

1.2 The role of the oceans in the global carbon cycle

The oceans represent one of the major global reservoirs of carbon, and play a crucial role in the global carbon cycle. Sigman and Boyle (2000) summarised the carbon cycle in the Holocene epoch as consisting of five reservoirs, of which the deep ocean

reservoir, containing an estimated 38,000 Pg C (1 Pg = 1 x 10^{15}g), is second only in size to the sediments and crust (Figure 1.1), and holds over ten times more carbon than the terrestrial, atmospheric and surface ocean combined. The surface ocean inventory is estimated to be comparable in size to that of the atmosphere, holding ~700 Pg C.

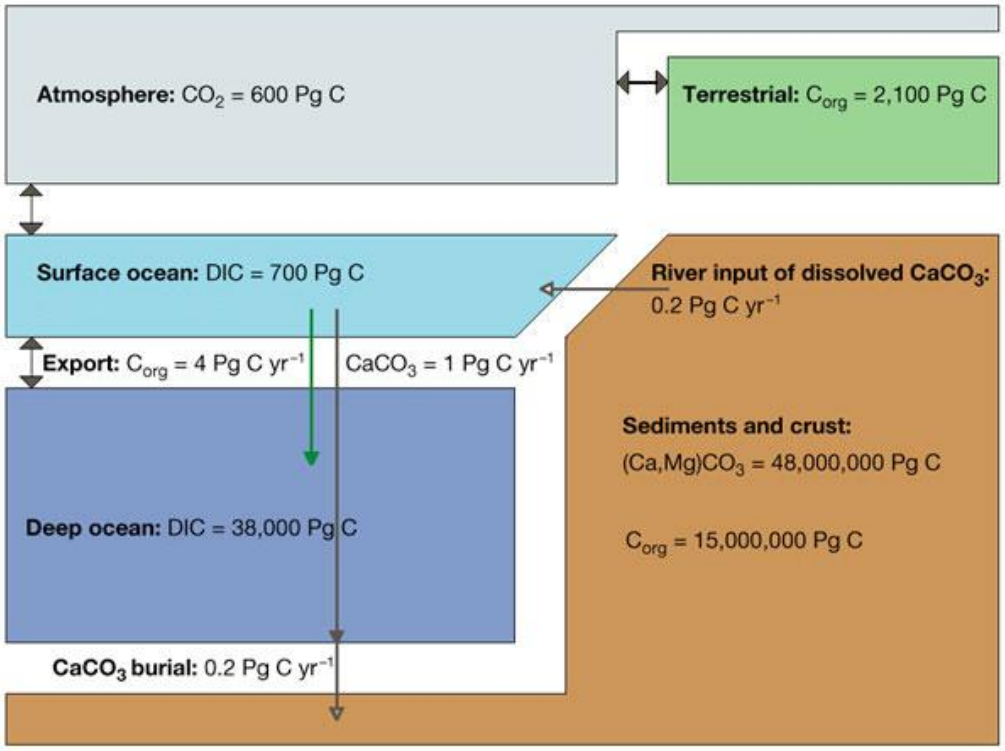

Figure 1.1: A simplified representation of the Holocene carbon cycle, showing only the major reservoirs thought to be important for glacial/interglacial variations in atmospheric carbon dioxide levels (values are in Pg = 1 x 10^{15} g). Also shown are some of the (pre-industrial) fluxes into and out of the surface ocean. Reproduced from Sigman and Boyle (2000).

Anthropogenically-forced deviations from the natural carbon cycle over the past two hundred years, through combustion of fossil fuels, deforestation and production of cement, have led to an increase in atmospheric CO_2 concentrations from 281 ± 2 parts per million (ppm) in 1800 to almost 384 ppm by 2007 and 392 ppm by 2011 (Sabine *et al.*, 2004; Doney *et al.*, 2009; Keeling *et al.*, 2012). It is estimated that oceanic uptake of CO_2 has removed around a third of the total emissions over this time, meaning that without this uptake the current atmospheric CO_2 would be almost 450 ppm (Doney *et al.*, 2009).

Along with inputs via rivers to coastal and shelf regions, the main input of carbon to the ocean is through the ocean-atmosphere interface, with exchange of CO_2 occurring in both directions. If no other factors were involved, the atmosphere and upper ocean

would eventually reach equilibrium, with atmospheric and oceanic CO_2 concentrations remaining stable. However, both physical and biological processes serve to transfer CO_2 from the surface to the deep ocean; the export to deep waters of dissolved inorganic carbon in cold, downwelling water and the sinking of particulate organic material (Schneider *et al.*, 2003). These two processes are known as carbon "pumps" because they maintain a concentration gradient of carbon between the surface and deep ocean, with total carbon dioxide (ΣCO_2) concentration greater in deep water than in the surface mixed layer (Volk and Hoffert, 1985). The first of these mechanisms is known as the solubility pump and is a physico-chemical process that exists due to greater solubility of CO_2 in cold surface water in the polar regions, which are also areas of deep-water formation (Volk and Hoffert, 1985). The second process is driven by biological uptake of carbon dioxide and is known as the biological carbon pump.

1.3 The biological carbon pump

The biological carbon pump, or "biological pump" (Figure 1.2), is defined as the downward export of biogenic particles through the water column (Boyd and Trull, 2007). It begins through the photosynthetic fixation of dissolved inorganic carbon and nutrients by phytoplankton in the euphotic zone (most commonly defined as the water column down to the depth at which 1 % or 0.1 % of surface incident light penetrates). Within this relatively thin layer of the upper ocean, these photoautotrophs produce biomass that forms the basis of the marine food web, with an estimated 45 – 50 Pg of organic carbon fixed globally by marine phytoplankton each year (Falkowski *et al.*, 1998). Within the surface and subsurface ocean, zooplankton and higher trophic organisms feed on the phytoplankton, and the resulting faecal pellets and detritus are colonised by heterotrophic bacteria, which are able to use the organic carbon for their own growth. This then provides a food source for other heterotrophs, and so energy is passed on through the various trophic levels of the marine ecosystem.

At each stage of the process, some material is metabolised as an energy source, rather than being incorporated into new biomass). Dissolved organic carbon (DOC) is released into the water column, while the excretion of faecal pellets and "sloppy" feeding by zooplankton and other heterotrophs produces detrital fragments of organic matter. Some of this particulate organic matter (POM) is large and dense enough to sink down through the water column, transferring organic carbon to depth. Although remineralisation continues throughout the water column, some material may reach the ocean floor and become part of the marine sediment. Organic carbon that sinks below the depth of seasonal convective overturning is less likely to be returned to the surface

ocean on annual timescales and is considered to be sequestered (removed and isolated) from the atmosphere for time periods up to the mean deep water residence time of ~1000 years.

Thus by the production, sinking and incomplete remineralisation of POM, carbon is continually transferred from the surface to the deep ocean and sediments, forcing ΣCO_2 concentrations near the ocean-atmosphere interface away from equilibrium with atmospheric CO_2 concentrations, and so driving uptake of CO_2 by the oceans (Volk and Hoffert, 1985). The effect of this is significant and it is thought that during the last glacial maximum a stronger biological pump contributed to a 30 ppm reduction in atmospheric CO_2 concentrations (Sigman and Boyle, 2000).

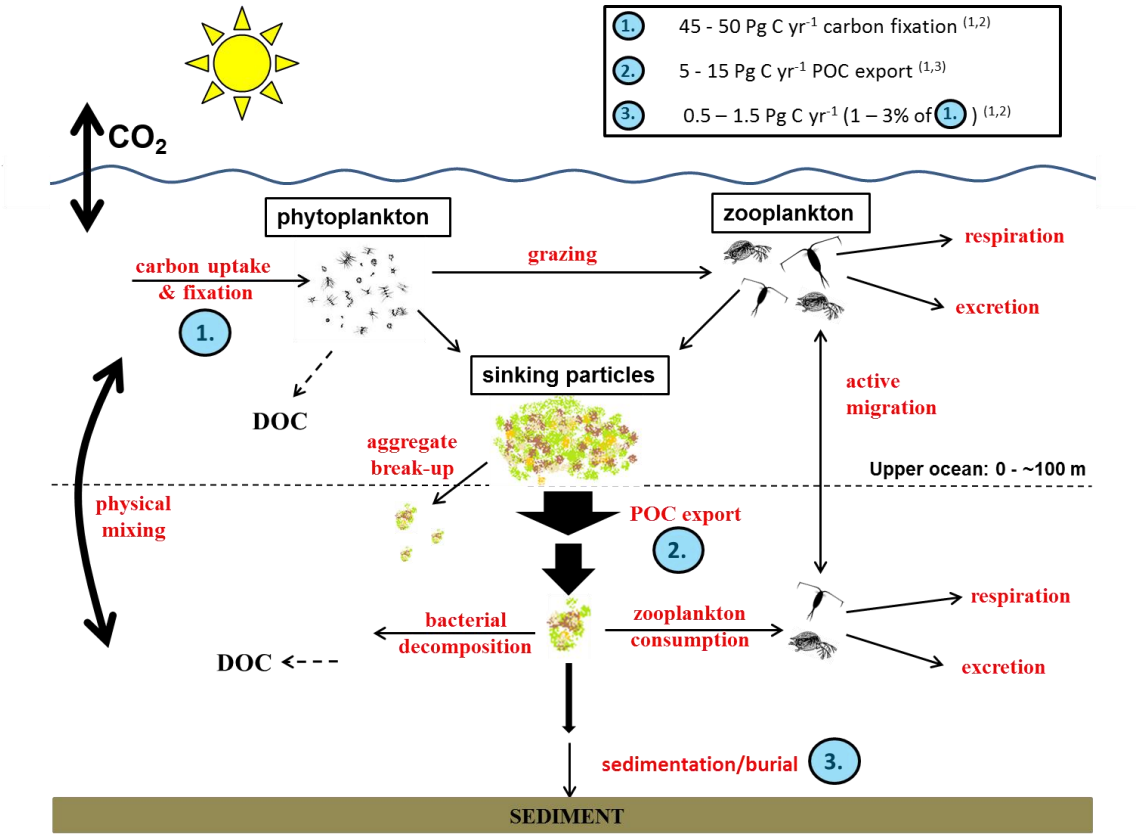

Figure 1.2: Schematic of the biological carbon pump, showing the main transport pathways of carbon (named in red), from photosynthetic uptake to sedimentation and burial. Adapted from a figure in "A New Wave of Ocean Science" (U.S.JGOFS, 2001). Estimated magnitudes of carbon transfer are given for the numbered processes. *References: (1)* Falkowski *et al.* (1998), *(2)* De La Rocha and Passow (2007), *(3)* Henson *et al.* (2011).

As it sinks, however, POM is steadily metabolised back to its inorganic constituents due both to feeding and respiration by zooplankton and microbial breakdown by heterotrophic bacteria, which then release the dissolved carbon and nutrients into the surrounding water. In this way, organic carbon may be recycled many times through

the "microbial loop" before it even leaves the surface ocean (Azam *et al.*, 1983). Consequently, the fraction of photosynthetically fixed carbon that is exported to the ocean interior is fairly small, with estimates ranging from 10 – 40 % of net global primary production exported from the euphotic zone (Eppley and Peterson, 1979; Henson *et al.*, 2011). The magnitude of this carbon export is controlled by a number of factors, including nutrient supply to the upper ocean, mixed layer depth, depth of the euphotic zone, food web structure and microbial loop efficiency (Falkowski *et al.*, 1998; Rivkin and Legendre, 2001; Buesseler and Boyd, 2009). For example, bacterial growth efficiency is inversely related to temperature, meaning that a larger fraction of assimilated carbon is respired in the upper ocean at low latitudes where surface waters are warmer. A greater proportion of production can therefore be exported in polar regions than in tropical systems (Rivkin and Legendre, 2001) and whereas in many areas export from the euphotic zone may only be 1 – 10 % of net primary production, in polar regions it can exceed 50 % (Buesseler, 1998; Neuer *et al.*, 2002).

Below the euphotic zone there is essentially no new production of particles by phytoplankton, but the feeding actions of zooplankton and microbial colonisation and breakdown of organic material continue to attenuate the carbon flux (Buesseler and Boyd, 2009), while also releasing dissolved material that can potentially be mixed back up to the euphotic zone. Of this further reduction in sinking flux, the greatest change occurs in the region known as the mesopelagic, between the base of the euphotic zone and around 1000 m depth. An estimated 6 – 25 % of material exported from the euphotic zone sinks beyond 1000 m (Martin *et al.*, 1987; Francois *et al.*, 2002; Boyd and Trull, 2007). Attenuation of the sinking particle flux is therefore of a similar magnitude in the subsurface ocean as in the surface ocean. Lutz *et al.* (2002), estimated that the amount of organic carbon that reaches depths of more than 1500 m ranges from 0.28 – 30 % (average of 5.7 %) of the export flux from the euphotic zone, equating to 0.1 – 8.8 % (average of 1.1 %) of primary production. Similarly, De La Rocha and Passow (2007) estimated that 1 – 3 % of carbon fixed by phytoplankton each year reaches the deep sea and sediments.

The sinking rate of a particle through a fluid is described by Stoke's Law, which relates the velocity to the particle radius and the difference in density between particle and fluid, as well as the fluid viscosity. Thus, increases in the density or size of particles increase their sinking velocity through the water column. Processes important in controlling the efficiency of the biological pump (*i.e.* what proportion of exported POM sinks beyond a particular depth) are those which affect the balance between sinking speed and degradation rate of the sinking particles: microbial remineralisation rates, the aggregation, disaggregation and repackaging of organic rich particles, which are in turn affected by zooplankton grazing and faecal pellet production, and the interaction between organic material and particulate minerals present (Armstrong *et al.*, 2002;

Francois *et al.*, 2002; Klaas and Archer, 2002; De La Rocha and Passow, 2007). The extent to which these processes dominate POM transfer to the deep ocean remains a matter of debate (Klaas and Archer, 2002; Passow, 2004; Trull *et al.*, 2008; Lee *et al.*, 2009; Henson *et al.*, 2012).

Contributions to sinking particle flux include faecal pellets, planktonic carcasses, detrital material from feeding processes, and mucus matrices such as transparent exopolymer particles (TEP; Alldredge and Silver, 1988; Alldredge *et al.*, 1993), as well as lithogenic mineral grains and fragments of (or complete) biomineral shells and tests. The various sources result in a wide range of particle size, density and porosity and therefore sinking velocity and susceptibility to remineralisation (De La Rocha and Passow, 2007). Particles that are too small to sink individually may remain suspended in the water column until they are either remineralised or become aggregated to other material.

Large composite particles of >500 μm diameter are collectively known as "marine snow" (Alldredge and Silver, 1988). They originate in several ways but these can be grouped together into two general pathways. One way is through the actions of organisms such as appendicularians, which produce gelatinous structures from mucopolysaccharides for feeding. These structures collect phytoplankton, bacteria and faecal pellets and are regularly discarded by the organism. The second route is through biologically-enhanced physical coagulation of smaller component particles, such as phytoplankton, inorganic particles and faecal pellets (Alldredge and Silver, 1988). In this latter route, TEP plays an important role as a matrix and glue for the various components (Alldredge *et al.*, 1993; De La Rocha and Passow, 2007).

As it sinks, marine snow is subject to further microbial decomposition and grazing by zooplankton, which break the aggregates up (as can the swimming motion of zooplankton). The resulting particles may be too small to sink on their own and so become part of the suspended particulate material (SPM) pool, from where they may form new aggregates. The sinking rate of particles varies according to composition and size but is typically tens to hundreds of metres per day for marine snow and phytodetritus, while faecal pellets may sink at >1000 m d^{-1} (Alldredge and Silver, 1988; Ittekkot, 1993; Turner, 2002) on their own, but may also become incorporated into aggregates.

1.3.1 Chemical composition of particulate material

Although the biological pump is important for its role in the transfer of carbon from the atmosphere and the euphotic zone to the deep-ocean and benthic sediments, not

all of the material reaching the seafloor contributes quantitatively to this transfer. By the time that they reach the deep sea, sinking particles only contain a fairly constant 5% of particulate organic carbon (POC) by weight (De La Rocha and Passow, 2007). Biogenic minerals such as opal (biogenic silica, bSi), calcite and aragonite (two forms of calcium carbonate, $CaCO_3$, which are together described as particulate inorganic carbon (PIC)) are produced by certain planktonic organisms, using dissolved minerals, and also contribute to the sinking flux. Lithogenic materials are also present throughout the water column, having entered mainly through riverine and atmospheric inputs of weathered continental material (Jickells and Spokes, 2001). The relative contribution and importance of these different fractions to the sinking particulate flux and to the SPM pool varies with depth, with time, and from region to region.

1.3.1.1 Particulate organic material (POM)

Most studies of sinking particle flux discuss the organic component in terms of POC, and indeed it is specifically the carbon flux that defines the strength of the biological pump (Volk and Hoffert, 1985; Buesseler and Boyd, 2009). But the material involved in this flux is composed of a whole suite of organic molecules (proteins, lipids, carbohydrates *etc.*) that contain not just carbon but also other elements such as nitrogen and phosphorus. Also, although dissolved organic carbon, by definition, does not sink, it may become associated with POM through its interstitial incorporation into colloids and aggregates (De La Rocha and Passow, 2007).

Recycling of organic carbon through the microbial loop means that more labile organic molecules are rapidly removed from POC by heterotrophic bacteria, leaving a higher proportion of refractory organic carbon in sinking POM. In a Pacific Ocean study by Sheridan *et al.* (2002), particulate material collected from the surface ocean was similar in composition to phytoplankton, while that collected from mesopelagic depths (200 – 1000 m) contained labile particulate material (amino acids, pigments, fatty acids, neutral lipids) that was increasingly degraded with depth due to microbial action (and possibly dilution of deeper SPM pools by more refractory material from fast-sinking particles). Similarly, the fraction of molecularly uncharacterised POC (organic molecules not measured by conventional techniques) has been shown to increase in deeper POC samples due to increased degradation of sinking particles (Hedges *et al.*, 2000).

Furthermore, the elemental composition of POM changes with depth due to preferential remineralisation of certain fractions of organic material: various studies show a trend for more rapid remineralisation of particulate organic nitrogen (PON) and phosphorus than POC. A comparison of POM measurements from a wide range of

sources by Schneider *et al.* (2003) found a global mean C:N ratio of sinking marine particles in the surface water of 7.1 ± 0.1 (*cf.* 6.6 expected from the Redfield ratio), with a systematic increase of the ratio with depth of 0.2 ± 0.1 per 1000 m, suggesting that nitrogen is remineralised from POM at shallower depths than carbon. A similar relationship has been documented for the C:P ratio (Shaffer *et al.*, 1999), while Honjo *et al.* (1982) found that in samples collected at mesopelagic depths in the Atlantic and Pacific Oceans, the C:N:P ratio had changed to 200:21:1, and then to 300:33:1 at bathypelagic depths.

This difference in remineralisation length scales of C, N and P is a driving force of the biological pump. More rapid remineralisation of N and P results in not only a higher C/nutrient ratio in sinking organic material, but a lower ratio in the surrounding water, meaning that upward mixing water is enriched in nutrients over the Redfield ratio to carbon. Utilisation of these nutrients by phytoplankton thus forces surface ocean CO_2 concentrations away from equilibrium, leading to further uptake of CO_2 by the ocean (Christian *et al.*, 1997).

1.3.1.2 Particulate Inorganic Carbon (PIC)

Calcium carbonate, in the form of calcite or its polymorph aragonite, is precipitated by certain plankton (coccolithophores, foraminifera, pteropods and calcareous dinoflagellates) as plates, shells or tests, which together comprise PIC. The sinking of these hard structures, either individually or as components of aggregates, provides another pathway for the flux of carbon from the surface and subsurface ocean to the seafloor. It is also thought that this denser material (calcite has a density of 2.7 g cm^{-3}, compared to ~1.1g cm^{-3} for organic matter) increases the efficiency of the biological pump through ballasting organic aggregates with which it becomes associated, thus increasing their sinking speed (Ittekkot, 1993).

However, the role of PIC in the biological pump is complex. The process of calcification increases dissolved CO_2 concentrations in the surface ocean by an average of 0.6 moles per mole of $CaCO_3$ precipitated, thereby acting to reduce CO_2 uptake by the ocean (Volk and Hoffert, 1985; Frankignoulle *et al.*, 1994). Thus the positive influence of its formation on the transfer of carbon from atmosphere to deep-ocean is offset. In order to positively contribute to sequestration of CO_2, each mole of carbonate exported must therefore result in an increased export of 0.6 moles POC (*i.e.*, a POC/PIC export ratio of ≥ 0.6 must be achieved).

Coccolithophores are thought to be responsible for 50 – 70 % of PIC production, but the tiny plates precipitated and discarded by them tend to remain suspended in the

water column until they become incorporated into aggregates large enough to sink (De La Rocha and Passow, 2007). In contrast, the tests of foraminifera are relatively large and heavy, and sink on their own, so that 32 – 80 % of the 1.1 Pg yr^{-1} calcite reaching the sea floor is thought to derive from foraminifera, with 12 % from coccolithophores, 10 % from pteropods and 3.5 % from calcareous dinophytes (Milliman *et al.*, 1999; Schiebel, 2002).

Thermodynamic dissolution of carbonate is not generally thought to take place at significant rates above the depth of the lysocline (~2,000 m for most of the ocean), above which the water is saturated with calcite (although this view is challenged by Feely *et al.* (2004)). However, models, laboratory experiments and flux measurements have found that the most significant decrease (40 – 80 %) in PIC flux takes place between 100 – 700 m, which is attributed to grazing and organic matter degradation creating microenvironments with a pH significantly lower than the surrounding water (Milliman *et al.*, 1999; Schiebel, 2002). As both of these require oxygen, it is not surprising that greater calcite preservation has been observed in low oxygen environments (Schiebel, 2002).

1.3.1.3 Biogenic silica (bSi)

As with calcite and aragonite, biogenic silica is incorporated into the physiological structures of certain autotrophic and heterotrophic plankton; in this case diatoms, radiolaria and silicoflagellates. Silicic acid ($Si(OH)_4$) is taken up from surface water by diatoms and other silicifying phytoplankton and deposited as bSi, with an estimated biogenic silica production of 6.7 ± 1.1 Pg Si yr^{-1} (Tréguer *et al.*, 1995). Diatoms in particular play an important role in the biological pump, as they tend to dominate the phytoplankton community during conditions optimal for growth and unusually high export: spring blooms, equatorial divergences, decay of ocean eddies, atmospheric dust inputs (Buesseler, 1998; Ragueneau *et al.*, 2000).

On a regional scale, bSi fluxes can vary by two orders of magnitude. The highest annual fluxes are found in areas of the Southern Ocean, with a general decrease towards lower latitudes (where calcite fluxes dominate), but with upwelling areas such as the equatorial Pacific providing exceptions to the trend (Ragueneau *et al.*, 2000). Like calcite, opal has a greater density (2.1 g cm^{-3}) than organic matter and can thus increase the sinking rate of aggregated material. Unlike calcite, biogenic silica is unsaturated in the ocean, and significant dissolution takes place in the upper ocean (as much as 50 – 60 % within the upper 100m (Tréguer *et al.*, 1995; Boyd *et al.*, 2004)) though not to the same extent as POC remineralisation (Nelson *et al.*, 2002). Of that

sinking out of surface waters, about 25 % reaches the sea floor and the global average preservation efficiency of bSi (burial in seabed as a fraction of production in surface waters) is estimated at only 3% (Tréguer *et al.*, 1995). Nevertheless, opal-rich sediments are widespread, and particularly prevalent in the high nutrient low chlorophyll (HNLC) regions (Ragueneau *et al.*, 2000).

1.3.1.4 Lithogenic material

Along the ocean margins, riverine sediment loads dominate the input of lithogenic material to the marine environment. Resuspension of shelf sediments also plays an important role. The material being transported consists of the erosion products of rocks and of soil, and so can be thought of as a mixture of minerals (including terrestrial carbonate and silicate) and POM. Most of this material is laid down in sediments along the continental margins and does not contribute to sinking particulate material in the open ocean, though there is evidence that some material from the continental shelf can be transported hundreds of miles into the ocean by lateral advection (Lam *et al.*, 2006; Lam and Bishop, 2008; Lamborg *et al.*, 2008a).

The main input of lithogenic material over the large areas of the surface ocean remote from land masses is through atmospheric dust deposition, transported primarily from arid and semi-arid areas of the continents. Globally, an estimated 0.9 Pg yr^{-1} of mineral aerosol is added to the surface ocean by atmospheric deposition, though the distribution of this is uneven and depends on prevailing wind patterns and proximity of dust sources: much of the North Atlantic receives 1 – 10 g m^{-2} yr^{-1} of mineral aerosol, whereas areas of the Southern Ocean and remote South Pacific receive <0.01 g m^{-2} yr^{-1} (Duce *et al.*, 1991).

Lithogenic material in the open ocean water column tends to consist mainly of aluminosilicate clay minerals, though other minerals associated with these may include small amounts of a large variety of other elements, including calcium, sulphur, iron and many other metals. In the open ocean, where the main input of lithogenic material is through deposition of dust carried hundreds or thousands of miles, the particles are typically small in size. Some may be large enough to sink individually, as the density of lithogenic material is relatively high (~2.7 g cm^{-3}; Klaas and Archer, 2002). Others may remain in the suspended particulate pool until they become incorporated into aggregates and, like the biominerals, add ballast to the organic material. Sediment trap studies show that the contribution of lithogenic material to the mineral fraction of material sinking in the deep-ocean ranges from 0 – 68 % (Francois *et al.*, 2002), and commonly contributes > 25 % of the total sinking particle flux (Wefer, 1989).

1.3.2 Measuring sinking particle flux

Measurements of the fixation of carbon by primary production in the surface ocean and export from the euphotic zone are useful for the information that they provide about uptake of CO_2 by the marine ecosystem and the proportion of this that is transferred downwards, away from the surface ocean (*i.e.*, the strength of the biological pump). But this information has its limitations, as the material sinking out of the euphotic zone is still subject to significant remineralisation in the mesopelagic zone. Due to a variety of processes such as seasonal variations in thermocline depth, dynamics of mode water eddies and upwelling, remineralised organic material in these subsurface waters can be returned to surface waters over relatively short timescales (months to years).

Direct measurement of sinking particle flux at a range of depths and for a suitable duration can provide useful information about the change in particle flux composition and magnitude with depth and how this varies regionally and temporally. However, there are known issues with traditional sediment traps and more novel approaches are now in use to tackle these problems. In situations where the use of traps is not favourable, radioisotope tracer methods can be used to estimate aspects of particle flux.

1.3.2.1 Traditional sediment traps

Sediment traps deployed at known depths of the water column can provide a wealth of information about sinking particles. A suitably planned trapping program, with traps deployed at different depths and set up for time-series sampling, can provide information on flux magnitude and attenuation with depth, changes in composition of particles, regional variations and temporal variations on interannual, seasonal and shorter timescales. First used in the late 1970s, the majority of sediment traps in widespread use are variations on the cylindrical VERTEX "MULTITRAPS" design (Knauer *et al.*, 1979) and the funnel-based "PARFLUX" trap (Asper, 1996). All work on the same basic "rain gauge" premise, with an opening at the top of the trap through which sinking particulate material is collected into the body of the trap. Most are deployed with a layer of brine, denser than the surrounding water, at the bottom of the collecting tube/sample cup in order to minimise resuspension and loss of any particles that are collected, and also to retain any poison or preservative used and any solubilisation products of the material collected (see below).

Since they were first used, there have been several inter-comparison projects carried out (*e.g.*, Honjo *et al.*, 1992) to compare the effectiveness of different trap designs and deployment strategies, such as bottom-moored (secured to a heavy weight on the seafloor) versus surface-tethered (connected to a drifting float at the sea-surface). There have also been numerous reviews of the various issues associated with the use of sediment traps for measuring sinking carbon flux (U.S.GOFS, 1989; Honjo, 1996; Gardner, 2000; Buesseler *et al.*, 2007), and attempts to calibrate these measurements using radionuclide methods (Bacon *et al.*, 1985; Buesseler, 1991; Buesseler *et al.*, 1994). A common theme of reviews on the topic of sediment traps is the issue of the main drawbacks associated with the method. These vary depending on the depth and duration of deployment. For example, traps in the deep ocean are more likely to collect material that has originated far from the sample location as there is a lot more opportunity for lateral transport as it sinks to the bathypelagic – *i.e.*, there is a larger "statistical funnel" from which particles arriving in the trap could have originated (Buesseler *et al.*, 2007).

Hydrodynamic issues are relevant for any tethered trap, regardless of depth, but are a more significant problem where lateral currents are stronger, which is more often the case in surface and subsurface waters. Also, if mesopelagic traps are tethered to a surface float, subject to wind stress, or if several traps are deployed at different depths on the same mooring, the traps will move at different speeds relative to the surrounding water. Lateral flow across the mouth of the trap causes turbulence which may deflect sinking material into or out of the trap and may cause aggregates to break up (thus changing their sinking characteristics as well as the composition of the sinking material). The trap mouth may also tilt towards or with the flow, thus changing the aspect ratio of the opening into which particles can sink (Buesseler *et al.*, 2007).

If traps are deployed for a long time, material collected may undergo substantial degradation before the sample can be processed, especially if local conditions promote microbial activity (*e.g.*, warm, oxic waters), and this can result in particulate material being lost to the surrounding supernatant (Antia, 2005). To reduce the degradation of material collected in traps, a poison or preservative is generally added in a suitable concentration to prevent or minimise microbial activity, examples being mercuric chloride, sodium azide, formaldehyde and chloroform. Various studies have been carried out to measure the effectiveness of different poisons/preservatives (Lee *et al.*, 1992) and their *in situ* effects on chemical composition of the material collected (Knauer *et al.*, 1984). The US GOFS 1989 planning report on sediment trap sampling lists some advantages and disadvantages of the various options commonly used (U.S.GOFS, 1989).

Zooplankton "swimmers" are another major problem for surface and subsurface sediment trap sampling. The term refers to zooplankton that are thought to actively enter sediment traps (Buesseler *et al.*, 2007), although some may be carried in by turbulent flow around the trap mouth. The swimmer problem is more of an issue in the upper water column and decreases with depth. They consist of crustaceans, such as copepods, amphipods and euphausiids, which are easily recognized and can be picked out of sample cups, but also gelatinous zooplankton that are difficult to see and distinguish from detrital material; so-called "cryptic swimmers" (Michaels *et al.*, 1990).

The numbers of swimmers can be very large compared to the sinking flux, with one study estimating that up to 96% of the measured carbon flux was due to swimmers (Michaels *et al.*, 1990). But they can also affect trap measurements in several other ways. By feeding on the material collected and then swimming out of the trap they cause an underestimation of sinking flux. They may also release faecal pellets while in the trap, either from previous feeding, or from feeding within the trap, thus causing a change in the amount and the chemical composition of material in the trap. Their swimming and feeding behaviour may also break up aggregates, altering the size spectrum of trap material and releasing DOM (and therefore contributing to excess elemental contributions in the trap brine). The use of poisons and preservatives is effective at killing zooplankton that make their way into the trap, though may lead to larger numbers of swimmers remaining in the trap (Lee *et al.*, 1992).

As swimmers do not contribute directly to the sinking particulate flux, the consensus is that any found in sediment trap samples should be removed where possible, though the method of doing so varies. Picking out individual swimmers under a microscope can be very time consuming and requires a certain level of experience in identifying items to be removed. The alternative is to screen the sample through a mesh to remove the larger swimmers before processing. However, this method may also result in some of the larger sinking particles being removed from the sample, while missing some of the smaller swimmers.

Although sediment traps suffer from these short-comings, and invite caution in analysis of data collected with them, they remain the most common method of measuring downward POC flux, especially in the deep ocean.

1.3.2.2 Radionuclide disequilibria

Estimates of particle settling fluxes have also been made using measurements of various radionuclide disequilibria, a technique which has also been used to try and quantify the errors associated with sediment traps. The method involves the use of

members of natural radioactive decay series as tracers. Those (daughter members) used must have two characteristics: be supplied to the water column by radioactive decay of parent nuclides at known rates, and be particle reactive so that they can be collected with material in sediment traps. The integrated deficiency of the daughter nuclide in the water column above the trap is determined in order to calculate its expected flux at the depth of the trap. Comparing this to the measured flux then gives an assessment of the trapping efficiency.

This method was first used for deep-sea sediment traps, with measurements made of several radionuclides in collected material (Brewer *et al.*, 1980; Bacon *et al.*, 1985). Measured fluxes of long-lived ^{230}Th and ^{231}Pa have been used to verify the collection efficiency of bathypelagic traps as being close to 100 %, while showing those in the mesopelagic to be more erratic (Scholten *et al.*, 2001; Yu *et al.*, 2001). In the upper water column shorter-lived radioisotopes in the ^{238}U decay chain have been used. Disequilibria of ^{234}Th/^{238}U (^{234}Th half-life = 24.1 days) have been used to estimate POC flux over timescales of weeks (*e.g.*, Buesseler, 1998) and test the sampling efficiency of sediment traps in the upper 300 m (Buesseler, 1991; Buesseler *et al.*, 1994), while ^{210}Pb (half-life = 22.3 years) and ^{210}Po (half-life = 138.4 days) have been used to study particle export over timescales of months (*e.g.*, Verdeny *et al.*, 2008).

1.3.2.3 Other methods

In the past twenty years, adaptations of the traditional sediment trap designs have arisen in order to either overcome some of the known issues or to focus research on specific aspects of sinking particle flux. The development of neutrally-buoyant sediment traps (Valdes and Price, 2000; Saw *et al.*, 2004) allows mesopelagic-depth deployments that are relatively free of the hydrodynamic concerns associated with surface-tethered or moored traps. This may also have a beneficial effect upon the issue of swimmers by reducing the numbers of zooplankton carried into the traps through turbulence generated by horizontal flow across the trap mouth. These traps are discussed in more detail in Section 2.3 and Appendix A.

Indented rotating sphere (IRS) sediment traps contain a valve that can be used to isolate the collected material from swimmers and reduce the risk of washout of sample, while allowing a time-series collection to be made (Peterson *et al.*, 1993). The design has also been adapted to enable sampling of material based on discrete particle settling velocity ranges, allowing studies in which flux magnitude is combined with knowledge of the distribution of material between different sinking rates (Peterson *et al.*, 2005; Trull *et al.*, 2008; Lee *et al.*, 2009).

Traps containing a polyacrylamide gel rather than poisoned brine enable collection of particles without subsequent aggregation of the material within the trap, allowing examination of individual particles to study the prevalence of different particle types and their characteristics (Ebersbach and Trull, 2008; McDonnell and Buesseler, 2010).

Though they do not specifically sample sinking particles, *in situ* large volume pumps and Go-Flo bottles, or similar, are used for bulk collection of marine particulate material, including both sinking and suspended fractions. These are discussed in more detail in Section 2.4 and Appendix B. Similarly, the marine snow catcher is a 100 L water bottle with a detachable reservoir and can be used to study suspended and sinking particulate material and to isolate individual sinking particles (Riley *et al.*, 2012).

Optical sensors are also used to investigate particle and POC concentrations and fluxes. Examples range from transmissometers fitted to CTD systems, through the Carbon Explorer (an Argo float outfitted with a transmissometer (Bishop and Wood, 2009), to underwater video microscope platforms such as the Video Plankton Recorder and Underwater Video Profiler (McDonnell and Buesseler, 2010; Jouandet *et al.*, 2011) and the use of sensors on gliders to measure backscattering due to particles (Briggs *et al.*, 2011).

1.3.3 Predicting POC flux

Though long time-series of sediment trap measurements exist and are useful in studying episodic, seasonal and annual variations in sinking POC flux, especially when traps are deployed at multiple depths, it is not possible to achieve global coverage. Short-term deployments during research cruises can take up valuable time, especially if traps are free-drifting and subject to movement with local currents, and, though they can provide useful information, the measurements represent snapshots of the continuous, complex and variable processes taking place. But the importance of the biological carbon pump to the redistribution of carbon and other elements from the atmosphere and surface ocean to the deep necessitates an improved understanding of its strength and efficiency on a global scale and of the factors that determine the variability of these, in order to accurately predict how they will change in a changing climate.

For this reason, there have been numerous attempts to deduce general trends or relationships that can then be included in global climate models to predict POC transfer from the euphotic zone using satellite derived data or existing deep-ocean flux measurements (Suess, 1980; de Baar *et al.*, 1983; Martin *et al.*, 1987; Francois *et*

al., 2002; Klaas and Archer, 2002; Lutz *et al.*, 2002; Henson *et al.*, 2012). In particular, understanding controls on the remineralisation length scale of POC (and other flux components) in the mesopelagic is key to balancing carbon budgets (Burd *et al.*, 2010), understanding the resupply of dissolved materials to the surface ocean (Christian *et al.*, 1997) and determining how rates of carbon sequestration will change as anthropogenic CO_2 emissions continue to influence global climate (Kwon *et al.*, 2009).

Suess (1980) first attempted to empirically describe the POC flux measured at depth as a function of primary production in the overlying waters, using data collected in the eastern subtropical Pacific and north-western Pacific. However, while the derived equation may have fitted the data used, primary production cannot always be relied upon to predict flux magnitude. The relationship suggested by Martin *et al.* (1987), in which flux to depth is linked to POC export from the surface ocean by a simple power-law function with an attenuation coefficient, *b*, has been more enduring and is used widely in biogeochemical models (*e.g.*, Doney *et al.* (2004) and references therein), though the initial definition of a globally applicable *b* value now appears an oversimplification (Berelson, 2001; Buesseler *et al.*, 2008). The "Martin curve" is described in more detail in Section 3.2.1.

Armstrong *et al.* (2002) challenged the notion that "all the information necessary for prediction is contained in the carbon flux itself" as implied by the original Martin work. Working from a large database of deep-sea sediment trap measurements, a strong correlation between POC and mineral fluxes was used to argue that fluxes of minerals determine the transport of POC to deep water though ballasting interactions. This ballast hypothesis was based on the ideas of minerals increasing the density and therefore the sinking velocity of particles (Ittekkot, 1993) and of POM in micropores of mineral surfaces or incorporated into biomineral tests being protected from enzymatic decomposition (Lowenstam and Weiner, 1989; Mayer, 1994). In contrast, it was argued, unballasted POC is remineralised in the upper ocean, so that the total flux of POC (F_{total}) at any depth (z) could be estimated using Equation 1.1, where F_{ballast} and F_{free} are fluxes of POC associated and not associated with ballast minerals, respectively, and $f_{ballast}$ is the POC-carrying coefficient of mineral ballast.

This idea was expanded upon by Klaas and Archer (2002), with the ballast-associated POC flux split into three separate terms; that associated with opal (F_{opal}), with calcite (F_{calcite}) and with lithogenic material ($F_{\text{lithogenic}}$), each with a specific POC-carrying coefficient (f_{opal}, f_{calcite} and $f_{\text{lithogenic}}$ respectively). This is shown in Equation 1.2.

$$F_{total}(z) = F_{free}(z) + f_{ballast}.F_{ballast}(z) \qquad \text{(Eqtn. 1.1)}$$

$$F_{total}(z) = F_{free}(z) + f_{opal}.F_{opal}(z) + f_{calcite}.F_{calcite}(z) + f_{lithogenic}.F_{lithogenic}(z) \quad \text{(Eqtn. 1.2)}$$

Klaas and Archer assigned carbonate the highest carrying coefficient and opal the lowest, with that for the lithogenic fraction highly variable, indicating that the source/mineralogy of lithogenic particles affect their transfer of POC. Francois *et al.* (2002) also derived an algorithm from deep-sea trap data suggesting that the settling flux of POC in deep sea sediment traps normalized to export production (from satellite-derived estimates of export production) increases with the flux of carbonate. The profiles of POC flux predicted by the different algorithms (which were derived from overlapping datasets) agree well below 2000 m. However, for the mesopelagic zone they diverge widely, highlighting that the algorithms were derived largely from trap data restricted to >2000 m depth. Additionally, the cause and effect relationship of the correlation between POC and biominerals has been questioned (Passow, 2004; Henson *et al.*, 2012).

More recently, Buesseler and Boyd (2009) suggested an overhaul of the traditional way of comparing POC flux at set depths, instead taking into account regional/temporal variations in the euphotic zone depth. They argue that not doing so skews interpretation of mesopelagic zone processes. Using this method, they find that for the data used, transfer efficiencies of POC at the various locations converged to ~20 – 30 % by 300 m below the euphotic zone depth.

1.4 The marine biogeochemistry of iron

Iron (Fe) is the fourth most abundant element in the Earth's crust, with an estimated concentration of 3.2 – 3.5 % by weight (Taylor and McLennan, 1995; Wedepohl, 1995). However, due to the low solubility in seawater of the thermodynamically stable form of iron, dissolved Fe (dFe) is generally present in the ocean at low (<2 nmol L^{-1}) concentrations, and often at picomolar concentrations in the upper ocean (de Baar and de Jong, 2001). Nevertheless, iron is an essential trace nutrient for phytoplankton, with multiple iron atoms contained in the redox intermediates involved in electron transfer during photosynthesis, while it is also required in many enzymes that are involved in nitrogen fixation, respiration and nitrate reduction (Morel *et al.*, 1991; 2004). Consequently, iron plays a crucial role in setting rates of primary productivity in the oceans (Martin *et al.*, 1991), with some models suggesting that it is the limiting nutrient for phytoplankton in ~40 % of the world ocean (Moore *et al.*, 2002). Understanding the pathways through which iron is introduced to and removed from

the marine environment and its biogeochemistry in the ocean is therefore important to our understanding of the marine carbon cycle.

1.4.1 Sources and sinks of iron in the surface ocean

Iron is introduced to the ocean through three major pathways: atmospheric deposition to the ocean surface, riverine input along the continental margins and hydrothermal input through oceanic crust. Its ultimate sink in the ocean is through sedimentation of particulate Fe (pFe) and its burial and eventual lithification (Figure 1.3).

Riverine concentrations of dissolved and particulate iron (~1 μmol L^{-1} and ~1 mmol L^{-1} respectively) are much higher than those in the open ocean, but mixing with seawater causes flocculation and scavenging which reduces the input substantially (Sholkovitz, 1976), with most fluvial pFe being deposited in coastal and shelf waters (Ussher *et al.*, 2004). Even so, rivers are estimated to make a sizeable contribution to dFe inputs to the ocean of 1.5 Tg yr^{-1} (1 Tg = 1 x 10^{12} g) (Jickells *et al.*, 2005). Hydrothermal inputs supply ~14 Tg Fe yr^{-1} to the ocean (Jickells *et al.*, 2005) through vent fluids with high reduced iron concentrations (1-3 mmol L^{-1}). Though oxidation to Fe(III) and precipitation as iron sulphides and oxyhydroxides, or scavenging by other particles can strip this iron out of the water column within a few hundred metres of the vent (Statham *et al.*, 2005), a recent study suggested that ligand concentrations were high enough to stabilise ~4 % of the vent-emitted dFe (Bennett *et al.*, 2008). Authigenic fluxes, released from sediments during diagenesis are estimated to contribute a further 5 Tg Fe yr^{-1} (Jickells *et al.*, 2005).

Atmospheric inputs include deposition of aluminosilicate materials from arid and semi-arid regions such as Saharan and sub-Saharan Africa, central Asia, Patagonia and Australia (Mahowald *et al.*, 2005); volcanic ash emissions (Duggen *et al.*, 2010); and anthropogenic emissions from biomass burning and combustion of fossil fuels (Guieu *et al.*, 2005; Sholkovitz *et al.*, 2009). Together these amount to an estimated input of 16 Tg Fe yr^{-1} to the surface ocean, though this is not evenly distributed, with local deposition rates ranging from <1 to >1000 mg m^{-2} yr^{-1} (Duce and Tindale, 1991). Atmospheric iron input is split between wet and dry deposition, the balance of which varies regionally and is not particularly well constrained – it has been estimated that wet deposition accounts for 30 – 95 % of the total (Jickells *et al.*, 2005).

Beyond these inputs, upwelling, seasonal convective mixing and entrainment of deeper waters are also important in redistributing iron to the upper ocean (Watson, 2001). On regional scales, lateral advection from continental margins can carry pFe offshore (Lam *et al.*, 2006; Planquette *et al.*, 2011), along with dissolved Fe(II) that has been

mobilised from marine sediments by the anoxic conditions created by organic material decomposition (Berelson *et al.*, 2003; Elrod *et al.*, 2004). Eddies have also been shown to be important in lateral transport and vertical mixing of iron and other nutrients to the surface (Johnson *et al.*, 2005; McGillicuddy *et al.*, 2007). In polar regions, melting of sea ice and icebergs helps in the redistribution of material originating from atmospheric deposition or glacial scouring (Sedwick and DiTullio, 1997; Grotti *et al.*, 2001; Lin *et al.*, 2011).

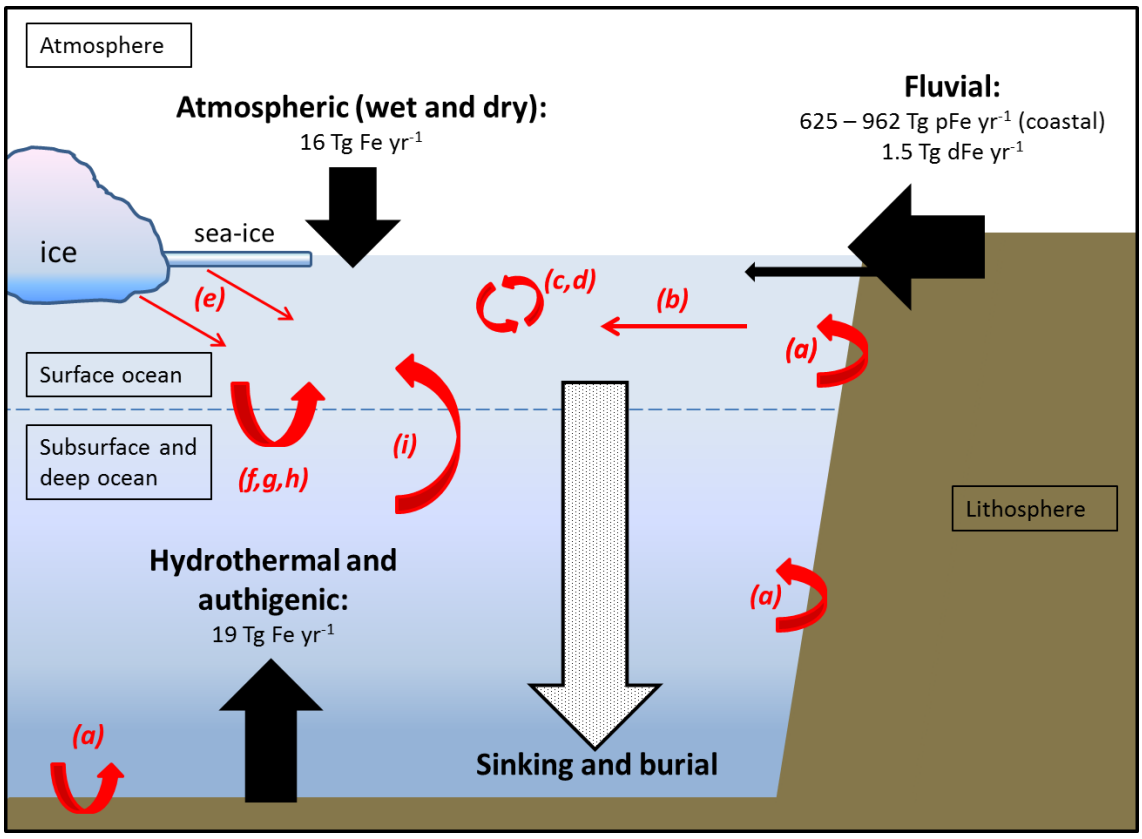

Figure 1.3: Schematic showing the main inputs (black arrows) and sink (shaded arrow) of iron in the ocean. Flux estimates are given for inputs in Tg Fe yr^{-1} (1 Tg = 1 x 10^{12} g) Red arrows summarise processes important in the redistribution of iron in the ocean: *(a)* remobilisation of Fe in margin and deep sea sediments, *(b)* lateral advection, *(c,d)* biological uptake and remineralisation, *(e)* transport and release by sea ice and icebergs, *(f – h)* supply to the surface ocean by upwelling, vertical diffusion and seasonal convective overturning, *(i)* transport by eddies. Flux estimates are from Jickells *et al.* (2005).

In summary, on a global scale the supply of iron to the euphotic zone of the open ocean largely takes place through wet and dry atmospheric deposition and through exchange with deeper water (through convective overturning, upwelling and entrainment). There is some uncertainty regarding the balance of these two sources globally (Archer and Johnson, 2000; Fung *et al.*, 2000), though on a regional scale the relative importance undoubtedly varies. Iron removal from the surface ocean ultimately takes place through gravitational settling (following active biological uptake and

incorporation into faecal pellets or detrital material), aggregation of small lithogenic particles with organic material, or scavenging of colloidal iron by detrital material (see Section 1.4.3).

1.4.2 The speciation of iron in seawater

In the open ocean, dFe is typically present at concentrations <0.5 nmol L^{-1} in surface waters and 0.3 – 1.4 nmol L^{-1} in the deep, though variations from this can result from the processes described above (de Baar and de Jong, 2001; Boyd and Ellwood, 2010). Particulate iron is often present in higher concentrations than dFe, though not all of it is bioavailable.

In oxygenated seawater, the redox speciation of dFe is dominated by the oxidised ferric form, Fe(III), which is mostly associated with organic complexes. The very low concentrations of dissolved inorganic Fe(III) (~0.07 pmol L^{-1}; Rue and Bruland, 1995) exist mainly as the inorganic hydrolysis complexes, $[Fe(OH)_n]^{(3-n)+}$ (where n = 1 – 3), with a tiny contribution from the free Fe^{3+} ion (Millero, 1998). Though the ferrous ion (Fe^{2+}) is considerably more soluble in seawater, dissolved Fe(II) is not thermodynamically stable in oxygenated seawater and, in the absence of organic matter, has a half-life of only 3 – 4 minutes, being continually oxidised back to Fe(III) by oxygen and hydrogen peroxide (Moffett, 2001; Rose and Waite, 2002). However, Fe(II) is also produced in the upper water column by photoreduction, with a clear relationship observed between UVB irradiance and Fe(II) concentrations during incubation experiments (Rijkenberg *et al.*, 2005).

The majority of dFe in seawater (>99 %) exists in complexes with one of two classes of organic ligands (Rue and Bruland, 1995; van den Berg, 1995; Wu and Luther, 1995). A bacterial/planktonic source is thought likely for these, due to the stability constants of some being very similar to those of siderophores, which are released in response to iron stress by numerous photosynthetic and heterotrophic bacteria (Barbeau *et al.*, 2001). It has also been demonstrated that organic, iron-binding compounds contain functional groups and exist within the size range consistent with biologically-produced siderophores (Macrellis *et al.*, 2001).

Particulate iron in the surface ocean is sometimes considered to be made up of lithogenic (mineral grains and dust particles from atmospheric deposition) and biogenic (incorporated into organic material) fractions (Frew *et al.*, 2006; Planquette *et al.*, 2009), the relative proportions of which vary regionally. A further fraction – detrital – may also be considered. In this case, iron incorporated into phytoplankton cells may be considered algal, while that included in faecal pellets or adsorbed onto organic

matter (and mineral grains) is termed detrital iron (Boyd *et al.*, 2010). Particulate iron concentrations range from ~0.1 nmol L^{-1} in the open ocean to hundreds of nanomoles per litre in coastal areas, with 50 – 90 % of pFe estimated to be refractory and the remaining fraction readily dissolved by a gentle leach or weak acid (de Baar and de Jong, 2001). A large proportion of the lithogenic fraction in particular may be refractory in nature; estimates of aerosol iron solubility range from 0.01 – 80 %, depending on aerosol source (Aguilar-Islas *et al.*, 2010), size (Baker and Jickells, 2006), atmospheric processing (Chen and Siefert, 2004) and the method used to assess solubility (Buck *et al.*, 2006).

1.4.3 Iron cycling in the upper ocean

Figure 1.4 summarises the biogeochemical cycling of Fe in surface waters. Active uptake of dFe by phytoplankton and bacteria plays an important role in controlling its concentration and distribution in the euphotic zone. This dissolved iron may be supplied by one of the external inputs described above, but as with other nutrients, recycled iron also plays an important role in meeting the iron demands of euphotic zone phytoplankton and bacteria (Hutchins *et al.*, 1993). Uptake occurs through binding of the metal ion to a ligand on the cell surface, followed by transfer across the cell membrane. Due to the high specific affinity of organic ligands for iron, this process is deemed to occur much faster for hydrated or inorganically complexed iron than for the organically complexed forms (Morel *et al.*, 1991). Reduction of organically-complexed iron species can, however, result in release of Fe(II), which can then be assimilated by phytoplankton. This reduction step can occur through the photolysis of Fe(III)-siderophore complexes, which simultaneously produces low affinity Fe(III) ligands (Barbeau *et al.*, 2001), or as a result of enzymatic activity, such as through the observed release of an iron-reductase enzyme by diatoms at times of iron deficiency (Maldonado and Price, 2000).

There is evidence for differing uptake strategies between prokaryotic and eukaryotic plankton, with the former able to utilise siderophore-bound iron much more readily, while the latter rely on Fe bound to porphyrin complexes, produced by zooplankton-mediated degradation and release of cellular material (Hutchins *et al.*, 1999). Furthermore, differing iron demands are exhibited between different taxa and in different conditions. Diazotrophy has been demonstrated to require Fe/C ratios 2.5 – 5 times higher than growth on ammonium (Kustka *et al.*, 2003), while cellular iron requirements also vary between neritic and oceanic species (Sunda and Huntsman, 1995). Luxury iron uptake has been observed in experiments with high dFe

concentrations, with the Fe/C ratio increasing by a factor of 20 – 30 between iron limited and iron replete conditions (Sunda and Huntsman, 1995; Price, 2005).

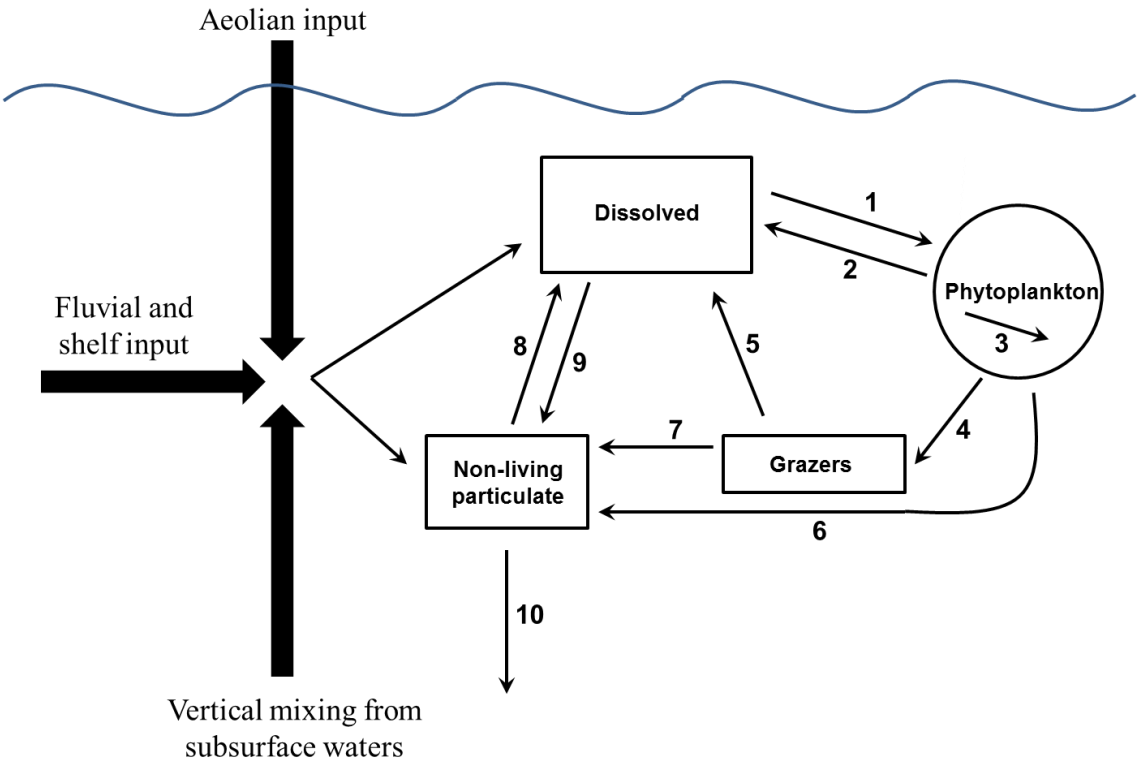

Figure 1.4: Summary of Fe biogeochemical cycling in the surface ocean. Thick arrows show inputs of new Fe. Numbered transfer paths are *(1)* passive adsorption and complexation of Fe to surface ligands of phytoplankton cells, *(2)* desorption from phytoplankton cell surfaces, *(3)* assimilation of cell surface-bound Fe, *(4)* transfer of Fe to zooplankton by grazing, *(5)* remineralisation through action of grazers, *(6)* phytoplankton death, producing detrital Fe, *(7)* zooplankton contribution to detrital Fe through faecal pellet production, death, cell break-up *etc.*, *(8)* solubilisation of minerals, desorption from and remineralisation of detrital Fe, and photoreduction of pFe, *(9)* scavenging of dFe through adsorption, precipitation and colloidal aggregation, *(10)* export of pFe from the surface ocean. Reproduced from Hutchins *et al.* (1993).

Following biological iron uptake, the resulting biogenic pFe is consumed by zooplankton, heterotrophic bacteria and viruses (Mioni *et al.*, 2005; Strzepek *et al.*, 2005; Sarthou *et al.*, 2008), which regenerate a proportion of the biogenic iron for further uptake within the euphotic zone. This cycling of iron has been dubbed the "ferrous wheel" (Kirchman, 1996). Its size and "spinning rate" (*i.e.*, the rate at which iron is acquired and regenerated) varies with depth and with region, depending on the community structure, and affects the ratio of new to recycled iron within the total iron supply (Boyd and Ellwood, 2010). The proportion of biogenic iron that is not regenerated through the turning of the ferrous wheel is the fraction that is lost from the upper ocean through export of biogenic material (*i.e.* the biological pump).

As well as active biological uptake, dFe may adsorb onto the surface of particles (scavenging). This can take place on all particle sizes, meaning that some dFe inevitably adsorbs onto sinking material and is lost from the euphotic zone before it is released back into the dissolved phase. During an iron enrichment experiment in the Southern Ocean it was estimated that 12 – 49 % of the observed decrease in dFe was due to colloidal iron hydrolysis species being scavenged onto large, sinking particles (Bowie *et al.*, 2001). Dissolved iron also adsorbs onto smaller particles that make up the suspended particulate pool and so remains available through reductive release of Fe(II) (see above). Aggregation and disaggregation of particles can therefore change the distribution of pFe between sinking material and SPM, while the latter process also releases colloidal and soluble iron back into the water column.

In the subsurface ocean, biological uptake of dFe is much diminished, and the partitioning of iron between dissolved and particulate pools is governed mainly by release of iron into the soluble and colloidal pools through remineralisation of sinking material (more so from labile organic material than from mineral particles), adsorption of dFe onto sinking or suspended particles, and aggregation of colloidal iron (Boyd and Ellwood, 2010). The latter processes represent a decoupling of iron from sinking organic material, as they result in remineralised iron returning to the particulate phase and sinking further in the water column, resulting in an increased Fe/C (or Fe/N, Fe/P) ratio with depth (Frew *et al.*, 2006; Lamborg *et al.*, 2008a). This can result in depleted dFe concentrations to greater depths, relative to macronutrients, thus affecting their stoichiometry in water supplied back to the upper ocean. This reduced supply of new iron, relative to new major nutrients, can result in iron limitation of primary production if there is not an additional supply to the euphotic zone of new bioavailable iron (*e.g.*, through atmospheric deposition) or sufficient recycled iron.

1.4.4 Iron limitation

The potential for limitation of oceanic primary production by iron availability was first proposed in the 1930s (Gran, 1931), though validation was hindered by the lack of suitably "trace-metal clean" equipment and methodology. As these methods developed, the link between low surface ocean dFe concentrations in areas of excess major nutrients such as the Southern Ocean, equatorial Pacific and north-east Pacific became apparent. Bottle incubation experiments, which showed increased growth rates of phytoplankton when dissolved iron was added, gave support to the hypothesis that iron limitation was responsible for incomplete nutrient drawdown in these HNLC areas (Martin and Fitzwater, 1988; Martin *et al.*, 1991).

Further laboratory experiments and mesoscale iron addition experiments have since confirmed the importance of Fe as a limiting nutrient in HNLC regions, which are typically remote from sources of atmospheric dust and consequently receive low aerosol iron inputs (*e.g.*, Coale *et al.*, 1996; Boyd *et al.*, 2000). Recent incubation experiments in the high latitude North Atlantic (another area of relatively low dust input) has found evidence of seasonal iron limitation (Nielsdóttir *et al.*, 2009), while the high iron demands of nitrogen-fixing cyanobacteria (Kustka *et al.*, 2003) demonstrate potential for iron limitation of diazotrophs in other oceanic regimes (Moore *et al.*, 2009). Model results suggest iron may be the limiting factor for phytoplankton growth in 30 – 40 % of the world ocean and also influence the phytoplankton community structure (Moore *et al.*, 2002; Moore *et al.*, 2004), thus highlighting its importance to primary production, nitrogen fixation and the marine carbon cycle.

1.5 Thesis objectives

The two principal motivations for this work were to gain new insights into processes that control the strength and efficiency of the biological carbon pump, in the hope of improving our ability to predict regional variations and future changes; and to improve our understanding of the role played by particulate material in the upper ocean biogeochemistry of iron, in terms of supply and removal of biologically available iron to and from the euphotic zone.

The work itself contributes to two specific research projects. The objective of the first was to compile a vertical carbon budget for the Porcupine Abyssal Plain (PAP) site, in the North Atlantic, with a particular focus on mechanisms leading to POC export from the upper ocean, and on the process of remineralisation in the mesopelagic. To this end, one of the objectives of this work was to measure and characterise the sinking particulate flux at the PAP site and to explain the behaviour of POC associated with it.

The second project had the objective of studying iron biogeochemistry in the high latitude North Atlantic to ascertain whether community productivity in parts of the region becomes iron limited following the spring bloom, and to establish what factors may lead to such a situation. As part of this, one goal of this work was to determine the concentration of pFe in the upper ocean in the region, and to estimate the distribution of this iron between refractory and biologically available fractions. A further aim was to determine the concentration of iron and nutrients in sedimenting material, in order to calculate their ratios and study how these change with depth.

The work described here also provided an opportunity to add to the total number of measurements of sinking particle flux made by neutrally-buoyant sediment traps (in this case, PELAGRA traps), with additional objectives being to directly compare POC and biomineral flux measurements made by the traps at separate North Atlantic locations, and to determine if the PELAGRA trap design is suitable for measurements of trace metals in sinking particles.

1.6 Thesis structure

Chapter 2 presents a description of the methods used in this work, including brief overviews of the two main sample collection methods (complemented by Appendices A and B), descriptions of the procedures used for POC(N), PIC and bSi determination and a description of the protocol used for quantifying trace metal concentrations in labile and refractory phases of particulate material. More details of the methods for particulate trace metal analysis are given in Appendix C.

In Chapter 3, the results of PELAGRA deployments in the North Atlantic are presented, with emphasis upon the observed trends in POC flux attenuation and upon the measurements of sinking particulate trace metals. Appendix D supplements this with information regarding trap deployments. Chapter 4 presents the results of measurements of POC, PON and trace metals in bulk particulate material collected by high volume *in situ* pumps deployed in the upper ocean of the high latitude North Atlantic. Deployment details for the pumps are tabulated in Appendix E.

In Chapter 5, the pFe data presented in the previous two chapters is used to begin putting together iron budgets for the high latitude North Atlantic, with a comparison made between “normal” conditions and a period of high inputs from nearby volcanic activity. The main findings of the work are summarised in Chapter 6, and this is followed by suggestions for future work.

Chapter 2: Sampling methods and analytical techniques

2.1 Overview

This chapter first gives an overview of the cleaning procedures that were used to prepare for the trace-metal work carried out during this research. Following this, a general description is presented of the two major methods of sample collection used, with context provided by a summary of the other techniques that have previously been used in similar work. More detailed accounts of sampling and sample processing protocols are given in Appendices A and B.

The analytical techniques used in this work for measurement of the major phases of particulate material are also described here, along with details on blanks and limits of detection for each. Finally, the same is done for the two-step leach/digest treatment and subsequent analysis used to examine trace metal content of the material collected, with a brief review of methods used by others. A more thorough description of this protocol is detailed in Appendix C.

2.2 Precautions for trace metal work

Due to the very low concentrations of iron and other trace metals that are observed in the oceans, great care needs to be taken when designing sampling and sample processing methodologies, in order to reduce the risk of contamination from external sources (atmospheric dust, emissions from ships' funnels, fibres from clothing, *etc.*). Considerations include the use of clean air laboratories and clean vans where possible for equipment preparation and sample processing, and laminar flow hoods for the more critical work. The use of appropriate clothing in these working environments (Tyvek coveralls, hairnets, shoe covers, gloves) is also very important to maintain the integrity of the working environment and samples. Similarly, the choice of materials and equipment used for sampling and for the processing of samples needs to be carefully considered in order to reduce the risk of samples being contaminated by metals leaching out of the materials used.

2.2.1 Cleaning of plastic ware

The selection of materials is typically combined with rigorous, time-consuming, but essential cleaning procedures to first remove any surface contaminants from the material and then to remove any impurities that may otherwise gradually leach from it into the sample it comes in contact with. The general cleaning procedures utilised for plastic ware to be used in oceanographic trace metal sampling are now well established, and the methods used in this work are based on those described by Achterberg *et al.* (2001).

Typically, Nalgene low density polyethylene (LDPE) or polypropylene (PP) bottles were used for trace metal sample splits or for samples before they were divided into subsamples. These bottles were rinsed with reverse osmosis (RO) water, and then soaked in a bath of Decon 90 detergent (2 % v/v) for at least 48 hours in order to remove any dust and residual organic material. They were then rinsed four times with RO water to remove any detergent, before being placed in a bath of 6 M hydrochloric acid (HCl; Fisher Scientific AR grade) and left to soak for 3 – 7 days. The bottles were then rinsed four times with RO water and placed in a bath of 6 M nitric acid (HNO_3; Fisher Scientific AR grade) for 3 – 7 days.

After removal from HNO_3, the bottles were capped and the outsides rinsed with Milli-Q (MQ) water (resistivity >18.2 MΩ.cm), then bagged up and transferred to a dedicated class 100 clean room laboratory. Here they were rinsed four times inside and out with MQ water, then partially filled with MQ water. For sample bottles (LDPE, 125 mL or 500 mL), this water was acidified to ~pH 2 with HCl (Romil, Ultra Purity (UpA) grade) for storage. All rinsed plastic ware was double-bagged in re-sealable plastic bags until needed.

Other miscellaneous LDPE laboratory equipment used for trace metal work (measuring cylinders, wash bottles) were cleaned following the procedure described above, then rinsed with MQ water in the clean laboratory after removal from the 6 M HNO_3 bath. Teflon plastic ware (filter rigs, Teflon sheet, digestion pots) was also cleaned in this way, but left to soak in the respective acid baths for longer.

Carboys (20 L, Nalgene LDPE) used for preparation and storage of brine were first rinsed with RO water, then filled with a 2 % (v/v) Decon 90 solution and left to soak for one week. They were then rinsed four times with RO water and filled with 10 % HCl and left to soak for another week, then rinsed four times with MQ water and bagged up with a small amount of MQ water inside.

2.2.2 Choice of reagents

Where reagents were added to or used in the treatment of samples, high-purity grades were used, to minimise any potential addition of trace metals. This involved either the purchase of certified high-purity chemicals (*e.g.*, Romil UpA grade) or the use of sub-boiling distilled acids, which had been purified using dedicated stills. Where high purity reagents were not directly available, efforts were made to treat lower-grade varieties in order to remove potential contaminants before use. These details are specified in the methods as required.

2.3 Sampling of sinking particulate material

As described in Section 1.3.2, sediment traps are the main tool for sampling sinking particulate material, but they have a number of methodological challenges associated with them. This is particularly true when sampling in the surface ocean and at mesopelagic depths, where horizontal currents can be large relative to sinking rates, where zooplankton are more abundant, and where a larger proportion of the sinking material is relatively labile (Buesseler *et al.*, 2007).

One of the platforms mentioned in Section 1.3.2 that has been developed to counter these issues is the free-drifting, neutrally buoyant sediment trap. The first designs for such a trap were produced in the mid-1990s (Asper, 1996, and reference within), but the first to be in frequent use – the NBST (Neutrally Buoyant Sediment Trap) – was developed at Woods Hole Oceanographic Institution in the late 1990s. The aim of the NBST design was to minimise the hydrodynamic flow interferences described in Section 1.3.2 by being able to drift freely with the ambient current (Valdes and Price, 2000). NBSTs have since been used alongside traditional tethered traps on numerous occasions (*e.g.*, Buesseler *et al.*, 2000; Stanley *et al.*, 2004; Buesseler *et al.*, 2008).

Other designs of such traps have since been developed. The PELAGRA (Particle Export measurement using a LAGRAngian trap) sediment trap has demonstrated reduced swimmer contamination compared to surface tethered traps (Saw *et al.*, 2004) and is now an established platform, though still evolving (Salter *et al.*, 2007; Lampitt *et al.*, 2008; Martin *et al.*, 2011). More recently the LST (Lagrangian Sediment Trap) has been used for sampling carbon export underneath icebergs in the Southern Ocean (Sherman *et al.*, 2011; Smith *et al.*, 2011).

2.3.1 The PELAGRA sediment trap

PELAGRA (Figure 2.1) is a free-drifting, neutrally-buoyant sediment trap capable of sampling down to depths of 1000 m. The trap design (Saw *et al.*, 2004; Lampitt *et al.*, 2008) is centred around a commercially available Autonomous Profiling Explorer (APEX) float (Webb Research Corporation), which includes conductivity, temperature and depth (CTD) sensors and an external oil-filled bladder used in active buoyancy control. Such floats are widely used for autonomous profiling operations as part of the international Argo programme.

Figure 2.1: A PELAGRA trap, complete with sample pots

The APEX float can operate in two modes: using an "isobaric" approach, the float is programmed to sink to a specific pressure surface, where it will remain within ±10

dbar of the target pressure, while for an "isopycnal" deployment strategy, a predetermined density surface is targeted and the float will remain within ±0.01 sigma-theta of that density throughout the sampling period. For this work, as with previous uses of PELAGRA, the latter strategy was used.

One adjustment was made to the APEX float in early 2009 in order to make the PELAGRA trap more suitable for collecting samples for trace-metal analysis. The sacrificial zinc anode, previously located at the top of the float, was relocated to the base, below the collection funnels.

In this work, multiple PELAGRA traps (between 2 and 5) were deployed at different depths between 50 m and 700 m, for periods of 2 to 6 days. Sample cups were filled with poisoned brine before deployment to limit microbial degradation of collected material and feeding by swimmers. Following recovery, samples were first filtered through a mesh to isolate swimmers and then split into sub-samples for the analyses listed below. Full details of trap design and operation, preparations for sampling, and initial treatment of samples are given in Appendix A.

2.3.2 Processing of sample splits

The main parameters measured on PELAGRA samples were mass, particulate organic carbon and nitrogen (POC, PON), particulate inorganic carbon (PIC), biogenic silica (bSi), trace metals, thorium-234 (^{234}Th), lead/polonium isotopes (^{210}Pb/^{210}Po) and taxonomy. Splits for ^{234}Th, ^{210}Pb/^{210}Po and taxonomy were analysed by other members of the research team and are not described here. Splits for the other parameters listed were filtered while at sea and the filters stored in petri dishes at –20 ˚C until analysis back in the laboratory. For each of these splits, full details of filter types, sample treatment and analytical procedures are given in Sections 2.5 and 2.6. Details of conversion of the amounts measured in individual splits to trap totals and to fluxes are given in Appendix A.

2.4 Bulk collection of marine particulate material

Sediment traps collect particulate material that is sinking down through the water column, but this only accounts for a fraction of the total particulate material present. Particles only sink when they are dense enough, relative to the surrounding water, to be negatively buoyant (De La Rocha and Passow, 2007), and the various physical and

biological processes that act upon particulate material – aggregation, heterotrophic feeding *etc.* – mean that their sizes change with time. As a result, particulate material moves between pools of sinking and suspended material, as well as changing in its chemical character by remineralisation, adsorption and precipitation. Sediment traps, as discussed, are useful tools for directly measuring the flux of material with depth and for studying changes in the properties of sinking material as it moves through the water column. But bulk collection of sinking and suspended particulate material can also contribute to estimating inventories of particle-associated elements at specific depths and therefore elucidating important biogeochemical processes in the water column.

Other than the use of towfish systems to pump near-surface water on-board for sampling (*e.g.*, Frew *et al.*, 2006; Berger *et al.*, 2008), there are two main methods that are commonly used for collection of particulate material without a direct discrimination between sinking and suspended particles:

- Go-Flo bottles, or similar, collect a discrete water sample (typically 5 – 30 L in volume), that is then brought back to the surface and filtered as the bottle is drained (Brewer *et al.*, 1976; Landing and Bruland, 1987; Twining *et al.*, 2010).
- Large-volume *in situ* pumps that filter 100s – 1000s of litres of seawater at depth. Several designs of pump are in use, including the Multiple Unit Large Volume *in-situ* Filtration System (MULVFS; Bishop and Edmond, 1976; Bishop *et al.*, 1985; Lam and Bishop, 2008), SAPS (Planquette *et al.*, 2009; see below), and the Rotating Automatic Pump for Particulate Inorganics Determination (RAPPID; Sherrell and Boyle, 1992).

Both methods have their own advantages and drawbacks. The use of bottles restricts the size of sample that can be collected and filtered, especially if other demands are also made on the water sample (*e.g.*, for analyses of dissolved constituents). This restricted sample size can be especially important when studying large particles, which comprise a small amount of the total particle pool but make a large contribution to the redistribution of material over depth (Bishop *et al.*, 1977). In addition, there have traditionally been concerns about sample bias by larger particles settling to the bottom of the bottle before filtration (Gardner, 1977), though recent work during the GEOTRACES inter-calibration cruises found no systematic bias in bottle-collected samples (Planquette and Sherrell, 2012). In the case of *in situ* pumps, the sampling cannot always be carried out at the same time as CTD measurements/collection of dissolved phase samples, and pump design means that the used filter will be exposed to other parts of the water column as the pump is recovered.

Collection of bulk particulate material (whether by bottle or pumps) also allows size fractionated studies of the material to be carried out in order to determine the

distribution of an element/substance over different particle size classes (Weinstein and Moran, 2004; Frew *et al.*, 2006; Lam *et al.*, 2011). The >53 (or >50) μm size fraction is one that is commonly sampled by *in situ* pumps because of studies suggesting that it is particles above this size that dominate the vertical transport of material (Bishop *et al.*, 1985). As a result, determination of the chemical composition of particles >53 μm, sampled by pumps, has been used to estimate downward fluxes of various chemical species (Weinstein and Moran, 2005; Planquette *et al.*, 2011).

In this study, *in situ* Stand Alone Pump Systems (SAPS; Challenger Oceanic) were deployed during the high latitude North Atlantic cruises (D350, D351, D354) in 2010 to collect samples for pFe analysis. SAPS units were used to filter large volumes of water (~150 L to >2000 L), typically through both 53 μm and 1 μm filters. The pumps were deployed at depths within the mixed layer (~20 m) and just below the mixed layer (~50 m), and also down to 150 m and occasionally 400 m.

Filters from SAPS were initially stored frozen (-20 ˚C) until back on land. Next, the material was rinsed off onto smaller polycarbonate filters for digestion and analysis. Sub-samples for POC/PON analysis were also taken. A full description of the pumps, along with preparation, deployment and sample processing procedures is detailed in Appendix B.

2.5 Analysis of the major fractions of particulate material

From PELAGRA samples, splits were used for determination of fluxes of the major components of sinking particles:

- particulate organic material (in the form of POC and PON measurements). Sub-samples from SAPS were also taken for this analysis.
- particulate inorganic carbon (PIC, quantified through calcium concentration).
- opal (measured as biogenic silica, bSi).

Mass flux was also determined gravimetrically from several splits. This section describes the protocols followed for each of these analyses.

2.5.1 Mass

All polycarbonate filters used for trace metal work during D341 and D354 were individually pre-weighed (after acid-washing and drying; see Section 2.6.2.1) using a

Sartorius ME-5 microbalance with a precision of ±1 µg. During D354, the 25 mm polycarbonate membranes used for PIC and bSi work were also pre-weighed on the same balance. Following sample collection and filtration, filters were again dried in a desiccator and then weighed multiple times to ensure a stable weight. Sample mass was calculated as the difference between measurements before and after filter use. Where two or more filters were used for a single split, mass was calculated as the sum of sample mass on the individual filters. Unused filters and those used as filter blanks (*e.g.*, see description of PIC filter blanks, Section 2.5.3) were also reweighed to check the consistency of mass measurements.

As only two splits dedicated to trace metal analysis were used for mass measurements during D341, the comparison between the two estimated flux values for each sample was susceptible to bias by inhomogeneity in the water/particle mixture during splitting. The mean value was calculated from each pair of duplicates, along with the percentage difference between them. The percentage difference between duplicates ranged from 2 % to 57 %, with an average value of 22 %.

For D354 samples, the number of replicate splits on which mass measurements were made varied depending on the number of splits used for PIC, bSi and trace metal analyses, with n = 3 – 7. In this case, the mean value was calculated for each sample, along with the standard deviation. The relative standard deviation (RSD) was generally <9 %, except for two samples (15 % and 16 %), and the mean RSD was 8 %. For process blanks taken during D354, which gave much lower mass measurements than samples, the RSD of replicates was understandably higher; when considering all replicates of all nine process blanks, the RSD was 75.6 %.

Combusted GF/F filters used for POC/PON analysis of SAPS sub-samples and of D354 PELAGRA splits were also pre-weighed, then reweighed after samples were dried. The PELAGRA POC/PON split sample weights did not agree well with those measured on PIC, bSi and trace metal splits, presumably due to sea salt retention by the GF/F filters, which had not been rinsed after sample filtration (Stavn *et al.*, 2009). However the SAPS samples were rinsed with several hundred millilitres of pH-adjusted MQ water (salinity measured in the rinse was negligible), so sea salt retention should not have been such an issue.

2.5.2 Particulate organic carbon and nitrogen

PELAGRA splits for POC and PON analysis were filtered under vacuum while at sea through one or more pre-combusted (450 °C for 12 hours), pre-weighed 25 mm glass fibre filters (Whatman GF/F, 0.7 µm nominal pore size) and stored frozen (-20 °C) in

Petri dishes. Back on land, filters from both PELAGRA and SAPS samples (see Appendix B for SAPS POC(N) sub-sampling details) were prepared following a method adapted from Poulton *et al.* (2006). They were first dried at 60 °C for 48 hours and then reweighed. Next, they were fumed using ~100 mL concentrated sulphurous acid (Fisher Scientific; technical grade) in an evacuated desiccator for 48 hours, in order to degrade any inorganic carbon present (Verardo *et al.*, 1990), then again dried at 60 °C for 24 hours.

Each filter was then pelleted inside a square of pre-combusted (450 °C, 12 hours) aluminium foil, using a method derived from Hilton *et al.* (1986). Filters with high particle loading were cut into halves or thirds, which were pelleted individually. The samples were analysed using a Thermo Finnigan Flash EA1112 elemental analyser based at Plymouth Marine Laboratory. Analytical precision of the instrument is <0.1 %.

Filter blanks were prepared in the same way as samples, using unused but pre-combusted GF/F filters. Table 2.1 lists the mean and standard deviation values for POC and PON on filter blanks carried out for D341 PELAGRA samples, D354 PELAGRA samples, and SAPS samples. Also shown are the calculated detection limits for blank-corrected samples, based on three times the standard deviation of the filter blanks.

Table 2.1: Filter blank means and standard deviations, and the resulting limit of detection values for filter blank-corrected POC and PON. All values are in µg.

	POC filter blank ***($\bar{x}$ ± 1σ)***	***POC limit of detection*** ***(3σ)***	***PON filter blank*** ***($\bar{x}$ ± 1σ)***	***PON limit of detection*** ***(3σ)***
D341 PELAGRA (*n*=10)	15.0 ± 6.9	20.8	1.54 ± 0.34	1.02
D354 PELAGRA (*n*=7)	18.4 ± 1.1	3.1	0.39 ± 0.06	0.17
SAPS (*n*=11)	17.4 ± 7.9	23.7	0.76 ± 0.34	1.03

All POC and PON measurements for PELAGRA process blanks and samples and SAPS samples were above the detection limit. Brine blank replicates, carried out during D354 by filtering 100 mL of unused poisoned brine through GF/F filters (POC = 9.2 ± 1.1 µg, PON = 1.2 ± 0.2 µg; n = 3), were also above the relevant detection limit, but were lower than process blanks and samples.

Although the nature of the sampling meant that replicate samples were typically not taken, four separate PELAGRA samples collected during D354 had triplicate splits taken, for which the RSDs of calculated POC fluxes were <5 % (mean RSD = 4.1 %) and those for PON fluxes were mostly <10 % (mean RSD = 8.3 %). These mean RSD values

were subsequently applied as an analytical uncertainty to all PELAGRA POC and PON samples for which replicates were not measured. In addition, duplicate splits were analysed from all process blanks during D354 and used to calculate a mean process blank value. Due to the lower concentrations measured in these process blanks, the RSD of the POC and PON analyses were slightly higher, calculated at 33.9 % and 33.2 % respectively (n = 18).

2.5.3 Particulate inorganic carbon

The PIC splits of PELAGRA samples were filtered under vacuum at sea. Each split was filtered through one or more pre-weighed 25 mm polycarbonate membranes (Whatman Nuclepore; 0.8 µm pore size), which were then rinsed with a small amount of pH-adjusted (pH 9, using ammonium hydroxide) MQ water to remove any sea-salt. Used filters were stored frozen (-20 °C) in individual Petri dishes. In the laboratory, filters were dried at 60 °C for 24 hours and then stored in a desiccator until reweighed (D354 only). Each filter was then transferred to a centrifuge tube, to which 20 mL 0.4 M HNO_3 was added gravimetrically in order to dissolve biogenic calcium carbonate ($CaCO_3$). After two days of exposure to this weak acid digest, the sample solutions were transferred by syringe to pre-cleaned sample tubes. Each solution was filtered through a Whatman 25 mm diameter 0.45 µm PTFE syringe filter during this step to ensure no particles passed into the sample tube.

The samples were analysed for Ca concentration by inductively coupled plasma optical emission spectrometry (Perkin Elmer Optima 4300 DV ICP-OES), which was set up to measure Ca at three different wavelengths and also sodium (Na), so that corrections could be made for any remaining sea salt (this turned out to be negligible). Limits of detection for the instrument, calculated as three times the standard deviation of ten replicate blank (0.4 M HNO_3) determinations were 2.1 ng g^{-1} for Na and 4.0 ng g^{-1} for Ca. Instrument precision for Ca at each of the three wavelengths has previously been measured as <1 % (Green *et al.*, 2003).

Samples were run alongside standards, prepared gravimetrically using certified element reference solutions (Romil PrimAg-xtra). Ca concentrations (µg g^{-1}) measured at the three wavelengths were in good agreement throughout (RSD <5 %). Following drift corrections, an average value was calculated from the three. Sample values were then corrected for filter blanks, which had been loaded onto the filter rig and rinsed with pH-adjusted MQ water, then treated in the same way as samples. Filter blank details are shown in Table 2.2. All samples were above the limit of detection calculated from filter blank analyses, except for brine blanks carried out during D354, which had

had 100 mL of poisoned brine filtered through them and were not significantly different to the filter blanks.

Table 2.2: Filter blank means and standard deviations, and the resulting limit of detection values of filter blank-corrected Ca analyses for D341 and D354 PELAGRA samples (all values are in µg).

	Filter blank ***($\bar{x}$ ± 1σ)***	***Method limit of detection*** ***(3σ)***
D341 (*n*=5)	0.23 ± 0.05	0.15
D354 (*n*=7)	0.53 ± 0.36	1.07

Sample Ca measurements were used to calculate a flux of biogenic Ca (µg m^{-2} d^{-1}), which was then used to calculate $CaCO_3$ and PIC fluxes using Equations 2.1 and 2.2 below:

$$CaCO_3 \text{ flux } (\mu g\ m^{-2}\ d^{-1}) = (Ca \text{ flux} / 40.08) \times 100.09 \quad \text{(Eqtn. 2.1)}$$

$$PIC \text{ flux } (\mu g\ m^{-2}\ d^{-1}) = (Ca \text{ flux} / 40.08) \times 12.01 \quad \text{(Eqtn. 2.2)}$$

where 40.08 = atomic mass of Ca, 100.09 = molecular mass of $CaCO_3$ and 12.01 = atomic mass of carbon.

As with other analyses, it was generally not possible to carry out PIC analyses on replicate splits. Of the two samples during D354 for which triplicate splits were set aside for PIC analysis, one gave a precision of 2 % (IB3 P4), but the other gave a precision of 25 % (IB1 P6). With two such different estimates of precision as this it seems imprudent to take a mean value of the two to apply to other samples. It also seems unlikely that the traps would be routinely as precise as IB3 P4 in terms of PIC collection: the nature of PIC in sinking material is as fragments of planktonic shells and tests and so it would be expected that these will be more heterogeneous in their distribution in particles than organic matter. For this reason, the higher RSD of 25 % has been applied to all remaining samples, though it is recognised that this may represent an unusually high degree of uncertainty. For the process blanks, which had much lower PIC concentrations, the precision when considering all process blank splits was 57 % (*n* = 16).

2.5.4 Biogenic silica

PELAGRA splits designated for bSi analysis were also filtered at sea. As with PIC splits, pre-weighed 25 mm polycarbonate membranes (Whatman Nuclepore; 0.8 µm pore size) were used and samples were filtered under vacuum. Where necessary, more than one filter was used. Filter blanks were loaded onto filter rigs, but had nothing filtered through them. Brine blanks (D354 only) had 100 mL of poisoned brine filtered through them. Samples and blanks were stored frozen (-20 ˚C) until analysis back in the laboratory.

Filters were first dried (60 ˚C, 24 hours) and reweighed (D354 only), then processed and analysed using a method adapted from Brown *et al.* (2003) and from Ragueneau and Treguer (1994). Each filter was transferred to a centrifuge tube and heated (80 ˚C) with 2.5 mL of 0.2 M sodium hydroxide (NaOH) for 90 minutes to dissolve biogenic silica, then cooled and neutralised with 0.1 M HCl solution. Samples were then centrifuged, before transferring the solution to sample vials for analysis. For filters with high loading of particulate material, a factor of ten dilution was carried out using MQ water.

Dissolved silicate (orthosilicic acid) was measured on a SEAL QuAATro Segmented Flow Analysis autoanalyser, which measures the intensity of the blue-coloured solution formed by the reaction of orthosilicic acid with molybdate and the subsequent reduction of the resulting silicomolybdate compound by a metol and oxalic acid solution. Detection limit of the instrument is 0.3 µg L^{-1}. Table 2.3 shows the results of filter blanks run following D341 and D354, and the methodological detection limits derived from these in each case. Brine blanks during D354 were typically slightly above the detection limit but much lower than samples.

Table 2.3: Filter blank means and standard deviations, and the resulting limit of detection values of filter blank-corrected bSi analyses for D341 and D354 PELAGRA samples (all values are in µg).

	Filter blank ***($\bar{x}$ ± 1σ)***	***Limit of detection*** ***(3σ)***
D341 (*n*=3)	3.62 ± 0.62	1.87
D354 (*n*=7)	5.11 ± 0.03	0.11

For some samples suspected of having high bSi content, the filter was put through another digestion/neutralisation cycle. In these cases, the recovery efficiency of the first extraction was calculated to be 91.9 ± 3.0 %, which is in good agreement to that calculated by Salter (2007) using a very similar analytical method (89.4 ± 4.0 %).

The data obtained from the autoanalyser (dissolved silicate; μmol L^{-1}) was first converted into a mass of silicon mobilised from the sample, and then into an elemental silicon flux. This was then converted into silica (SiO_2) flux by multiplying by 2.14 (see Equation 2.3). Based on the assumption that no lithogenic silica was mobilised by the sample treatment, this value is considered to be biogenic silica. The flux of opal (Equation 2.4) was calculated using the assumption that diatomaceous opal has a relatively constant water content of ~10 % and therefore has the chemical formula $SiO_2.0.4H_2O$; (Mortlock and Froelich, 1989).

$$bSi\ flux\ (\mu g\ m^{-2}\ d^{-1}) = Si\ flux \times 60.08 / 28.09 \quad \text{(Eqtn. 2.3)}$$

$$opal\ flux\ (\mu g\ m^{-2}\ d^{-1}) = Si\ flux \times 67.29 / 28.09 \quad \text{(Eqtn. 2.4)}$$

where 28.09 = atomic mass of Si, 60.08 = molecular mass of SiO_2 and 67.29 = molecular mass of $SiO_2.0.4H_2O$.

Only one sample during D354 had triplicate splits analysed for bSi (IB1 P6), and this demonstrated good agreement between the three (RSD = 2.7 %). Duplicate splits were analysed on a further sample and these also agreed well (IB2 P6; percentage difference = 3.5 %). However, given the higher RSD values observed for other fractions of the material collected, and RSD values for previous bSi measurements in PELAGRA samples (RSD <10 % in Salter *et al.* (2007); percentage difference between duplicates mostly <10 % in Martin *et al.* (2011)), it seems rather optimistic to apply this low value to all of the samples. Therefore, an uncertainty of what is considered to be a conservative value of 10 % of the bSi measurement is applied for all other samples from D354 and D341. For the lower bSi concentrations measured in the process blanks, the calculated precision was 44.0 % (n = 18).

2.6 Analysis of trace metals in particulate material

2.6.1 Overview of methods used in previous studies

One of the challenges of understanding the biogeochemical cycling of elements is in identifying the biological availability of that element in the different chemical forms in which it naturally occurs, and in quantifying the amount of the element in each form.

In the case of iron associated with oceanic particulate material, contributions to the total inventory are from phytoplankton, non-living biological (detrital) matter and lithogenic material (Hutchins *et al.*, 1993; Morel and Price, 2003). The latter of these has itself contributions from numerous different minerals and chemical forms of iron, such as aluminosilicates, carbonates and crystalline and amorphous oxyhydroxides (Landing and Bruland, 1987; Moffett, 2001). In addition, iron may be incorporated into the interior of particulate material, whether as organic matter or as part of a crystal matrix, or scavenged onto adsorption sites on the particle surface from the surrounding water (Bowie *et al.*, 2001; Tovar-Sanchez *et al.*, 2003). The same is true of other biologically important trace metals.

This complexity in the pFe inventory makes it very difficult to define biological availability of Fe in such a way that it can be easily measured by an established technique (Wells *et al.*, 1995). Measurements of total pFe will overestimate the bioavailable portion of the metal, while multi-step sequential extractions, though useful in shedding light on geochemical partitioning, are time-consuming and yet do not necessarily reveal the extent of biologically available iron (Berger *et al.*, 2008). Instead, previous work has typically focused on a two-step analysis, with an initial extraction step to isolate an operationally defined "labile" fraction, followed by a total digest of the remaining material to quantify the "refractory" fraction.

Within this category of analysis, one of the more common techniques used for characterising the labile fraction of trace metals in marine particulate material is some variation on the 25 % acetic acid (HAc) leach described by Chester and Hughes (1967). Typically, this involves a 2 hour leach of the material at room temperature using a 25 % v/v solution of HAc at pH 2 (Landing and Bruland, 1987; Fitzwater *et al.*, 2003; Hurst and Bruland, 2007; Planquette *et al.*, 2009), which extracts Fe weakly adsorbed to surfaces, bound by organic matter and associated with carbonate minerals and amorphous oxyhydroxides (Wells *et al.*, 2000).

Recently, Berger *et al.* (2008) argued that the room temperature leach with HAc alone is not sufficient to release a portion of the more tightly-bound trace metals associated with phytoplankton. Their work suggested that a more appropriate leach for releasing all of the labile metal, particularly for samples from coastal zones, was to include a reducing agent (hydroxylamine hydrochloride) and a heating step in the traditional 25 % HAc approach.

Another method, in which samples are washed with oxalate, aims to discriminate between Fe scavenged onto particle surfaces ("extracellular") and "intracellular" Fe, which is incorporated into interior particle matrices (Tovar-Sanchez *et al.*, 2003). However, it should be considered when applying the method to natural samples that

the "intracellular" fraction may contain not only Fe in phytoplankton cells, but also that within lithogenic particles (Frew *et al.*, 2006).

The digest procedure used to determine the "refractory" phase of particulate iron, or simply the total pFe content, also varies between studies. Many use a mixture of concentrated HNO_3 and HF, though the relative amounts vary (*e.g.*, Sherrell and Boyle, 1992; Weinstein and Moran, 2004; Frew *et al.*, 2006; Lamborg *et al.*, 2008a). In other studies, HCl is also used in the digestion mixture (Landing and Bruland, 1987; Planquette *et al.*, 2009; Prego *et al.*, 2009), while some methods include perchloric acid to break down refractory organic material (Kuss and Kremling, 1999b). Similarly, digestion takes place either by heating the sample and acid mixture on a hotplate (Cullen *et al.*, 2001; Pohl *et al.*, 2004), in a water bath (Wells *et al.*, 2000), or with the use of a microwave (Stanley *et al.*, 2004; Berger *et al.*, 2008).

Several published methods describe difficulties in getting the filter (usually polycarbonate) to fully digest. In some cases, this is tackled by the addition of extra steps to aid complete digestion of the filter, such as the addition of ammonium hydroxide (Lamborg *et al.*, 2008a). In others, the partially-digested filter is simply removed (Cullen *et al.*, 2001; Weinstein and Moran, 2004), though this introduces the risk of losing some of the digest solution when the filter is taken out.

Digested (and leached) samples are typically analysed for multiple elements using an inductively-coupled mass spectrometer (ICP-MS; *e.g.*, Lamborg *et al.* (2008a), Planquette *et al.* (2009)) although older studies typically used atomic adsorption spectrometry methods (Sherrell and Boyle, 1992).

2.6.2 Protocol for leach and digest of particulate material

It was decided to employ a two-step procedure during this work, based on that used by Planquette *et al.* (2009), but with changes made to the digest procedure, including the acid mixture used and with an added step of spreading the filter on the wall of the vial. This results in the refluxing acid mixture digesting the particulate material as it runs down over the filter, while making the filter easier to remove without loss of digest solution from the vial. The method therefore consists of an initial leach of the material by 25 % HAc at room temperature, followed by a total digestion using a mixture of concentrated nitric and hydrofluoric acids.

2.6.2.1 Preparations and sample filtration

All filters used for trace metal measurements were 47 mm polycarbonate track-etched membranes (Whatman Nuclepore). Those used for PELAGRA samples during D354 had a 1.0 µm pore size. Unfortunately these were not available during D341, so the samples during that cruise were filtered through membranes with 0.4 µm pore size. All SAPS samples were filtered through 0.4 µm membranes when processed. Filters were cleaned before use by being soaked in a 1 L LDPE bottle filled with 10 % HCl solution for 2 – 3 weeks, rinsed thoroughly with MQ water, then air-dried under a class 100 laminar air hood. After further drying in a silica gel desiccator, the filters were weighed as described in Section 2.5.1 and stored until use in individual acid-washed Petri dishes. Some filters were kept to be used as filter blanks.

PELAGRA trace metal splits were filtered at sea and the filters stored frozen (-20 ˚C) until they could be processed on land. Original SAPS samples were rinsed off onto the smaller filters in the laboratory as described in Appendix B. Samples (and blank filters) were dried and weighed before further processing, using the same approach as described in Section 2.5.1.

2.6.2.2 Leach procedure

Using acid-cleaned plastic tweezers, filters were folded, particle side inward, and placed in the bottom of clean PFA Teflon 30 mL vials (Savillex), to each of which 4 mL of 25 % v/v acetic acid (Romil, SpA grade, prepared with MQ water) was added – enough to completely cover the filter. Samples were left in the leach solution for 2 hours at room temperature, and then centrifuged (15 minutes at 3000 rpm).

The leachates were transferred by auto-pipette to clean Teflon 15 mL vials, then each acidified with 100 µL concentrated HNO_3 (sub-boiling distilled) before being taken to dryness on a hotplate (100 ˚C). Residues were each redissolved in 2 mL of 2 % v/v HNO_3 (sub-boiling distilled, prepared with MQ water) and transferred to pre-weighed, acid-washed 30 mL LDPE bottles. Initial sample dilution with further 2 % HNO_3 was carried out to give volumes of approximately 12 mL, and the bottles then reweighed to determine the precise mass of acid used.

2.6.2.3 Total digest procedure

Following the transfer of the leachate to a fresh pot, the leached samples were heated with a concentrated acid mixture to release trace elements from the remaining material. First, each filter was unfolded and spread onto the interior wall of the 30 mL Teflon vial, particle-side exposed. Next, a mixture of 2.5 mL concentrated HNO_3 (sub-boiling distilled) and 0.5 mL concentrated hydrofluoric acid (HF; Romil Super Purity (SpA) grade, 47-51 %) was added to each.

Vials were sealed and heated at 130 °C for 4 hours, then uncapped and taken to dryness. A second digest step was then carried out using concentrated HNO_3 only (1.5 mL; 2 hours at 130 °C), and the solutions again dried down. The polycarbonate membranes were removed as vials approached dryness. If any particulate material remained on the membrane at this point, the digest procedure was repeated.

Sample residues were redissolved in 5 mL of 2 % v/v HNO_3 and transferred to pre-weighed, acid-washed 30 mL LDPE bottles. Initial sample dilution with further 2 % HNO_3 was carried out to give volumes of 15 – 20 mL, and the bottles then reweighed.

2.6.3 Analysis by ICP-MS

The solutions resulting from the leach and digest of SAPS and PELAGRA trace metal splits were analysed by high resolution inductively coupled plasma mass spectrometry (Thermo Fisher Scientific Element 2 XR HR-ICP-MS; Bremen, Germany). Elements measured were Li, Al, P, Ti, V, Cr, Mn, Fe, Co, Ni, Cu, Zn, Ga, As, Rb, Sr, Cd, Sn, Cs, Ba, Pb, Th and U, though here the focus will be on Fe and Al. Full details of the instrument set-up and data processing are given in Appendix C.

Samples were run along with a series of multi-element standards prepared gravimetrically from certified single-element reference solutions (Romil PrimAg-xtra and Inorganic Ventures), with 2 % HNO_3 as the diluent. Many samples were further diluted with more 2 % HNO_3 before analysis in order to bring expected concentrations into the range covered by the standards.

2.6.3.1 Reagent and filter blanks for Fe and Al

Instrument detection limits for Fe and Al (based on three times the standard deviation of ten replicate acid blanks) were run-dependent, but typical values were 0.13 ng g^{-1} for Al and 0.014 ng g^{-1} for Fe. Filter blanks for 47 mm polycarbonate membranes were put through the same leach and digest procedure as described for the samples. The values obtained for Fe and Al in reagent blanks and for filter blanks carried out during SAPS and PELAGRA studies are summarised in Tables 2.4 (leach fraction) and 2.5 (total digest fraction), along with the methodological detection limits calculated from the filter blanks (in ng). Full details of reagent/filter blanks for all elements analysed are given in Appendix C.

Table 2.4: Mean (±1σ) reagent blank and filter blank values for Fe and Al from ICP-MS analyses of leach samples, along with corresponding method limit of detection values (3σ). All values are in ng.

	25 % HAc leach Fe *($\bar{x}$ ± 1σ)*	*Fe limit of detection (3σ)*	*25 % HAc leach Al* *($\bar{x}$ ± 1σ)*	*Al limit of detection (3σ)*
Reagent blank (n = 17)	1.4 ± 0.9	**2.7**	6.6 ± 4.2	**12.6**
SAPS (n = 11)	2.7 ± 1.7	**5.2**	8.5 ± 3.4	**10.2**
D341 PELAGRA (n = 7)	2.6 ± 0.9	**2.6**	33.3 ± 12.9	**38.6**
D354 PELAGRA (n = 7)	1.4 ± 0.3	**0.8**	20.4 ± 6.7	**20.2**

2.6.3.2 Sample precision

During D341, duplicate splits were taken for trace metal analysis from all PELAGRA samples. As duplicate samples do not allow for calculations of precision, the percentage difference between the two values is instead considered. Leachable Fe and Al measurements from duplicates were susceptible to variations in the water/particle mixture between splits, but generally agreed fairly well (within a factor of two). The

same was true for the digests. During D354, most samples only had one split designated for trace metal analysis, though triplicate splits were analysed for two separate samples, while another had duplicate splits processed. For the triplicate measurements, Fe leach replicates had a precision of 36 % for one and 40 % for the other, while Al leach replicates had precisions of 18 % and 11 %. Replicate digest values for Fe had RSD values of 16 % and 19 % and those for Al were 9 % and 36 %. For the remaining samples, it was decided to apply the higher of these values in each case.

Process blanks from each trap deployment during D354 showed precision of 44 % for Fe and 187 % for Al in the leach fraction (*n = 18*), though the latter were typically below the detection limit, as defined by the filter blanks. For the digest fraction, process blank replicates had an RSD of 46 % for Fe and 107 % for Al (*n = 18*), with the latter values again lower than the detection limit determined by filter blank analysis.

Table 2.5: Mean (± 1σ) reagent blank and filter blank values for Fe and Al from ICP-MS analyses of digest samples, along with corresponding method limit of detection values (3σ). All values are in ng.

	Acid digest Fe *($\bar{x}$ ± 1σ)*	*Fe limit of detection (3σ)*	*Acid digest Al* *($\bar{x}$ ± 1σ)*	*Al limit of detection (3σ)*
Reagent blank (n = 17)	3 ± 1	**3**	7 ± 4	**12**
SAPS (n = 11)	18 ± 5	**14**	28 ± 16	**49**
D341 PELAGRA (n = 7)	18 ± 10	**30**	72 ± 49	**148**
D354 PELAGRA (n = 7)	14 ± 3	**7**	75 ± 36	**108**

2.6.3.3 Digest method verification

To ensure that the digest method used was successful in releasing all of the trace elements of interest from samples, a selection of certified reference materials (CRMs) were treated using the same protocol. With each batch of samples, one or two of the following CRMs (listed with the organisation from which they were obtained) were treated using the same digest procedure:

- HISS-1: marine sediment; NRC-CNRC, Canada

- NIST 1573a: tomato leaves; NIST, USA
- TORT-2: lobster hepatopancreas; NRC-CNRC, Canada
- NIST 1648a: urban particulate matter; NIST, USA

These materials cover a range of organic, lithogenic and anthropogenic source materials and so should be useful in indicating the success of the digest method in treating the samples collected. For each CRM digestion, 50 – 250 mg of material was transferred to a digestion pot and then treated in the same way as the samples, though when >100 mg of material was used, the amount of each acid used was doubled.

The recovery values for iron and aluminium are shown in Table 2.6. Mean Fe recovery was typically >95 % for the reference materials, with the exception of NIST1648a (mean recovery of 89 %). Mean Al recovery from NIST1648a was also 89 %, and 87 % from HISS-1, but 97 % from NIST1573a. Unfortunately, no certified value for Al in TORT-2 is available.

Table 2.6: Certified concentrations (in bold red) of Fe and Al in reference materials, compared to results obtained using the described digest protocol. All concentrations are in ppm. Also shown (in brackets) is the number of replicates analysed in each case. Values in italics represent mean percentage recovery.

	HISS-1	*NIST1573a*	*TORT-2*	*NIST1648a*
Fe	**2460 ± 90**	**368 ± 7**	**105 ± 12**	**39200 ± 2100**
	2361 ± 85 (*n* = 7)	353 ± 8 (*n* = 7)	104 ± 23 (*n* = 10)	34715 ± 1043 (*n* = 9)
	96 %	*96 %*	*99 %*	*89 %*
Al	**7300 ± 500**	**598 ± 12**	-	**34300 ± 1300**
	6384 ± 136 (*n* = 7)	582 ± 13 (*n* = 7)	34 ± 10 (*n* = 10)	30515 ± 956 (*n* = 9)
	87 %	*97 %*	-	*89 %*

Chapter 3: Mesopelagic particle flux in the North Atlantic Ocean

3.1 Overview

This chapter presents the results of measurements of sinking particulate material made using PELAGRA sediment traps during two research cruises in the North Atlantic Ocean. Although the two cruises were for unrelated projects, it was hoped that the two different locations would allow an extension of the comparative studies of particulate carbon flux in the mesopelagic that were carried out during the VERTIGO programme, which are described in Section 3.2. Additionally, one of the aims of the first cruise was to determine the suitability of the PELAGRA trap for sinking particulate trace metal collection, while the determination of iron in sinking particles was a key aim of the second cruise.

3.2 Introduction

The mesopelagic is loosely defined as the depth interval of the ocean that lies 100 – 1000 m from the surface. More specifically, it can be considered the region extending down from the base of the euphotic zone, defined as the depth of either 1 % or 0.1 % light penetration (Jerlov, 1968; Buesseler and Boyd, 2009), to some depth (usually 1000 m) regarded as being beyond the depth of convective winter mixing. The low light levels and gradual decrease with depth of the remaining sunlight through this region has resulted in its alternative name of the "twilight zone". Alternatively, the mesopelagic has been described as lying below the pycnocline but above the lower limit of zooplankton/micronekton habitat, which can extend to between 1.5 – 2 km (Honjo *et al.*, 2008).

The twilight zone is characterised by significant biogeochemical changes with depth. The majority of the biogenic particulate material exported from the euphotic zone is returned to the dissolved pool before a remaining fraction manages to sink below the mesopelagic and into the bathypelagic ocean: it is estimated that 6 – 25 % of exported POC sinks below 1000 m, with the rest being remineralised within the mesopelagic (Boyd and Trull, 2007). The small fraction of organic material that sinks through the

mesopelagic and into the deep ocean is considered to be isolated from the surface for timescales of hundreds of years. This sequestered carbon is therefore not as likely to be exchanged back to the atmosphere, whereas any carbon that is remineralised at shallower depths can potentially be mixed back up to the surface on a seasonal time-scale and impact on the atmospheric carbon cycle.

Our current understanding of the various processes that control the remineralisation of POC within the twilight zone is hampered by the logistical problems associated with studying biogeochemical and ecological interactions in such an environment (Burd *et al.*, 2010). Direct sampling of sinking particulate material is usually carried out using traditional sediment traps, either moored or tethered to a surface float (*e.g.*, Martin *et al.*, 1987; Pohl *et al.*, 2004; Frew *et al.*, 2006). However, traps deployed in such a way at mesopelagic depths are considered to be particularly susceptible to the well-documented methodological problems associated with sediment traps in general (*i.e.*, hydrodynamic issues, swimmers and solubilisation of the collected material (Honjo, 1996; Gardner, 2000; Buesseler *et al.*, 2007)).

3.2.1 The "Martin" curve

A previous study of particle transport, VERTEX (VERtical Transport and EXchange), measured particle flux at depths of 100 – 2000 m at several sites in the northeast Pacific using traditional MULTITRAPS – a design of sediment trap deployed in series and attached to a surface float (Martin *et al.*, 1987). Data from this work led to the generation of the "Martin" curve (Equation 3.1), a power function relating particle flux at depth to a measured flux at some reference depth and a coefficient of attenuation:

$$F_z = F_{z_0}(z/z_0)^{-b} \qquad \text{(Eqtn. 3.1)}$$

where F_z is the flux at depth z, F_{z_0} is the flux at the reference depth, z_0, and b is the coefficient of attenuation.

Based on an "open ocean composite" data-set which included measurements of POC flux from six of the northeast Pacific stations occupied during VERTEX, the attenuation coefficient calculated by Martin *et al.* had a value of 0.858 (Figure 3.1). This value has since been used extensively in ocean biogeochemical models (*e.g.*, Sarmiento and Le Quéré, 1996; references in Doney *et al.*, 2004) and to normalise measured flux values to a particular depth so that direct comparisons can be made between traps deployed at different depths (Salter *et al.*, 2007) or from different regions (*e.g.*, Lampitt and Antia, 1997; Fischer *et al.*, 2000). More recent compilations of data sets have suggested a global range in the value of b of ~0.6 – 2.0 (Berelson, 2001; Francois *et*

al., 2002), though these are based on deep-sea trap measurements which do not include representation of the region of greatest change in POC flux (*i.e.*, the mesopelagic). Even the original sites from which the Martin curve was derived showed variations in *b* from 0.65 – 0.97 (Martin *et al.*, 1987), suggesting that there may be larger variations in the remineralisation rate of sinking particles in different oceanic regimes.

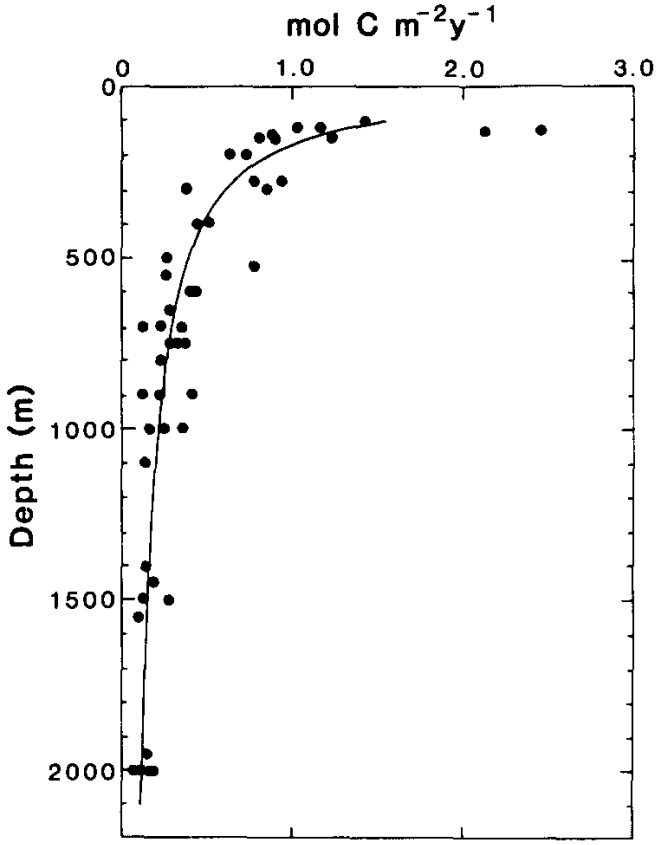

Figure 3.1: Open ocean composite of POC fluxes measured during the VERTEX programme, overlaid with the best-fit "Martin curve", $F = 1.53(z/100)^{-0.868}$. Reproduced from Martin *et al.* (1987).

The variation in remineralisation length scale of POC (*i.e.*, the depth over which a certain degree of flux attenuation takes place) has been demonstrated to have significant implications by Kwon *et al.* (2009), who suggest a global mean *b* value of 0.9 – 1.0. They used model studies to show that even a small increase (24 m) in the mean global remineralisation length scale of POC would result in a fall in atmospheric CO_2 concentration of 10 – 27 ppm. Nevertheless, due to the known methodological issues with using traditional sediment traps in the mesopelagic, further studies of the regional and seasonal variation of *b* largely ignored this region of most dynamic flux variation until the development of neutrally-buoyant sediment traps.

3.2.2 The VERTIGO programme

The VERtical Transport In the Global Ocean (VERTIGO) programme was designed to scrutinise the processes that control the efficiency of particle transport between the surface and deep ocean, based around two process studies at contrasting sites in the North Pacific. The multidisciplinary study focused on the two hypotheses that the efficiency of sinking particle transport (*i.e.*, the percentage of the sinking flux that remains after sinking through a certain depth) is determined by particle source characteristics and that processes in the twilight zone determine the transport efficiency (Buesseler *et al.*, 2008). The null hypothesis, that remineralisation rates do not change in response to either of these, would result in only one pattern of particle flux attenuation with depth (*i.e.*, a common value of *b*).

As part of the VERTIGO project, NBSTs (the Woods Hole Oceanographic Institute design of neutrally buoyant sediment traps) were deployed alongside traditional float-tethered sediment traps at three mesopelagic depths (150m, 300m, 500m) during research cruises at station ALOHA in the subtropical North Pacific and at K2, located in the northwest Pacific subarctic gyre. These traps were used to compare flux magnitudes and characteristics at the two sites of organic material, biogenic minerals and a selection of minor and trace elements (Lamborg *et al.*, 2008a;b).

A key finding of the study was that the *b* values observed for POC at the two sites were dramatically different. In the warm, oligotrophic waters at ALOHA, where conditions were relatively stable and the phytoplankton community was dominated by picoplankton, a *b* value of ~1.3 was measured. In contrast, in the colder, seasonal, mesotrophic conditions at K2, dominated at the time by diatom primary production, *b* was measured as ~0.52 (Lamborg *et al.*, 2008b). These results indicate that there was considerably higher transport efficiency for the POC flux at the latter, while sinking organic material was remineralised much more rapidly between 150 m and 500 m at ALOHA. This observation appears at odds with results from work based on deep-sea sediment traps and satellite-derived data (Francois *et al.*, 2002; Henson *et al.*, 2012), which suggest that the magnitude of *b* is lower at low latitudes and high at high latitudes.

One possible explanation for the higher transfer efficiency at K2 is the lower temperature in the mesopelagic at that site, which would reduce the extent of microbial remineralisation of sinking material. Alternatively, the logic of the ballast hypothesis, developed from the observed correlation between biomineral and POC in deep-sea sediment traps (Armstrong *et al.*, 2002; Klaas and Archer, 2002), suggests

that the transfer efficiency at K2 could have been enhanced by the high opal content of sinking material, although there was no evidence found at that site of higher proportions of biominerals in faster sinking particles (Trull *et al.*, 2008).

3.2.3 Iron in sinking particles

The VERTIGO study was also notable in that it provided some rare measurements of iron and other trace metals in sinking particles at mesopelagic depths (Lamborg *et al.*, 2008a). Although such measurements have often been made before in deep-sea trapping programs (Jickells *et al.*, 1984; Kuss and Kremling, 1999b; Kuss *et al.*, 2010), those made at mesopelagic depths have generally been made in coastal or shelf waters (Martin, 1990; Nameroff *et al.*, 2002; Pohl *et al.*, 2004). Exceptions to this include measurements at 200 m depth, using a bottom-moored trap in the northwest Mediterranean Sea (Quétel *et al.*, 1993); at 80 m and 120 m using surface-tethered free-drifting traps in subantarctic waters southeast of New Zealand (Frew *et al.*, 2006); and at 150 m and 300 m at the Bermuda Atlantic Time-Series (BATS) site in the Sargasso Sea, using both surface-tethered traps and NBSTs (Stanley *et al.*, 2004).

Sinking pFe data from the VERTIGO cruises showed contrasting behaviour at the two sites. At ALOHA, the pFe flux was fairly constant with depth, while at K2 a higher flux was found in the deeper traps, which was ascribed to the lateral advection of a plume of continental shelf-derived material. For comparison, Stanley *et al.* (2004) observed no difference between 150 m and 300 m depth using NBST traps, and a decrease with depth using surface-tethered traps. The two surface-tethered trap arrays deployed by Frew *et al.* (2006) as part of the FeCycle programme also showed differing trends for iron with depth (an increase in one and a decrease in the other).

Clearly, with such a small data set available, it is difficult to determine what the dominant controls are on the variation of sinking pFe within the mesopelagic. Particulate iron is present in the upper ocean in both lithogenic (*i.e.*, associated with continental material derived from atmospheric deposition) and biogenic (incorporated into living or detrital organic material) forms, as well as existing adsorbed onto other particles and as authigenic precipitates. While the limited previous work has shown little attenuation in downward pFe flux in the subsurface ocean, the FeCycle project showed evidence of a change in the character of particulate iron with depth, with that exported from the mixed layer containing a larger proportion of biogenic iron than material sampled in the euphotic zone, suggesting a transformation of lithogenic to biogenic iron in the surface ocean, prior to export (Frew *et al.*, 2006). Rapid attenuation of this biogenic Fe with depth is speculated to provide an important source

of dFe and iron-binding ligands in the upper mesopelagic that can be mixed back up to the surface ocean to be utilised during photosynthetic production, while sinking lithogenic iron is likely to have a much longer remineralisation length scale (Boyd *et al.*, 2010).

3.2.4 Aims and hypotheses

It was intended to investigate further the geographical variation in POC flux attenuation, using PELAGRA sediment traps to collect sinking particulate material at mesopelagic depths at different locations in the North Atlantic and analyse the changes in the relative composition of the material. With sampling sites in the sub-polar gyre and high latitude North Atlantic, it was hypothesised that these colder, mesotrophic regions, more similar to the K2 station from VERTIGO than the ALOHA site, would more closely resemble the former in terms of POC flux attenuation.

In addition, adding to the limited global inventory of upper ocean pFe flux measurements was a key aim of this work. The intention was to measure this flux, differentiating between the fraction which is accessible to heterotrophs, and can be readily remineralised for resupply to the upper ocean, and the more refractory fraction that is transferred to the deep ocean and sediments. The hypothesis was that downward flux of the former fraction would show a rapid attenuation with depth, while that of the latter would be relatively invariant with depth, or increase as a result of scavenging of dissolved iron onto sinking particles.

3.3 Overview of the two research cruises

The results shown here are from two separate research cruises, associated with two different projects. The first, to the Porcupine Abyssal Plain (PAP) site, was part of a dedicated study of the biological carbon pump and mesopelagic remineralisation, while the second, to the Irminger and Iceland Basins, formed part of a project examining the possibility of seasonal iron limitation in the high latitude North Atlantic (HLNA). Consequently, the demands made on sampling activities (*e.g.*, sample depths, spatial coverage of sample collection) were slightly different during the two cruises. Figure 3.2 shows the relative locations of the two study areas.

The details below are given to provide some context for the samples collected, and to point out any differences in the methods used between the two cruises. Throughout,

PELAGRA trap deployments during the two cruises are referred to as either PAP*a* P*b* or IB*a* P*b*, where PAP and IB refer to cruises D341 and D354 respectively, *a* is the deployment number during that cruise and P*b* relates to the specific trap used (P2, P4, P5, P6 or P7).

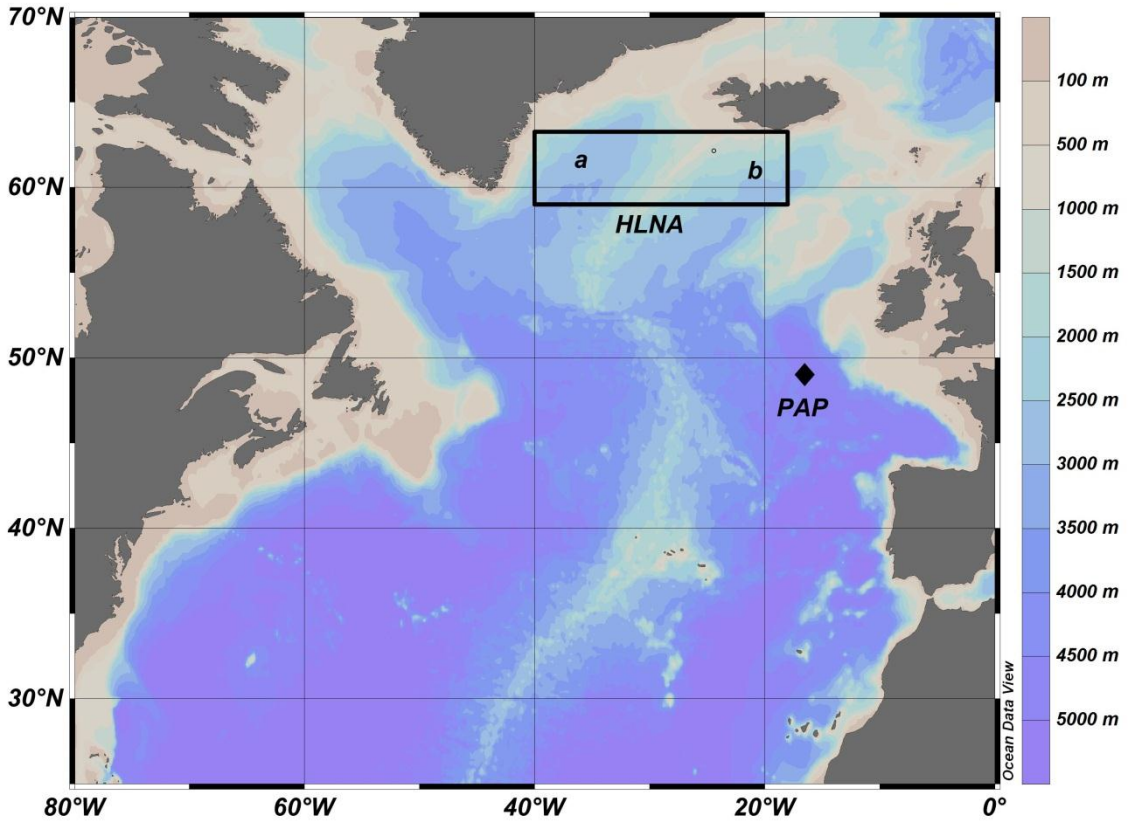

Figure 3.2: Locations of the study areas for research cruises D341 (PAP site, 49 °N 16.5 °W) and D354, to the high latitude North Atlantic (HLNA). In the black box, *a* represents the Irminger Basin and *b*, the Iceland Basin, defined by the Reykjanes Ridge separating these regions.

3.3.1 Cruise D341: PAP site, summer 2009

The PAP site (49° 00' N 16° 30' W) has been established as the site of a long-term, deep-sea sediment trap mooring since 1992, replacing a previous mooring 350 km to the southwest that was used during the North Atlantic Bloom Experiment (NABE) from 1989 – 1990 (Lampitt *et al.*, 2001). It has since been used as a site for both benthic and pelagic biogeochemical process studies (Billett and Rice, 2001; Lampitt *et al.*, 2010 and references in each). The time-series mooring is situated in water ~4850 m deep, in an area with fairly flat bathymetry and remote from both the continental slope and the mid-ocean ridge.

Located within what Longhurst (1998) termed the North Atlantic Drift Province (NADR), in the southeast part of the subpolar gyre, the area around the PAP site is characterised by winter convective mixing to 400 m or deeper, with a spring bloom initiated following restratification in the spring (Hartman *et al.*, 2010). As nutrients in the upper mixed layer are used up, surface production rates drop, though they can respond to episodic nutrient inputs through the summer, with mesoscale features such as eddies being one of the means by which this may occur.

RRS *Discovery* cruise D341 was carried out at the PAP site during summer (13th July – 9th August) 2009. One of the aims of the cruise was to compile a vertical carbon budget for the site, with particular focus on export from the upper ocean and processes within the mesopelagic. With this in mind, it was planned to perform several deployments of multiple PELAGRA traps in the vicinity of the PAP site, thus sampling the sinking particle flux concurrently at up to five depths between the base of the mixed layer and ~700 m. In most cases, two of the four sample pots on each trap were used for the work described here, with a third used to collect material for particle sinking experiments and the fourth set aside for work on organic chemistry.

PELAGRA deployments were made on four occasions over a three and a half week period. In each case, five traps were deployed simultaneously, with target depths of 50 m (trap P2), 150 m (P4), 300 m (P5), 450 m (P6), and 600 m (P7). Of the twenty individual trap deployments, four were completely unsuccessful in that they did not provide usable samples. Some other traps did not stabilise at their programmed depths, but did still yield potentially useful samples. Full details are below. All four deployments took place within the vicinity of the PAP site. Figure 3.3 summarises D341 sample coverage, while full details on individual trap deployments are given in Appendix D, along with depth profiles for each.

The first deployment (PAP1; 14th – 17th July) was planned as a test deployment, with the traps programmed to only collect material for 48 hours. All traps sank deeper than programmed due to over-ballasting. Traps P4 and P6 sank too deep, released their emergency weights and returned to the surface early in the deployment. The other three traps eventually stabilised at 156 m (P2), 287 m (P5) and 669 m (P7), though did not reach stable depths until 8 – 12 hours after the sample pots opened.

During PAP2 (19th – 26th July; 132 hours sampling time), P5 stabilised at a depth of 312 m, P6 at 449 m and P7 at 565 m. P2 remained at the surface until the sample pots opened and then sank, stabilising at 52 m some twelve hours later (average depth over the sampling period was 68 m). P4 also remained at the surface until the sample cups opened, and then sank too deep, triggering the over-depth release and returning to the surface. It was therefore discarded.

During PAP3 (28th July – 2nd August; 76 hours sampling) P2 stabilised at 49 m. P5 and P7 each initially sank but returned to the surface, then sank again once the sample pots opened. P5 quickly (~3 hours) reached and stabilised at 48 m, while P7 stabilised at 205 m some 12 hours after the sample cups had opened (average depth during the entire sampling period was 198 m). P4 behaved in a similar way to P5 and P7, but remained at the surface for a few hours after the pots opened and did not stabilise (222 m depth; average depth over sampling was 171 m) until 27 hours into the sampling period. P6 behaved in a similar way to P4 but remained at the surface for over half of the deployment time and so was discarded.

The final deployment (3rd – 7th August; 48 hours sampling) saw all five traps reach and stabilise at or close to their target depths before the sample cups opened: P2 at 51 m, P4 at 184 m, P5 at 312 m, P6 at 446 m and P7 at 589 m.

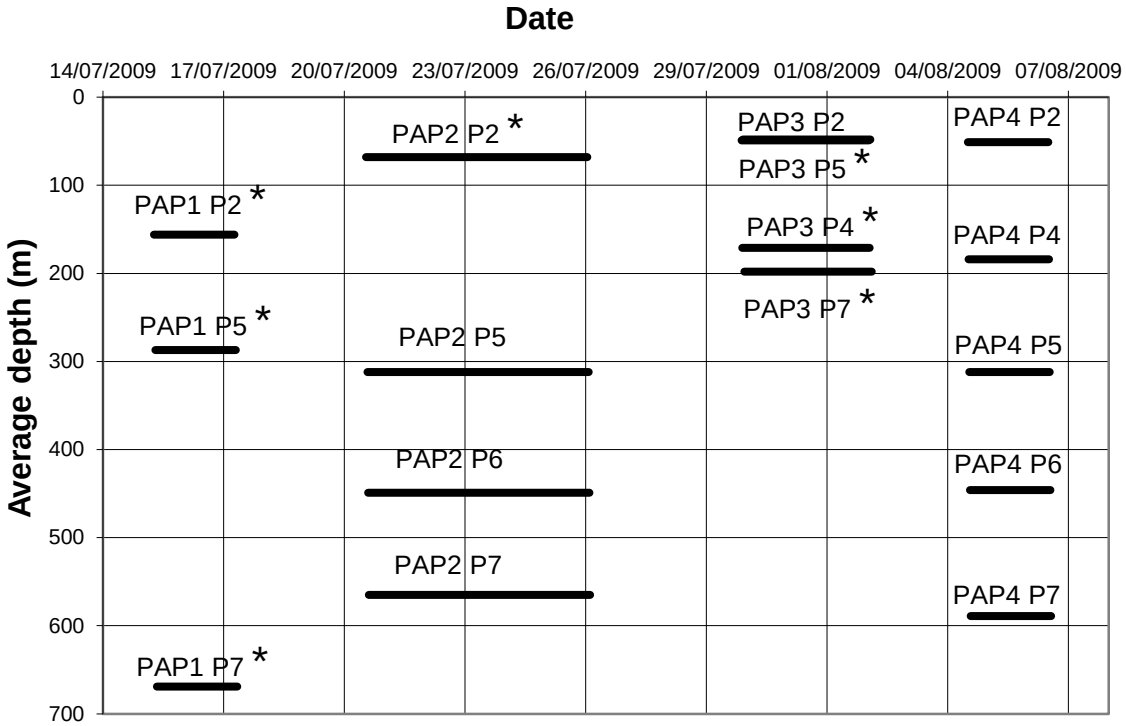

Figure 3.3: Depth and temporal coverage of PELAGRA traps during D341. Asterisks denote traps that were not stable for the entire deployment

3.3.2 Cruise D354: Irminger and Iceland Basins, summer 2010

As at the PAP site, the nutrient resupply to the euphotic zone in the HLNA takes place through annual convective mixing of the water column to 400 – 1000 m in the winter (de Jong *et al.*, 2012). Together with thermal stratification and increasing light levels in

the spring, this annual resupply results in a pronounced spring bloom with chlorophyll concentrations of >2 μg L^{-1} in places. The HLNA is characterised by residual concentrations of nutrients in the summer (~2 μmol L^{-1} nitrate in the Irminger Basin), which has led to speculation that seasonal iron limitation may be a feature of the region (Sanders *et al.*, 2005; Forryan *et al.*, 2012). This argument is reinforced by low rates of supply by dust deposition to the area inferred from modelling studies (Jickells *et al.*, 2005), while *in vitro* iron addition experiments carried out in the Iceland Basin have demonstrated enhanced net growth rates for the resident phytoplankton community (Nielsdóttir *et al.*, 2009).

As part of a larger project to study potential seasonal iron limitation in the Irminger and Iceland Basins, PELAGRA traps were used during RRS *Discovery* cruise D354 in the summer of 2010 (9th July – 7th August). Although five traps were taken to sea, storm damage incurred during transit to the study area rendered two of the traps unusable for the duration of the cruise, with a further one in need of substantial repairs before it was ready for use half-way through the cruise. Due to the limitations that this placed on sampling strategy, PELAGRA deployments only covered depths of 80 – 400 m during D354. Trap P4 was targeted at 80 m, P6 at 150 m and, for the third and fourth deployments, P7 at 400 m.

Most deployments during the cruise were carried out with one sample pot on each trap dedicated as a process blank (*i.e.*, programmed to not move underneath the collection funnel for the duration of the deployment). The other three pots were programmed to open and close at the same time and were pooled together during processing (described in Appendix A). For all deployments, the traps were programmed with a 24 hour period to reach and stabilise at the sampling depth. Figure 3.4 shows coverage of PELAGRA sampling during D354, along with trap deployment positions marked on a map of the study area. Full details of deployment/recovery positions and times are listed in Appendix D, along with depth profiles for each trap.

PELAGRA deployment IB1 (12th – 14th July, deployed at 60.0 °N 20.0 °W) was again used as a test deployment, with the traps programmed for 30 hours of sampling. P6 sampled successfully, stabilising at 156 m. P4 stabilised at 83 m for the first 25 hours of sampling time but surfaced five hours too early, which will have corrupted the samples.

IB2 took place from 18th – 21st July, with the traps deployed at 60.1 °N 35.0 °W and programmed for 54 hours sampling time. P4 again stabilised at 83 m for the first 25 hours but surfaced with sample cups open due to a technical fault, compromising the sample, while P6 stabilised at 152 m and sampled successfully.

For IB3 (25th– 28th July; deployed at 60.9 °N 31.6 °W), P4 was stable at 84 m for the 44 hours that it was programmed to sample for, P6 was stable at 154 m for 50 hours of sampling and P7 was stable at 402 m for its 44 hours of sampling.

During the final deployment, IB4 (3rd – 6th August; traps deployed at 62.2 °N 24.4 °W), all three traps again sampled successfully. P4 was stable at 82 m for 40 hours of sampling, P6 at 152 m for 46 hours and P7 at 402 m for 40 hours.

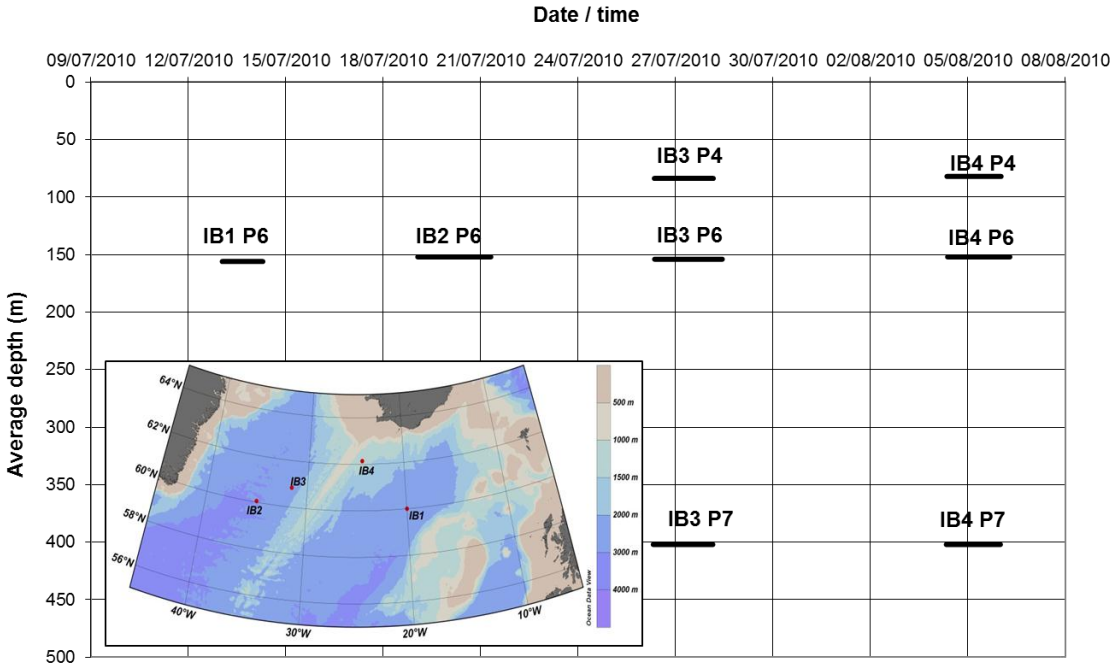

Figure 3.4: Depth and temporal coverage of PELAGRA traps during D354, along with (inset) deployment locations.

3.4 Results

3.4.1 Process blanks

During the VERTIGO project, one tube of the trap array was used as a process blank during each deployment and kept covered throughout, but otherwise treated in the same way as the sample tubes (Lamborg *et al.*, 2008b). The results of that project showed that, especially in regions of low particle flux, the process blank often represented a meaningful fraction of the measured sample flux, although samples were usually well above the resulting detection limits.

Due to demands on trap samples, it was not possible to carry out regular process blanks during D341. Only three were carried out, all on the first deployment, using traps P2, P4 and P6, and the latter two of these traps spent most of their time at the surface and were considered unusable. However, during D354 one pot was designated as a process blank for every trap deployment. The measurements made on these process blanks were converted into "fluxes" and the mean values taken, and these blanks then applied to all samples collected during both D354 and D341, as the flux magnitudes observed on the two cruises were similar. In the case of aluminium, calculated concentrations in both the leach and digest fractions of the process blanks were below the detection limit calculated from replicate filter blanks, so sample concentrations were instead considered relative to the filter blank detection limit.

As found during VERTIGO, sample values were generally well above the detection limit resulting from the process blanks, and the blank values themselves are comparable to those measured by Lamborg *et al.* at station ALOHA, and lower than those from K2.

3.4.2 D341 results

3.4.2.1 Seasonal context and hydrography

MODIS (Moderate Resolution Imaging Spectroradiometer) satellite-derived chlorophyll concentrations for a 100 km x 100 km area centred on the PAP site during 2009 (Figure 3.5) show that cruise D341 began four or five weeks after the peak of the spring bloom and that mean chlorophyll concentrations over the area were ~0.5 – 0.7 mg m^{-3} during the cruise, having peaked at around 1.1 mg m^{-3}.

Hydrographic data collected during the cruise showed a mixed layer of typically 32 – 45 m depth (interquartile range from all CTD profiles) and 15 – 16 °C, below which the water temperature decreased to 10 – 11 °C at 500 m. Euphotic zone depth, taken as the depth of 1 % light penetration, varied from 42 – 47 m. The CTD fluorescence signal was either fairly stable from surface to the base of the mixed layer, or else showed a maximum anywhere between 15 and 40 m depth. Nutrients measured from CTD bottle samples were typically low in the mixed layer (nitrate < 0.3 – 0.7 µmol L^{-1}).

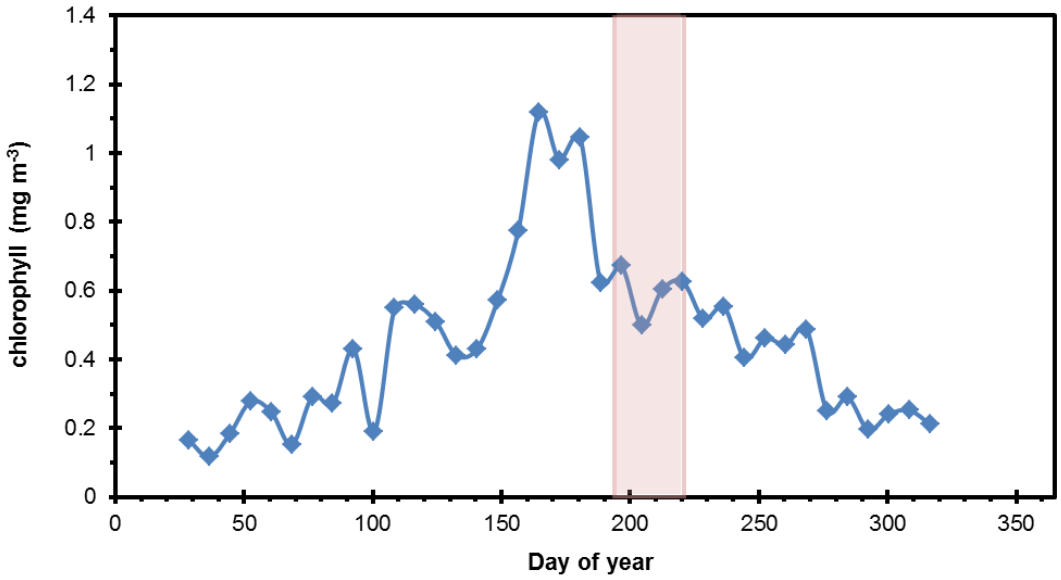

Figure 3.5: MODIS satellite-derived chlorophyll concentrations for 2009 at the PAP site, based on the mean values of 8-day time intervals. Timing of research cruise D341 is shown by the shaded box (days 194 – 221).

3.4.2.2 Geographical coverage of the traps

Free-floating traps deployed individually in the ocean are susceptible to divergence from each other, especially if they are stationed at different depths and therefore possibly influenced by disparate currents. The magnitude of this divergence is likely to be more significant the longer the traps are deployed. In this case it was hoped that short deployments of between 66 and 156 hours would minimise the potential for substantial separation of the traps; nevertheless it was found that traps floated in opposite directions during three of the four deployments. Figure 3.6 shows the locations of all 16 successful trap deployments at the PAP site (*i.e.*, not including the four traps that resurfaced too early), along with the first location transmitted by each trap upon resurfacing.

Although it is not possible to follow the precise trajectory of the traps while submerged, it is apparent from the first coordinates transmitted after resurfacing that during deployment PAP1, trap P2 drifted in the opposite direction to traps P5 and P7, resurfacing 25 – 30 km from the other two traps, which were around 7 km apart. During the longest deployment, PAP2, traps P5, P6 and P7 resurfaced south or south-southwest of their deployment position, having diverged from each other by 20 – 45 km, while P2 resurfaced to the northeast, over 140 km away from any of the others. During PAP3, traps P2 and P7 resurfaced within ~10 km of each other, roughly

northeast of the deployment site, while P4 and P5 did so (within ~15 km of each other) roughly 45 km away to the southwest.

Only during PAP4 did all five traps seem to have travelled in the same direction. For this deployment the maximum distance between any two traps at the time of the first transmission after surfacing was <9 km, with most of the traps being within 5 km of each other. Although it cannot be claimed with absolute certainty that all of the traps took the same trajectory to reach their destination, it seems improbable that they would all resurface in such proximity after 72 hours having followed different currents while submerged.

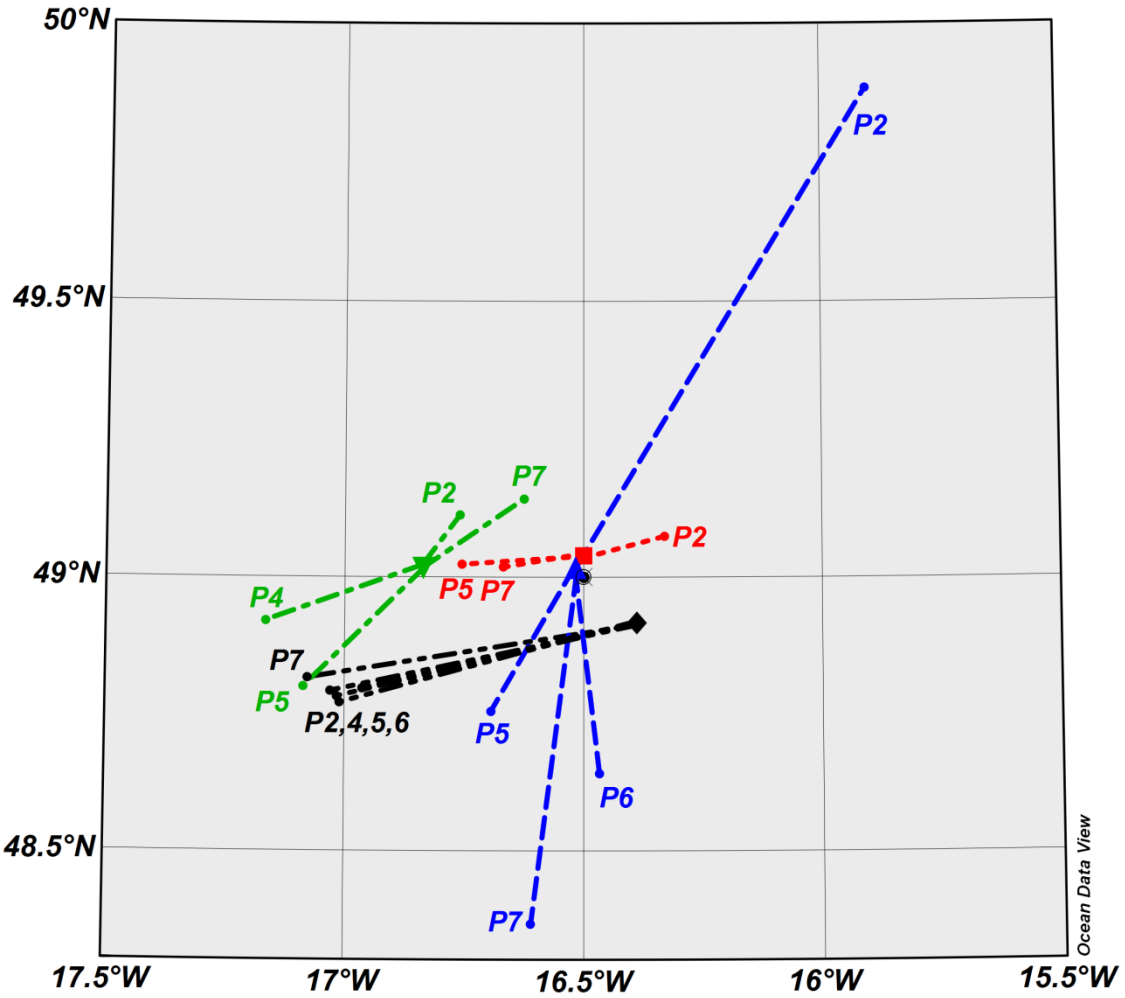

Figure 3.6: Deployment positions of traps for PAP1 (red square), PAP2 (blue triangle), PAP3 (green inverted triangle) and PAP4 (black diamond) and approximate locations of traps upon surfacing. Dashed/dotted lines depict straight-line transit of each trap while submerged.

3.4.2.3 PELAGRA fluxes

Tables 3.1 and 3.2 and Figure 3.7 summarise the fluxes measured during D341, including mass, POC, PON, PIC (derived from Ca), bSi, Al, Fe, P and Mn. Values shown for the metals and P are total values (*i.e.*, the sum of leach and digest fractions). Also included in the tables are the calculated "fluxes" from the process blanks carried out during D354. All sample fluxes shown have been corrected using the process blank.

PAP3 P4 data is highlighted in red in the tables and is not included in Figure 3.7 as the trap spent a significant amount of the sampling time shallower than the stable depth shown, while those traps italicised in the tables were not stable at the start of sampling, but were either ascending to the sampling depth at a rate of ~20 m hr^{-1} or immediately started sinking from the surface at a rate of ~70 m hr^{-1} upon the sample pots opening (see Appendix D). There is no particular evidence to suggest that this behaviour significantly affected the sampling efficiency of these traps over the deployment periods, but such features do introduce uncertainty into the numbers calculated.

For the most part, fluxes of mass and the biogenic components of the sinking material were well above the detection limit, with the exception of bSi from PAP2 P2. Fe, Mn and Al fluxes were also usually above the detection limit, except for PAP2 P2, PAP3 P2 (all three metals), PAP3 P4 & P5 and PAP 4 P6 & P7 (Fe only). However, the leachable fraction of Fe was usually below the detection limit (data not shown in table).

The highest mass flux measured (Figure 3.7*a*) was 352 ± 60 mg m^{-2} d^{-1} at 51 m depth during PAP4. Other than two other measurements of >100 mg m^{-2} d^{-1} (at 198 m and 312 m depth), all other values fell in the range of 46 – 94 mg m^{-2} d^{-1}. Considering the dataset as a whole, there was no significant trend in mass flux with depth, though less variation was measured below 400 m.

Magnitude of flux for POC and PON (Figure 3.7*b,c*) each showed a similar distribution to mass, with the same three samples again providing the highest values, and the greatest flux measured at 51 m by PAP4 P2 (6.9 ± 0.3 mmol m^{-2} d^{-1} for POC and 0.83 ± 0.07 mmol m^{-2} d^{-1} for PON). The lowest fluxes (0.8 and 0.1 mmol m^{-2} d^{-1} POC and PON respectively) were also measured at ~50 m depth, by PAP3 P2 and P5. As with mass, it can be said that there was less variation in measured flux below 400 m depth than in the upper 350 m, but no simple linear trend of flux with depth was apparent. The data for phosphorus flux (Figure 3.7*h*) showed a similar pattern to POC and PON, with values ranging from 3 – 63 µmol m^{-2} d^{-1}.

Table 3.1: Flux summaries for mass and biogenic components of particulate material during D341 (corrected for process blanks). DL = detection limit, based on 3σ of process blank. Samples in italics had not stabilised before sample cups opened, while PAP3 P4 (highlighted in red) spent a significant time at a shallower depth than the stable depth shown (see text and Appendix D).

Sample	Depth (m)	Mass (mg m^{-2} d^{-1})	POC (mmol m^{-2} d^{-1})	PON (mmol m^{-2} d^{-1})	PIC (mmol m^{-2} d^{-1})	bSi (μmol m^{-2} d^{-1})
PAP1 P2	*156*	*76 ± 10*	*1.46 ± 0.07*	*0.17 ± 0.02*	*0.34 ± 0.08*	*16 ± 2*
PAP1 P5	*287*	*84 ± 54*	*1.76 ± 0.08*	*0.19 ± 0.02*	*0.30 ± 0.07*	*42 ± 5*
PAP1 P7	*669*	*96 ± 3*	*1.80 ± 0.09*	*0.19 ± 0.02*	*0.35 ± 0.09*	*151 ± 15*
PAP2 P2	*68*	*48 ± 6*	*1.81 ± 0.09*	*0.23 ± 0.02*	*0.05 ± 0.01*	*<DL*
PAP2 P5	312	187 ± 26	5.47 ± 0.23	0.71 ± 0.06	0.41 ± 0.10	74 ± 8
PAP2 P6	449	93 ± 4	2.08 ± 0.10	0.24 ± 0.02	0.40 ± 0.10	99 ± 10
PAP2 P7	565	77 ± 17	1.96 ± 0.09	0.22 ± 0.02	0.28 ± 0.07	106 ± 11
PAP3 P2	49	56 ± 38	0.88 ± 0.05	0.10 ± 0.01	0.28 ± 0.07	3 ± 1
PAP3 P4	*171*	*42 ± 5*	*0.70 ± 0.05*	*0.08 ± 0.01*	*0.14 ± 0.04*	*9 ± 2*
PAP3 P5	*48*	*56 ± 19*	*0.76 ± 0.05*	*0.09 ± 0.01*	*0.32 ± 0.08*	*4 ± 1*
PAP3 P7	*198*	*210 ± 21*	*4.65 ± 0.20*	*0.57 ± 0.05*	*0.25 ± 0.06*	*5 ± 1*
PAP4 P2	51	352 ± 60	6.87 ± 0.29	0.83 ± 0.07	1.33 ± 0.33	19 ± 2
PAP4 P4	184	84 ± 24	2.33 ± 0.11	0.29 ± 0.03	0.21 ± 0.05	29 ± 3
PAP4 P5	312	60 ± 13	1.39 ± 0.07	0.13 ± 0.01	0.22 ± 0.05	42 ± 5
PAP4 P6	446	48 ± 9	1.20 ± 0.06	0.12 ± 0.01	0.22 ± 0.05	47 ± 5
PAP4 P7	589	61 ± 10	1.33 ± 0.07	0.14 ± 0.01	0.23 ± 0.06	39 ± 4
D354 blank [a]	(80-400)	10 ± 3	0.12 ± 0.04	0.013 ± 0.004	0.003 ± 0.002	2.4 ± 1.1

[a] For D354 process blank mean, each process blank measurement was divided by the trap deployment time to obtain a nominal flux, and the mean and standard deviation of all values was calculated (n = 18). Process blank replicate measurements were made during D354.

Table 3.2: Flux summaries for Al, Fe, P and Mn during D341 (corrected for process blanks). Values shown are total values (leach + digest). DL = detection limit, based on 3σ of process blank. Samples in italics had not stabilised before sample cups opened, while PAP3 P4 (highlighted in red) spent a significant time at a shallower depth than the stable depth shown (see text and Appendix D).

Sample	Depth (m)	Al (μmol m^{-2} d^{-1}) [b]	Fe (μmol m^{-2} d^{-1})	P (μmol m^{-2} d^{-1})	Mn (nmol m^{-2} d^{-1})
PAP1 P2	*156*	*0.57 ± 0.10*	*0.39 ± 0.10* [c]	*10.9 ± 0.8*	*7.4 ± 1.1*
PAP1 P5	*287*	*2.04 ± 0.16*	*1.61 ± 0.40* [c]	*13.0 ± 1.2*	*30.0 ± 1.4*
PAP1 P7	*669*	*7.67 ± 0.33*	*2.19 ± 0.35*	*4.3 ± 0.3*	*92.4 ± 4.4*
PAP2 P2	*68*	*<DL*	*<DL*	*19.3 ± 0.4*	*<DL*
PAP2 P5	312	3.40 ± 0.78	0.83 ± 0.13 [c]	26.2 ± 0.5	19.8 ± 3.0
PAP2 P6	449	2.43 ± 0.17	0.36 ± 0.12 [c]	8.3 ± 1.6	58.0 ± 1.9
PAP2 P7	565	2.13 ± 0.45	0.28 ± 0.17 [c]	5.8 ± 2.6	45.8 ± 6.3
PAP3 P2	49	<DL	<DL	10.9 ± 0.2	<DL
PAP3 P4	*171*	*0.23 ± 0.04*	*<DL*	*11.0 ± 0.2*	*2.7 ± 0.9*
PAP3 P5	*48*	*0.19 ± 0.05*	*<DL*	*11.1 ± 1.1*	*5.8 ± 1.3*
PAP3 P7	*198*	*2.67 ± 1.29*	*0.45 ± 0.10*	*62.6 ± 1.3*	*12.3 ± 1.7*
PAP4 P2	51	1.10 ± 0.59	0.69 ± 0.25	39.4 ± 9.5	27.4 ± 10.5
PAP4 P4	184	1.25 ± 0.33	0.76 ± 0.15 [c]	8.6 ± 0.4	14.6 ± 1.7
PAP4 P5	312	1.14 ± 0.24	0.52 ± 0.32 [c]	4.5 ± 0.3	12.5 ± 2.0
PAP4 P6	446	1.07 ± 0.17	<DL	3.3 ± 0.2	21.4 ± 2.0
PAP4 P7	589	1.42 ± 0.13	<DL	6.2 ± 0.3	38.0 ± 1.3
D354 blank [a]	(80-400)	<DL	0.18 ± 0.08	0.36 ± 0.15	2.2 ± 0.9

[a] For D354 process blank mean, each process blank measurement was divided by the trap deployment time to obtain a nominal flux, and the mean and standard deviation of all values was calculated (*n* = 18). Process blank replicate measurements were made during D354.
[b] Process blank for Al was below filter blank detection limit, so filter blank detection limit is used instead of process blank.
[c] Leach fraction of total was below detection limit defined by process blank measurements.

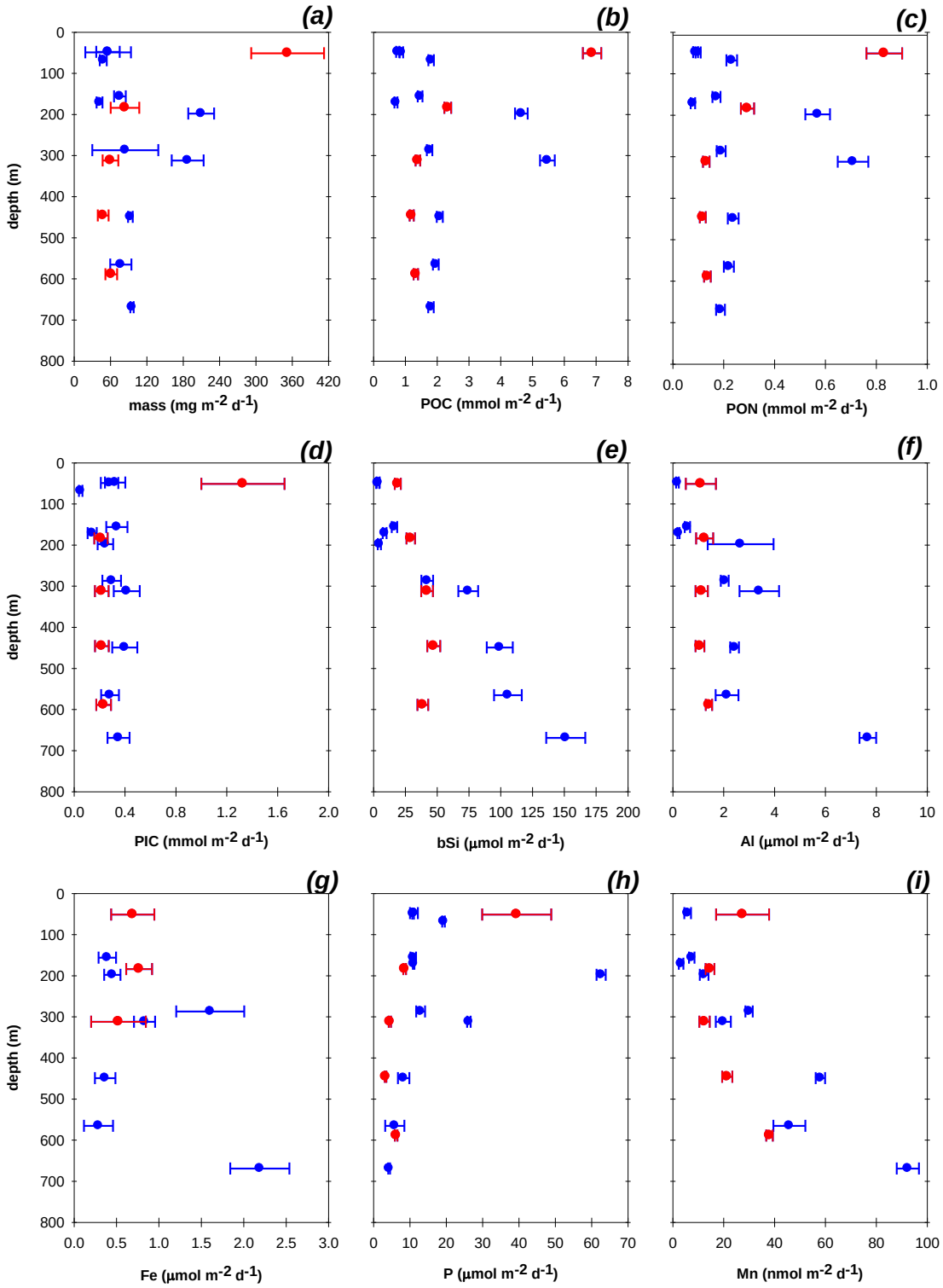

Figure 3.7: Fluxes of *(a)* mass, *(b)* POC, *(c)* PON, *(d)* PIC, *(e)* bSi, *(f)* aluminium, *(g)* iron, *(h)* phosphorus and *(i)* manganese during D341. Measurements from PAP1 - PAP3 are shown in blue; those from PAP4 in red. All values are corrected for process blanks.

The two main biominerals displayed very different patterns with depth. Calcite flux (PIC; Figure 3.7*d*) showed very little variation with depth, generally falling in the range 0.2 – 0.4 mmol m^{-2} d^{-1}, with only two exceptions. During deployment PAP4, P2 (51 m) recorded a flux of 1.3 ± 0.3 mmol m^{-2} d^{-1}, while PAP2 P2, which had drifted over 100 km from the PAP site, measured a flux of only 0.05 ± 0.01 mmol m^{-2} d^{-1} PIC. In contrast, bSi fluxes (Figure 3.7*e*) showed a statistically significant relationship of greater flux measured at increased depth (Spearman rank-order correlation; P <0.001, n = 16). Values of bSi flux fell in a range from below the detection limit (DL) to 151 µmol m^{-2} d^{-1}, with the lowest flux measured at 48 m depth during PAP3 and the highest at 669 m during PAP1.

As with bSi, the lowest measured fluxes of Al and Fe were at ~50 m during PAP3 (both below detection limit for P2) and the highest at 669 m during PAP1 (7.7 ± 0.3 µmol m^{-2} d^{-1} for Al, 2.2 ± 0.3 µmol m^{-2} d^{-1} for Fe; Figure 3.7*f,g*). The relationship of greater Al flux with depth was statistically significant (P < 0.01, n = 16), while that for Fe was not. Manganese (< DL – 92 nmol m^{-2} d^{-1}; Figure 3.7*i*) also showed a significant correlation between depth and flux magnitude (P <0.001, n = 16).

3.4.3 D354 results

3.4.3.1 Seasonal and hydrographical context

Although sampling during D354 covered a much greater geographical area, with PELAGRA deployed in both the Iceland and Irminger Basins over a four week period, the mixed layer depth in both at the time of the cruise was typically <35 m, with a euphotic zone extending to between 33 and 43 m depth. CTD data shows that the upper water column of the Irminger Basin was slightly colder and fresher than the Iceland Basin.

MODIS satellite imagery of the region from 2010 (Figure 3.8) suggests that much of the Irminger Basin was under bloom conditions for the duration of the cruise, with peak chlorophyll concentrations later than usual and coinciding roughly with the halfway point of the cruise. Chlorophyll *a* concentrations for the Iceland Basin were generally lower at the time, having peaked in mid-May and again in early June. The MODIS data shows the highest chlorophyll concentrations in the study area at the time of the cruise were in the Reykjanes Ridge region, positioned between the two basins, where chlorophyll concentrations peaked early in the cruise, before decreasing rapidly. Nevertheless, the highest values seen from underway measurements of chlorophyll

during the cruise were in the Irminger Basin (mean value, 2.3 µg L^{-1}; mean for Iceland Basin, 1.3 µg L^{-1}, for Reykjanes Ridge, 1.9 µg L^{-1}).

Underway surface nutrient measurements carried out during the cruise also showed differences between the two basins. In the Irminger Basin TON (Total Oxidised Nitrogen = nitrate + nitrite) concentrations ranged from <0.09 – 6.5 µM (median: 3.2 µM), phosphate from 0.03 – 0.52 µM (median: 0.26 µM) and silicate from 0.1 – 4.3 µM (median: 1.8 µM), while in the Iceland Basin, TON ranged from <0.09 – 2.7 µM (median: 0.3 µM), phosphate from 0.04 – 0.18 µM (median: 0.07 µM) and silicate from 0.18 – 1.74 µM (median: 0.65 µM).

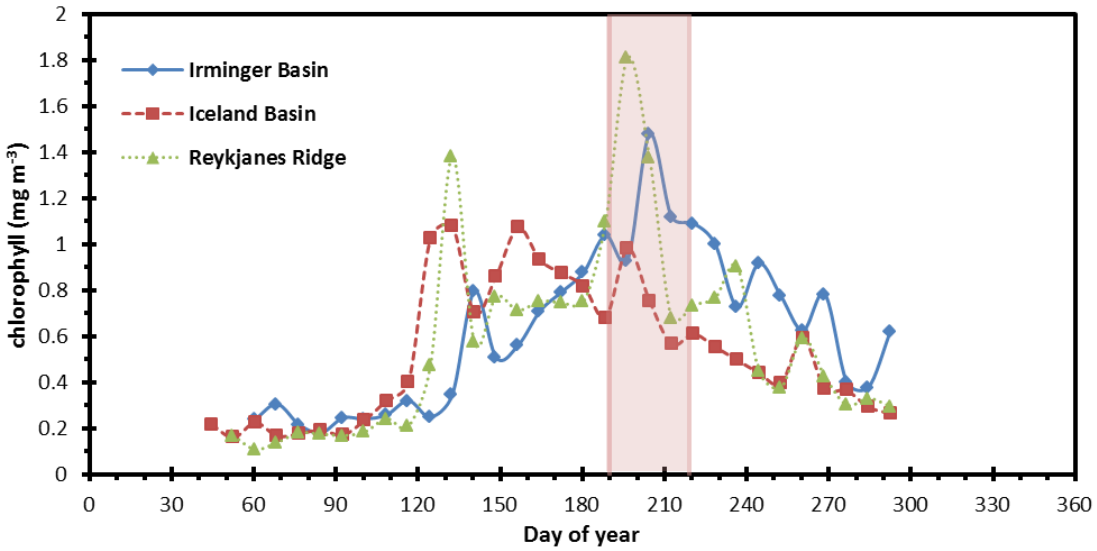

Figure 3.8: MODIS satellite-derived chlorophyll concentrations for 2010 in the Irminger and Iceland Basins and the Reykjanes Ridge region between the two. The timing of cruise D354 is shown by the shaded area between days 190 - 219.

3.4.3.2 PELAGRA trap geographical coverage

Figure 3.9 shows for each set of PELAGRA deployments the location of deployment and the location of the first transmission from each trap upon resurfacing. As before, the general direction of travel while submerged is shown for each trap, although the true trajectory cannot be known.

During IB1 and IB2, trap P6 surfaced roughly east-northeast of the deployment locations. Unfortunately, there are no coordinates available for trap P4 upon resurfacing during IB3. Instead, the recovery coordinates are used, though it should be noted that this took place approximately nine hours after the trap surfaced. During the same deployment, P6 drifted ~3.2 km northeast in 7 hours between surfacing and

recovery, while P7 drifted ~3.4 km north-northwest in 7 hours, so P4 probably surfaced within 5 km of the position given. All three traps surfaced roughly southwest of the deployment location during IB3, with traps P6 and P7 surfacing ~7.5 km apart, while P4 was recovered approximately 20 - 25 km further to the west.

During IB4, P4 appears to have travelled roughly due west from the deployment location, and surfaced ~22 km distant from both P6 and P7. However, these two traps ended up ~39 km from each other, with P6 having taken a more south-westerly trajectory and P7 surfacing slightly further north of P4 and closest to the deployment site.

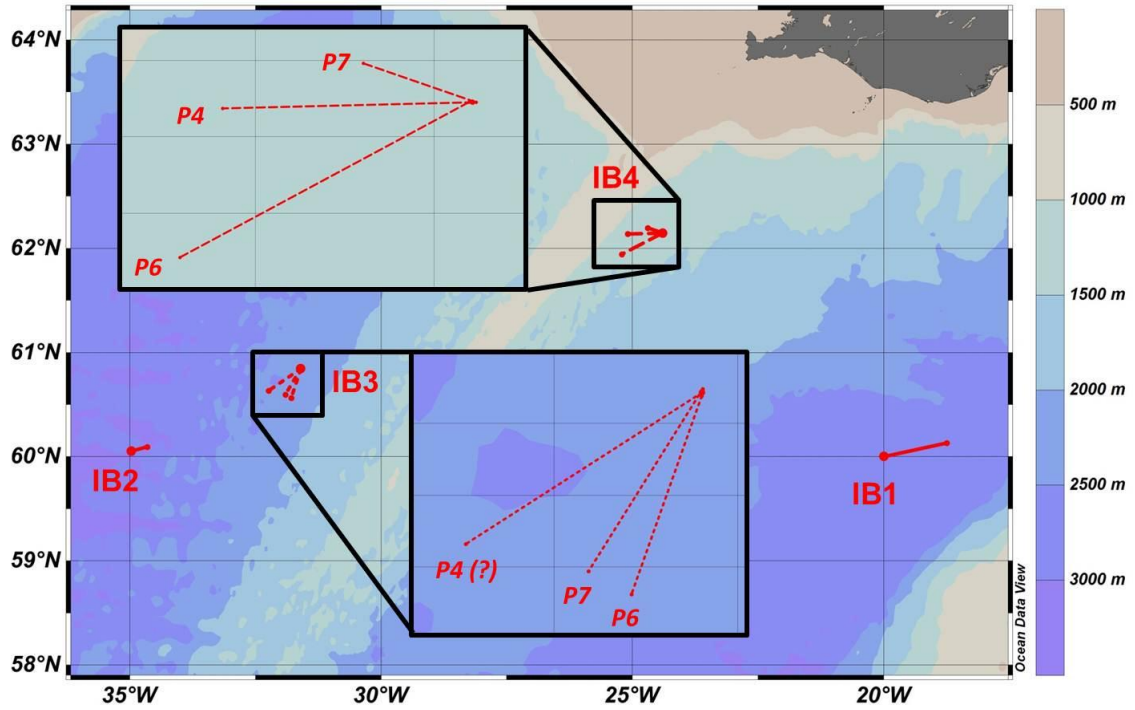

Figure 3.9: Locations of PELAGRA deployments during D354, and the first recorded locations of the traps upon resurfacing. For IB3 P4 see comments in text.

3.4.3.3 Measured fluxes

The fluxes of mass, POC, PON, PIC and bSi measured during D354 are listed in Table 3.3, while those for aluminium, iron, phosphorus and manganese are shown in Table 3.4. Figure 3.10 shows the depth profiles of the calculated fluxes for all successful trap deployments.

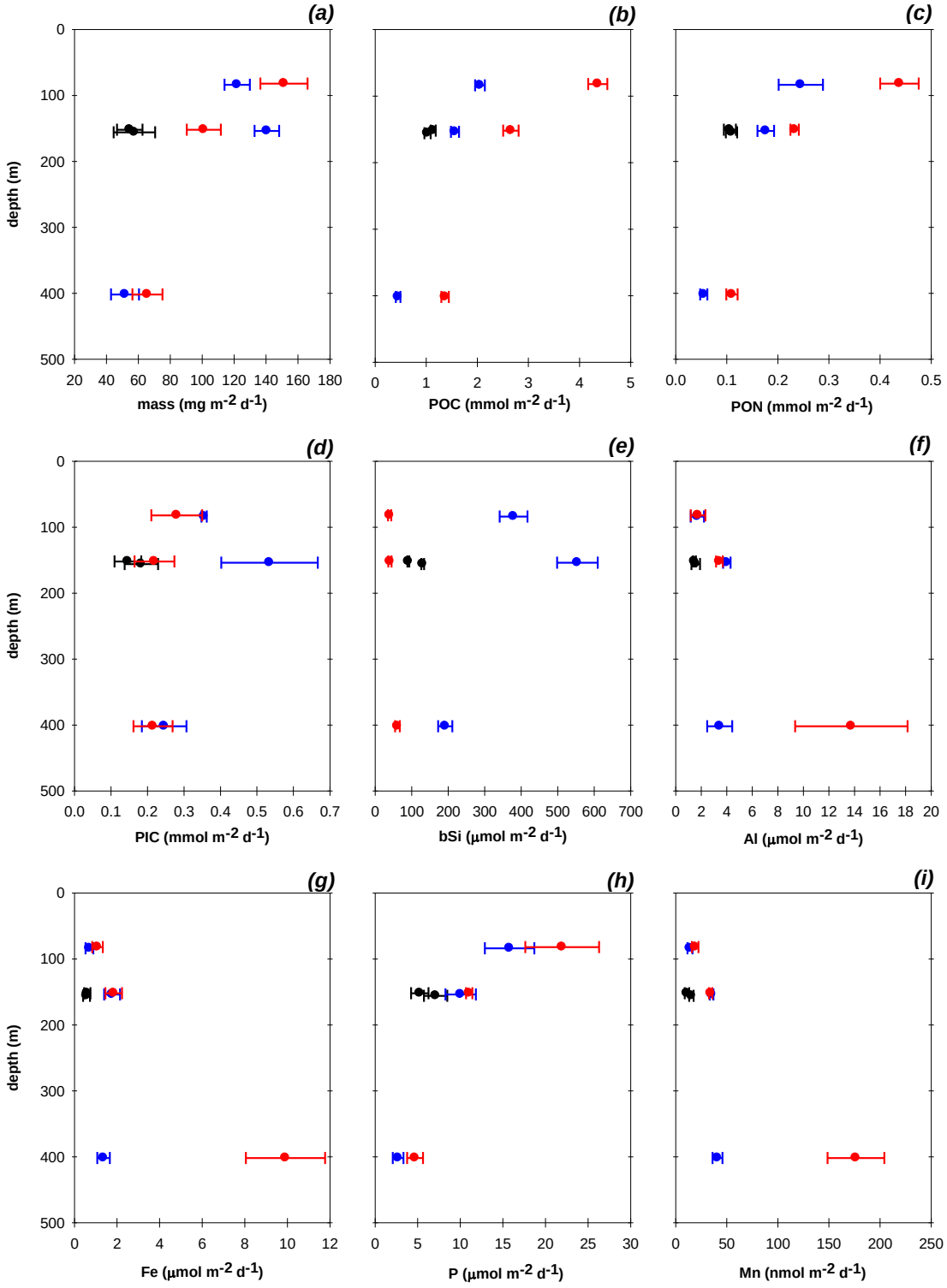

Figure 3.10: Fluxes of *(a)* mass, *(b)* POC, *(c)* PON, *(d)* PIC, *(e)* bSi, *(f)* aluminium, *(g)* iron, *(h)* phosphorus and *(i)* manganese during D354. Measurements from IB1 and IB2 are shown in black, those from IB3 in blue, and those from IB4 in red. All values are corrected for process blanks.

Observed mass flux (Figure 3.10*a*) ranged from 52 – 151 mg m^{-2} d^{-1}, a similar range of values to those measured at the PAP site during D341. The results for IB3 and IB4 differed from each other in that during the latter, mass flux reduced from 151 ± 15 mg m^{-2} d^{-1} at 80 m to 101 ± 11 mg m^{-2} d^{-1} at 150 m, while there was a slightly higher flux at 150 m than at 80 m during IB3. In both cases the flux measured at 400 m was the lowest of the three depths.

The highest POC and PON fluxes measured during D354 (Figure 3.10*b,c*) were also collected by the shallowest trap during IB4 (4.4 ± 0.2 and 0.44 ± 0.04 mmol m^{-2} d^{-1} respectively), with POC flux observed by this trap twice as high as that measured at the same depth during IB3. For both POC and PON, a larger flux was also measured by the deepest trap during IB4 compared to IB3, although the latter did not reduce as quickly between 80 and 150 m. The same relationship was observed for phosphorus (Figure 3.10*h*). The observed fluxes for all three were of the same order of magnitude as those measured during D341, with POC and PON fluxes measured at 400 m during IB3 being the lowest seen during either cruise.

In contrast to the organic constituents of the sinking particle flux, the largest fluxes of PIC and bSi measured in the course of D354 (Figure 3.10*d,e*) were during IB3, in the Irminger Basin. In each case the observed flux was greatest at 150 m depth (0.53 ± 0.13 mmol m^{-2} d^{-1} for PIC, 0.55 ± 0.06 mmol m^{-2} d^{-1} for bSi). The flux of bSi measured by the shallower two traps during IB3 was around a factor of ten greater than that measured during IB4 (and about three times greater at 400 m depth), and higher also than any of the bSi flux measurements at the PAP site in 2009.

The fluxes of Al, Fe and Mn measured during D354 (Figure 3.10*f,g,i*) were typically of a similar magnitude to those observed on the earlier cruise. Both Al and Fe exhibited a greater flux at 150 m than at 80 m or 400 m during IB3, in the Irminger Basin. Leachable iron values were typically below the detection limit during D354, while 10 – 20 % of total Al and 20 – 30 % of total Mn were present in the leach fraction. The greatest fluxes measured for all three trace metals were in the deepest trap during IB4. These values (13.8 ± 4.4 and 9.9 ± 1.9 µmol m^{-2} d^{-1} respectively, for Al and Fe; 177 ± 28 nmol m^{-2} d^{-1} for Mn) were 4 – 5 times higher than any others measured during the cruise.

Table 3.3: Flux summaries for mass and biogenic components of particulate material during D354 (corrected for process blanks).

Sample	Depth (m)	Mass (mg m^{-2} d^{-1})	POC (mmol m^{-2} d^{-1})	PON (mmol m^{-2} d^{-1})	PIC (mmol m^{-2} d^{-1})	bSi (µmol m^{-2} d^{-1})
IB1 P6	156	58 ± 13	1.02 ± 0.06	0.11 ± 0.01	0.18 ± 0.05	130 ± 4
IB2 P6	152	55 ± 8	1.14 ± 0.05	0.11 ± 0.01	0.15 ± 0.04	91 ± 3
IB3 P4	84	122 ± 8	2.05 ± 0.10	0.24 ± 0.04	0.36 ± 0.01	379 ± 38
IB3 P6	154	141 ± 8	1.56 ± 0.08	0.18 ± 0.02	0.53 ± 0.13	554 ± 56
IB3 P7	402	52 ± 9	0.45 ± 0.05	0.06 ± 0.01	0.25 ± 0.06	192 ± 19
IB4 P4	82	151 ± 15	4.36 ± 0.19	0.44 ± 0.04	0.28 ± 0.07	40 ± 4
IB4 P6	152	101 ± 11	2.66 ± 0.15	0.23 ± 0.01	0.22 ± 0.05	41 ± 4
IB4 P7	402	66 ± 9	1.37 ± 0.07	0.11 ± 0.01	0.22 ± 0.05	61 ± 6
D354 blank [a]	(80-400)	10 ± 3	0.12 ± 0.04	0.013 ± 0.004	0.003 ± 0.002	2.4 ± 1.1

[a] **For D354 process blank mean, each process blank measurement was divided by the trap deployment time to obtain a nominal flux, and the mean and standard deviation of all values was calculated (*n* = 18).**

Table 3.4: Flux summaries for Al, Fe, P and Mn during D354 (corrected for process blanks). Values shown are total values (leach + digest). DL for Al D354 blank = detection limit, based on 3σ of filter blank.

Sample	Depth (m)	Al (μmol m^{-2} d^{-1})	Fe (μmol m^{-2} d^{-1})	P (μmol m^{-2} d^{-1})	Mn (nmol m^{-2} d^{-1})
IB1 P6	156	1.57 ± 0.34	0.57 ± 0.16[b]	7.1 ± 1.4	15 ± 2
IB2 P6	152	1.47 ± 0.12	0.60 ± 0.15[b]	5.3 ± 1.0	11 ± 2
IB3 P4	84	1.70 ± 0.52	0.71 ± 0.18[b]	15.8 ± 2.9	14 ± 2
IB3 P6	154	4.00 ± 0.30	1.77 ± 0.38[b]	10.0 ± 1.8	35 ± 2
IB3 P7	402	3.45 ± 0.98	1.37 ± 0.29	2.7 ± 0.6[c]	41 ± 5
IB4 P4	82	1.75 ± 0.57	1.08 ± 0.25[b]	22.0 ± 4.3	19 ± 3
IB4 P6	152	3.42 ± 0.26	1.85 ± 0.39[b]	11.1 ± 0.4	34 ± 2
IB4 P7	402	13.75 ± 4.40	9.92 ± 1.86	4.7 ± 0.9	177 ± 28
D354 blank[a]	all (80-400)	<DL	0.18 ± 0.08	0.36 ± 0.15	2.2 ± 0.9

[a] For D354 process blank mean, each process blank measurement was divided by the trap deployment time to obtain a nominal flux, and the mean and standard deviation of all values was calculated (*n* = 18).
[b] Leach fraction numbers were below detection limit – numbers shown are for digest only.
[c] No P leach fraction value available for IB3 P7 – number shown is for digest only.

3.5 Discussion

3.5.1 Comparison to previous data

Previous measurements of flux in the upper water column at the PAP site have been limited to less extensive use of PELAGRA traps between 2003 and 2006 (Lampitt *et al.*, 2008), though surface-tethered traps were used during the nearby NABE project (centred on 47 °N 20 °W) in 1989 (Martin *et al.*, 1993). There is also a relatively extensive set of time-series data available for fluxes measured in the deep ocean at the PAP site (Lampitt *et al.*, 2001; Salter *et al.*, 2010). The mass flux measured during D341 (46 – 352 mg m^{-2} d^{-1}) generally falls within the range measured at 1000 m at the site over several annual cycles (0.6 - 279 mg m^{-2} d^{-1}; Lampitt *et al.*, 2001), with only the highest measured flux (from 51 m during PAP4) above this range. The flux measured is, however, generally less than that measured in the upper water column during NABE (183 – 774 mg m^{-2} d^{-1}), though sampling during that work targeted the spring bloom period, when higher fluxes may be expected. Similarly, measured POC fluxes during D341 (0.8 – 6.9 mmol m^{-2} d^{-1}) generally overlap with those measured in the upper 750 m during NABE (2.7 – 9.5 mmol m^{-2} d^{-1}), and with previous PELAGRA deployments at the PAP site (1.3 – 8.6 mmol m^{-2} d^{-1}).

With the exception of the 1.3 mmol m^{-2} d^{-1} measured at 50 m during PAP4, the range of PIC fluxes measured during D341 fell below that measured during bloom conditions in NABE (1.23 – 1.97 mmol m^{-2} d^{-1}), but within the 0.05 – 1.66 mmol m^{-2} d^{-1} range observed in the 1000 m time-series trap deployed at the PAP site (Lampitt *et al.*, 2001). Unfortunately, no previous data could be found regarding mesopelagic bSi fluxes at PAP, but the range observed during D341 lay within that observed in the 1000 m time-series trap (3 – 700 µmol m^{-2} d^{-1}) by Lampitt *et al.* (2001).

In May 2008, PELAGRA was used to study sinking particle flux during a spring bloom in the Iceland Basin (Martin *et al.*, 2011). POC flux measured during the first three weeks of the bloom (0.8 – 2.5 mmol m^{-2} d^{-1}) corresponds fairly well with that measured during D354, but in the later stages, the 2008 bloom led to a POC flux significantly higher than that measured in 2010, and at greater depths (6.2 – 13.7 mmol m^{-2} d^{-1} measured at 400 – 750 m). The same is true for PON and PIC. For bSi, the highest fluxes measured during D354, during deployment IB3, were of a similar magnitude to those measured during the early part of the 2008 bloom. The highest bSi flux measured in

the earlier cruise was ~30 times higher than any measured during D354, while the highest mass flux was around twelve times as large.

3.5.2 Trends in organic material and biominerals

Figure 3.7 presents superimposed snapshots of particle flux in the area around the PAP site, collected over windows of 48 – 132 hours in a total observation period spanning approximately three and a half weeks. During this time, composite satellite data for an area of 100 x 100 km around the PAP site shows slight changes in chlorophyll concentrations (Figure 3.5) and primary production rate; they also indicate that the sampling commenced some 2 – 4 weeks after the peak of the spring bloom. Furthermore, the tracks taken by the traps means that total coverage spread over approximately a degree of latitude and a degree of longitude, which means that mesoscale and sub-mesoscale variations in production and export could have had significant influence upon the material collected by the traps.

These details make it a difficult task to provide simple interpretations for the distribution of flux measurements shown in Figure 3.7. The results from the K2 site during VERTIGO showed to what magnitude fluxes can change over the space of two or three weeks (Lamborg *et al.*, 2008b). What can be said is that for the calculated fluxes of mass, POC, PON and particulate phosphorus there was less variability in the values below 350 m depth, which may be due to the majority of attenuation of flux for each of these parameters at the PAP site taking place in the upper 350 m. However, this observation is based on only five measurements made below 350 m depth (and on ten from 50 – 350 m).

There is a statistically significant trend in the D341 data of greater bSi flux with increasing depth. This is an unexpected finding and is most obvious when considering the fluxes measured during the first three deployments: there is a suggestion of an increase from 51 to 446 m during PAP4, but the fluxes measured at 446 m and 589 m fall well below those measured at similar depths during the first two deployments. This suggests that the observed pattern is a temporal feature, which could have been caused by slow-sinking remnants of the earlier diatom bloom.

The distribution of particle sinking speeds has been demonstrated previously to be extensive, with faecal pellets observed to sink at rates of 5 – 220 m day^{-1} and marine snow at 16 – 368 m day^{-1} (Turner, 2002, and references therein). In the Southern Ocean Ebersbach *et al.* (2011) observed a fairly uniform distribution of sinking rates, with ~1/3 of POC sinking at >100 m day^{-1} and ~1/3 sinking at <10 m day^{-1}, while sinking particles in the eastern subtropical North Atlantic have been described as having a

bimodal distribution of settling velocities, with ~62 % of total POC flux accounted for by particles sinking at <11 m day^{-1} and ~25 % by particles sinking at >326 m day^{-1} (Alonso-González *et al.*, 2010). Particle settling experiments carried out on material collected at 50 m depth during cruise D341 also found two pools of sinking material; a fast sinking pool, consisting of marine snow aggregates and aggregate-protist complexes and with a weighted average sinking velocity of 181 ± 8 m day^{-1}, and a slow sinking pool with a sinking velocity of 0 – 18 m day^{-1} (average of 9 m day^{-1}; Riley *et al.*, 2012).

Assuming that the opal collected by trap PAP2 P7, at 565 m depth, was associated with the slow sinking fraction of material, using the average sinking velocity would mean that it could have been exported from 50 m depth around 57 days previously, in late May. This corresponds approximately to two weeks before the peak satellite-derived chlorophyll conditions shown in Figure 3.5. A faster sinking speed of 15 m day^{-1} (still within the range for the slow-sinking fraction calculated by Riley *et al.*) would allow for the collected opal to have been exported from 50 m depth during the height of the spring bloom and reach 565 m by the time of the trap deployment. Using this reasoning, the opal collected by PAP4 P7 should also have descended from 50 m depth not long after peak chlorophyll concentrations. This idea of bSi flux associated with slow sinking material is supported by evidence in the deeper PELAGRA traps of diatoms of the genus *Bacteriastrum*, which was present in surface water plankton samples (collected by Continuous Plankton Recorder) from the PAP site region during the month of May but not during the June – August period (J. Riley, *pers. comm.*).

POC and PON flux were very tightly correlated at the PAP site: Spearman's rank order correlation coefficient, r_s, was 0.991 ($P < 0.0001$, $n = 16$). However, neither bSi nor PIC fluxes showed a significant linear correlation with POC flux. This lack of relationship between biominerals and organic carbon suggest that the former were not playing a significant role in transfer of POM at the PAP site at the time of sampling. In the case of bSi, this does not include any contribution from material that may have returned to the dissolved phase while in the trap (Antia, 2005). However, given the observed trend of greater bSi flux measured at depth it is unlikely that including this would result in a significant correlation with depth-attenuated POC flux.

During D354 both multi-trap deployments showed decreasing fluxes of POC, PON and P with depth, though the rate of change with depth differed, as will be discussed in more detail in Section 3.5.3. At IB4, mass flux also decreased with depth, while there was not much change in PIC flux. The bSi flux measured during IB4 did not show the same trend observed at the PAP site during D341, though there was a slightly higher flux in the deepest trap. In contrast, measured bSi and PIC (and as a result, mass)

fluxes at IB3 were greatest in the middle trap. This could potentially be due to spatial heterogeneity in the sinking particle flux, with the 150 m trap collecting material underneath an area of slightly greater flux than the 80 m trap, or material advected from an area of higher flux. Alternatively it could be that, as at the PAP site, the 150 m trap collected slow sinking bSi-rich particles from a period of higher export flux that had already descended past 80 m by the time sampling commenced.

The different biomineral profiles at the two HLNA sites were complimented by different phytoplankton community structures, as established by Scanning Electron Microscopy (SEM) analyses of samples collected by CTD in the mixed layer and of material from the PELAGRA traps. At IB3, coccolithophores contributed ~30 % of the total cell abundance (based on enumeration of coccolithophore and diatom species), with the dominant taxa being *Syracosphaera sp*. and *Rhabdosphaera sp*., while the diatoms *Thalassiosira sp*. and *Pseudo-nitzschia sp.* each made up 30 – 35 % of the population. By contrast, IB4 showed a dominance of coccolithophores (~50% *Rhabdosphaera sp.* and ~40 % *Syracosphaera sp*. by cell numbers per unit volume), with the remainder being non-specified diatoms (A. Poulton, *pers. comm*.). Similarly, in the PELAGRA samples, at IB3, where the total number of cells counted was greater, coccolithophores contributed only 4 – 20 % of the total, with the remainder being *Thalassiosira* and *Pseudo-nitzschia*. At IB4, coccolithophores amounted to 75 % of the total cell abundance at 80 m. This number decreased with depth to 50 % at 150 m and only 2 % at 400 m, where *Pseudo-nitzschia* was the dominant genus. At each site, *Coccolithus pelagicus* numerically dominated the coccolithophore community below the 80 m trap.

Despite these differences, as at the PAP site, POC and PON fluxes measured throughout D354 showed a significant correlation, with $r_s = 0.952$ ($P < 0.0001$, $n = 8$), while there was no linear correlation between POC and bSi or PIC.

3.5.3 Attenuation of POC flux

The data from PAP4, IB3 and IB4 provide three instances of multiple PELAGRA traps being deployed concurrently at different depths. This provides an opportunity to study the change in POC flux with depth to try and ascertain how rapidly sinking organic material is remineralised at the three sites.

Figure 3.11 shows the POC flux from PAP4, IB3 and IB4 combined on one plot. Interestingly, the data points for PAP4 and IB4 all seem to fit on one curve, with the POC fluxes measured between 82 – 402 m at IB4 falling within the range observed between 51 – 589 m during PAP4, while those of IB3 are separate, with lower flux measured at all three depths. From this distribution of data it would appear that, as

well as the absolute POC flux being lower at IB3 than at IB4 and PAP4, the remineralisation of POC followed a different pattern with depth at the former site: the three data points for IB3 appear to describe a more linear decrease in POC flux with depth.

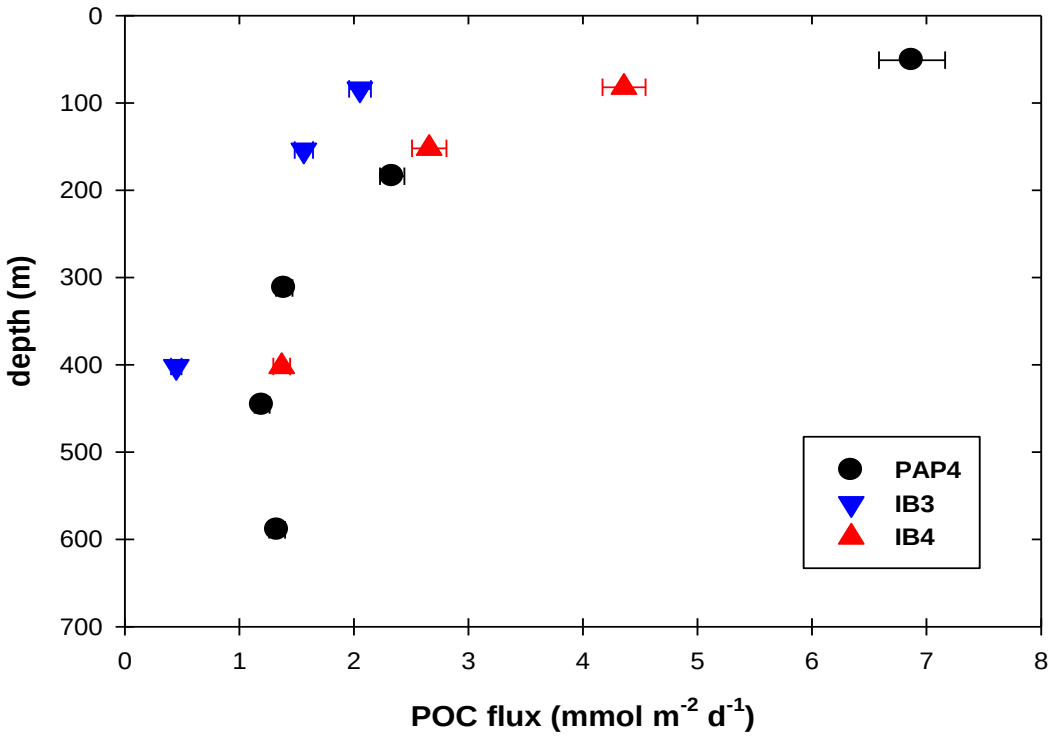

Figure 3.11: Observed POC flux profiles from PAP4 during D341 and from IB3 and IB4 during D354.

3.5.3.1 Calculation of *"b"* values for the PAP site and HLNA

As discussed in Section 3.2.2, the two contrasting sites studied during VERTIGO showed very different attenuation coefficients. In the warm, oligotrophic conditions at ALOHA, where the phytoplankton community was dominated by picoplankton, the high *b* value of ~1.3 indicated a rapid remineralisation of a large proportion of exported organic material in the upper mesopelagic. Conversely, the low value of ~0.5 observed during a large diatom bloom in the colder waters at K2 suggested that a relatively large proportion of the export flux was sinking beyond 500 m depth.

Using Equation 3.1, the flux data from D341 and D354 were used to estimate the non-linear least squares fits for the attenuation coefficient of POC flux at each site, giving values of 0.73 ± 0.10 (r^2 = 0.950) for PAP4, 0.72 ± 0.03 (r^2 = 0.998) for IB4 and 1.00 ±

0.23 (r^2 = 0.951) for IB3. The values for PAP4 and IB4 are almost identical, corroborating the apparent agreement in flux profiles shown in Figure 3.11, while the *b* value for IB3 is somewhat larger than the other two, suggesting a more rapid remineralisation of sinking POC with depth at the Irminger Basin station. IB3 does however have a relatively large standard deviation associated with it compared to the other two stations, highlighting the fact that the three data points do not give a particularly good fit to the curve described by the Martin power-law function.

These values of *b* represent the first estimates of the POC attenuation coefficient to be calculated in the Atlantic Ocean entirely from measurements made with multiple neutrally buoyant sediment traps. Table 3.5 presents a list of other *b* values calculated from mesopelagic measurements of POC flux. As there have been very few measurements made anywhere with such traps the table also includes some other relevant measurements of *b,* either made using surface-tethered traps (Martin *et al.*, 1987; Martin *et al.*, 1993) or with traps deployed at just two depths at the PAP site (Lampitt *et al.*, 2008).

Table 3.5: A comparison of mesopelagic measurements of "*b*" at a range of locations.

Location	"*b*" value	Traps used	Depth range (m)	Reference
K2 (deploy 1)	0.57	NBSTs	150 – 500	(Lamborg *et al.*, 2008b)
K2 (deploy 2)	0.49	NBSTs	150 – 500	
ALOHA (deploy 1)	1.25	NBSTs	150 – 500	(Lamborg *et al.*, 2008b)
ALOHA (deploy 2)	1.36	NBSTs	150 – 500	
VERTEX composite	0.86	tethered[a]	50 – 2000	(Martin *et al.*, 1987)
NABE	0.95	tethered[a]	150 – 2000	(Martin *et al.*, 1993)
PAP (July 2006)	1.7	PELAGRA	150 & 250	(Lampitt *et al.*, 2008)
PAP (August 2009)	0.73	PELAGRA	51 – 589	*This study (PAP4)*
Irminger Basin	1.00	PELAGRA	84 – 402	*This study (IB3)*
Iceland Basin	0.72	PELAGRA	82 – 402	*This study (IB4)*

[a] **traditional sediment traps tethered to a surface float.**

All three calculated *b* values from this study fall in between those calculated for the two North Pacific stations occupied during VERTIGO, and all three are similar to the composite value of 0.858 described by Martin *et al.* for the North Pacific VERTEX sites. The *b* value of 0.73 calculated following PAP4 was lower than that determined at the

same location in 2006 (b = 1.7; Lampitt *et al.*, 2008). However, in that earlier work the attenuation coefficient was estimated from only two POC flux measurements, which leaves considerable ambiguity over the shape of the associated flux profile, given the scatter around the fitted functions seen in the original VERTEX work.

The PAP4 b value is also slightly lower than that calculated from surface-tethered trap data collected at a relatively close location during NABE (47° N 20° W; b = 0.95), suggesting a longer remineralisation length scale in this more recent study. This seems surprising as the NABE measurements were made towards the end of the spring bloom, compared to several weeks after the bloom peak for PAP4, and so it may be expected that the NABE flux attenuation would more closely resemble that during the large diatom bloom at K2 (*i.e.*, have a lower b value). There were, however, methodological differences between the PAP4 and NABE flux measurements. While the work carried out during NABE covered a greater depth range than that at PAP (150 – 2000 m), it did not include traps deployed in the upper water column where the greatest flux attenuation takes place. Additionally, the b value of 0.95 was calculated by pooling flux measurements from three separate two-week deployments of traps, spanning April 24th – June 1st and so represents an integration of temporal changes in flux magnitude as well as depth-related attenuation of POC.

In the high latitude North Atlantic, the higher attenuation coefficient calculated for POC flux at IB3 than at IB4 may suggest that material collected at the former shares more characteristics with that collected at station ALOHA and the latter with material collected at K2. Figure 3.12 shows the relative proportions of the four main flux components in material collected at PAP4, IB3 and IB4: particulate organic material (POM), opal, calcite ($CaCO_3$) and lithogenic material. The POM flux was determined by multiplying mass flux of POC by 2.2 (Klaas and Archer, 2002; Lamborg *et al.*, 2008b), $CaCO_3$ by multiplying mass flux of Ca by 2.5 (based on atomic and molar masses of Ca and $CaCO_3$), opal by multiplying bSi mass flux by 2.4 (Mortlock and Froelich, 1989), and lithogenics by multiplying Al flux by 12.56 (Wedepohl, 1995). Table 3.6 compares the range in values observed for the three sites to those recorded at K2 and ALOHA.

It is evident from the figure that in some cases the total of the four fractions adds up to slightly more than 100 % of the total mass measured and in some cases to a little under the total. This is in part due to the uncertainty associated with each measurement from the methods used and may also be partly due to the conversion factors used. The translation from bSi to opal as described by Mortlock and Froelich is based upon an average water content of diatomaceous silica of 10 % (*i.e.*, opal = $SiO_2.0.4H_2O$), though it is plausible that the average value in any one location varies according to seasonal and other controls. Conversion of POC to POM followed the value of 2.2 used by Klaas and Archer, but values used in the literature range at least

from 1.87 (Anderson, 1995) to 2.3 (Jickells *et al.*, 1998). Similarly the conversion of Al to lithogenic flux was based upon the average crustal abundance of aluminium of 7.96 % by weight. The other global average estimates are similar to this value (*e.g.*, 8.04 % (Taylor and McLennan, 1995)), but regional variations away from this value may be more significant (*e.g.*, 7.1 % Al in Saharan dust (Guieu *et al.*, 2002), 4.5 % Al in Australian soil/dust (Frew *et al.*, 2006)).

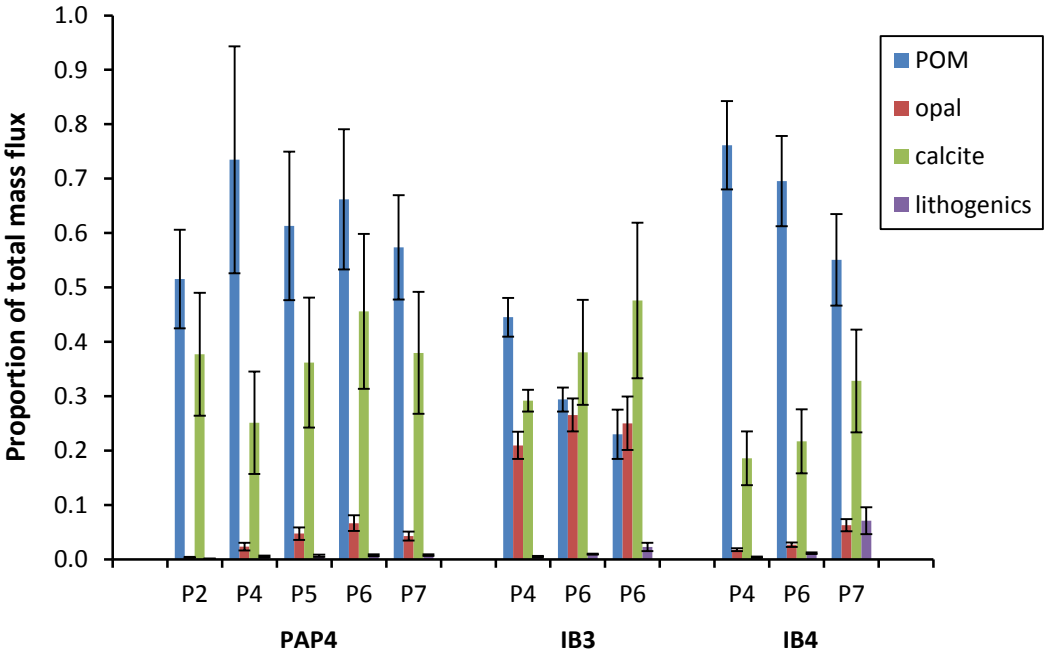

Figure 3.12: Composition of material collected in PAP4, IB3 and IB4 traps, by proportion of total mass flux.

Table 3.6: Relative contributions (by weight) of the four main flux components to material collected during PAP4, IB3, IB4 and at the VERTIGO stations.

	IB3	IB4	PAP4	ALOHA	K2
POM	23 – 45 %	55 – 76 %	52 – 73 %	~40-70 %	~10 %
Opal	21 – 27 %	2 – 6 %	<1 – 7 %	~10 %	~80 %
$CaCO_3$	29 – 48 %	19 – 33 %	25 – 46 %	~15 – 35 %	<6 %
Lithogenics	<1 – 2 %	<1 – 7 %	<1 %	~10 %	<6 %

Figure 3.12 and Table 3.6 show that it is actually the material collected at IB4 (and at PAP4) which has the higher proportion of POM, and relative proportions of the four

main flux components more similar to ALOHA. The material collected at IB3 appears to be intermediate in character between ALOHA and K2: a lower percentage of the content is POM than at ALOHA, but higher than at K2, while the opposite is true for opal. This suggests that it is not a high relative POC content that causes a rapid attenuation in POC flux, or a high relative biomineral content that leads to low POC flux attenuation, as may have been inferred from the VERTIGO data alone; evidently other characteristics of a region need to be considered in order to explain or predict POC flux attenuation.

Kwon *et al.* (2009) highlight that the remineralisation depth of POC is dependent on the balance between sinking speed of particles containing organic material and the rate of decay of that material. Factors proposed as important in controlling the remineralisation of exported POC or its transport through the water column include concurrent mineral fluxes (Armstrong *et al.*, 2002), particularly calcite (Klaas and Archer, 2002), which may increase the sinking speed or protect organic material from remineralisation; oxygen concentrations, with lower oxygen acting to lower the rate of microbial respiration (Devol and Hartnett, 2001); export flux magnitude, with a positive correlation between *b* and POC export at 100 m demonstrated by Berelson (2001). Additionally, processes that have been identified as important in determining the fraction of primary production that is exported from the surface ocean – notably plankton community structure, total chlorophyll concentration and water temperature (Dunne *et al.*, 2007) – may also be influential in determining flux attenuation in the mesopelagic.

The calculated *b* values for the VERTIGO sites, PAP site and high latitude North Atlantic were plotted against various properties measured at the time of or just prior to sampling, in an attempt to gauge any correlations and thus highlight possible factors in setting the remineralisation length scale. A selection of the scatter plots are shown in Figure 3.13. Properties looked at were percentage contribution to total mass of biominerals/lithogenics (individually and combined) in the 150 m trap or averaged over all traps, molar ratios of the two biominerals to POC, magnitude of POC flux at 100 m (extrapolated using the calculated *b* values), temperature and oxygen concentrations averaged over either the mixed layer or various extents of the upper 500 m, and concentrations of dissolved nutrients in the upper water column. The results show very little correlation between upper ocean POC flux attenuation and calcite content of the sinking material (Figure 3.13*a*), or indeed any of the permutations of biomineral/lithogenic material fluxes that were used (*e.g.*, Figure 3.13*b,c*). Similarly, no significant correlations were found between *b* and the upper water column PIC/POC ratio (Figure 3.13*d*), the 100 m POC flux (not shown), or upper ocean nutrient concentrations (*e.g.*, phosphate, Figure 3.13*e*).

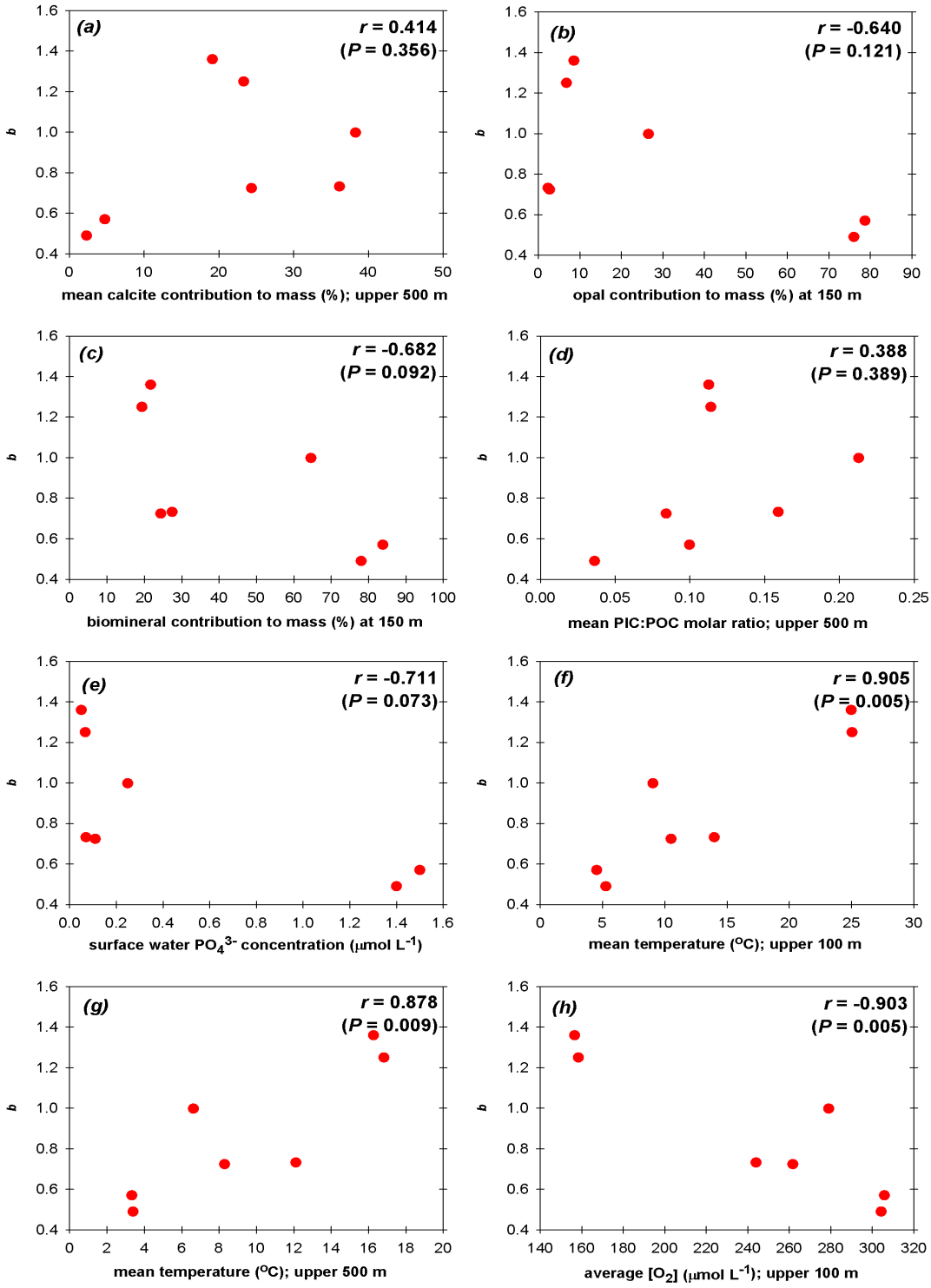

Figure 3.13: Selected plots of *b* versus various properties of the water column/sinking particulate material, with details of any correlation found (using Pearson product-moment correlation; *P* <0.05 is considered significant). For all plots, *n* = 7. Parameters are: *(a)* mean calcite contribution to mass in traps over upper 500 m, *(b)* opal contribution to mass in 150 m trap, *(c)* biomineral contribution to mass in 150 m trap, *(d)* mean PIC:POC ratio of trap material, *(e)* surface water phosphate concentration, *(f)* mean temperature over upper 100 m, *(g)* mean temperature over upper 500 m, *(h)* mean O_2 concentration over upper 100 m.

However, all of the correlations between *b* and water column temperature (whether considering the mixed layer temperature or the average temperature over the upper 100 m, 200 m... up to 500 m; *e.g.*, Figure 3.13*f,g*) were significant (Pearson Product Moment correlation, $P < 0.05$), with the highest correlation coefficient being that using the average temperature over the upper 100 m of the water column ($r = 0.905$, $P < 0.01$, $n=7$). This suggests that, at least in this small dataset, the attenuation of POC flux in the mesopelagic is more closely linked to variations in upper water column water temperature than to any metric of biomineral content of the sinking material.

Oxygen concentration over the upper water column was also found to be correlated with the calculated attenuation coefficients, though negatively so (Figure 3.13*h*). Statistically significant correlations ($P < 0.05$) were found using the mixed layer and upper 200 m average O_2 concentrations, but the most significant was that between *b* and the average O_2 concentration over the upper 100 m ($r = -0.903$, $P < 0.01$, $n = 7$). As the relationship between O_2 concentration and *b* is an inverse one, it seems more likely that, rather than oxygen concentration determining *b* through capacity for microbial respiration in the upper water column, as proposed by Devol and Hartnett (2001), in this case it is the remineralisation efficiency within the upper water column that is causing lower oxygen concentrations (*i.e.*, a relatively high remineralisation rate, as at ALOHA, uses up more oxygen, resulting in lower concentrations).

This dataset is relatively small, and it is possible that the observed correlations are forced to a certain extent by the ALOHA data, which shows substantially higher temperature and lower oxygen as well as a higher attenuation coefficient than any of the other stations. Hopefully the dataset can be added to through measurements made in other regions with different characteristics (*e.g.*, upper water column temperatures of <5 °C or 15 – 25 °C, to fill in the gaps in Figure 3.13*a*).

For each station, PAP4, IB3 and IB4, the Martin curve was also applied to measured PON fluxes, with respective *b* values of 0.82 ± 0.13 ($r^2 = 0.93$), 0.91 ± 0.18 ($r^2 = 0.96$) and 0.86 ± 0.08 ($r^2 = 0.99$) respectively. For PAP4 and IB4, these values are higher than the respective values for POC, indicating that PON in sinking material was remineralised more rapidly with depth than POC, and consistent with observed increases with depth in the C/N ratio of material collected. For IB3, the *b* value of POC is slightly higher than that for PON, while the C/N ratio did not show a clear trend with depth.

3.5.3.2 Implications of the calculated *"b"* values

The attenuation coefficients calculated using data from cruises D341 and D354 have been used to extrapolate the measured POC flux over the depth range 100 – 1000 m, with the same done for the results from VERTIGO. These fluxes were then normalised to 100 m in order to directly compare the attenuation of flux with depth (Figure 3.14). In this way, the canonical Martin *"b"* value of 0.858 implies that, of the POC flux at 100 m depth, approximately 14 % sinks as deep as 1000 m, with the rest being remineralised in the mesopelagic. The plot shows that, for this small data set, K2 and ALOHA represent extremes in variation from this pattern, with only around 5 % of the 100 m POC flux at ALOHA sinking past 1000 m, compared to ~30 % at K2. The PAP site and Iceland Basin data each show a slightly more efficient biological pump than suggested by the VERTEX work, with 19 % of the 100 m flux sinking deeper than 1000 m, while the Irminger Basin measurements show a slightly lower efficiency of POC sequestration, despite the higher biomineral content of the material sampled at that site compared to IB4 and PAP4.

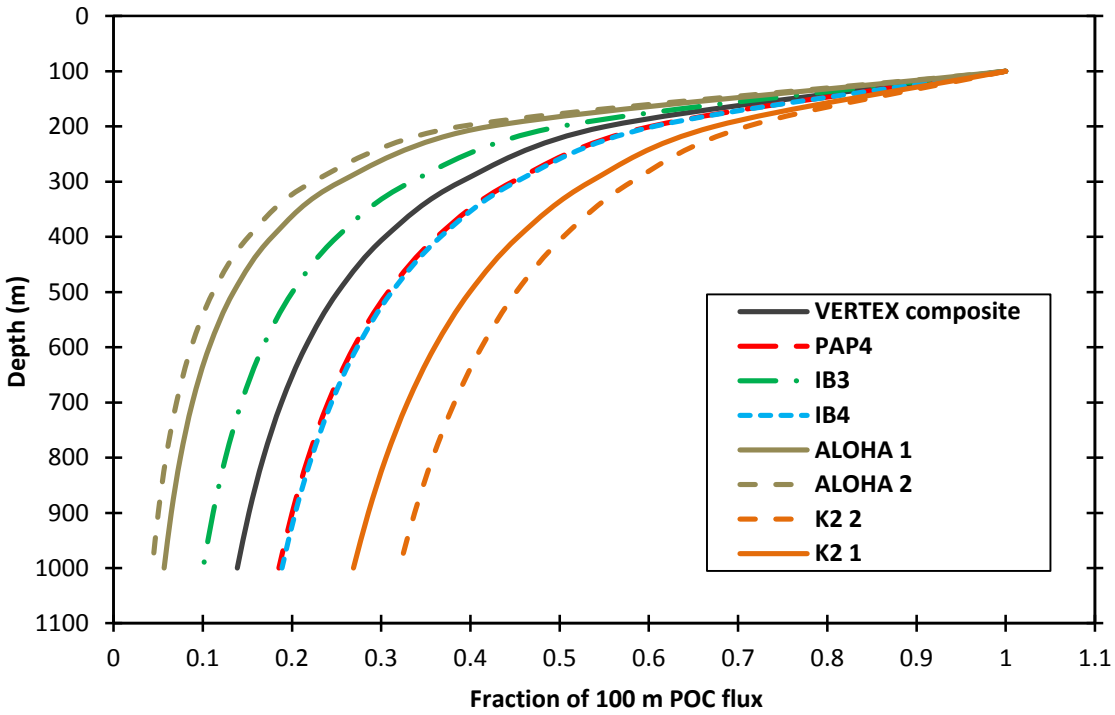

Figure 3.14: Comparison of POC flux attenuation for Pacific and Atlantic Ocean sites, using calculated *b* values and flux normalised to 100 m.

Using the POC flux measured at 80 m and the calculated *b* values for each station during D354, the flux was extrapolated to the base of the euphotic zone, using the observed average euphotic zone depth of 40 m. This gave an estimate for the export flux at the time of sampling at IB3 (26th – 28th July) of 4.3 mmol m^{-2} d^{-1}. The satellite derived estimate of export production for the Irminger Basin at around the time of IB3 (20th – 27th July) was ~14 mmol m^{-2} d^{-1}, a factor of three greater. Similarly, the satellite-derived estimate for the Iceland Basin and Reykjanes Ridge regions over the period 28th July – 12th August were ~9 and ~ 12 mmol POC m^{-2} d^{-1}, compared to the 7.3 mmol m^{-2} d^{-1} extrapolated by trap measurements during IB4 (4th – 6th August). The values for both regions are given here because the area where the traps were deployed and recovered during IB4 lies approximately where the distinction between the two was made when the satellite data was processed.

All of the satellite-estimated fluxes are higher than those derived from the PELAGRA traps. However, comparison between the two estimates should be treated with caution. The algorithm used for satellite-derived export estimates is based on a sea-surface temperature to export ratio algorithm (for which the relationship shows greater scatter at colder temperatures; Henson *et al.* (2011)), multiplied by the satellite-derived primary production estimate, the algorithm for which also has an error of ~40 % associated with it. Additionally, satellite data is based on measurements made of the ocean surface only, rather than the entire mixed-layer, and so can misrepresent the characteristics of the latter as a whole. Furthermore, the values used in calculating the satellite data were averaged over a 1˚ x 1˚ grid, with the final figure for each region consisting of an average of all the grid-squares in that region. Thus, the satellite-derived estimate represents a large-scale integration of POC export, whereas the PELAGRA data measured a relatively local contribution to that value.

Extrapolating PELAGRA-measured POC fluxes at IB3 and IB4 to 50 m depth gave estimated fluxes at that depth of 3.4 and 6.2 mmol m^{-2} d^{-1} respectively, while estimates derived from ^{234}Th measurements on particles >53 µm made at around the same time were 8.9 ± 4.5 and 9.5 ± 1.5 mmol C m^{-2} d^{-1} respectively (F. Le Moigne, *pers. comm.*). These values, though slightly higher than the values extrapolated from PELAGRA, agree reasonably well. It should be considered that the ^{234}Th method measures particle flux integrated over a period of ~1 month, as opposed to the 2 – 3 days measured by the traps, and so the higher values obtained by the former may be influenced by greater flux in the days/weeks before the traps were deployed. By the same argument, the slightly lower Th-derived POC flux measured just prior to commencement of sampling for PAP4 (3.8 ± 0.8 mmol m^{-2} d^{-1} *cf.* 6.9 ± 0.3 mmol m^{-2} d^{-1} measured by the PELAGRA trap) may reflect generally lower POC flux in the days running up to the trap deployment.

Annual export production for the Irminger Basin has been estimated at ~60 g POC m^{-2} yr^{-1} using satellite-based measurements of sea-surface temperature and chlorophyll *a* concentrations (Henson *et al.*, 2006). Using the *b* value calculated during IB3 and assuming the depth for the base of the euphotic zone to remain between 30 – 60 m, gives an estimate of 1.8 – 3.6 g POC m^{-2} yr^{-1} sinking beyond 1000 m depth (taken as being beyond the typical depth of winter convective mixing) in the region. Considering the uncertainty associated with this *b* value (~23 %; $b = 1.00 \pm 0.23$) the estimate for flux beyond 1000 m becomes 0.8 – 6.9 g POC m^{-2} yr^{-1}. This value does however rely on many assumptions including the attenuation of POC following the same trend over an annual cycle.

3.5.4 Measurements of particulate iron flux

The calculated fluxes of iron (and Al and Mn) shown in Tables 3.2 and 3.4 are based upon the combined measurements of leachable and refractory forms of the metal(s) associated with particulate material collected on filters while processing sediment trap sample cups. It was hoped that using this two-step approach would provide information about the labile fraction of iron (consisting of iron weakly adsorbed onto organic matter and associated with amorphous oxyhydroxides and carbonates). In most cases, however, the leachable fraction of pFe was below the detection limit resulting from process blank analysis. In the few instances where this was not the case, it was calculated to contribute 1 – 6 % of the total pFe.

The flux data do not include any correction for potential solubilisation of particulate metals between material entering the sample cups and processing of the samples. Degradation of material can occur between sample collection and processing, particularly in time-series traps that are deployed for long periods, and this results in elevated concentrations of certain elements in the collection cup supernatant (Antia, 2005). Previous studies that have looked at in-trap solubilisation of trace metals by analysis of the supernatant suggest that Fe remains mostly (>95 %) in the particulate phase, even in trapping experiments where several months elapse between sampling and processing (Knauer *et al.*, 1984; Kuss and Kremling, 1999b; Pohl *et al.*, 2004). In contrast, the same studies found that a significant proportion of the total Mn in a trap can be found in dissolved form, even after short trap deployments (*e.g.*, >70 % (Knauer *et al.*, 1984), 49 ± 21 % (Pohl *et al.*, 2004)). Measurements of dissolved aluminium in the supernatant are less common, but in deep-sea traps deployed for 5 – 12 months it was found that <1 % of the total aluminium was in dissolved form (Kuss and Kremling, 1999b). Based on this information, it is assumed that no significant correction is

needed of the iron and aluminium fluxes shown in Tables 3.2 and 3.4, but that the manganese values may be too low by a factor of 2 – 5.

As mentioned previously, there have been relatively few measurements of pFe associated with sinking material in the mesopelagic. Table 3.7 summarises fluxes measured between 50 – 800 m depth using sediment traps, including the values from this work. The fluxes measured using PELAGRA in the North Atlantic comfortably fall within the range observed during previous work at open ocean sites, which include studies in the Pacific and Southern Oceans and at the BATS site in the subtropical North Atlantic. The lowest iron fluxes listed were observed in the Southern Ocean (0.07 – 0.2 μmol m^{-2} d^{-1}) and in HNLC waters southeast of New Zealand (0.2 – 0.6 μmol m^{-2} d^{-1}), though some of the measurements made at the PAP site were below the method detection limit of ~0.1 μmol m^{-2} d^{-1}.

Of the data in Table 3.7, those of Lamborg *et al.*, Frew *et al.,* Ho *et al.* and Quetel *et al.* include measurements made simultaneously at two or more depths and they show no common trend between Fe flux and depth. The FeCycle measurements consisted of concurrent deployments of two separate surface-tethered sediment trap arrays, with traps at 80 m and 120 m on each (Frew *et al.*, 2006). One trap array recorded a greater iron flux at 80 m than at 120 m, while the reverse was true for the second array. Part of the DYFAMED dataset includes results from traps deployed at both 80 m and 200 m: in eight of the eleven time periods, iron flux measured by the 200 m trap was greater than that measured at 80 m (Quétel *et al.*, 1993). Ho *et al.* (2010) also observed both trends in traps at 100 m and 160 m, while data from the same time period at 120 m and 600 m on a moored trap generally showed greater flux in the deeper trap during periods of low flux at 120 m, but the opposite trend during periods of higher shallow flux. The measurements of pFe flux at the VERTIGO sites found no significant change with depth at ALOHA, consistent with a steady-state supply and removal of aeolian dust inputs, but a greater flux with depth at K2, which was ascribed to the influence of a plume of material laterally advected from a continental shelf (Lamborg *et al.*, 2008a).

3.5.4.1 PAP site Fe data

The combined pFe flux measurements from the PAP site, shown in Figure 3.7*g*, do not show a clear trend with depth. Only two measurements were above 1 μmol m^{-2} d^{-1}, both during PAP1. These measurements may signify a dust event having occurred in the region prior to the cruise – certainly aluminium flux in the deepest trap from PAP1 was also elevated. The profile of pFe flux from PAP4 shows values of ~500 – 750 nmol m^{-2} d^{-1} in the upper 300 m, dropping to 180 nmol m^{-2} d^{-1} in the two deeper traps (below the detection limit resulting from process blank measurements).

Table 3.7: Particulate iron (pFe) fluxes measured by neutrally buoyant, free-drifting or moored sediment traps between 50 - 800 m depth.

pFe flux (μmol m^{-2} d^{-1})	Site/region	Depth range (m)	Trap type	Reference
0.6 – 9.9	High latitude N. Atlantic	80 – 400	PELAGRA	This study
<~0.1 – 2.2	PAP	50 – 670	PELAGRA	This study
1.4 – 9.0/11.5	K2	150 – 500	NBSTs/surface tethered	(Lamborg *et al.*, 2008a)
1.7 – 5.8/6.7	ALOHA	150 – 500	NBSTs/surface tethered	(Lamborg *et al.*, 2008a)
1 – 18	BATS	150	NBSTs	(Stanley *et al.*, 2004)
0.22 – 0.55 (total) 0.11 – 0.35 (bio) 0.11 – 0.20 (lith)	HNLC region, SW Pacific	80 – 120	Surface-tethered	(Frew *et al.*, 2006)
0.07 – 0.2	Southern Ocean	150	Surface-tethered	(Bowie *et al.*, 2009)
~1.2	N. Pacific (16°N,107°W)	150	Surface-tethered	(Knauer *et al.*, 1984)
33 – 69	South China Sea	100, 160	Surface-tethered	(Ho *et al.*, 2010)
0.2 – 79.3	South China Sea	120, 600	Moored	(Ho *et al.*, 2011)
0.4 – 62	Mediterranean Sea	80 – 200	Moored	(Quétel *et al.*, 1993)
1.3	BATS	500	Moored	(Huang and Conte, 2009)
<10 – 140	Gotland Basin	120	Moored	(Pohl *et al.*, 2004)

The iron to aluminium ratio for the D341 data (Figure 3.15*a*) showed a significant trend of decreasing Fe/Al with increasing depth (Spearman's rank-order coefficient, r_s = -0.732, $P < 0.01$), with values in the upper 300 m elevated over that of the typical crustal ratio (*e.g.*, 0.19 mole Fe/mole Al; Wedepohl, 1995). In previous work (*e.g.*, Frew *et al.*, 2006; Planquette *et al.*, 2011), the average crustal ratio of Fe to Al has been used to determine the amount of Fe in particulate material that is lithogenic in nature and so to estimate the biogenic Fe fraction by difference of the lithogenic fraction from the total. Doing so here using the Wedepohl value for crustal Fe/Al of 0.19, the resulting "biogenic Fe" flux values are plotted against depth in Figure 3.15*b.*

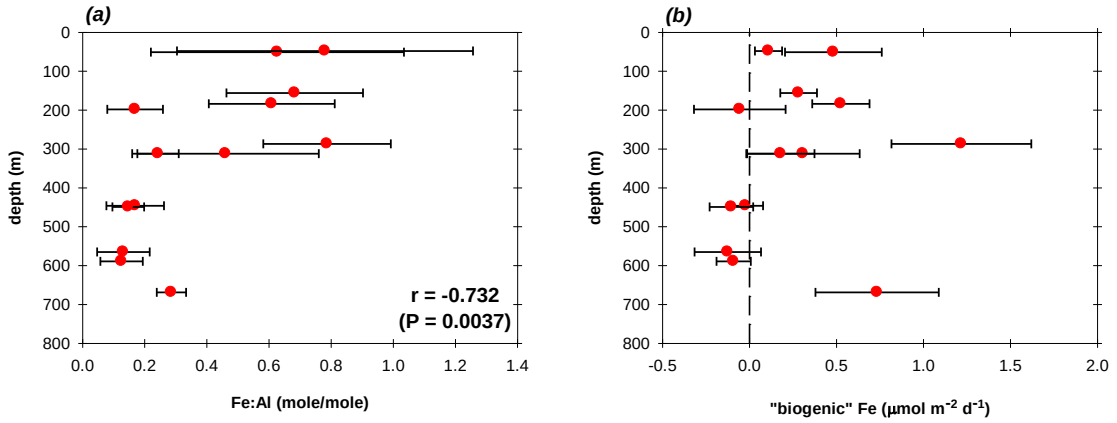

Figure 3.15: Plots for D341 data of *(a)* Fe/Al molar ratio against depth, and *(b)* "biogenic" Fe against depth. Biogenic pFe is calculated by assuming an average crustal Fe/Al of 0.19 (Wedepohl, 1995) and applying this to the measured pAl flux to estimate lithogenic pFe flux, then subtracting this from the total pFe flux. The dashed line is included to highlight that some of the calculated biogenic pFe fluxes are < 0 µmol m^{-2} d^{-1}.

Several of the resultant "biogenic" pFe (bioFe) fluxes are <0 µmol m^{-2} d^{-1}, though not by values greater than the related uncertainties. In these cases, it seems that no biogenic iron was associated with the sinking material and that, either some of the lithogenic iron had been accessed and utilised and then remineralised, or that excess aluminium had been scavenged onto the material from the surrounding water column, resulting in an over-estimate of the lithogenic pFe fraction. These values include all but one of the fluxes calculated for samples collected deeper than 400 m (the exception being the deepest trap from the very first deployment), suggesting that biogenic pFe was mostly remineralised in the upper 400 m.

For the remaining data, the resulting bioFe/POC ratio ranged from 33 – 690 µmol mol^{-1}, which is generally higher than the range of ~3 - ~100 µmol mol^{-1} cited for phytoplankton stoichiometry from previous studies (tabulated in King *et al.*, 2012). This discrepancy may however be due to "luxury uptake" of Fe by phytoplankton in an iron replete environment (Sunda and Huntsman, 1995) or to contribution from a non-

lithogenic, non-biogenic fraction of sinking particulate iron flux. For example, Ho *et al.* (2010) highlighted the contribution of anthropogenic aerosol deposition to the South China Sea to explain similarly Fe-enriched sinking particles. The fact that this component appears to be absent from material sinking beyond 300 m (*i.e.*, Fe/Al approaches crustal values) may however suggest that it, like the biogenic iron, is more labile and more easily lost to the dissolved phase as the material sinks.

It should be noted that the choice of lithogenic Fe/Al ratio has a major influence on interpretation of the partitioning of Fe between lithogenic and biogenic pools in this way. As well as the value of 0.19 used here and by others (Frew *et al.*, 2006; King *et al.*, 2012), a value of 0.33 (from Taylor (1964)) is often used (Ho *et al.*, 2007; Lamborg *et al.*, 2008a), while Planquette *et al.* (2009) used a value of 0.51 based on the average Fe/Al ratio of crustal basalt in the vicinity of the study area. Using the higher global average estimate (0.33) here would result in more negative values for bioFe flux. Unfortunately there is no aerosol data available for the PAP site at the time of the PELAGRA sampling and so application of any "input" Fe/Al ratio is merely speculation. Though the north-eastern North-Atlantic is known to be influenced by episodic inputs of Saharan dust (Arimoto *et al.*, 1995), backward air mass trajectory analysis carried out for the site for the weeks immediately before and during the cruise (carried out using the NOAA Air Resources Laboratory HYSPLIT model (Draxler and Rolph, 2012)) suggest that, at the time, air masses reaching the PAP site typically had arrived from the west or north of the PAP site, rather than from the south.

3.5.4.2 High latitude North Atlantic iron data

The pFe flux data for IB3 and IB4 showed a similar change between 80 m and 150 m, both increasing approximately two-fold (Figure 3.10*g*). However, whereas the 400 m trap from IB3 recorded a flux intermediate between the two shallower traps, that at IB4 collected the highest pFe flux measured in this study, roughly five-fold greater than that at 150 m during the same deployment. The same is true for pAl and pMn. The three metals show statistically significant correlations with each other when considering the entire D354 dataset ($P < 0.001$, using Spearman's rank correlation; $n = 8$): for pFe and pAl, plotted in Figure 3.16*a*, the correlation coefficient, $r_s = 0.905$, for pFe and pMn, $r_s = 0.833$, and for pAl and pMn, $r_s = 0.952$. Though influenced to a certain extent by the high fluxes of each measured by IB4 P7, these correlations remain if that sample is not considered. This would suggest that most of the pFe collected by PELAGRA during cruise D354 was lithogenic in origin, a hypothesis given support by the lack of a significant correlation between pFe and POC ($P = 0.46$).

Figure 3.16*b* shows the Fe/Al of D354 samples plotted against depth, with vertical lines representing commonly cited crustal average values of 0.19 and 0.33. All of the measured values lie above these two ratios, suggesting that the source material over the region has a higher Fe/Al ratio than the global crustal average, either through Fe-enriched lithogenic material (relative to the global average) or through deposition of aerosols that are anthropogenically enriched in Fe, or through the influence of hydrothermal activity. The calculated Fe/Al values for IB4 (0.54 – 0.72) were all higher than those at the other stations (0.36 – 0.44).

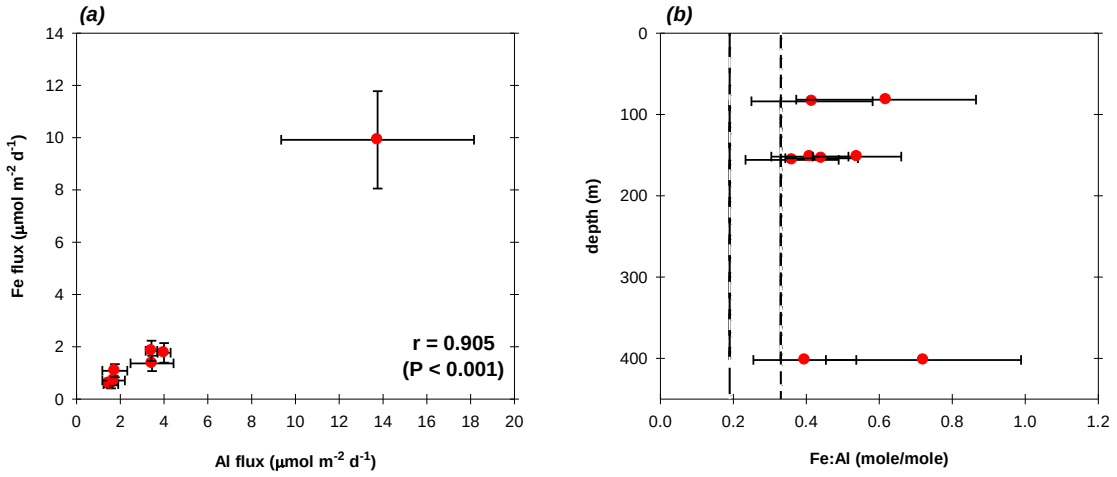

Figure 3.16: *(a)* correlation between Fe and Al fluxes during D354, with Spearman's rank-order correlation coefficient, r_s = 0.952 (*P* < 0.001, *n* = 8). *(b)* Fe/Al molar ratio of D354 sinking particles plotted against depth. Dashed lines represent estimates of global crustal average Fe/Al ratio: long-dashes = 0.19 (Wedepohl, 1995), short-dashes = 0.33 (Taylor, 1964).

Aerosol samples collected during D354 showed a mean Fe/Al ratio of 0.21 ± 0.04 mol mol^{-1}, similar to the global crustal average of 0.19 calculated by Wedepohl (1995). The average dust deposition rate during the cruise was calculated to be 151 ± 60 µg m^{-2} d^{-1}, based on Al concentrations measured using a high-volume collector, an average Al concentration in crustal material of 8 % by mass (Wedepohl, 1995), and an assumed deposition velocity of 0.7 cm s^{-1} (A. Baker, *pers. comm.*). This falls short of the lithogenic flux calculated from particulate Al measured in PELAGRA trap samples (317 – 2969 µg m^{-2} d^{-1}). Though model estimates for annually averaged atmospheric dust input to the region (~550 – 2740 µg m^{-2} d^{-1}; Jickells *et al.*, 2005; Mahowald *et al.*, 2005) are more comparable to the sediment trap measurements , the low measured values and lower Fe/Al ratio of the aerosol material suggest that another source contributed to the observed flux.

A study into the composition of basalts dredged along the mid-Atlantic Ridge by Schilling *et al.* (1983) estimated an average (± 1σ) value for the Fe/Al ratio along the

Reykjanes Ridge section of 0.61 ± 0.08. This is much closer to the values observed during IB4, which was carried out just to the east of the Reykjanes Ridge. It is possible that the high Fe/Al ratios measured in sinking particles during this deployment are due to the influence of material that had been resuspended from the ridge or the continental shelf and advected laterally through the basin; an explanation that would also account for the relatively high fluxes of pFe, pAl and pMn measured at 400 m during this deployment. Dissolved Fe and Al data from a CTD deployment in the general vicinity (61.92 °N 26.28 °W) of the trap deployment give some support to this idea, with evidence of increased concentrations at ~400 m over the ridge (1.6 nM dFe, 13 nM dAl). Additionally, Holliday *et al.* (2006) show the surface and mid-depth currents in the area around IB4 as being dominated by south-westerly flow along the length of the ridge from the Icelandic continental shelf, a situation which could result in lateral transport of shelf material in the area. The mixing of such basaltic material with atmospheric inputs could also account for the observed Fe/Al ratio of material collected during IB3.

Alternatively, it is possible that the IB4 values show a hydrothermal influence. Although the Reykjanes Ridge is a known spreading centre as part of the Mid-Atlantic Ridge, there has only been one hydrothermal vent-field reported in the region; the Steinahóll vent-field at 63.1 °N 24.5 °W, where a plume has been documented in ~350 m water depth (German *et al.*, 1994; Ernst *et al.*, 2000). However, this is within ~50 nautical miles of the deployment location of the IB4 PELAGRA traps. The elevated metal flux measured by the 400 m trap, along with the elevated Fe/Al ratio for that material (0.72) is consistent with the material collected being influenced by a lateral plume of iron-enriched material originating at the vent-field.

The calculated Fe/C ratios for material collected by each PELAGRA trap during D354 indicate a significant lithogenic contribution, with a range of 249 – 7240 μmol mol^{-1}, compared to 3 – 136 μmol mol^{-1} measured in previous studies of natural phytoplankton assemblages (King *et al.*, 2012 and references therein). Similarly, the values measured for Fe/N ratio in trap material (~2500 – ~90,000 μmol mol^{-1}) were much greater than the value of ~470 μmol mol^{-1} suggested for the elemental stoichiometry of marine phytoplankton by Ho *et al.* (2003).

Conversely, from the aerosol samples collected during D354, it is estimated that the dry deposition of operationally defined soluble Fe to the region averaged ~ 6.5 nmol Fe m^{-2} d^{-1} over the three week period from 17th July – 6th August (A. Baker, *pers. comm.*). If it is assumed that this represents the only supply of bioavailable Fe to the surface ocean during the cruise and that the system was in a steady state, it could be expected that the biogenic iron flux would also be of the order of 6.5 nmol Fe m^{-2} d^{-1}. Combining

this figure with the 80 m POC and PON fluxes measured during IB3 and IB4 of 2.05 and 4.36 mmol POC m^{-2} d^{-1} and 0.24 and 0.44 mmol PON m^{-2} d^{-1} respectively, would result in bioFe/POC and bioFe/PON ratios of 1.5 – 3.2 μmol mol^{-1} and 14.8 – 27.1 μmol mol^{-1} in that order. In this case, the bioFe/PON ratio is well below the ratio of Fe/N in marine phytoplankton of ~470 μmol mol^{-1} suggested by Ho *et al.*, while the bioFe/POC ratio falls correspondingly short of the ~60 μmol mol^{-1} suggested in the same study and almost all of the previously published phytoplankton Fe/C values (King *et al.*, 2012).

The low ratios indicate that the proposed input of 6.5 nmol m^{-2} d^{-1} of soluble aerosol iron represents a minimum estimate of iron input. The soluble iron input quoted here is an operationally defined value determined by leaching the sample at pH 4.7 with ammonium acetate and may not be an accurate representation of the fraction of total aerosol iron that is biologically available. Neither does it take into consideration inputs of iron by wet deposition during the same time period. Additional sources of iron to the euphotic zone, such as vertical turbulent flux are also likely to be extant.

3.6 Summary

Measurements of biogenic and lithogenic contributions to sinking particulate flux were made using multiple PELAGRA neutrally buoyant sediment traps during two research cruises in the North Atlantic. Similar magnitudes of flux were observed at the PAP site (49 °N 16.5 °W) and at two sites in the high latitude North Atlantic. Fluxes measured at the PAP site sat within the range of observations made at the site from previous PELAGRA deployments and a time-series trap deployed at 1000 m depth, while fluxes measured in the Iceland Basin were significantly lower than those measured during a large export event associated with a spring diatom bloom.

An observed trend of higher opal flux with increasing depth observed at the PAP site suggests a contribution to sinking flux in the mesopelagic of a slow-sinking fraction which includes the remains of diatoms present at the site during the peak of the spring bloom some two months earlier. No correlation was found during either cruise between POC flux and opal, calcite or combined biomineral flux.

The PELAGRA traps were also used to measure the sinking flux of particulate iron during the two research cruises. Comparison of Fe data to that of Al and Mn suggests that in the Irminger and Iceland Basins, Fe flux was dominated by lithogenic material, with evidence of lateral advection of material from the continental shelf or the Reykjanes Ridge observed at 400 m depth in the Iceland Basin. At the PAP site, lack of correlation between Fe and Al data suggests that the lithogenic fraction did not appear to be as dominant as at the HLNA sites, while the decrease in Fe/Al ratio with depth

may indicate a preferential remineralisation of iron over aluminium in the upper water column, as the biogenic fraction is broken down. A lack of information about the Fe/Al ratio of source materials is, however, a hindrance to determining relative contributions from biogenic and lithogenic material.

During both cruises, measured fluxes of pFe showed a similar range (0.3 – 2.2 μmol m^{-2} d^{-1} during D341 *cf.* 0.6 – 9.9 μmol m^{-2} d^{-1} during D354), as did pAl, POC and PON. However, the observed Fe/C and Fe/N ratios of material collected during D354 showed greater ranges and were generally higher, and showed more significant increases with depth, suggesting greater loss of pFe from the upper ocean relative to POC and PON than at PAP site. If a typical characteristic, this could have important consequences for the HLNA region in terms of development of seasonal iron limitation. However, if the greater observed increase in Fe/C is due to additional material being advected from the continental shelf and gradually sinking (*i.e.*, not material that has sunk from the surface mixed layer) this would not necessarily be the case.

The measured POC flux at the PAP site and in the Irminger and Iceland Basins was used to estimate values for each location of the attenuation coefficient, *b,* and these values combined with those calculated in the North Pacific during the VERTIGO programme to give a small dataset of *b* values determined by neutrally-buoyant sediment traps deployed at mesopelagic depths. The widely used Martin curve, with a set *b* of 0.868 for the global ocean, has been shown to be inadequate at representing regional variations in the character of POC flux attenuation (Buesseler *et al.*, 2008). Allowing for a regionally variable *b* value gives a better description of POC flux attenuation, but will only be useful in modelling studies if this characteristic can be accurately described. It appears from this small dataset that the upper water column temperature (and consequently the rate of microbial activity) is the most important control on *b,* or at least is the most suitable of the parameters used here to help predict the variability of *b.* This apparent trend invites further study of mesopelagic-depth POC fluxes and the determination of the POC attenuation coefficient in order to expand the dataset in terms of geographic coverage, temperature range and, ideally, seasonal comparisons in locations where the upper water column temperature varies significantly over a seasonal cycle.

In terms of describing the attenuation of POC flux to the deep ocean, this small data set does not show the trend demonstrated where estimates of *b* are calculated from deep sea sediment traps and/or satellite data; *i.e.*, lower *b* values in lower latitudes (Klaas and Archer, 2002; Henson *et al.*, 2012). This is explained in previous work in terms of the export of relatively fresh, labile material at high latitudes which is quickly remineralised as it sinks, while at low latitudes, organic matter is recycled and

repackaged much more extensively before being exported, resulting in more refractory sinking POC (or a greater association of POC with calcite), a greater proportion of which is not remineralised before reaching the deep ocean. However, if *b* is derived from deep sediment traps and primary production or export data, without direct measurements of flux in the upper mesopelagic where change in flux is greatest, there is a lot more scope for miscalculation of the attenuation coefficient when trying to best-fit the Martin equation to the data.

This data suggests a situation in which low latitude (*i.e.*, warm water) regions demonstrate stronger relative attenuation of POC flux if considering mesopelagic depths, but weaker attenuation when considering flux to the deep ocean (and the reverse for high latitude regions). Such a scenario makes it important to accurately consider the depth below which sinking POC is considered sequestered and isolated should it be remineralised. What is the likelihood of POC remineralised below, say, 1000 m, being returned to the surface ocean within a few years? Or the possibility of POC remineralised at ~500 m depth at low latitude remaining isolated from the atmosphere for climatologically significant time-scales?

Chapter 4: Particulate trace metals in high latitude North Atlantic surface waters

4.1 Overview

This chapter focuses on particulate trace metal distributions, with an emphasis on iron and aluminium, using data from bulk particulate material samples collected by *in situ* pumps, deployed in the upper water column of the high latitude North Atlantic. Two size fractions of particles were collected within the mixed layer and at different depths below the mixed layer during three research cruises in 2010. The aim of this study was to improve our understanding of the role of particles in the biogeochemical cycling of metals in the high latitude North Atlantic, and to provide an independent estimate of particulate iron fluxes to those from the PELAGRA traps. Sample coverage encompassed the spring bloom and post-bloom period (two cruises in early- to mid-May and one from mid-July to mid-August). The two earlier cruises also coincided with an eruption of the Icelandic volcano, Eyjafjallajökull, in the vicinity of the study region, thus giving an opportunity to examine the effects of volcanic ash deposition on the particulate metal inventory.

4.2 Introduction

In Chapter 2 it was discussed how information on the composition of suspended particulate material (SPM), as well as that of sinking particles, is useful, due to the exchange of material between the two pools, and between particulate and dissolved pools. Large, sinking particles of marine snow collect smaller, non-sinking particles including fine mineral grains as they descend through the water column, due to the presence of mucus matrices such as transparent exopolymer particles (TEP; Alldredge and Silver, 1988; Passow, 2004). Conversely, the feeding habits of zooplankton may break up sinking particles into smaller fragments that are too small to sink (De La Rocha and Passow, 2007). POC concentrations and fluxes are theoretically linked by sinking speed and this was exploited by a recent study, which used a compilation of

POC concentration profiles, collected through the use of mesopelagic depth *in situ* pumps, to study the strength and efficiency of the biological pump (Lam *et al.*, 2011).

Furthermore, an understanding of how other biologically important elements transfer to and from particles is necessary in order to understand their biogeochemical cycles and how these influence, and are influenced by, that of carbon. The exchange of trace elements between the dissolved and particulate phases throughout the water column plays a major role in controlling their distribution and concentrations in the world's oceans, and the trace element composition of marine particles reflects the effects of numerous processes that are physical, chemical and biological in nature. Studying different characteristics of particulate trace elements (*e.g.*, size fractionation, elemental ratios, lability, variation of concentration with depth) can therefore help to explain processes affecting production.

4.2.1 Concentrations of suspended particulate trace metals: previous studies

The trace metal concentrations of marine particles are typically measured on material collected on filters: either directly, through the use of *in situ* pumps at depth (Sherrell and Boyle, 1992) or a towed fish connected to a ship-based pump (Frew *et al.*, 2006), or through collection of discrete samples using 5 – 30 L bottles deployed on a hydro-wire (Landing and Bruland, 1987). Data are sometimes shown in terms of trace metal content per unit mass of material collected (*e.g.*, μmol g^{-1}, or ppm, as shown in Kuss and Kremling (1999a)), but are more often converted to concentration in seawater by consideration of the volume of water filtered and/or the SPM concentration measured.

Tables 4.1 and 4.2 summarise some of the particulate trace metal concentrations measured in the upper 500 m of the ocean in previous studies, reported on a *moles per gram of SPM* and a *moles per volume of seawater* basis respectively. It is evident from Table 4.1 that upper ocean *per gram* concentrations of metals in SPM can vary by several orders of magnitude in some areas. Similarly, Table 4.2 shows that *per volume* particulate metal concentrations can vary over at least a couple of orders of magnitude (*e.g.*, Frew *et al.*, 2006; Planquette *et al.*, 2009), with studies covering larger geographical areas showing even larger ranges (Landing and Bruland, 1987; Fitzwater *et al.*, 2003). In the data sets summarised in the two tables, particulate Fe (pFe) concentrations range from 0.1 nmol L^{-1} in open ocean waters to 360 nmol L^{-1} in an upwelling plume off the coast of California (Gordon *et al.*, 1998; Fitzwater *et al.*, 2003), and from ~ 0.3 μmol g^{-1} in open ocean waters of the Atlantic to ~980 μmol g^{-1} in the Gotland Basin (Helmers, 1996; Pohl *et al.*, 2004).

Table 4.1: Summary of literature values for *per gram* concentrations of selected metals in suspended particulate material. All concentrations are in μmol g^{-1}. n/a = details not available.

Study region	*Depth (m)*	*Size (μm)*	*Fe*	*Al*	*Mn*
***North Atlantic*[(1)]**	7	*n/a*	0.8 – 1.5	6 – 38	0.33 – 0.35
***Atlantic*[(2)]**	12	>0.4	0.3 – 18	11 - 104	0.08 – 0.22
***Crozet Islands*[(3)]**	30–340	>53	3 – 496	3 – 960	n/a
***Gulf of Alaska*[(4)]**	20–220	>0.4	1 – 860	1 – 2221	n/a
***Ross Sea*[(5)]**	2–380	>0.4	0.5 – 425	n/a	0.01 – 59
***California upwelling*[(6)]**	~2	>0.4	0.4 – 174	2 – 1130	n/a
***Gotland Basin*[(7)]**	5–250	*n/a*	215 – 980	408 – 1330	18 - 346

References: *(1)* Kuss and Kremling (1999b), *(2)* Helmers (1996), *(3)* Planquette *et al.* (2009), *(4)* Martin *et al.* (1989), *(5)* Grotti *et al.* (2001), *(6)* Fitzwater *et al.* (2003), *(7)* Pohl *et al.* (2004).

Depth profiles of particulate metal concentrations in the upper ocean are rare and are subject to local influences, but aluminium and iron both show a general increase in concentration with depth through the whole water column (Orians and Bruland, 1986; Johnson *et al.*, 1997). This contrasts with concentrations of SPM in general, which decrease with depth from a maximum near the base of the mixed layer (Bishop *et al.*, 1977), highlighting the decoupling of such trace metals from the biogenic fractions of material that generally dominate SPM mass (*i.e.*, POM, opal, calcite).

Studies of size-fractionated particulate trace metals are also limited in number. SPM studies carried out with *in situ* pumps tend to differentiate only between material >53 μm and material of 1 – 53 μm, with the larger size fraction often operationally defined as the "sinking" fraction (Sherrell and Boyle, 1992; Planquette *et al.*, 2009). In some cases the gap between "particulate" and "dissolved" is closed by near-simultaneous deployment of Go-Flo bottles to collect material for filtering through 0.4 μm filters (Weinstein and Moran, 2004). Weinstein and Moran showed lower variability of >53 μm particulate Fe, Al and Mn concentrations, compared to smaller sized material in the Labrador Sea, with totals dominated by the latter. In HNLC waters in the south-west Pacific Ocean, the largest size fraction measured (>20 μm) had the greatest contribution (43 ± 6 %) to total pFe (Frew *et al.*, 2006).

Table 4.2: Summary of literature values for *per volume* concentrations of selected particulate metals in the upper 500 m of the water column. Data shown are either ranges (References 1 – 8) or calculated mean values (References 9 – 11). Fe and Al data are in nmol L^{-1}; all other metals are in pmol L^{-1}.

	Depth (m)	*Size (µm)*	*Fe*	*Al*	*Mn*	*Cu*	*Co*	*Pb*	*Ni*
***Sargasso Sea*[1]**	10 – 500	>1	0.1 – 0.9	0.7 – 2.5	8 – 242	3 – 24	0.3 – 1.8	0.8 – 2.9	5 – 16
***Equatorial Pacific*[2]**	20 – 150	>0.4	0.1 – 1.1	0.1 – 1.2	9 – 56	8 – 39	0.1 – 3.1	—	14 – 81
***N. & S. Atlantic*[3]**	"surface"	>0.45(?)	1 – 11	1 – 29	11 – 425	23 – 618	—	—	14 – 412
***Pacific Ocean*[4]**	15 – 500	>0.3	0.1 – 64	0.1 – 267	3 – 3311	—	—	—	—
***Crozet Islands*[5]**	30 – 340	>53	0.2 – 13	0.1 – 26	—	—	—	—	—
***SW Pacific*[6]**	10	>0.2	0.5 – 0.9	2.0 – 4.7	—	—	—	—	—
***Gulf of Alaska*[7]**	20 – 220	>0.4	0.2 – 150	0.2 – 386	—	—	—	—	—
***California upwelling*[8]**	~2	>0.4	0.2 – 368	1 – 2380	—	—	—	—	—
***N. & S. Atlantic*[9]**	12	>0.4	0.43	1.46	17	11	—	0.68	—
***Labrador Sea*[10]**	0 – 250	0.4–10	2.5	3.6	55	32	4.3	4.0	—
***Gulf of Maine*[10]**	0 – 300	>0.4	34.8	109	—	96	22.4	24.8	—
***North Atlantic*[11]**	7	n/a	1.0	3.9	70	130	8.1	5.1	35

References: *(1)* Sherrell and Boyle (1992), *(2)* Gordon *et al.* (1998), *(3)* Krishnaswami and Sarin (1976), *(4)* Landing and Bruland (1987), *(5)* Planquette *et al.* (2009), *(6)* Frew *et al.* (2006), *(7)* Martin *et al.* (1989), *(8)* Fitzwater *et al.* (2003), *(9)* Helmers (1996), *(10)* Weinstein and Moran (2004), *(11)* Kuss and Kremling (1999a).

4.2.2 Labile versus refractory particulate metals

In a handful of studies, variations of a two-step, acetic acid leach and concentrated acid total digest method (Chester and Hughes, 1967; Wells *et al.*, 2000) have been applied to SPM in an attempt to estimate the fraction of particulate metals (iron in particular) that is readily available to phytoplankton. The leach aims to solubilise metals associated with carbonate minerals, amorphous oxyhydroxides and adsorbed onto particle surfaces. These fractions could represent an additional source of new iron to the surface layer (for example, labile iron associated with recently deposited atmospheric material) or represent a source of recycled iron, consisting of the metal included in cell fragments and faecal pellets. Landing and Bruland (1987) considered the acetic acid leachable fraction (HAc) of metals to be an indicator of scavenging of dissolved metals onto particle surfaces and suggested that high ratios of HAc to refractory (Ref) metals are indicative of the scavenging process. Observed general increases with depth of the HAc/Ref ratio for pFe and particulate aluminium (pAl) are attributed to active scavenging with depth.

Based on studies in the eastern Pacific Ocean, the HAc fraction of aluminium (HAc-Al) was suggested by Orians and Bruland (1986) to typically account for 5 – 10 % of total suspended pAl, rising to 10 – 15 % in areas of low pAl concentrations (though values of 20 – 50 % were measured in the upper 500 m at one station in the South Pacific). Furthermore, they showed a more constant HAc-Al concentration with distance from the continent than was seen for refractory pAl (Ref-Al), the labile fraction thus interpreted as being due to an authigenic source of Al. Iron recovered by the HAc leach (HAc-Fe) was always <10 % and averaged ~2 % of the total pFe in samples collected by Martin *et al.* (1989) in the upper 200 m of the Gulf of Alaska, and generally <20 % in samples from the upper 500 m of a larger study area of the Pacific (Landing and Bruland, 1987). In the region around the Crozet Islands in the Southern Ocean, <1 % of both pFe and pAl were typically present in the leachable fraction (Planquette *et al.*, 2009). By contrast to Fe and Al, particulate manganese (pMn) is typically present mostly in the leachable fraction (32 - 99 %; Landing and Bruland, 1987).

Measurements of leachable metals in open ocean SPM using the acetic acid technique are for the most part limited to Al, Fe and Mn, but Gordon *et al.* (1998) showed that in the upper 150 m of the equatorial Pacific Ocean, the leachable fraction dominated for cadmium, zinc and nickel as well as manganese, while the refractory fraction dominated for copper, iron and aluminium, with cobalt fairly evenly split between the two phases.

4.2.3 Molar ratios of particulate trace metals

For SPM samples in which several trace metals have been determined following a shared processing protocol, the relative molar concentrations can be readily compared. This is most frequently done by calculating the molar ratio of other metals (M) to aluminium, which is generally considered to be a good tracer of lithogenic material. Comparing the observed M/Al ratio with average crustal values thus enables an estimation of the lithogenic contribution to the metal of interest (though low Ti/Al ratios in biogenic sediments have been used as an argument that a significant scavenged contribution to Al in some regions may reduce the validity of this practice (Murray and Leinen, 1996)). Using this approach, the Fe/Al ratio of SPM in the Sargasso Sea was shown to cluster within 40 % of the crustal value used as a comparison (Sherrell and Boyle, 1992), with the same true for particles collected in an upwelling plume in the western Pacific (Fitzwater *et al.*, 2003).

Crustal M/Al ratios are generally applied in one of two ways. The M/Al value calculated for a sample can be compared directly to the literature crustal value and an enrichment factor (EF) calculated for the metal with respect to the crustal value, following Equation 4.1. Though more commonly used to assess the anthropogenic contribution to atmospheric trace metal inputs (*e.g.*, Sholkovitz *et al.*, 2009) this method of interpretation has also been applied to trace metal studies of marine particulate material (Kremling and Streu, 1993; Kuss and Kremling, 1999a).

$$E.F. = \left[\frac{M}{Al}\right] sample \Big/ \left[\frac{M}{Al}\right] crust \qquad \text{(Eqtn. 4.1)}$$

Alternatively, the observed pAl concentration is multiplied by the crustal M/Al ratio to calculate the concentration of the metal that is expected to be present due to lithogenic material. This is then subtracted from the total particulate metal to leave a remaining fraction that has been defined as biogenic (Frew *et al.*, 2006; Planquette *et al.*, 2009) or as an alternative definition of a labile fraction (Kuss *et al.*, 2010).

While most studies use the total particulate metal data when considering M/Al ratios, Martin *et al.* (1989) used just the refractory fraction, as determined from the leach/total digest method, presumably because inclusion of the leachable fraction may skew the results through contributions from scavenged Al and other metals. Fitzwater *et al.* (2003) considered the Fe/Al of leachable and refractory fractions separately, and found the former to be enriched in iron while the latter resembled the crustal average.

4.2.4 Aims and hypotheses

The work described here was carried out as part of a project to study iron biogeochemistry in the high latitude North Atlantic, a region suspected to be subject to seasonal HNLC conditions due to iron limitation. An overriding aim of the work was therefore to provide a regional synthesis of iron and nutrient inputs and sinks, with an estimate of particulate iron flux from SAPS sampling (by linking the Fe measurements to measurements of ^{234}Th depletion) intended to complement direct measurements made using PELAGRA (see Chapter 3). Comparison of pFe measurements to POC and PON data were intended to help evaluate if iron is preferentially retained in the surface mixed layer by recycling.

Through the concurrent measurement of aluminium in bulk particulate material, a further aim was to estimate the division of pFe between lithogenic and biogenic material and to study the variation of this distribution with depth and between small (1 – 53 μm) and large (>53 μm) size fractions of material. Additionally, the analysis of samples by ICP-MS provided the opportunity to simultaneously determine particulate concentrations of several other important trace metals, thus adding to the rather sparse global dataset of such measurements.

The dynamics of pFe in surface and sub-surface waters have not been studied very extensively, with the FeCycle study in HNLC waters of the southwest Pacific being the most significant (Boyd *et al.*, 2005; Frew *et al.*, 2006). Based on the findings of FeCycle the working hypothesis for this work was that an increase in the Fe/C and Fe/N ratios would be observed with depth below the mixed layer, due to a preferential loss of POC and PON by remineralisation, along with scavenging of remineralised iron back on to sinking particles. This loss of Fe from the surface ocean, relative to N, if not offset by a sufficiently increased Fe/N ratio in inputs to the surface ocean, would represent a process by which the euphotic zone could become iron-limited as the season progressed.

The FeCycle study observed an approximate two-fold decrease in the proportion of lithogenic iron in exported material relative to that in the mixed layer, through transformation of lithogenic to biogenic pFe within the mixed layer, prior to export, and it was hypothesized that the same feature would be observed in the HLNA.

Finally, the timing of two of the cruises coincided with an eruption of the Icelandic volcano, Eyjafjallajökull, which emitted an estimated 270 x 10^6 m^3 of particles to the atmosphere as tephra during April – May 2010 (Dellino *et al.*, 2012). Much of this was deposited over the north-western Atlantic Ocean, including part of the study area, and

it was hypothesised that the sampling stations within the region of ash deposition would show noticeably higher concentrations of particulate trace metals relative to those more distant from the ash plume.

4.3 Overview of the research cruises and sampling strategy

SAPS samples were collected on three research cruises that formed part of the Irminger Basin Iron Study. Appendix E lists the deployment dates and locations for each sample, along with sample collection depth, volume of seawater filtered, size fractions and the mass of SPM collected (calculated as the sum of material rinsed onto smaller filters for trace metal and POC analyses). During the first cruise, RRS *Discovery* cruise D350 (26th April to 9th May 2010), eight deployments of multiple SAPS units were carried out. Sampling started in the middle of the Irminger Basin, and an eastward transect along 60 °N was then followed into the Iceland Basin, with a SAPS deployment carried out each day. The cruise track then turned north-east and then north, towards Iceland, with the final two deployments both taking place at stations on the 20 °W meridian (Figure 4.1*a*). The final SAPS sample was carried out ~35 nautical miles from the erupting Eyjafjallajökull volcano, off the south coast of Iceland.

During D350, the SAPS samples for trace metal analyses (TM-SAPS) were carried out in parallel with the collection of samples at the same depths for ^{234}Th, POC and PON, opal and $CaCO_3$ analyses (Th-SAPS). To minimise the potential for contamination of the trace metal samples, TM-SAPS were secured to the hydro-wire above the Th-SAPS. Due to a limited number of available pumps and to time constraints, samples were collected at only two depths at most stations: one TM-SAPS/Th-SAPS pair was deployed at approximately 50 m depth, with the other TM-SAPS/Th-SAPS pair deployed concurrently a further 100 m deeper in the water column. At the final station it was possible to deploy a third TM-SAPS, at 15 m depth, although no corresponding Th-SAPS was deployed.

SAPS samples were also collected at three stations during RRS *Discovery* cruise D351 (10th – 28th May 2010; Figure 4.1*a*), which followed the Extended Ellett Line from Iceland to Scotland. The TM-SAPS deployments targeted roughly the same depth horizons as during D350, guided by the surface mixed layer depth: one pump was deployed ~10 m below the base of the mixed layer and the second one 100 m deeper. During the first deployment, which was a reoccupation of a station visited six days earlier (during D350), a third SAPS unit was deployed within the mixed layer. No corresponding Th-SAPS were carried out during D351.

Finally, SAPS samples were collected during RRS *Discovery* cruise D354 (4th July – 11th August), with sample coverage spanning both the Irminger and Iceland Basins (Figure 4.1*b*). TM-SAPS deployments typically occurred jointly with Th-SAPS as in D350, with depths of ~10 m and ~110 m below the base of the mixed layer targeted. A third TM-SAPS was deployed within the mixed layer at most stations, though it was not paired with simultaneous POC(N) measurements from a Th-SAPS. At a couple of stations, additional TM-SAPS deployments took place to depths of 300 – 400 m.

For the sake of simplicity, the main samples will be referred to as being "50 m" and "150 m" depth throughout this chapter, though the former were collected at depths between 50 m and 70 m during D350 and D351, and at 40 m or 50 m during D354 (depending on hydrographic conditions), while the latter were always collected 100 m deeper. Shallower samples collected during D354 are referred to as "20 m" or "mixed layer" samples. Exact sample collection depths for each station are listed in Appendix E.

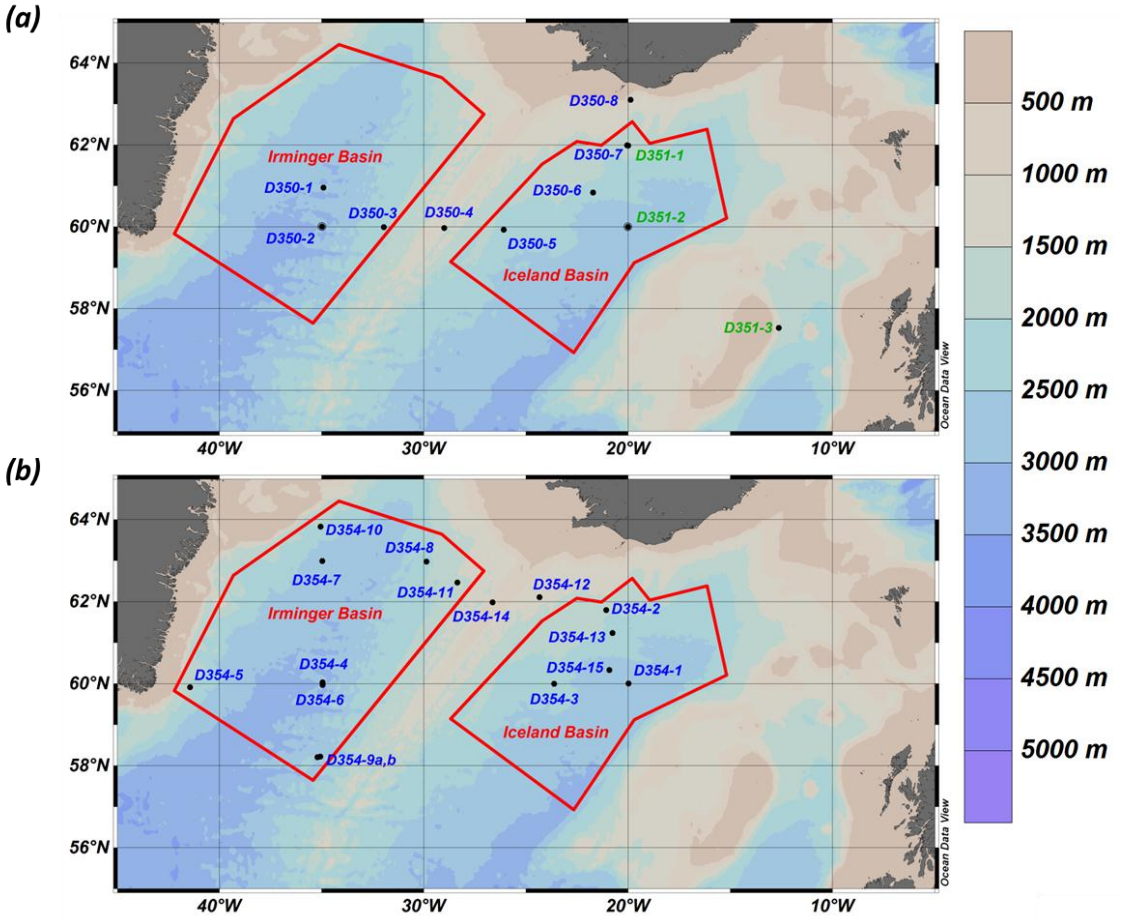

Figure 4.1: Locations of SAPS sampling stations during cruises *(a)* D350 and D351, and *(b)* D354. Red outlines surround stations in >1500 m deep water in the Irminger or Iceland Basins (as labelled). Stations D350-4, D354-12 and D354-14 were in water <1500 m deep above the Reykjanes Ridge, while D350-8 was in <1500 m deep water over the continental slope south of Iceland.

4.4 Results and discussion

4.4.1 Hydrographic context

The areas covered by SAPS sampling stations during each of D350 and D354 largely fell into groupings within the Irminger Basin, and Iceland Basin, with a couple in the Reykjanes Ridge region (Figure 4.1). CTD data from D350 and D354 showed the water column to 500 m depth in the Irminger Basin to be colder and slightly fresher than the Iceland Basin during both cruises. In each basin, temperature and σ_θ data during D354 showed a clear surface mixed layer typically spanning the upper 30 – 40 m. Such a feature was generally less defined during D350.

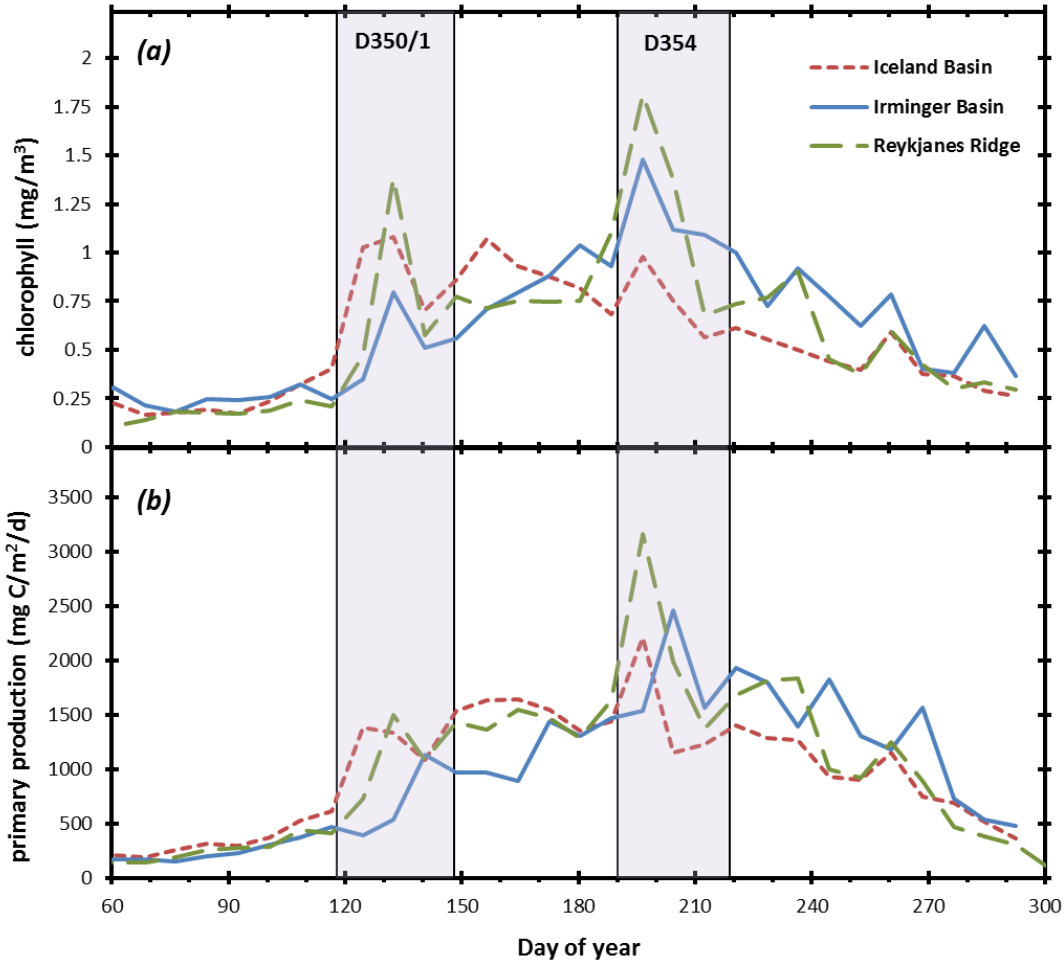

Figure 4.2: High latitude North Atlantic data for *(a)* chlorophyll, and *(b)* primary productivity in 2010. Data is derived from MODIS satellite images, with regions defined by a southerly limit of 58 °N and with water depths of >1500 m for the Irminger and Iceland Basins.

Surface chlorophyll data during 2010 for the Iceland and Irminger Basins and the Reykjanes Ridge is shown in Figure 4.2*a.* Data was derived from MODIS satellite imagery using standard algorithms, and the three regions defined by the 58th parallel as a southerly extent and the 1500 m depth contour for each basin. The data suggests that in the Iceland Basin, chlorophyll concentrations associated with the spring bloom were at their maximum during the period in which samples were collected for D350 and D351, before dropping off in late May and then peaking again in early June. A further, slightly smaller peak coincided with sampling during D354. This is corroborated by underway chlorophyll data (Table 4.3), which showed slightly higher values during D350 (median 1.8 μg L^{-1}) than during D354 (median 1.4 μg L^{-1}).

In the Irminger Basin, the MODIS data showed low but increasing chlorophyll concentrations during D350. A continued general increase until mid-July resulted in the highest concentrations roughly coinciding with the first SAPS sampling in the Irminger Basin during D354, then stayed relatively high for the remainder of the cruise. Figure 4.2*a* shows that chlorophyll in the Irminger Basin was lower than in the Iceland Basin during D350, with the opposite being true during D354. This is also shown in the underway data, which increased from a median value of 0.8 μg L^{-1} in the Irminger Basin during D350 to a median of 2.3 μg L^{-1} during D354.

Table 4.3: Surface nutrients and chlorophyll data from underway measurements made during D350 and D354. Data shown is the range of values in each region, with the median value in brackets.

		Chlorophyll (μg L^{-1})	*TON (μM)*	*PO_4 (μM)*	*Si (μM)*
Iceland Basin	**D350**	0.78 – 3.51 (1.8)	5.4 – 12.3 (9.9)	0.34 – 0.72 (0.60)	0.14 – 6.0 (3.8)
	D354	0.23 – 3.53 (1.4)	<0.09 – 2.7 (0.3)	0.04 – 0.18 (0.07)	0.18 – 1.7 (0.65)
Irminger Basin	**D350**	0.36 – 1.49 (0.8)	11.2 – 14.5 (12.9)	0.69 – 0.84 (0.75)	3.8 – 5.5 (4.7)
	D354	0.87 – 4.44 (2.3)	<0.09 – 6.5 (3.2)	0.03 – 0.52 (0.26)	0.12 – 4.3 (1.8)
Reykjanes Ridge	**D350**	0.71 – 1.63 (1.2)	10.1 – 13.1 (11.2)	0.64 – 0.75 (0.70)	3.0 – 5.8 (4.8)
	D354	0.32 – 3.7 (1.9)	<0.09 – 2.8 (0.3)	0.02 – 0.23 (0.08)	0.63 – 3.9 (1.2)

Finally, the Reykjanes Ridge region also showed increasing chlorophyll concentrations, coinciding with the start of the spring bloom, during D350, and peaking soon afterwards (Figure 4.2*a*). Underway measurements during D350 had a median value of ~ 1.2 μg L^{-1}. A second, higher maximum in the MODIS data from mid-July was followed by a sharp decrease through the rest of D354. The median chlorophyll concentration measured for the Ridge region during D354 (1.9 μg L^{-1}) suggests that sampling did not coincide with the peak bloom conditions observed by MODIS.

Nutrient data from underway samples collected during D350 and D354 (Table 4.3) also provide evidence for significant blooms in the region over the period spanned by the cruises, with significant reductions in dissolved nutrients observed in both basins. Furthermore, the continued higher nutrient concentrations in the Irminger Basin, relative to the Iceland Basin, support the MODIS satellite data (Figure 4.2*b*) in implying that rates of primary production in the latter increased earlier in the year and were generally higher up until mid-July (coincident with the timing of cruise D354).

4.4.2 Methods critique

This section evaluates the protocol used to process TM-SAPS samples and assesses the uncertainties associated with it in terms of interpretation of the data. The protocol (described in full in Chapter 2 and Appendix B) involved rinsing off the collected material from the 293 mm SAPS filters onto smaller and more manageable 47 mm diameter polycarbonate Nuclepore membranes (0.4 μm pore size), following the method of Planquette (2008). One variation from the Planquette approach was the method of collecting subsamples for POC(N) analysis. In the previous work, a small amount of material was scraped from the 47 mm Nuclepore membrane after drying and weighing, and transferred to a pre-weighed silver cup, which was then reweighed. In this work, subsamples were taken by syringe from the water/particle mixture of the filter tower, following the first rinsing of material from the SAPS filter, then filtered through a pre-weighed GF/F filter. The GF/F filters were dried, reweighed, pelleted and sent away for analysis, as described in Section 2.5.2.

4.4.2.1 Mass measurements: significance for estimates of SPM concentrations

It was estimated during the previous application of this method, through weighing the SAPS filters and 47 mm Nuclepore membranes before and after use, that on average 80 % of the material collected on the SAPS filters (>53 μm material only) was recovered on

the smaller filters (Planquette, 2008). During this work, however, it was found that obtaining an accurate, stable mass for the large filters was very problematic, particularly for the Nitex filters. Uncertainties in the mass difference (between unused filter and used, rinsed filter) were typically of the same order of magnitude as the mass of material collected on the smaller filters (tens of milligrams) and as a result, calculations sometimes resulted in a clearly erroneous negative value for mass of material remaining on the filter. This is ascribed to the fact that, pre-cruise, washed filters were dried under a flow hood for a couple of days before weighing, whereas after use and rinsing they were subjected to the more thorough process of freeze-drying.

The significance of this is that it introduces uncertainty into the particulate metal results in terms of moles of element per litre of seawater. Assuming an average 80 % recovery as previously described would allow a correction to be applied to the calculated values, but there would be no way of confirming the accuracy of the assumption. Furthermore, individual samples would undoubtedly vary significantly from the average value. Consequently, no correction has been applied to the data, but the subsequent interpretation must come with the caveat that the values measured represent minimum estimates.

4.4.2.2 POC and PON measurements: comparison to Th-SAPS results

During the CROZEX (CROZet natural iron bloom and EXport experiment) work, TM-SAPS subsamples for POC and PON were analysed alongside subsamples from Th-SAPS (>53 μm size fraction only). For the latter, material was rinsed off the SAPS filters while at sea, within a couple of hours of recovery, using one litre of thorium-free, filtered seawater. The water/particle mixture was then split with a Folsom splitter and a ¼ split completely filtered and used for POC(N) analysis (Morris *et al.*, 2007; Le Moigne, *pers. comm.*). The measured POC(N) was multiplied by four and then divided by the volume of seawater filtered by the SAPS unit. TM-SAPS POC(N) estimates were calculated by multiplying the POC(N) content of the subsample (mmol g^{-1}) by the total mass of material collected and dividing by the volume of seawater filtered.

Comparison of the TM-SAPS POC and Th-SAPS POC concentration estimates during CROZEX showed percentage differences ranging in magnitude from 1 – 172 % (mean of 44 %), and plotting of the estimates resulted in a best-fit line whereby TM-SAPS POC = 0.71 x Th-SAPS POC (r^2 = 0.47, n = 18; Planquette, *pers. comm.*). This comparison (TM-SAPS POC being 71 % of Th SAPS POC) is close to the 80 % mass recovery that was stated earlier. As the Th-SAPS POC analysis was carried out on a larger amount of

material and thus considered to be a more accurate representation of the material collected, where possible the Th-SAPS POC data was used in conjunction with TM-SAPS pFe and pAl data for the CROZEX work.

A similar comparison of TM-SAPS and Th-SAPS results was carried out during this work where possible, with each size fraction of material considered. Both POC and PON results were compared in this way, with the POC(N) content of the TM-SAPS subsample (in mmol g^{-1}) multiplied by the sum of the mass on the subsample GF/F filter and the 47 mm membrane(s) used for TM analysis, then divided by the volume of seawater filtered to give a μmol L^{-1} concentration. Scatter plots of Th-SAPS POC against TM-SAPS POC are shown in Figure 4.3 for (*a*) 53 μm Nitex filters, (*b*) 1 μm Nitex filters and (*c*) 1 μm polycarbonate filters.

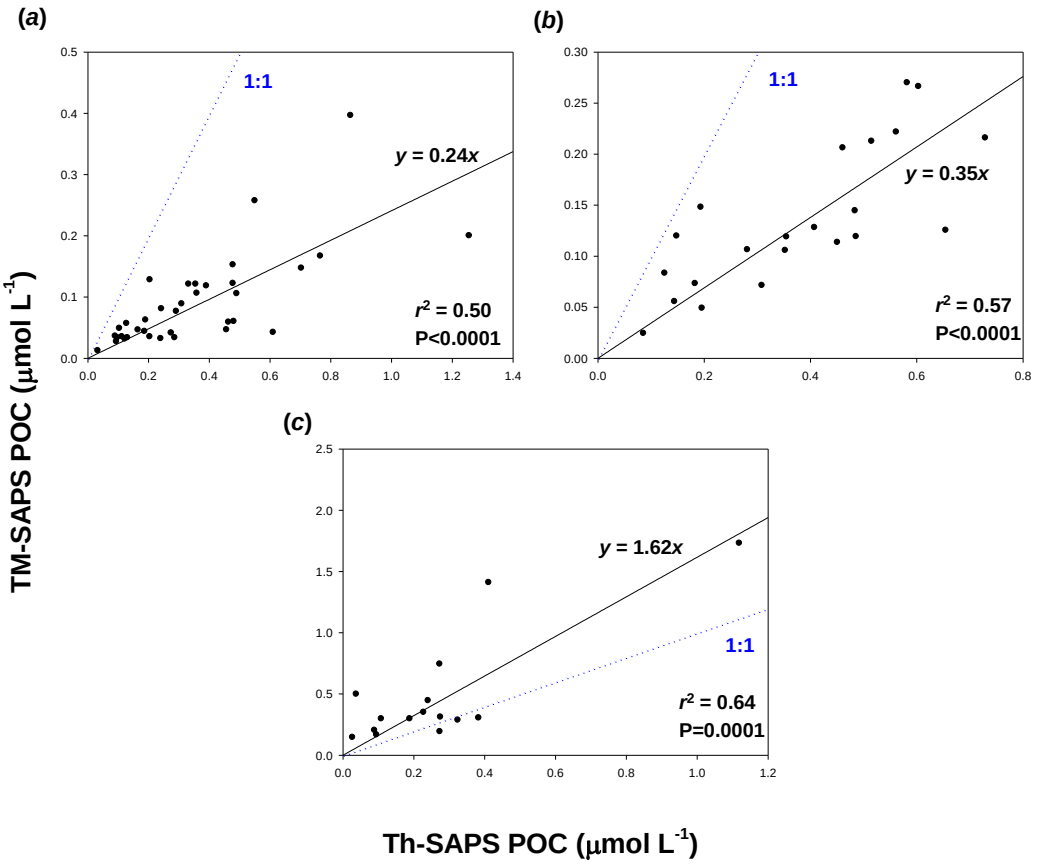

Figure 4.3: Comparison of POC concentrations determined from Th-SAPS and TM-SAPS, where *(a)* 53 μm Nitex filters have been used for both, *(b)* 1 μm Nitex filters have been used for both, and *(c)* 1 μm Nitex filters have been used for Th-SAPS and 1 μm polycarbonate filters have been used for TM-SAPS.

It is clear from Figure 4.3*a* that, for the >53 μm size fraction POC results, the TM-SAPS and Th-SAPS were a lot further from a 1:1 ratio than in the CROZEX study. In this case

the best-fit line was given by TM-SAPS POC = 0.24 (± 0.04) x Th-SAPS POC (r^2 = 0.50, n = 36, P <0.0001), where 0.04 is the standard error of the line gradient. A similar relationship was found for the 1 – 53 μm size fraction (Figure 4.3*b*), with TM-SAPS POC = 0.35 (± 0.05) x Th-SAPS POC (r^2 = 0.57, n = 22, P <0.0001) and for the corresponding PON measurements: >53 μm size fraction TM-SAPS PON = 0.22 (± 0.04) x Th-SAPS PON (r^2 = 0.52, n = 36, P <0.0001), 1 – 53 μm size fraction TM-SAPS PON = 0.25 (± 0.05) x Th-SAPS PON (r^2 = 0.37, n = 22, P <0.0001). This implies that, for some reason, the method used for estimating POC and PON from the TM-SAPS gave, on average, a value only 22 – 35 % of the Th-SAPS estimate, whereas the different sub-sampling procedure followed during CROZEX gave a value equal to around 71 % of the Th-SAPS estimate.

Why this should be the case is uncertain. Possibly the material collected in the HLNA had properties that made it more prone to adhering to the Nitex mesh after freezing than that collected during CROZEX. If this is the case it would imply that mass recovery from the SAPS filters during this work was also only between one quarter and one third of the total, though visual inspection of the filters suggests that this is unlikely. Alternatively, it may be a result of the different sub-sampling methods used: whereas in the CROZEX work the POC sub-sample was a fraction of the material collected on a 0.4 μm pore-size membrane, in this work it was material that was collected on a GF/F filter with nominal pore size of 0.7 μm (though Th-SAPS POC samples were also rinsed off onto GF/F filters). It is also possible that removal of the rinse/particle mixture from the filter tower by syringe gave an under-representative subsample of organic material, though on occasions where more than one subsample was taken for POC analysis, the amount of POC per gram of material agreed within ~10 % between subsamples.

Where a polycarbonate membrane was used to collect the 1 – 53 μm size fraction of the TM-SAPS samples (compared to a Nitex mesh used for the Th-SAPS), plotting corresponding samples (Figure 4.3*c*) gave a best-fit line described by TM-SAPS POC = 1.62 (± 0.30) x Th-SAPS POC (r^2 = 0.64, n = 15, P = 0.0001), with a similar result for PON. This suggests that, whatever aspect of the sub-sampling method caused the apparent differences between CROZEX and this study in POC recovery, relative to the Th-SAPS method, this effect was masked by the difference observed when comparing collection of material using two different filter types during sampling (*i.e.* a smooth polycarbonate membrane with sharply defined pore size and a Nitex mesh).

These findings cast further uncertainty on estimates of absolute particulate elemental concentrations per volume of seawater, though as the same method of POC subsampling was used throughout the work, there is still merit in qualitative use of the data. The different relationships of TM-SAPS results to Th-SAPS results when polycarbonate membranes and Nitex mesh were used suggest that comparisons between samples that used the different filter types should be avoided, at least in

terms of concentrations per volume of seawater, as the data implies that the Nitex filters would give a downward bias relative to the polycarbonate membranes. However, comparison of data from D354 for samples collected using polycarbonate and Nitex filters showed no significant differences in *per gram* values between the two.

4.4.2.3 Consideration of the rinse filtrate

In previous studies using *in situ* pumps, or where seawater samples or sediment trap samples have been filtered in order to analyse the particulate material, there have been differing approaches to the issue of sea-salt trapped within the collected material. In some cases, sodium in the collected material is measured and used to apply a correction to the measured dry-weight mass (Bishop and Edmond, 1976; Lam and Bishop, 2007). In others, the filter is rinsed with a small amount of deionised water (sometimes adjusted to a pH close to that of seawater) in order to remove residual sea-salt before measuring the dry-weight mass of the material collected (Pohl *et al.*, 2004; Lamborg *et al.*, 2008a). However, doing so may result in a significant fraction of the labile metals also being lost with the filtrate, which has been attributed to loss of material through cell lysis (Collier and Edmond, 1984).

In this work, a fairly large volume of deionised water (typically 200 – 400 mL) was used in the rinsing of material from SAPS filters, and so there was a concern that a significant proportion of certain metals would be lost to the rinse. The amount of water used to rinse material off each filter was therefore determined gravimetrically, and a 125 mL sample of it kept for trace metal measurements. Although it was not possible to analyse every sample, a selection of filtrates relating to different cruises, sample depths and filter types were analysed by ICP-MS and the concentration of metals in each one calculated. Following a blank correction (the amount of metal measured in deionised water passed through an unused polycarbonate membrane), these values were compared to the calculated metal concentrations in the acetic acid leach and total acid digest fractions.

The results, summarised in Table 4.4, show that for all filter types, a large amount of phosphorus was present in the rinse, relative to the amount determined by analysis of the leach and digest solutions; on average phosphorus in the rinse accounted for ~73 % of the total. Several other elements also had a significant fraction “lost” to the rinse, notably V, Cu, Co, Mn, Cd and Ni. Only 8 % of Zn and 4 % of Pb, on average, were in the rinse, while the values for Fe, Al and Ti were all insignificant (<1 %). It should be noted that these values are based on two major assumptions:

- Leach and digest metal values from analysis of the 47 mm Nuclepore membranes were adjusted to account for the extra mass collected on the GF/F filters; it is assumed that the material collected on the two filter types had the same composition.
- The calculations assume that all of the metals in the rinse fraction were derived from the material that was collected on the Nuclepore and GF/F filters. If a significant fraction of the collected material remained on the large SAPS filter, it is likely that some of the rinse contents will have derived from that material, in which case the values in Table 4.4 represent an upper limit to the percentage lost to the deionised water rinse.

Table 4.4: Amount of each element measured in deionised water rinse as a percentage of the total measured in the rinse, leach and digest fractions. Values shown are the mean value and standard deviation for the number of samples (*n*) from which the rinse was analysed.

	D350/1 53µm Nitex (n = 4)	*D354 53µm Nitex (n = 4)*	*D354 1µm Nitex (n = 3)*	*D350/1 1µm PC (n = 2)*	*D354 1µm PC (n = 2)*	*Overall (n = 15)*
P	76 ± 4 %	78 ± 8 %	66 ± 12 %	70 ± 13 %	70 ± 1 %	**73 ± 8 %**
Al	0 ± 0 %	0 ± 0 %	0 ± 0 %	0 ± 0 %	0 ± 1%	**0.1 ± 0.2 %**
Ti	0 ± 0 %	0 ± 0 %	0 ± 0 %	0 ± 0 %	0 ± 0 %	**0.0 ± 0.0 %**
V	40 ± 21 %	54 ± 8 %	40 ± 18 %	36 ± 33 %	69 ± 11 %	**47 ± 19 %**
Mn	22 ± 18 %	56 ± 17 %	54 ± 21 %	4 ± 2 %	35 ± 12 %	**37 ± 24 %**
Fe	0 ± 0 %	0 ± 0 %	0 ± 0 %	0 ± 0 %	2 ± 0 %	**0.5 ± 0.5 %**
Co	23 ± 13 %	51 ± 17 %	40 ± 25 %	16 ± 13 %	61 ± 7 %	**38 ± 21 %**
Ni	31 ± 3 %	30 ± 11 %	19 ± 10 %	19 ± 11 %	23 ± 8 %	**25 ± 9 %**
Cu	45 ± 11 %	53 ± 16 %	27 ± 13 %	41 ± 26 %	42 ± 15 %	**43 ± 16 %**
Zn	10 ± 4 %	11 ± 7 %	6 ± 2 %	3 ± 2 %	7 ± 1 %	**8 ± 5 %**
Cd	41 ± 21 %	39 ± 21 %	24 ± 18 %	12 ± 7 %	12 ± 3 %	**29 ± 20 %**
Pb	6 ± 4 %	5 ± 1 %	3 ± 1 %	1 ± 1 %	3 ± 0 %	**4 ± 3 %**

4.4.3 Variations in SPM, POC and PON concentrations

The total mass of material rinsed from each SAPS filter onto 47 mm membranes and GF/F filters is shown in the tables in Appendix E. In Table 4.5, the range of values

calculated for SPM concentration (in μg L^{-1}) are shown for each cruise on a depth-related basis, along with the mean and standard deviation of the values. The values are shown as total SPM (>1 μm) and as >53 μm and 1 – 53 μm size fractions. For all three cruises, the SPM concentrations were found to generally decrease between 50 m and 150 m; a trend apparent in both size fractions. The extension of the depth range during D354 (with samples also collected at 20 m and occasionally down to 400 m) showed a continuation of the trend, though at the two stations where samples were collected at both 300 m and 400 m there was no significant difference in SPM between the two depths.

Table 4.5: Size-fractionated and total suspended particulate material concentrations for D350, D351 and D354. For each depth, the range, mean and standard deviation are shown.

		SPM (μg L^{-1})		
		>53 μm	**1 – 53 μm**	**Total**
D350				
15 m	Value (n = 1)	6	136	142
50 - 60 m	Range	2 - 25	17 – 214	19 – 231
	Mean ± 1σ	11 ± 9	86 ± 67	97 ± 73
150 – 160 m	Range	3 – 8	22 – 42	26 – 48
	Mean ± 1σ	5 ± 2	35 ± 9	40 ± 9
D351				
25 m	Value (n = 1)	7	10	17
50 - 70 m	Range	8 – 21	7 – 84	15 – 105
	Mean ± 1σ	13 ± 7	56 ± 43	69 ± 48
150 – 170 m	Range	7 – 9	11 – 35	14 – 46
	Mean ± 1σ	8 ± 1	19 ± 14	35 ± 18
D354				
20 m	Range	5 – 62	4 – 95	22 – 118
	Mean ± 1σ	26 ± 15	30 ± 31	55 ± 30
50 - 60 m	Range	2 – 9	6 – 27	10 – 31
	Mean ± 1σ	6 ± 3	11 ± 6	17 ± 6
150 – 160 m	Range	1 – 7	2 – 24	4 – 26
	Mean ± 1σ	3 ± 2	9 ± 7	12 ± 7
300 m	Range	1 – 2	3 – 4	4 – 5
	Mean ± 1σ	1 ± 1	3 ± 0	5 ± 0
400 m	Range	1 – 1	3 – 8	5 – 9
	Mean ± 1σ	1 ± 0	5 ± 3	6 ± 2

The data suggest an increase in the percentage of SPM within the >53 μm size fraction between cruises D350 and D354, but this is most likely a sampling artefact resulting from the change in the type of 1 μm filter used for most samples in the latter cruise (see Section 4.4.2). What is apparent is that, within each cruise period (*i.e.*, D350 or D354), there was no statistically significant difference, between 50 m and 150 m depth, in the fraction of SPM lying within the >53 μm pool. During D350, 14 ± 5 % of SPM was in the >53 μm size fraction at 50 m (*n = 5*), compared to 12 ± 7 % at 150 m (*n = 4*), while during D354 the average values were 40 ± 11 % at 50 m (*n = 11*) and 34 ± 9 % at 150 m (*n = 11*). However, during D354 there was a higher contribution to total SPM by the >53 μm size fraction in samples collected within the mixed layer, with a mean of 67 ± 14 % (*n* = 9). This is statistically different ($P < 0.001$) to the values at 50 m and 150 m and suggests the presence in the mixed layer of particle aggregates or large diatom cells that are quickly broken up upon sinking from the mixed layer.

When all of the samples collected between 50 m and 150 m during D354 were considered, there was also no clear difference between the two basins in the contribution from the >53 μm size fraction: 33 ± 10 % in the Iceland Basin (*n = 8*) compared to 40 ± 10 % in the Irminger Basin (*n = 14*). During D350, however, there appeared to be a greater proportion of large particles in samples from the Irminger Basin (17 ± 4 %; *n = 5*) than those from the Iceland Basin (8 ± 1 %; *n = 4*).

The calculated concentration of POC from TM-SAPS ranged from 0.2 – 3.7 μmol L^{-1} during D350/1 and from 0.1 – 3.3 μmol L^{-1} during D354, while PON ranged from 0.02 – 0.43 μmol L^{-1} and from 0.01 – 0.41 μmol L^{-1} respectively. Average POC and PON concentrations at the depths sampled during D350 and D354 are shown for each basin in Figure 4.4. Despite the large standard deviations in the data, due to variations over the extensive spatial coverage of the datasets, the attenuation of organic matter concentration with depth is evident, particularly between the mixed layer and 50 m during D354. It is also apparent that during D350 POC and PON were higher at 50 m depth in the Irminger Basin than in the Iceland Basin, and that during D354, mixed layer concentrations of POC(N) were greater in the Iceland Basin than in the Irminger Basin, though this did not hold true below deeper in the water column.

Figure 4.4 suggests that there were generally higher POC and PON concentrations observed during D350 than D354. However, as with the apparent increase between the two cruises in the large particle contribution to total SPM (above), it is thought that this may be a sampling artefact, resulting from the change from 1 μm polycarbonate membranes during D350 to a 1 μm Nitex mesh for most samples during D354. For the sake of clarity, when comparing between depths or basins for the D354 data, results from three stations for which polycarbonate membranes were used have been left out of Figure 4.4. More details on the effects of filter-type used are given in Section 4.4.2.

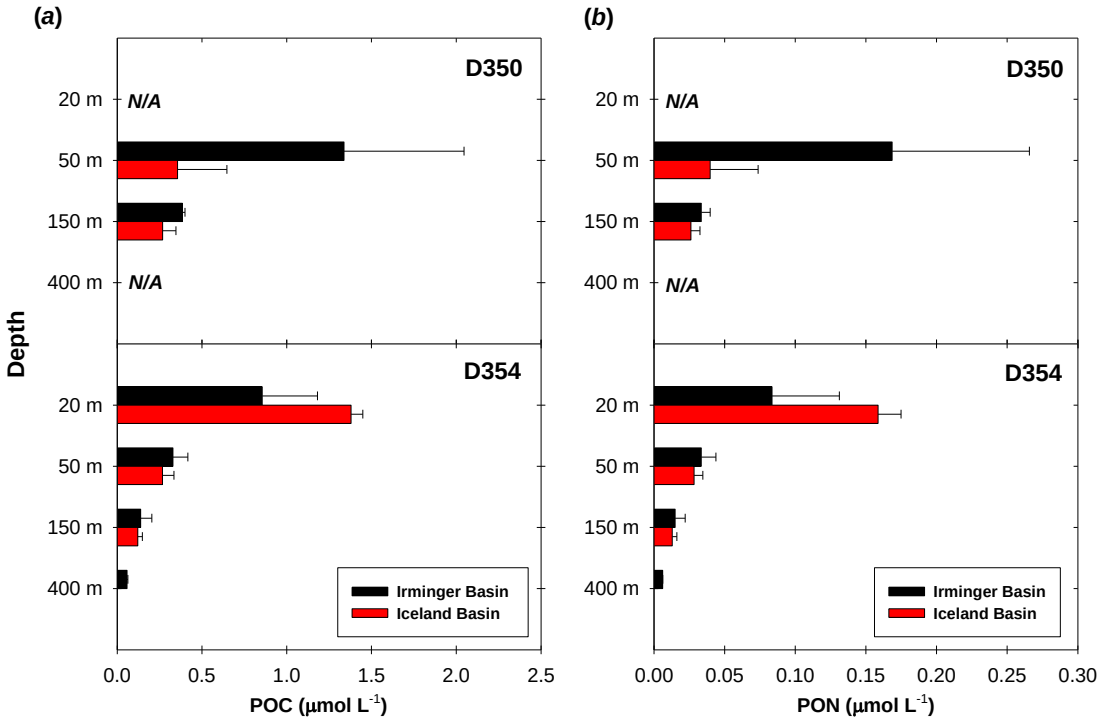

Figure 4.4: Depth-related comparisons of *(a)* mean POC, and *(b)* mean PON concentrations in the Irminger and Iceland Basins during D350 and D354. Error bars represent one standard deviation.

4.4.4 Trace metal, POC and PON concentrations within SPM

Through the analysis of the known amount of material rinsed from SAPS filters onto 47 mm Nuclepore membranes, the concentrations within the collected particulate material of several trace metals and phosphorus were calculated. This was carried out in such a way as to estimate a "labile" fraction (from an acetic acid leach) and a "refractory" fraction (from a concentrated nitric and hydrofluoric acid digest), which were combined to give the "total" content of each element in the collected material (see Chapter 2 and Appendix C for method details). Table 4.6 lists the median and range of values of the total *per gram* concentrations for each element during each cruise, though it does not show adjustments made for the loss of some metals to the deionised water rinse (see Section 4.4.2). Also given are the *per gram* concentrations of POC and PON in particulate material.

Most of the trace metals listed showed a large range of *per gram* concentrations during each research cruise, typically spanning at least one order of magnitude, and three orders of magnitude in the case of iron during D350. Nevertheless, the measured values for Al, Fe, Mn and Cu fall within the combined range of the literature values listed in Table 4.1, while the ranges of other elements are also comparable to previous

Table 4.6: Summary of POC, PON, P and total trace metal (leach + digest) concentrations in SPM collected during cruises D350, D351 and D354. POC and PON values are in mmol g^{-1}, Co and Pb in nmol g^{-1}, and all others in μmol g^{-1}.

	D350 – May 2010			*D351 – May 2010*			*D354 – July/August 2010*		
	Min	**Max**	**Median**	**Min**	**Max**	**Median**	**Min**	**Max**	**Median**
POC	5	12	9	8	34	12	10	32	18
PON	0.5	1.5	1.1	0.8	3.6	1.4	0.9	3.4	1.8
P	30	68	52	37	118	51	43	111	64
Al	14	751	44	80	887	223	5	370	54
Ti	0.4	57.5	2.6	3	65	12	0.4	25.6	2.9
V	0.03	0.75	0.12	0.11	0.78	0.25	0.04	0.68	0.16
Mn	0.2	8.4	0.4	0.6	9.8	2.0	0.2	7.5	0.7
Fe	4	352	23	24	393	85	3	173	25
Ni	0.07	0.80	0.27	0.09	0.58	0.29	0.26	4.43	0.69
Cu	0.07	0.53	0.28	0.13	0.71	0.30	0.10	1.62	0.43
Zn	0.5	1.9	1.7	0.8	3.6	1.8	0.5	3.2	1.4
Cd	0.04	0.07	0.05	0.05	0.16	0.06	0.02	0.20	0.06
Co	4	93	10	9	100	27	10	109	22
Pb	6	48	19	9	30	18	11	614	19

measurements (Helmers, 1996; Kuss and Kremling, 1999a; Pohl *et al.*, 2004). As a result of the large ranges observed, it is difficult to discern statistically significant differences between cruises. What is apparent is that, whilst the ranges of values measured for Al, Ti, V, Mn and Fe were all greater during D350, with greater maximum values and minimum values greater than or equal to those during D354, the median values were higher during D354. The highest values for each of those elements were observed during D351, when the median values for Al, Ti, Mn and Fe were all statistically different to those during the other two cruises (P <0.05 using a Mann-Whitney U test).

Unlike the trace elements, *per gram* concentrations of POC and PON (and also P) only varied by a factor of two or three during each cruise and there was a significant (P <0.001 using a Mann-Whitney U test) increase in the mean concentration of each between D350 and D354, with POC increasing from 9 ± 2 to 19 ± 5 mmol g^{-1} and PON from 0.9 ± 0.3 to 1.9 ± 0.5 mmol g^{-1}. The POC and PON data from D351 would more closely resemble that from D350, but for one SAPS deployment outside of the main study area, east of Rockall (on 19th May; see D351-3 in Figure 4.1). Excluding the data from this sample results in a statistically significant difference between the mean *per gram* POC concentration measured during D351 (11 ± 3 mmol g^{-1}) and that during D354 (see above; P = 0.002 using a Mann-Whitney U test). The results for PON mirror those for POC.

Opal and PIC contributions to SPM mass were not measured on TM-SAPS samples, but data from Th-SAPS showed a large general increase between D350 and D354 in the POC/PIC ratio of material collected, and a smaller increase in the POC/opal ratio. This relative reduction in biomineral contribution to SPM accounts for the observed moles per gram increases in POC, PON and the various metals.

4.4.4.1 Spatial variation of pFe, pAl and organic material

The D350 metal data was dominated by the differences between concentrations observed in the Irminger Basin and those measured at station D350-8 (in ~1000 m deep water just south of Iceland) and within the Iceland Basin. Mean *per gram* concentrations of pFe and pAl in the Iceland Basin were approximately ten times and eight times greater respectively than those from the Irminger Basin, while absolute (*i.e. per volume*) concentrations were around five times greater. However, only three stations were occupied in each basin during D350, and the Iceland Basin data was heavily influenced by particularly high Fe and Al concentrations at station D350-7 (62 °N, 20 °W), as illustrated by the plot of *per gram* pFe concentrations shown in Figure

4.5. At the same station (D350-7), corresponding *per gram* pAl concentrations at 50 m were ~750 μmol g^{-1}, which, assuming a typical lithogenic source (8 % Al content by mass (Wedepohl, 1995)), suggests that lithogenic material accounted for approximately one quarter of the total SPM mass. The other two Iceland Basin stations showed a decrease in pFe and pAl concentrations with distance from Iceland, with those at D350-5 being indistinguishable from the Irminger Basin results. The same trend was broadly mirrored by absolute concentrations of pFe and pAl; absolute concentrations of pFe during D350 and D351 are included as an inset in Figure 4.5.

For the four stations during D350 at which samples were collected at two depths, *per gram* concentrations of pFe and pAl generally increased with depth (by up to a factor of ~10 between 50 m and 150 m at D350-4, above the Reykjanes Ridge). Absolute (nM) concentrations of particulate Fe and Al usually decreased slightly between the two depths in each case.

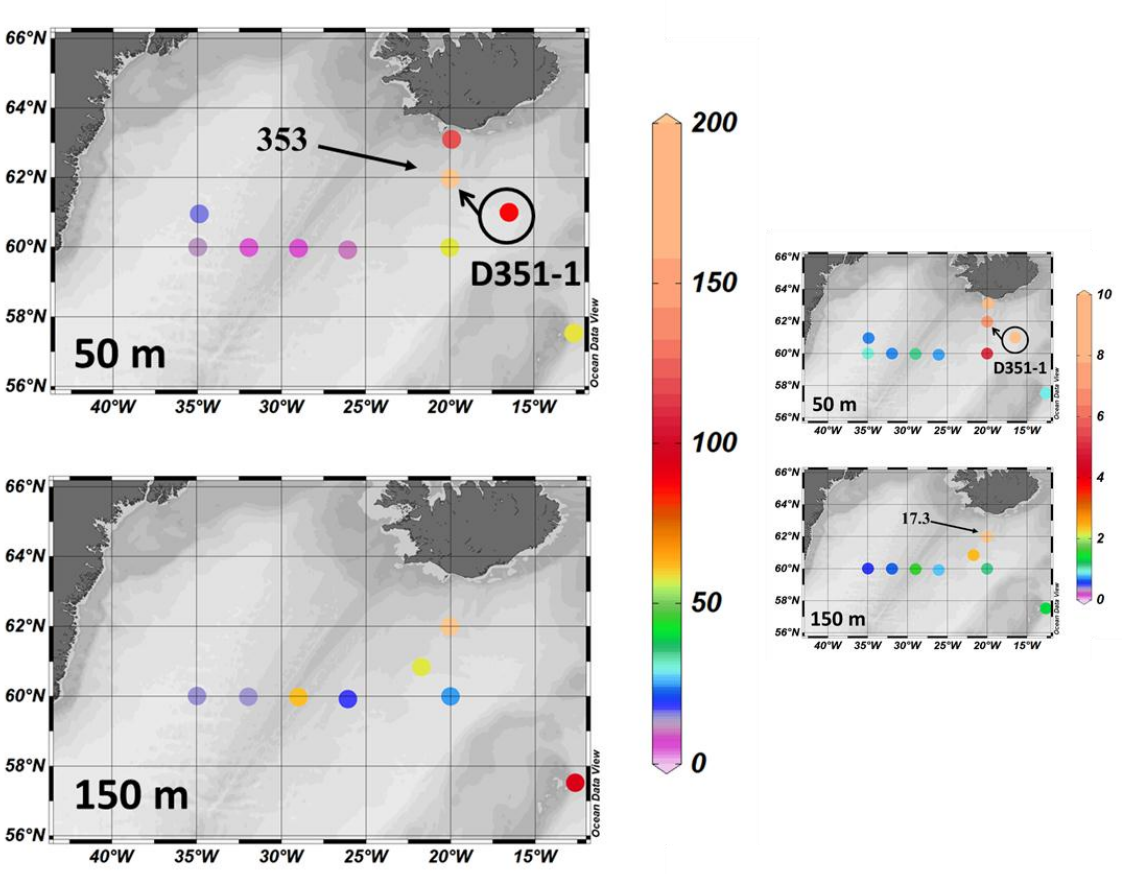

Figure 4.5: Iron concentrations in SPM during D350 and D351, in μmol g^{-1}, with (inset) absolute concentrations, in nmol L^{-1}, for comparison. Values are shown for 50 m and 150 m depth. Circled data point (D351-1) was collected at 62.0 °N 20.1 °W and has been displaced so that the data point for D350-7 can also be seen. Value for 50 m depth at D350-7 was 353 μmol g^{-1}.

POC and PON *per gram* concentrations were generally slightly lower in the Iceland Basin (mean PON: 0.69 ± 0.19 mmol g^{-1}, n = 4) than in the Irminger Basin (mean PON: 0.96 ± 0.41 mmol g^{-1}, n = 4), though that may be a result of the greater lithogenic influence on SPM composition in the former. With depth, *per gram* POC and PON concentrations either decreased or showed little change.

During D354, the concentrations for pFe and pAl (both absolute and *per gram*) in the Iceland Basin were again higher than those for the Irminger Basin, though to a lesser extent than during D350 (*per gram* pFe concentrations are shown in Figure 4.6, with absolute concentrations shown in the inset image). As before, one station in particular in the Iceland Basin had a significant influence in forcing up the average concentrations in the basin (in this case D354-2, located at 61.8 °N 21.1 °W), though with data from D354-2 excluded, the pFe and pAl concentrations were still generally higher in the Iceland Basin (Figure 4.6). Apart from at D354-2, mixed layer concentrations of iron in SPM were relatively low and uniform (though generally lower in the Irminger Basin). Concentrations of Fe and Al in SPM usually increased from the mixed layer to depth, while absolute pFe and pAl concentrations sometimes increased from the mixed layer to just below the mixed layer and sometimes decreased, and then usually increased from 50 – 150 m depth.

POC and PON concentrations within SPM did not show any significant difference between basins during D354 (PON was 2.0 ± 0.4 mmol g^{-1} in the Iceland Basin and 1.8 ± 0.4 mmol g^{-1} in the Irminger Basin). Concentrations per gram of SPM and per volume of seawater generally decreased with depth.

4.4.4.2 Size fractionation of pFe, pAl and organic material

During D350, material in >53 μm and 1 – 53 μm size classes each showed a decrease in POC and PON concentrations with depth, both per litre of seawater and per gram of SPM, as a consequence of remineralisation of material during sinking. During D354, the absolute concentrations again decreased with depth in each size fraction. However, the behaviour with depth of the *per gram* POC and PON concentrations for the >53 μm fraction varied between stations, sometimes increasing with depth, while concentrations in the 1 – 53 μm fraction showed a steady decrease (Figure 4.7*a,b*). Assuming that the larger particles represent relatively fast sinking material and that smaller particles are slower sinking or suspended, this suggests the loss of some material more labile than POM from the larger particles as they sink, resulting in an increase in the concentration of the remaining POC per unit mass. Biogenic silica seems the likely candidate for this more labile material, as preferential upper ocean

remineralisation of bSi relative to POC has been reported previously for the northeast Atlantic Ocean (Brown *et al.*, 2006). In contrast, the longer time taken for the smaller particles to reach depth means that the POC present will have undergone much more remineralisation and so show a decrease relative to the remaining mass.

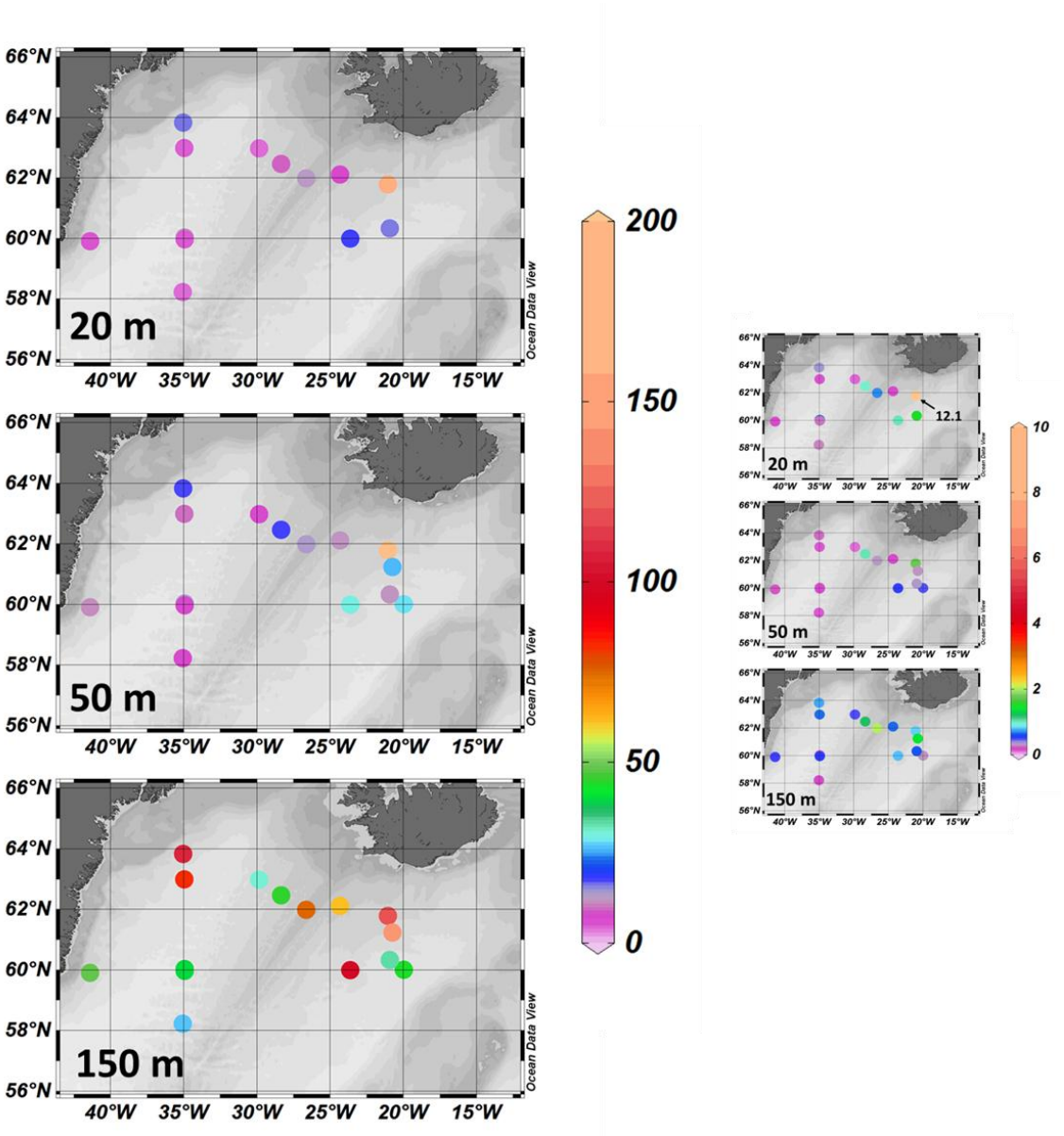

Figure 4.6: Iron concentrations in SPM during research cruise D354, in μmol g^{-1}, with (inset) absolute concentrations, in nmol L^{-1}, for comparison. Values are shown for 20 m, 50 m and 150 m depth. Colour bars are the same scale as those in Figure 4.5.

The increase with depth of Fe and Al concentrations in SPM was shown by both size fractions. During D350 and D351, higher *per gram* concentrations were usually found in the >53 μm size fraction at all depths, suggesting that larger particles were enriched in lithogenic material relative to smaller ones. Remineralisation of POC (and/or another

component of the particles) or scavenging of dissolved metals could serve to increase their concentration relative to the mass of material present as particles sank. Absolute concentrations of pFe and pAl in the > 53 µm size fraction showed a decrease or little change with depth during D350, suggesting that loss of POC, rather than scavenging was the dominant control to concentrate the metals in the SPM. The decrease in absolute concentrations of >53 µm pFe(Al) could be due to the break-up of sinking aggregates, or to recent increased input at the surface that had not yet sunk down through the upper water column. Absolute concentrations of pFe(Al) in the 1 – 53 µm size fraction showed little change with depth, which indicates that the breakup of larger particles was not the reason.

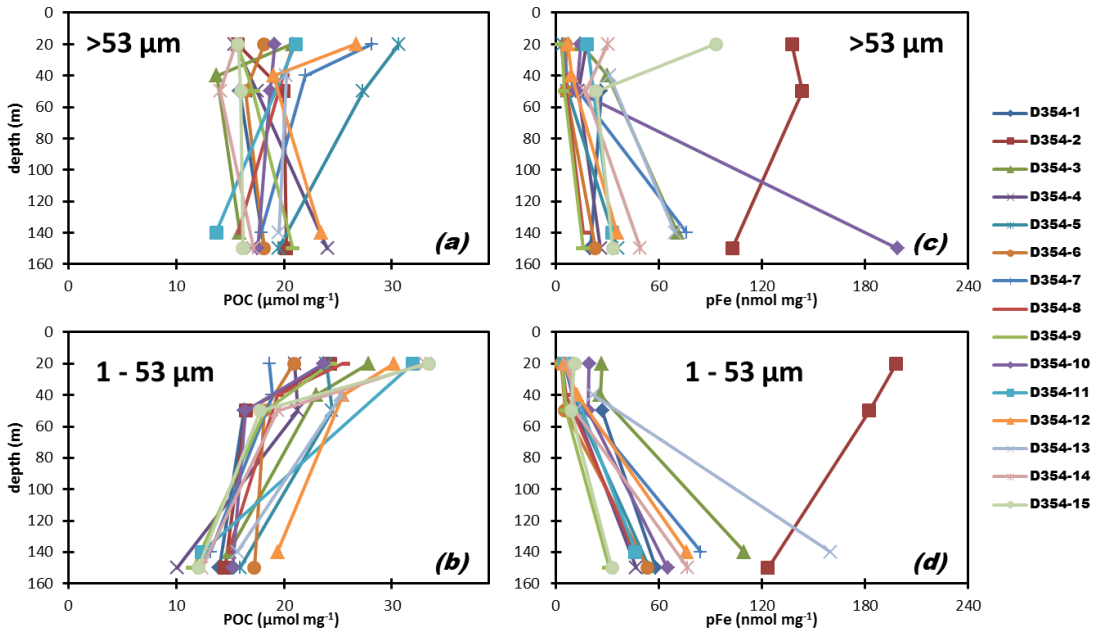

Figure 4.7: *Per gram* concentration results by size fraction for pFe and POC during D354. Plots show POC concentrations in SPM in *(a)* >53 µm and *(b)* 1 – 53 µm size fractions, and pFe concentrations in SPM in *(c)* >53 µm and *(d)* 1 – 53 µm size fractions.

During D354, the two size fractions generally had similar *per gram* concentrations of Fe and Al within the mixed layer (Figure 4.7*c,d*). Below the mixed layer, concentrations in both size fractions generally increased with depth, with those of the 1 – 53 µm size fraction usually slightly greater at 150 m depth than those of the larger particles. Thus, the situation was different to that during D350, where concentrations were greater in the >53 µm fraction. Furthermore, absolute concentrations of pFe and pAl generally increased with depth for the small size fraction while, for the larger particles, they often decreased slightly between the mixed layer and 50 m depth and then showed variable behaviour below that, sometimes increasing and sometimes decreasing with depth. Continuing the proposed explanation from above, it would appear that, in

contrast to D350, scavenging played a major role in the increase with depth of Fe and Al associated with SPM during D354, as well as the loss of POC through remineralisation. As before, the break-up of sinking aggregated material may explain the observed decrease in >53 μm pFe(Al) between the mixed layer and 50 m depth.

One station that did not fit in with the general observations during D354 was station D354-2. At D354-2 there was firstly a considerably higher *per gram* concentration of Fe and Al in particles in the upper water column, and secondly, these concentrations decreased with depth, as opposed to increasing at the other stations. The absolute concentrations of pFe and pAl did, however, decrease with depth at D354-2.

4.4.4.3 Leachable pFe and pAl

For each metal analysed (and phosphorus), the percentage of total particulate metal present in the labile fraction (*i.e.*, that proportion that was solubilized by acetic acid) was calculated for every sample, and the mean value and standard deviation for each cruise calculated. These results are shown in Figure 4.8. The figure includes corrections made for the amount of material lost to the deionised water rinse (see section 4.4.2), which it is assumed would otherwise contribute to the leach fraction for each element. The values calculated from the different cruises were in good agreement for each element, with the exception of significant differences for Mn and Co.

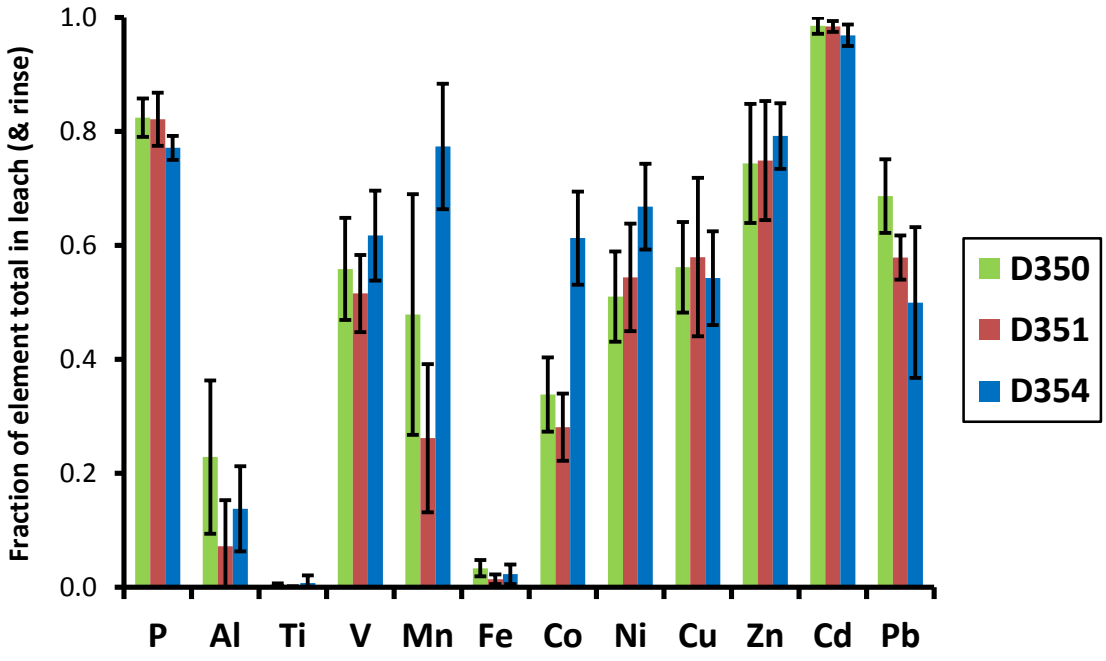

Figure 4.8: Average values, by element and by cruise, for the fraction of particulate metals present that was HAc-leachable. Error bars represent one standard deviation.

Cadmium was almost completely (~97 %) removed by the leach step, while zinc and lead were also found mostly in the leachable fraction. The most refractory elements in character were titanium and iron, for which <1 % and ~1.5 % respectively was leachable by acetic acid, while ~15 % of aluminium was removed on average. These elements also lost very little of their total particulate metal to the deionised water rinse.

Although only forming a small percentage of the total particulate iron throughout this study, the leachable fraction nevertheless showed variations. As with total pFe, the highest *per gram* concentrations were measured during D350 and D351, with the highest values at 62 °N 20 °W (22.3 μmol g^{-1} on >53 μm material collected at 50 m depth during D350-7), and at D350-8 (19 μmol g^{-1} in the >53 μm size fraction from 50 m). The percentage of pFe that was leachable showed a general increase with depth, best demonstrated by the three stations during D354 at which samples were collected down to 400 m depth (Figure 4.9). Aluminium showed a similar trend, though with a higher percentage of the total being leachable. As the leach is expected to displace adsorbed ions (Landing and Bruland, 1987), this trend is consistent with the leach removing scavenged Fe and Al from the surface of particles, with a greater proportion of the surface area coated by these ions at depth.

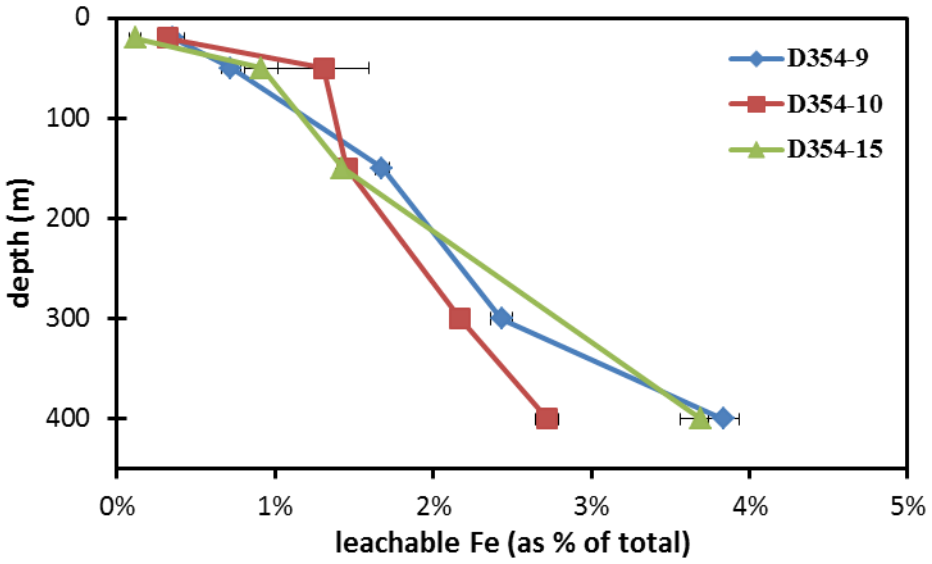

Figure 4.9: The percentage of total pFe present in leachable forms, as a function of depth, for three stations during D354. Error bars represent propagated errors from analytical uncertainties.

4.4.4.4 Consideration of elemental ratios

The total amount of pFe present in the upper water column does not necessarily represent a pool of available iron for uptake by phytoplankton, as can be deduced by consideration of its sources. The main supply routes for iron to the surface ocean are through upwelling and convective mixing of deeper water, atmospheric deposition, and lateral advection of surface waters that may have originated from shelf areas. Of these, atmospheric inputs are often of relatively refractory lithogenic material, with most of the iron locked up in aluminosilicate matrices and only sparingly soluble in seawater (*e.g.*, Buck *et al.*, 2006). Material introduced from below the mixed layer will likely consist of a mixture of refractory lithogenic iron and some contribution from iron that has been remineralised from biogenic particles and scavenged back onto particle surfaces.

The distribution of iron between different particle phases can be estimated by considering the contribution to the total SPM of the major types of particulate material (organic matter, lithogenic material, biomineral) and the typical degree of association of iron with them. In this study, biomineral (opal, calcite) contents were not measured as *per gram* contributions to SPM. The direct association of iron with them is assumed to be negligible (Collier and Edmond, 1984), though there is evidence for other metals such as aluminium to be incorporated into biogenic silica matrices at low molar ratios of 1 – 2 mmol mol^{-1} (Van Cappellen *et al.*, 2002; Middag *et al.*, 2009). The measured *per gram* POC concentrations were converted into POM concentrations by multiplying by a factor of 2.2 (Klaas and Archer, 2002). The average crustal content of ~8 % Al by weight (Wedepohl, 1995) was assumed to use pAl concentrations to estimate the lithogenic contribution to total mass (*i.e.*, pAl in μg g^{-1} multiplied by 12.5). Based on this, POM was calculated to make up 11 – 38 % (median 23 %) of the total SPM mass during D350/1 and 26 – 86 % (median 47 %) during D354, while lithogenic material contributed 0.5 – 30 % (median 4 %) during D350/1 and 0.2 – 12 % (median 2 %) of the total during D354. The remaining mass was presumably composed of opal and calcite associated with plankton and detritus.

Estimates of the Fe/C ratio of open ocean phytoplankton cells range from 3 – 136 μmol mol^{-1} (King *et al.* (2012) and references therein). If a conservative estimate of 10 μmol Fe mol^{-1} C (Twining *et al.*, 2004) is applied to the range of observed POC concentrations in this study, the algal pFe would account for just 0.01 – 2.9 % of total pFe during D350 and 0.1 – 8.0 % during D354. Using the highest Fe/C of 136 μmol mol^{-1}, the calculated biogenic Fe would amount to 0.2 – 40 % of the total during D350 and 1 – 106 % during D354.

A comparison of *per gram* pFe and POC concentrations (Figure 4.10) shows that no correlation between the two existed during D350/1, while during D354 they displayed a weak but statistically significant negative correlation (*i.e.*, pFe concentrations in SPM increased as POC decreased; r = -0.460, n = 47, P = 0.001). This agrees well with the observed changes of each with depth during D354 (Figure 4.7), and highlights the different processes acting upon the two elements in the upper water column (*i.e.*, remineralisation of POC, scavenging of dissolved and colloidal iron onto particles). Even if just the mixed layer samples for D354 are considered, there is no correlation between pFe and POC (r = 0.125, P > 0.05). This is presumably because, although a lower concentration of POM would decrease the relative mass of biogenic pFe in the material, it would simultaneously result in a proportionally greater contribution to the mass from any lithogenic pFe present.

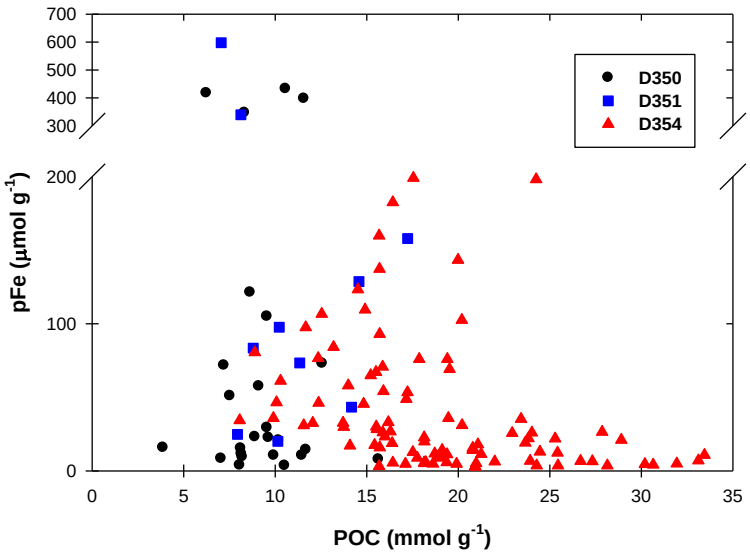

Figure 4.10: POC content of SPM against pFe content of SPM for cruises D350, D351 and D354. Note the change in scale for values of pFe above 200 µmol g^{-1}.

By contrast, comparison of the pFe data to pAl data showed a very good correlation for both cruise periods, with a correlation coefficient, *r,* of 0.979 for D350/1 (Figure 4.*11a*) and 0.965 for D354 (Figure 4.12*a*). Regression analyses for each plot of pAl against pFe, with the intercept set at zero, gave Fe/Al ratio values (the gradient of the regression line) of 0.46 mol mol^{-1} for D350/1 and 0.44 ± 0.02 mol mol^{-1} for D354. These values compare very well to the mean Fe/Al of aerosol material collected at sea during D350 (0.43 ± 0.06 mol mol^{-1}, calculated from five samples collected 29th April – 9th May 2010; A. Baker, *pers. comm.*), and also to that measured in ash samples collected during the Eyjafjallajökull eruption (0.47 mol mol^{-1}; Gislason *et al.* (2011)). In addition, correlations between pFe and pTi and between pTi and pAl were very strong

during both study periods (Figure 4.11*b & c*, and Figure 4.12*b & c*), with Fe/Ti and Ti/Al ratios also similar to those of ash collected from Eyjafjallajökull (5.9 mol mol^{-1} and 82 mmol mol^{-1} respectively; Gislason *et al.* (2011)).

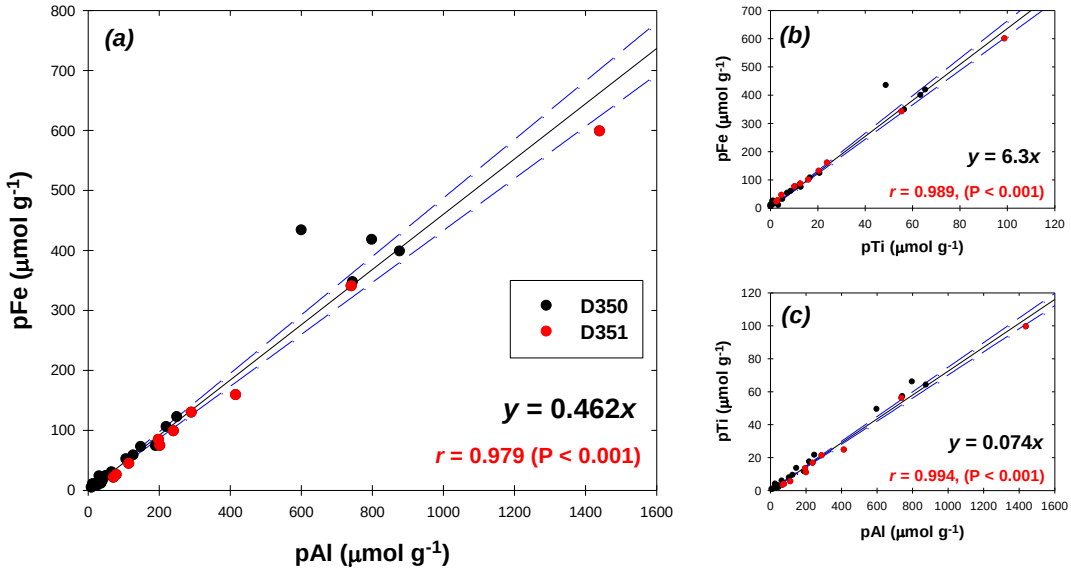

Figure 4.11: Scatter plots for D350 (black dots) and D351 (red dots) of concentrations in SPM of (a) pAl and pFe, (b) pTi and pFe, (c) pAl and pTi. Each includes the calculated regression line (solid black line) with 95 % confidence intervals (dashed blue lines), regression equation, correlation coefficient and P-value.

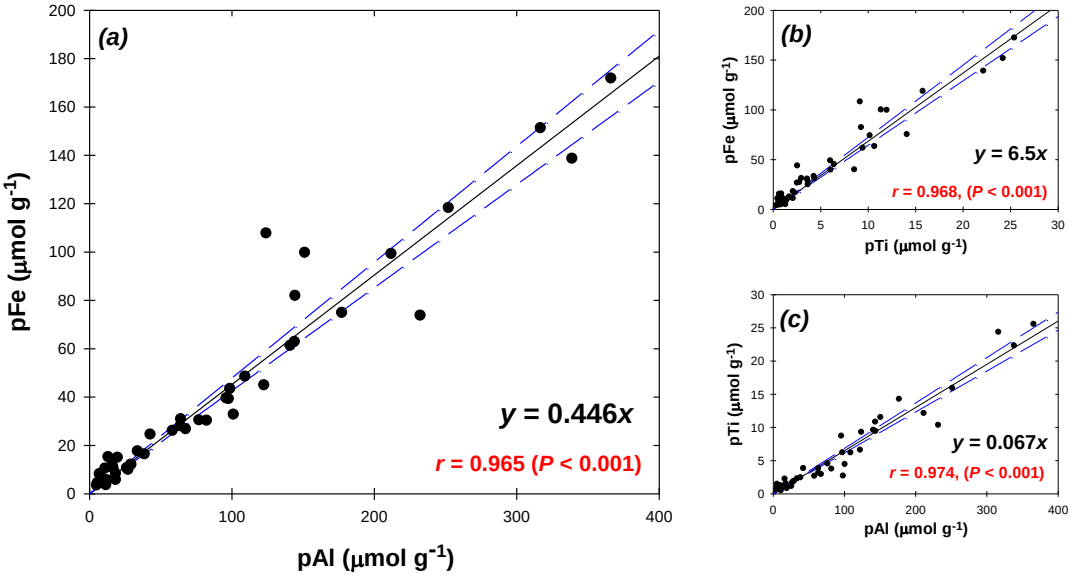

Figure 4.12: Scatter plots for D354 of concentrations in SPM of (a) pAl and pFe, (b) pTi and pFe, (c) pAl and pTi. Each includes the calculated regression line (solid black line) with 95 % confidence intervals (dashed blue lines), regression equation, correlation coefficient and P-value.

Clearly, *per gram* concentrations of pFe show closer behaviour to those of pAl than to POC, suggesting that the lithogenic fraction dominated pFe. Alternatively, it could just reflect that similar processes act to influence the relative concentrations of the two (*i.e.*, loss of organic material and scavenging of the metals). To study this idea more closely, the absolute concentrations of each were considered. Regression analysis of pFe with pAl for all three cruises, with the intercept set at zero gave an Fe/Al ratio of 0.395 ± 0.004 mol mol^{-1} (r = 0.9914, P < 0.0001; not shown), while doing the same for pFe with POC did not provide a significant relationship.

Plotting data from all three cruises for the absolute concentrations of pFe against POC, the data points did not show a clear single trend, but largely fell into two groups (Figure 4.13*a*). The first, consisting entirely of samples with pFe concentrations <5 nmol L^{-1}, showed a relatively small increase in pFe as POC increased. The second set showed a much greater increase in pFe concentrations with increasing POC, but with much more scatter.

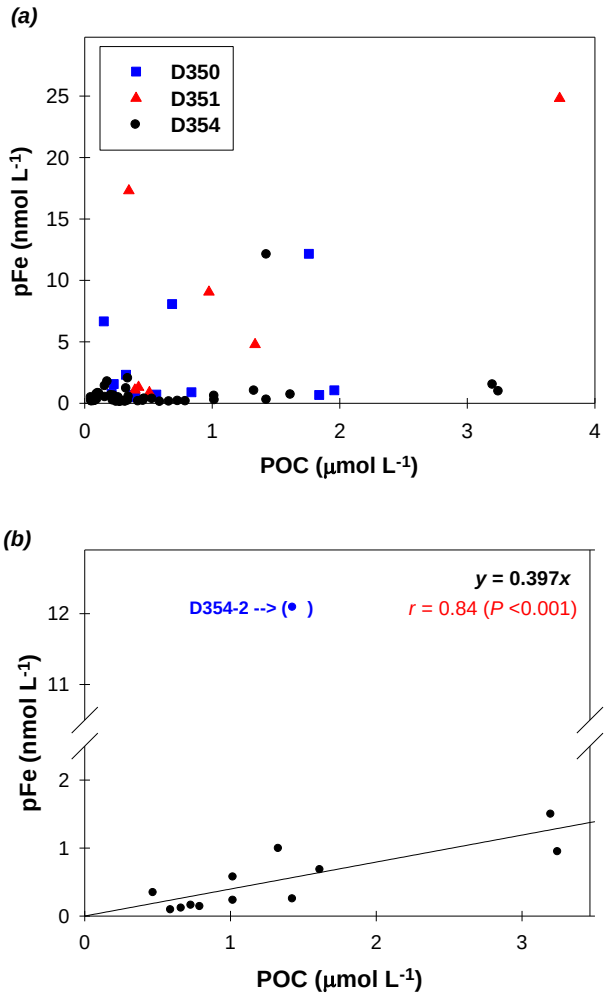

Figure 4.13: Absolute concentrations of POC plotted against those of pFe for *(a)* all samples from D350, D351 and D354, and *(b)* D354 mixed layer samples only, with regression line. Regression does not include sample D354-2, which had a much higher pFe concentration than any of the other stations.

Further investigation revealed that the first group was dominated by mixed layer data from D354. Considering only the mixed layer data from D354 (Figure 4.13*b*), there was a definite correlation between POC and pFe concentrations, with the exception of the results from station D354-2, which showed much higher pFe concentrations, relative to POC. With this data omitted, and the intercept set at zero, regression analysis of the data gave a pFe/POC ratio of 397 ± 82 μmol mol^{-1} (r^2 = 0.70, n = 12, P <0.001). This value is rather higher than the range of values collected by King *et al.*, though the regression analysis did not consider the lithogenic contribution to pFe.

4.4.5 Estimating the biogenic contribution to pFe

Due to the apparent dominance of the lithogenic contribution to pFe in the dataset as a whole, suggested by the correlations in Figures 4.11 and 4.12, the measured Fe/C ratios observed in particulate material were much higher than those reported elsewhere for predominantly biogenic material. Values ranged from 370 – 44,000 μmol mol^{-1} during D350, 1,960 – 50,800 during D351 and 146 – 10,000 during D354. However, not all of this pFe would be available for biological uptake. The inclusion of an acetic acid leach step in the sample treatment was to estimate the proportion of particulate iron that was readily available to phytoplankton. The leach is presumed to remove adsorbed metal ions and metals bound by organic matter, and to dissolve calcium and magnesium carbonates and amorphous (Fe and Mn) oxyhydroxides (Wells *et al.*, 2000). There is, however, evidence to suggest that such a leach does not remove all of the iron associated with biogenic material (Martin *et al.*, 1989; Hurst and Bruland, 2007; Berger *et al.*, 2008), and so estimates obtained using the method should be treated with care as probable underestimates of the bioavailable pFe.

As described in Section 4.4.4.3, only a small fraction of the total pFe collected with SAPS was removed using the acetic acid leach; typically <1 % in the surface mixed layer during D354, representing concentrations of only 1 – 21 pmol L^{-1}. Considering this fraction only, the ratio of "labile" Fe to POC (HAc-Fe/C) ranged from 6 – 1,700 μmol mol^{-1} during D350/1 and from 0.2 – 269 μmol mol^{-1} during D354. The highest values during D350/1 corresponded to the stations thought to be most influenced by ash inputs from Eyjafjallajökull and probably included a contribution from iron released by ash upon entering the ocean and then adsorbed back onto particle surfaces, while the lowest values, of <1 μmol mol^{-1}, were associated with mixed layer samples collected in the central Irminger Basin. The lower values are below the range of values reported for phytoplankton (King *et al.*, 2012), thus demonstrating that this approach generally represents a lower limit to the total biogenic pFe.

As discussed in Section 4.4.4.4, the D354 mixed layer data differed from the rest of the data set in that it showed a significant positive correlation between concentrations of POC and pFe, as well as between pFe and pAl. Multiple regression analysis of the data was carried out with respect to POC and pAl, again with the intercept set to zero, in order to see if variations in mixed layer pFe concentrations during D354 could be better explained by considering a combination of POC and pAl concentrations, as in Equation 4.2:

$$[pFe] = a.[POC] + b.[pAl] \qquad \text{(Eqtn. 4.2)}$$

where *a* and *b* are coefficients describing the ratio of pFe to the two relevant components of SPM. With the D354-2 data omitted, and using refractory pFe and pAl data so as to exclude contributions from scavenged material, the result gave values for *a* and *b* of (0.157 ± 0.049) x 10^{-3} ($P < 0.01$) and 0.420 ± 0.089 ($P < 0.0001$) respectively, with $r = 0.980$. In other words, the concentrations of pFe observed during D354 could be largely explained as consisting of a mixture of lithogenic material with a Fe/Al ratio of 0.42 ± 0.09 mol mol^{-1}, and biogenic material with a Fe/C ratio of 157 ± 49 μmol mol^{-1}.

The Fe/Al value is again close to that of the volcanic ash from the Eyjafjallajökull eruption, while the Fe/C ratio is higher than those listed by King *et al.* (2012), particularly the estimates based on single-cell analysis (6 – 40 μmol mol^{-1}) and radioisotope uptake experiments (3 – 11 μmol mol^{-1}). However, diatoms grown under iron-replete conditions have been shown to take up extra iron, reaching an Fe/C stoichiometry of ~300 μmol mol^{-1} (Sunda and Huntsman, 1995; Price, 2005). In addition, it should be considered that the metal and POC subsamples were collected on different filter types; the metal subsamples on polycarbonate membranes with a pore size of 0.4 μm and those for POC on GF/F filters with a nominal pore size of 0.7 μm. If a significant proportion of POC was present in the 0.4 – 0.7 μm size fraction, the Fe/C of samples would have been calculated higher than it should have, resulting in an overestimation of the POC coefficient in the multiple regression. Applying this Fe/C ratio to mixed layer samples gives an estimated range of biogenic pFe concentrations of 0.07 – 0.54 nmol L^{-1} (mean = 0.21 nmol L^{-1}).

When the same multiple linear regression approach was applied to the remaining D354 samples (*i.e.*, those collected below the mixed layer), no significant coefficient for the POC term was calculated, suggesting that the pFe data could be better explained by consideration of the pAl data alone. Similarly, the D350 & D351 data did not give a statistically significant value for the POC correlation coefficient. As the correlation between pFe and POC during D354 originated from consideration of the 20 m depth samples, it seems likely that the lack of pFe/POC correlation during the earlier cruises

stems from a dearth of samples from the surface mixed layer and a relative lack of biogenic pFe in the deeper samples that were collected.

An alternative approach to estimating the pool of biogenic Fe is through the difference between the total pFe pool and the contribution from lithogenic pFe, calculated from the pAl concentration and the Fe/Al ratio of the lithogenic material regarded as the source (*e.g.*, aerosol samples, eroded shelf sediments, local or global average crustal material). This method has been used during the FeCycle and CROZEX studies (Frew *et al.*, 2006; Planquette *et al.*, 2009), among others, while Martin *et al.* (1989) used a similar approach considering just the refractory fractions of pAl and pFe, presumably on the basis that the acetic acid leachable phase would mainly be associated with scavenged material.

The key to estimating biogenic pFe using this method is to select the correct Fe/Al ratio for lithogenic material in the study area. The FeCycle study used a value of 0.18 mol mol^{-1} (close to the global average of 0.19 suggested by Wedepohl (1995)), based upon analysis of Australian soil samples considered to be the main source following atmospheric transport to the study region (Frew *et al.*, 2006). Another estimate of the crustal global average Fe/Al ratio (0.33 mol mol^{-1}; Taylor, 1964) has also been used (Martin *et al.*, 1989). For the CROZEX study, the Fe/Al ratio of local basalt (0.51 mol mol^{-1}) was used, based upon the assumption that the main lithogenic source was lateral transport of material from the plateau (Planquette *et al.*, 2009).

In this study, the choice of Fe/Al ratio is complicated. Aerosol samples collected during D350 had an average Fe/Al of 0.43 mol mol^{-1}, due to influence from the Eyjafjallajökull eruption. During D354, aerosol samples had a much lower Fe/Al of 0.22 mol mol^{-1}, while basalt dredging along the Reykjanes Ridge has shown the local crustal material to have a ratio of ~0.61 mol mol^{-1} (Schilling *et al.*, 1983). The regression analysis carried out previously suggests that pFe concentrations of material collected by SAPS were linked to pAl concentrations by a ratio similar to that of the volcanic ash, suggesting that the much larger aerosol inputs during the spring, and the potential for transport of volcanic-derived material from the Iceland Shelf resulted in this material dominating the lithogenic SPM.

Nevertheless, the observed Fe/Al ratio of SAPS material showed significant variations. During D350, it ranged from 0.30 – 0.74 mol mol^{-1}, with a median value of 0.41 mol mol^{-1}. During D351 the range (median) was 0.29 – 0.44 (0.38) mol mol^{-1}, while during D354 it was 0.28 – 1.13 (0.44) mol mol^{-1}. The range, median and 25 % and 75 % quartiles for each cruise are compared in Figure 4.14*a*. The > 53 μm fraction generally showed a larger range in values than the 1 – 53 μm fraction, and typically had a higher median, as shown for D354 (Figure 4.14*b*), while the samples collected in the surface mixed layer during D354 also showed a higher median and greater range than those

collected at depth (Figure 4.14*c*). Some of these variations may be due to the amount of biogenic Fe present, especially where a higher Fe/Al is seen in the mixed layer during D354. Others, however, are likely to be due to variations in the Fe/Al ratio of source lithogenic material.

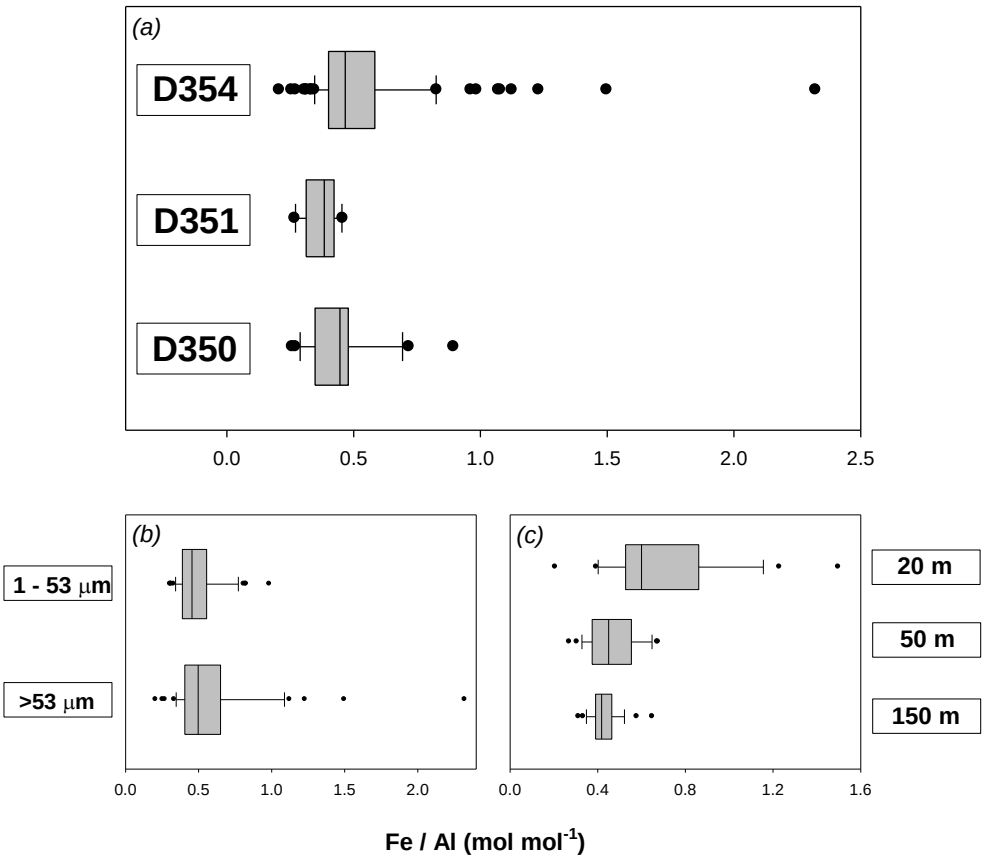

Figure 4.14: Box plots of measured Fe/Al molar ratios in total particulate material, showing variations between *(a)* cruises, *(b)* size fractions and *(c)* depth. Boxes represent interquartile range (left-hand and right-hand edges of box), divided by the median value; whiskers span values within 1.5 interquartile ranges of the quartiles and any values outside that range are represented as dots. For *(b)* and *(c)*, only data from D354 is used.

The two previously used crustal average Fe/Al estimates (0.19 and 0.33 mol mol^{-1}) were applied to refractory pAl and pFe data for the SAPS samples, along with the value of 0.43 mol mol^{-1} obtained from aerosol samples during D350 (assumed to be representative of volcanically-derived material). Table 4.7 shows the results calculated for the percentage of pFe in the lithogenic fraction, and for the concentration of biogenic pFe. In each case the range of values calculated is given, with the median value shown in brackets. The choice of Fe/Al ratio used for source lithogenic material has a significant impact on the calculated concentration of biogenic pFe; during D354 the biogenic pFe concentration calculated using 0.19 mol mol^{-1} as the Fe/Al ratio

averaged ~4 times greater than that using 0.43 mol mol^{-1}. Using the former gave calculated biogenic pFe concentrations in the mixed layer during D354 (excluding D354-2) of 0.1 – 1.1 nmol L^{-1}, while the latter gave concentrations of <0 – 0.7 nmol L^{-1}. The resulting biogenic Fe/POC ratio showed a similar variation. Applying a lithogenic Fe/Al ratio of 0.43 mol mol^{-1} resulted in an average biogenic Fe/POC ratio of 138 ± 145 μmol mol^{-1}, while applying the crustal average value of 0.19 mol mol^{-1} gave a biogenic Fe/POC of 258 ± 182 μmol mol^{-1}.

Table 4.7: Effect of the choice of Fe/Al ratio upon calculated values for the percentage of particulate Fe present in the lithogenic fraction and upon the calculated biogenic pFe concentrations. For each cruise and ratio, the ranges of calculated values are shown, based on pFe and pAl measurements. In each case the median value is shown in brackets.

	Fe/Al = 0.19	***Fe/Al = 0.33***	***Fe/Al = 0.43***
		Percentage lithogenic pFe	
D350	35 – 48 (38)	61 – 84 (65)	80 – 109 (85)
D351	43 – 61 (49)	74 – 105 (85)	97 – 137 (111)
D354	16 – 62 (39)	27 – 108 (68)	36 – 140 (88)
		Biogenic pFe concentration (nmol L^{-1})	
D350	0.3 – 7.0 (0.6)	0.1 – 3.0 (0.3)	<0 – 0.8 (0.1)
D351	0.5 – 12.7 (2.5)	<0 – 4.3 (0.7)	<0 – 0.5 (<0)
D354	0.1 – 7.3 (3.7)	<0 – 3.8 (1.9)	<0 – 1.4 (0.6)

In reality, it is unlikely that a single lithogenic Fe/Al ratio across the whole region is applicable in this case. The substantial deposition of volcanic ash to parts of the region during the eruption of Eyjafjallajökull in April/May 2010, along with transport of shelf sediments that may have originated in the same way (*i.e.* volcanic material with a similar Fe/Al ratio that has been resuspended and carried into the basin interior) may represent the dominant lithogenic source of material in parts of the region. But the aerosol samples collected during D354 showed that material from other sources also reached the region. Additionally, areas in the west of the Irminger Basin may receive inputs of material transported from the Greenland Shelf with a different elemental composition.

One result that is clear from Figure 4.14 is that during D354 the median Fe/Al was noticeably different between samples from the surface mixed layer (0.60 mol mol^{-1}) and samples collected deeper in the water column (~0.44 mol mol^{-1}). Assuming that

this general trend was not due to different source material for samples below the mixed layer, this decrease in observed Fe/Al must represent an increase in the percentage pFe contribution from the lithogenic fraction between the mixed layer and deeper water (from 69 % to ~86 %, using a source material Fe/Al of 0.43 mol mol^{-1}). This is the opposite to the situation observed during the FeCycle experiment, where the lithogenic component of pFe in the surface mixed layer of HNLC water was calculated to contribute 68 – 97 % of the total, compared to ~43 % at depths of 80 – 120 m (Frew *et al.*, 2006). In that study, the material sampled below the mixed layer consisted of sinking particles collected by sediment trap, and it was suggested that the low concentrations of pFe in the mixed layer (0.5 – 0.9 nmol L^{-1}) resulted in efficient conversion of the available lithogenic pFe to biogenic pFe during the estimated 100 day residence time, prior to export.

In this study, based on the use of a lithogenic Fe/Al ratio of 0.43 mol mol^{-1}, it would appear that despite similar mixed layer concentrations of pFe (0.1 – 1.5 nmol L^{-1}, with the exception of 12 nmol L^{-1} at D354-2), very little of the biogenic pFe from the mixed layer was exported to a depth of 50 m. This finding agrees with the correlation between pFe and POC, which was found for mixed layer samples only (Section 4.4.4); that a significant fraction of pFe at mixed layer depth during D354 was biogenic in character, but below the mixed layer that fraction quickly diminished.

The difference between this study and the FeCycle study is that here the observation is based on SPM at each depth, rather than mixed layer SPM and *sinking material* below the mixed layer. If the >53 μm size fraction (often used as a nominal sinking fraction) only is considered for material collected below the mixed layer, the relationship still exists but is weaker, with the percentage lithogenic contribution increasing from 69 % in the mixed layer to 78 % with depth.

4.4.6 Is there evidence of influence from the Eyjafjallajökull eruption during D350, D351 and D354?

The concentration ranges of several particulate metals, including pFe and pAl were generally higher during D350 and D351 compared to D354, with particularly high concentrations observed at stations D350-7, D350-8 and D351-1. The highest *per gram* concentrations measured in this project for Al, Ti, V, Mn, Fe, Co, Ni and Cu were all from D350-7 (62 °N 20 °W) or D351-1, a reoccupation of the same station six days later. This station, approximately 100 nautical miles south of the Eyjafjallajökull volcano, was located in a region thought to have received significant inputs of volcanic ash during the eruption, as was D350-8 (63.1 °N 19.9 °W; ~35 nautical miles south of

the volcano). It seems evident that the elevated concentrations of particulate metals observed at these stations were due to influence from the ash plume from Eyjafjallajökull.

However, elevated concentrations were also measured during the summer cruise, at station D354-2 (61.8 °N 21.1 °W), only ~35 nautical miles southwest of D350-7. Though the pFe and pAl concentrations measured were lower than those from D350-7 or from 170 m depth at D351-1, they were nevertheless elevated at all three depths and greater than those measured at 70 m depth at D351-1, suggesting a significant recent input of lithogenic material to the water column in that location and raising the possibility that the main source of particulate metals to the region may not be aerosol, but material advected from the continental margins. This raises the question of whether volcanic influence really was the cause of the high concentrations measured during the earlier cruises, D350 and D351.

Aerosol samples collected during D354 had a somewhat lower Fe/Al ratio (0.22 ± 0.04 mol mol^{-1}; mean of 5 samples collected 19th July – 6th August 2010 (A. Baker, *pers. comm.*)) than those during D350 (0.43 ± 0.06 mol mol^{-1}; mean of 7 samples collected 29th April – 9th May 2010). The latter showed the influence of the volcanic ash across the region during the eruption, having an Fe/Al ratio similar to that of ash collected closer to the volcano (Gislason *et al.*, 2011). Aerosol aluminium data from each cruise were used to estimate dust deposition rates, using an estimated deposition velocity of 0.7 cm s^{-1}. The D354 aerosol data gave an average value of 151 ± 60 μg dust m^{-2} d^{-1}, while data from D350 showed a large range from ~400 μg m^{-2} d^{-1} in the Irminger Basin and southern Iceland Basin to ~2000 μg m^{-2} d^{-1} in the central and northern Iceland Basin (stations D350-5 to D350-8) and up to 7 x 10^5 μg m^{-2} d^{-1} in the vicinity of the volcanic ash plume (A. Baker, *pers. comm.*).

The main volcanic eruption lasted ~6 weeks from mid-April to mid-May and although the main plume was generally located to the east of the study area, satellite imagery showed that local meteorological conditions sometimes resulted in low level ash being blown further west; a situation supported by the elevated dust concentrations observed in aerosol samples from the central Iceland Basin (an order of magnitude higher than measured during D354). Air mass trajectory analysis carried out using the NOAA Air Resources Laboratory HYSPLIT model (Draxler and Rolph, 2012) also showed that both the Irminger and Iceland Basins received air that had travelled over southern Iceland in the weeks prior to cruise D350 and during the volcanic eruption. Thus, it seems plausible that the higher Fe/Al ratio measured in SPM over the area during D354, relative to that of aerosol samples during the same cruise, was a result of significant material of volcanic origin from inputs during the eruption two months earlier.

The fact that the Fe/Al ratio of material collected by SAPS during D354 more closely resembled that of the aerosol samples from D350 seems to suggest that the greater amount of material deposited during the eruption was still dominating the lithogenic particle inventory of the upper ocean in both basins, either directly or through transport of material deposited elsewhere during the eruption and then resuspended and transported by local currents.

However, calculations made using PELAGRA data suggest a relatively short residence time for particulate Fe and Al in the surface mixed layer at the time of cruise D354, of 16 – 40 days, while fluxes derived from Th-SAPS at stations thought to be affected by high rates of ash deposition during D350 imply a residence time as short as half a day (see Chapter 5). This suggests that any atmospheric inputs of ash during the eruption should have been exported before the start of D354, consistent with the lower concentrations observed at most stations during that cruise.

Small sub-samples taken while rinsing material from SAPS filters were pipetted on to 25 mm diameter polycarbonate membranes and used for scanning electron microscopy (SEM). The images for samples collected at D350-7, D350-8 and particularly D351-1 revealed many lithogenic particles in the ~5 – 40 μm size range, many of which, when analysed by X-ray tomography, had a similar composition to ash samples collected by Gislason *et al.* (2011). This is consistent with the idea of the three stations being most affected by direct deposition of ash close to the time of sampling. Such particles were less evident in the sub-samples studied from D354-2, though not entirely absent. It seems likely that the majority of the higher particulate trace element concentrations measured at D354-2 were due to smaller granules of lithogenic material associated with aggregated organic material, rather than in the larger discrete particles, such as those observed in the D350 and D351 samples. This would be consistent with the micron-sized iron "hot spots" identified by Lam *et al.* (2006) in both 1 – 53 μm and >53 μm size fractions of material collected in the subarctic Pacific, which were hypothesised to have been transported to the open ocean from the continental margin.

4.4.7 A SAPS-derived estimate of sinking pFe flux

The radioactive isotope, ^{234}Th, is scavenged onto particles in the upper ocean and as a result, is employed in a technique to estimate export flux out of surface waters. ^{234}Th is formed through radioactive decay of naturally occurring ^{238}U, an isotope that behaves in a conservative manner in seawater and is therefore present in concentrations proportional to salinity (Chen *et al.*, 1986). As ^{234}Th is scavenged onto particles, which then sink out of the upper ocean, a deficit forms in the upper water column between

the total ^{234}Th activity, relative to that of ^{238}U. Thus, by quantifying the ^{234}Th/^{238}U disequilibrium, the extent of ^{234}Th loss through scavenging by sinking particles can be calculated.

If the POC/^{234}Th ratio in sinking material is also known, the POC flux can then be estimated. The method relies on an assumption that processes such as horizontal and vertical advection and turbulent diffusion, which can also influence the ratio of ^{234}Th to ^{238}U, are negligible (Morris *et al.*, 2007). From the resulting estimate of POC export, the concurrent export of other elements can be estimated if the ratio of those elements to POC (or to ^{234}Th directly) in sinking material is also measured at the depth considered. This process has been employed to estimate fluxes of biominerals (Sanders *et al.*, 2010) and trace metals (Weinstein and Moran, 2005; Planquette *et al.*, 2011).

During D354, Th-SAPS were deployed simultaneously with the 50 m and 150 m TM-SAPS at all but two stations (D354-10 and D354-15, when deployments were carried out separately with 12 and 6 hours delay respectively between TM-SAPS and Th-SAPS). Total (particulate and dissolved) ^{234}Th activities in the upper water column were measured, and Th-SAPS samples processed as described by Morris *et al.* (2007). From the resulting calculated ^{234}Th fluxes (dpm m^{-2} d^{-1}) and POC/^{234}Th ratios from material collected by Th-SAPS, a range of POC fluxes of 3 – 23 mmol m^{-2} d^{-1} were calculated for the >53 μm size fraction at 50 m depth (F. Le Moigne, *pers. comm.*). Using the molar Fe/C and Al/C ratios measured for the same size fraction from the corresponding TM-SAPS, pFe fluxes of 0.8 – 28 μmol m^{-2} d^{-1} and pAl fluxes of 2 – 54 μmol m^{-2} d^{-1} were calculated, with median values of 5.4 and 11.3 μmol m^{-2} d^{-1} respectively. These values are significantly higher than those measured using PELAGRA (see Chapter 3), the possible reasons for which will be discussed in Chapter 5.

For the earlier cruises, no Th-SAPS were deployed during D351, while POC fluxes calculated for the >53 μm size-fraction of 50 m samples during D350 ranged from 4 - 23 mmol m^{-2} d^{-1}, a similar range to that estimated during the summer cruise. Applying the pFe/POC ratios measured by the TM-SAPS resulted in estimated pFe fluxes of 2 – 342 μmol m^{-2} d^{-1}, with the highest value being that at D350-7, where elevated pFe concentrations coincided with a relatively low (12 nmol L^{-1}) POC concentration measurement by the TM-SAPS. Using the same approach, the 50 m depth, >53 μm size-fraction pAl fluxes during D350 ranged from 8 – 653 μmol m^{-2} d^{-1}.

4.5 Summary

Suspended particulate material samples were collected using *in situ* pumps during three cruises to the high latitude North Atlantic, in order to study variations in POC and particulate trace metal concentrations and to improve understanding of the biogeochemical cycling of iron. The first two cruises coincided with an eruption of the Icelandic volcano, Eyjafjallajökull, which was responsible for a large input of ash to the surface ocean in the region, as demonstrated by aerosol samples collected at the time. There was some evidence of this input increasing the particulate trace metal concentrations in stations closer to the volcano, with a general gradient of decreasing pFe and pAl concentrations with distance from the volcano observed within the Iceland Basin during D350, while Irminger Basin stations showed lower, more uniform concentrations.

However, high pFe and pAl concentrations at one of the Iceland Basin stations during D354 suggest that another source may also have contributed to the relatively high concentrations in the earlier cruises, with advection of material from the relatively close Iceland Shelf the likely origin. Results from D354 also showed a generally slightly higher concentration of particulate metals in the Iceland Basin, which, along with lower POC concentrations contributed to a greater contribution to total mass from lithogenic material.

The collection of samples within and at two or more depths below the mixed layer during D354 allowed the trends with depth of POC and pFe to be compared. POC concentrations in seawater decreased with depth for both small (1 – 53 μm) and large (>53 μm) particles, while the *per gram* concentration in large particles often showed little change with depth, with organic material calculated to contribute 40 – 60 % of the total mass in that size fraction. This is consistent with particles >53 μm being relatively fast-sinking, organic-rich aggregates, which drive export of POC to depth. In contrast, *per gram* pFe concentrations increased with depth in both size fractions, partially due to the reduction in organic (and perhaps opal) content in the material, while the increase in absolute concentrations of pFe sometimes observed show the effects of scavenging of remineralised iron back on to particle surfaces. This was also shown by the increase with depth of the relative contribution from leachable iron to the total pFe pool.

During D354, the Fe/Al ratio of particulate material was shown to be more variable and with slightly higher median values in the >53 μm size fraction and within the mixed layer. Despite the wider range observed during D354, the median Fe/Al values

observed during all three cruises were similar to those of ash ejected during the Eyjafjallajökull eruption. As aerosol samples collected during D354 suggested an input to the surface ocean of material with a considerably lower Fe/Al, it would seem that the lithogenic material in the upper water column was either dominated by the greater input during the eruption, or else mainly influenced by material with a non-atmospheric source, such as erosion products from the local continental shelf/slope that may have been distributed by the local currents. The short residence times (of the order to 1 – 3 days) calculated for pFe and pAl from Th-SAPS and TM-SAP data suggest that the latter is a more plausible explanation.

The Fe/C ratio observed varied from values close to those reported for phytoplankton to values ~1000 times higher in areas with a relatively strong lithogenic influence, while HAc-Fe/C ratios ranged from below reported cellular requirements to values observed in iron-replete diatoms (0.2 – 269 μmol mol^{-1} during D354). The variable Fe/Al ratios observed make it hard to choose a value that represents that of source lithogenic material suitable for all samples, but estimates using an Fe/Al of 0.43 mol mol^{-1} suggest that the contribution to pFe from biogenic Fe was greatest within the mixed layer during D354, with little of that material being exported as deep as the second pump (ten metres below the mixed layer). This is different to the findings of the FeCycle project, where a partial transformation of lithogenic to biogenic iron within the mixed layer, prior to export, was proposed.

Questions remain as to the contribution of the 0.4 – 1 μm fraction of SPM to particulate iron, as it was not considered in this study, and also to the primary source of the lithogenic fraction of pFe in the region, though SEM analysis of some samples suggests a greater number of large lithogenic particles in the stations thought to have had greatest volcanic ash inputs (D350-7, D350-8, D351-1). Data concerning dissolved and total dissolvable concentrations of Fe, Al and Mn in the region may help to further explain the observed distributions of the particulate metals.

Chapter 5: Towards the synthesis of iron budgets for the high latitude North Atlantic

5.1 Overview

The FeCycle programme culminated in a novel attempt to synthesise a biogeochemical iron budget in low iron HNLC waters (Boyd *et al.*, 2005). In this chapter, the pFe data collected from deployments of PELAGRA sediment traps and SAPS in the high latitude North Atlantic are used as the basis for constructing similar budgets for this region. Budgets are prepared for both basins using the data collected during D354, with another prepared for part of the Iceland Basin during the Eyjafjallajökull eruption. The features of these budgets are compared to previous budgets, and the nature of the similarities and differences between them addressed, and the implications for the cycling of iron are discussed. The fluxes measured by PELAGRA and estimated by SAPS are also compared.

5.2 Previous iron budgets

Putting together a biogeochemical budget provides a good way of summarising the information known about an element in a particular environment and highlighting what is not known. For iron, there have been very few such budgets produced, testament to the difficulties inherent in making many of the measurements.

Following the Southern Ocean Iron RElease Experiment (SOIREE), Bowie *et al.* (2001) summarised the standing stocks and fluxes that were measured, or estimated, in order to determine the fate of the dFe added during the experiment. Pools of dissolved and particulate iron were measured directly, while biogenic Fe pools were estimated from measurements of biomass and from measured and literature values of Fe/C ratios. The dominant Fe input for the budget was the known input of ferrous sulphate added during the fertilisation experiment, while many of the smaller inputs and loss terms were estimated from model and literature values. Sinking biogenic flux was based on POC flux and literature values for plankton species-specific Fe/C ratios, while non-biogenic sinking pFe flux was estimated by difference of input and output terms.

The FeCycle experiment, in which an area of water was labelled with SF_6, produced an iron budget for HNLC waters southeast of New Zealand. It did include direct measurements of sinking pFe flux, with differentiation made between lithogenic and biogenic contributions by consideration of the Fe/Al ratio of the sinking material (Frew *et al.*, 2006). The same distinction was made for the mixed layer pFe pool, which was measured directly throughout the study. Atmospheric input was estimated from literature data for the study region, while lateral advection and vertical diffusive supply were calculated using dFe measurements and by consideration of the SF_6 tracer data (Boyd *et al.*, 2005). The resulting budget is shown in Figure 5.1. The Fe/C ratio of particulate material in the mixed layer was calculated to have a mean value of 42 μmol mol^{-1}, while the residence time of pFe in the surface ocean was estimated from the export flux and mixed layer inventory to be ~100 days (Frew *et al.*, 2006).

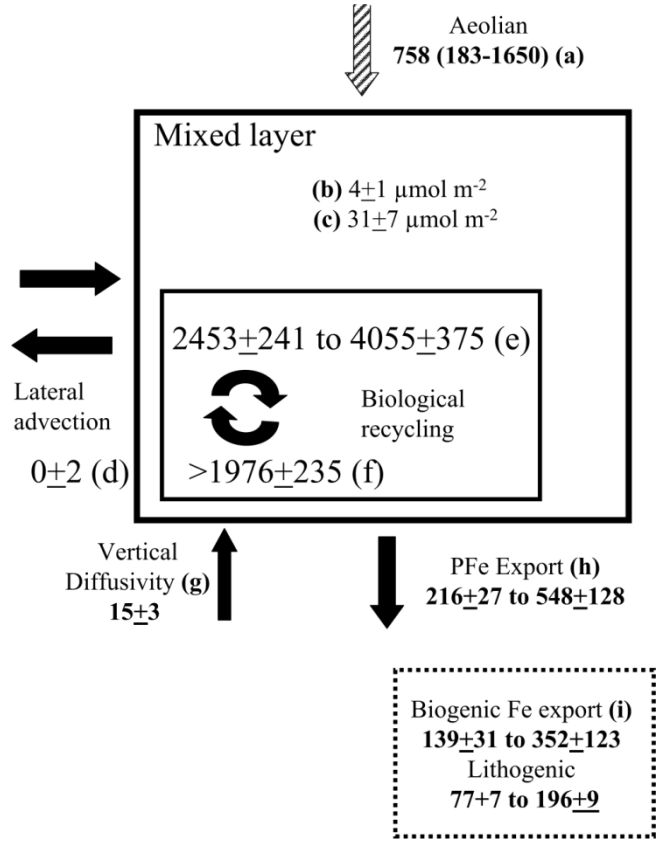

Figure 5.1: Iron budget for the surface mixed layer during FeCycle, reproduced from Boyd *et al.* (2005). All fluxes are in nmol Fe m^{-2} d^{-1}. Term "(a)" is the literature-derived atmospheric deposition rate, pools "(b)" and "(c)" are the calculated dFe and pFe inventories respectively, "(d)" is lateral advection of dFe, "(e)" and "(f)" are biological uptake and regeneration rates, "(g)" is vertical diffusive supply, "(h)" is measured pFe export and "(i)" is the estimated biogenic and lithogenic contribution to pFe export flux. Full details of measurements and construction of the budget are outlined in Boyd *et al.* (2005).

Iron budgets were also produced for three contrasting sites in subantarctic and polar frontal waters south of Australia during the SAZ-Sense project (Bowie *et al.*, 2009). Export of pFe and atmospheric deposition were measured directly, as were the dFe and pFe inventories, while lateral advection and vertical diffusion terms were calculated using a mixture of measurements, literature values and model results. In each case, atmospheric deposition seemed to be the dominant input, though the uncertainties associated with the numbers were large. With the same caveat, total inputs were larger than removal terms in each case. Calculated mixed layer particulate Fe/C ratios were measured at 32 ± 30 to 55 ± 14 μmol mol^{-1}. No consideration was given to the distribution of pFe between lithogenic and biogenic material.

An Fe budget was also prepared for the waters surrounding the Crozet Islands, in the Southern Ocean (Planquette *et al.*, 2011). Vertical and lateral advective inputs of dFe were calculated from measured concentrations and radium isotope data, and atmospheric Fe input was calculated using calcium and silicon concentrations in aerosol samples. Particulate Fe export through sinking particles was calculated using pFe/POC and POC/^{234}Th ratios of >53 μm particles, collected by *in-situ* pumps deployed 10 m below the base of the mixed layer, and from measurements of the integrated ^{234}Th flux. In addition, the flux of labile pFe was calculated from the ratio of acetic acid leachable pFe to POC in the >53 μm particles and the same ^{234}Th approach.

Although atmospheric inputs were estimated to be of a similar magnitude to those in the other studies, the input through lateral advection of dFe was calculated to be slightly higher, while the downward pFe flux calculated was considerably higher (typically ~100 times) than that measured using sediment traps during FeCycle or SAZ-Sense. POC export was also at least ten times higher than in the previous studies (Frew *et al.*, 2006; Bowie *et al.*, 2009; Planquette *et al.*, 2011). The large downward pFe flux was ascribed to a large flux of lithogenic pFe advected from the Crozet Plateau, some of which was available for conversion to biological pFe. The biological pFe downward flux estimates from CROZEX, at 840 – 50,000 nmol m^{-2} d^{-1}, were also considerably higher than those measured during FeCycle (see Figure 5.1). Due to the high pFe concentrations measured, the Fe/C ratios calculated for the waters surrounding the Crozet Islands (in particles below the mixed layer) were also higher than those during FeCycle and SAZ-Sense, at 404 – 39,000 μmol mol^{-1}. These features highlight the much greater influence of lithogenic material on the biogeochemical cycle of Fe at the Crozet Islands, relative to the regions studied during FeCycle and SAZ-Sense.

5.3 Iron measurements in the HLNA

This section brings together many of the relevant iron measurements made during research cruises D350 and D354. Where possible, a distinction is made between values calculated for the Iceland Basin and those for the Irminger Basin. Although finalised dFe data is not yet available, some estimates are made based on preliminary data, or on approximate expected values using literature sources.

5.3.1 Suspended pFe concentrations

As described in Chapter 4, SAPS were deployed at a total of fifteen stations during D354; eight of these were in the defined limits of the Irminger Basin and five within the Iceland Basin, with the two others being over the Reykjanes Ridge (see Figure 4.1). At most stations, a pump was deployed at 20 m depth (within the mixed layer), with further pumps deployed 10 m below the base of the mixed layer and a further 100 m deeper in the water column.

Measurements of the mixed layer pFe concentration (material >1 μm in size) ranged from 0.09 – 12.1 nmol L^{-1}, though apart from station D354-2, collected in the Iceland Basin on 13th July, all of the measured concentrations were <1.5 nmol L^{-1}. Excluding D354-2, the mean (± 1σ) mixed layer pFe concentration across the region was 0.50 ± 0.45 nmol L^{-1}. The average mixed layer depth in both basins (measured throughout the sampling period) was 35 m, giving estimated mixed layer pFe inventories for the basins of 12 ± 10 μmol m^{-2} for the Irminger Basin (n = 8) and 43 ± 12 μmol m^{-2} (n = 2; D354-2 excluded) for the Iceland Basin (total range for all stations across the region except D354-2 was 3 – 52 μmol m^{-2}).

Due to a limited number of SAPS units and to time constraints, only one SAPS deployment within the mixed layer was carried out during D350, with that taking place at D350-8 on 8th May 2010. At that station, expected to be influenced by volcanic ash deposition from the Eyjafjallajökull eruption, the measured pFe concentration (12.2 ± 0.2 nmol L^{-1}) was around an order of magnitude higher than any mixed layer concentrations measured during D354, except D354-2 (see above). It was similarly greater than any of the other pFe concentrations measured during D350, other than those at different depths at the same station and at D350-7. Thus, it seems likely that the value was influenced from volcanic material (possibly in addition to shelf-derived material) and not representative of the region as a whole. Applying the measured

concentration to the mixed layer depth, (~40 m on average, during D350), gives a pFe inventory of 510 μmol m^{-2}.

5.3.1.1 Lithogenic versus biogenic pFe in the surface mixed layer

As described in Chapter 4, the determination of lithogenic and biogenic fractions of pFe through the use of Fe/Al ratios of lithogenic material is rather subjective, particularly in studies that cover a reasonably large area, such as this. The choice of ratio can have a strong effect, and the assumption of a common source material, with a constant Fe/Al ratio, can lead to false interpretation of the data. Nevertheless an effort is made here to differentiate between the two. Two different Fe/Al ratios are considered; the global crustal average of 0.19 mol mol^{-1} (Wedepohl, 1995) is frequently cited and compares well to the Fe/Al ratio measured in aerosol samples collected during D354, while the value of 0.43 mol mol^{-1} represents the average measured in aerosols during D350 and resembles that of volcanic material (Gislason *et al.*, 2011) thought to have had a strong influence in the region (see Chapter 4).

Using an Fe/Al ratio of 0.19 mol mol^{-1}, the proportion of pFe in the Irminger Basin during D354 contributed by biogenic pFe was estimated to be 70 ± 15 % (*n = 8*), and that for the Iceland Basin 67 ± 8 %. Using the same ratio, the biogenic fraction at D350-8 was calculated to contribute 56 % of the total. Applying the ratio of 0.43 mol mol^{-1} to pAl data gave relative biogenic pFe contributions of 33 % and 25 % for the Irminger and Iceland Basins respectively during D354 and only 0.5 % for D350-8.

5.3.2 Mixed layer dFe concentrations

Surface water samples for dFe analysis were collected while underway using a trace-metal clean towed fish, with additional mixed-layer samples collected in 10 L trace metal clean Ocean Test Equipment sampling bottles with external springs, which were deployed using a titanium-frame CTD at each station. Unfortunately, data are not yet finalised. Previous measurements of dFe in the central Iceland Basin, during July to September 2007, averaged 0.09 nmol L^{-1}, with a range of <0.01 – 0.22 nmol L^{-1} (Nielsdóttir *et al.*, 2009). Initial results suggest a similar range during this study, while showing slightly higher surface dFe concentrations in the Iceland Basin than in the Irminger Basin. For the purposes of this budgeting exercise, average values are based on preliminary results and are taken to be 0.18 nmol L^{-1} for the Iceland Basin and 0.11

nmol L^{-1} for the Irminger Basin. This gives mixed layer dFe inventories of 6.3 and 3.9 μmol m^{-2} respectively.

As for D354, the dFe results for D350 are not yet finalised. Preliminary data shows a general increase along the cruise track from the Irminger Basin (~0.1 nmol L^{-1}) into the Iceland Basin (0.2 – 0.3 nmol L^{-1}) to ~0.4 nmol L^{-1} near SAPS stations D350-7 and D350-8. Using the latter value gives a mixed layer inventory of 16 μmol m^{-2}. Surface water dFe concentrations increased further as the ash plume itself was approached, reaching values > 3 nmol L^{-1}, which would yield a mixed layer dFe inventory of >120 μmol m^{-2}. No corresponding SAPS samples were collected so close to the ash plume.

5.3.3 Sinking flux of pFe

For the purposes of preparing a budget for iron in the surface mixed layer, the key measurement of sinking particle flux is the export flux. Ideally this would be measured immediately below the base of the mixed layer, but practical constraints make this implausible. PELAGRA traps were used to measure downward particle flux during D354, with two deployments of three traps each at depths of 80 m, 150 m and 400 m (see Chapter 3). In the Irminger Basin, the 80 m trap measured a sinking pFe flux between 26th – 28th July of 706 ± 183 nmol m^{-2} d^{-1}, while the trap deployed at 80 m in the Iceland Basin between 4th – 6th August measured a flux of 1083 ± 250 nmol m^{-2} d^{-1}.

As an alternative measure of pFe export, for each station, measurements from the TM-SAPS and Th-SAPS pumps deployed 10 m below the mixed layer were combined. SAPS-derived concentrations of pFe in the >53 m size fraction (assumed to constitute sinking material), along with the Fe/C ratio of the material, was combined with the C/^{234}Th ratio of material from the corresponding Th-SAPS, and the integrated ^{234}Th flux to provide an estimate of pFe flux at that depth. Measured values ranged from 0.8 x 10^3 – 19.3 x 10^3 nmol m^{-2} d^{-1} (excluding the value from D354-2), with mean values of 15.7 x 10^3 ± 3.4 x 10^3 nmol m^{-2} d^{-1} for the Iceland Basin (*n* = 3) and 4.0 x 10^3 ± 2.0 x 10^3 nmol m^{-2} d^{-1} for the Irminger Basin (*n* = 7). These are considerably higher than the fluxes measured by PELAGRA at 80 m, and the two approaches are discussed further in Section 5.4.1.

As no PELAGRA traps were used during D350, SAPS data only is used to estimate export flux of pFe. SAPS-derived concentrations of pFe in >53 μm size material at 10 m below the base of the mixed layer ranged from 0.1 – 0.3 nmol L^{-1} at the first five stations, then increased to values of 0.8 and 1.1 nmol L^{-1} at D350-7 and D350-8 respectively, again showing the influence of volcanic ash deposition and/or shelf water. The calculated estimates for export flux of pFe, based on Fe/C ratios of TM-

SAPS material and C/^{234}Th ratios from Th-SAPS, ranged from 2 – 48 μmol m^{-2} d^{-1} for the earlier stations and increased to ~340 μmol m^{-2} d^{-1} at D350-7 (no Th-SAPS data available for D350-8). As expected, the latter value was considerably higher than those estimated during D354 using the same method. The corresponding POC flux estimates (from Th-SAPS) ranged from 4 – 39 mmol m^{-2} d^{-1}, which compare well to ^{234}Th-derived POC export calculated in the region following a spring diatom bloom during a previous study (30 – 53 mmol m^{-2} d^{-1}; Martin *et al.* (2011)). Thus, the higher pFe fluxes calculated were likely due to a combination of a significant bloom/export event within the time integrated by the ^{234}Th method and elevated pFe concentrations resulting from volcanic ash inputs.

5.3.4 Aerosol Fe inputs

Aerosol samples were collected between 19th July and 6th August during D354 and had a mean Fe concentration of 161 ± 73 pmol m^{-3} (n = 5). This translates to a mean dry deposition flux of 98 ± 44 nmol m^{-2} d^{-1}, using an assumed average deposition velocity of 0.7 cm s^{-1} (A. Baker, *pers. comm.*). Due to the limited number of samples collected, most of which were collected while underway in the Irminger Basin, the value shown is taken as the estimated input for the entire HLNA region. There was no significant difference apparent in the one sample collected entirely within the Iceland Basin compared to those collected in the Irminger Basin. The calculated dry deposition flux was at the low end of annual mean aerosol iron deposition rate estimates for the region derived from models (49 – 490 nmol m^{-2} d^{-1} (Duce and Tindale, 1991), 340 – 860 nmol m^{-2} d^{-1} (Jickells *et al.*, 2005)). Of the aerosol Fe, 4 – 11 % was determined to be soluble (using an ammonium acetate leach at pH 4.7 as described in Baker et al. (2006)), giving an estimated soluble Fe flux of 7 ± 3 nmol m^{-2} d^{-1}. Wet deposition of Fe was not measured.

Aerosol sampling during D350 showed increasing influence of the volcanic eruption as the cruise track approached southern Iceland. The first two samples, collected between the Irminger Basin and southern Iceland Basin (*en route* to D350-5), showed an iron concentration of 0.7 – 1.1 nmol m^{-3}, corresponding to inputs of 420 – 640 nmol m^{-2} d^{-1} if using the same 0.7 cm s^{-1} deposition velocity. The estimated inputs increased to 2.1 x 10^{3} – 2.8 x 10^{3} nmol m^{-2} d^{-1} for samples collected in the Iceland Basin (up until station D350-8), while aerosol Fe input in the vicinity of the ash plume was calculated at 28 x 10^{3} – 920 x 10^{3} nmol m^{-2} d^{-1}.

5.3.5 Vertical turbulent diffusivity

A vertical turbulence profiler was deployed at 21 stations during D354, with ten profiles to at least 120 m depth completed at most stations. From these, an average diffusivity (across both basins) of 1.08 x 10^{-5} m^2 s^{-1} was calculated. Although a final figure for vertical turbulent diffusive flux of iron depends upon finalisation of the dFe data, a preliminary estimate of a mean 10 nmol m^{-2} d^{-1} has been calculated. This compares to a previous estimate for the Iceland Basin-averaged vertical turbulent flux of dFe of 2.6 nmol m^{-2} d^{-1} (Forryan *et al.*, 2012).

No measurements of vertical turbulent diffusivity were made during D350.

5.4 Discussion

5.4.1 Reasons for observed differences in D354 pFe flux estimates

There are a number of reasons why the flux measurements of pFe made during D354 by PELAGRA and by SAPS could differ. First of all, the shallowest SAPS-derived flux estimates are from just below the mixed layer depth; the relatively short collection time for each deployment allowed for the depth to be specifically targeted following an initial CTD deployment. The shallowest PELAGRA traps, by comparison, were deployed ~40 m below the base of the mixed layer in order to provide scope for potential deepening of the layer over the course of the longer deployment time (>48 hours), which also had the likelihood of covering a larger area. However, the large disparities in estimates also found for the deeper SAPS and PELAGRA traps (42 ± 37 μmol m^{-2} d^{-1} compared to 1.8 ± 0.6 μmol m^{-2} d^{-1}; both deployed at ~150 m depth), suggest that this was not a significant factor in the differences.

More significantly, the two methods measured fluxes over different timescales. Whereas sediment traps record the actual material sinking into the trap over the relevant sampling time (in this case ~48 hours), the $^{234}Th/^{238}U$ disequilibrium method provides an integration of fluxes over a period of ~1 month (half-life, $t_{1/2}$, of ^{234}Th is 24.1 days). Thus, the higher pFe fluxes estimated using SAPS measurements of concentrations and of the $^{234}Th/^{238}U$ disequilibrium may be due to a previous, elevated export of material in the region which was missed by the traps during their relatively short deployments. Furthermore, although the sediment traps sampled over a larger

area than each SAPS deployment, due to their drifting with local currents while collecting material, the greater number of SAPS deployments during the study period means that the latter gave greater spatial and temporal coverage of the region over the course of the cruise (see Figure 3.9 *cf.* Figure 4.1). In the Irminger Basin, for example, SAPS coverage during D354 extended over five degrees of latitude and thirteen degrees of longitude.

However, the pFe flux estimates calculated from SAPS data had much larger uncertainties associated with them. This is partly a direct result of the greater spatio-temporal coverage described; the mean and standard deviations shown above were no doubt influenced by patchiness in pFe export from the mixed layer. Another factor is the number of assumptions made in calculating pFe flux from SAPS data. The ^{234}Th method of estimating flux itself involves several assumptions, such as negligible influence of advection and turbulent diffusion in controlling ^{234}Th distribution (Morris *et al.*, 2007). Additionally, as the SAPS method relies upon the product of Fe/C and C/^{234}Th ratios of the sampled material and the ^{234}Th/^{238}U disequilibrium that developed over the weeks prior to sampling, it is possible that the C/^{234}Th of the SAPS material was not representative of the material responsible for the measured disequilibrium. The radionuclide ^{234}Th is thought to trace total mass flux rather than POC flux specifically (Verdeny *et al.*, 2009) and so an enhanced flux of biominerals or lithogenic material, relative to POC, prior to sampling could potentially lead to an overestimation of POC flux.

In addition to this, during this study the pFe and ^{234}Th measurements were made on separate samples, albeit ones that were collected simultaneously with the same type of pump and (>53 μm) filter, and at approximately the same depth (± ~2 m). Thus, having calculated the ^{234}Th activity flux, the pFe flux was determined using the POC/^{234}Th ratio of the Th-SAPS and the pFe/POC ratio of the TM-SAPS to calculate a pFe/^{234}Th ratio, which was then multiplied by the ^{234}Th activity flux. The differences in POC concentration between Th-SAPS and TM-SAPS deployed simultaneously (Section 4.4.2.2) highlight the potential for inaccuracy in estimating fluxes of other elements in this way. An overestimation of ^{234}Th activity flux, POC/^{234}Th ratio of the Th-SAPS or pFe/POC ratio of the TM-SAPS could all result in an overestimation of pFe flux using the SAPS technique.

Partly as a result of this, and partly because the most thorough Fe budgets previously published have estimated sinking flux from free-drifting sediment traps (Frew *et al.*, 2006; Bowie *et al.*, 2009), the pFe fluxes measured by PELAGRA are used here as the preferential choice for estimating flux in each basin. The SAPS-derived fluxes from D354 are compared to other studies that have used *in-situ* pumps rather than sediment traps, including the measurements made during D350.

5.4.2 High latitude North Atlantic iron budgets

5.4.2.1 D354 budgets

Figure 5.2 shows the iron budgets for (*a*) the Irminger Basin and (*b*) the Iceland Basin during summer 2010. At present the dFe inventory and vertical diffusion flux terms are provisional, being reliant on data that is not finalised, while there are no measurements available for lateral advection of dissolved or particulate iron. It is evident from the figure that the budgets for the two basins were similar during the period of study. The mixed layer inventory of iron was higher in the Iceland Basin, approximately by a factor of three, and the pFe export flux was also slightly higher. In both cases the measured export of pFe was significantly higher (by a factor of 6.5 to 10 times) than the measured inputs, suggesting either a missing input term or systems that were steadily losing iron from a diminishing reservoir.

Mixed layer residence times were calculated for pFe using the export flux and pFe inventory, as was done at the FeCycle site (Frew *et al.*, 2006) and yielded values of 16 days for the Irminger Basin (2 – 42 days, based upon associated uncertainties) and 40 days (23 – 66 days) for the Iceland Basin. Assuming that the measured export fluxes were representative of the respective basins and had not suddenly increased just before sampling took place, such residence times would have required a large standing stock of pFe in the mixed layer to have sustained the inventory up until the time of sampling, or must have been steadily replenished by another input.

One candidate for such an input is lateral advection of material from continental margins, which was not measured as part of the budget and was discussed in both Chapters 3 and 4 as a potential contributor to high particulate metal fluxes measured by a 400 m deep PELAGRA trap and to high pFe concentrations at station D354-2 respectively. Evidence for such transport has been shown for other regions with varying degrees of magnitude and to various distances from the continental shelf (Lam *et al.*, 2006; Lamborg *et al.*, 2008a; Planquette *et al.*, 2009). Unfortunately, with only one successful 80 m trap deployment in each basin, there is also the chance for enhanced local fluxes to bias export results, which could account for the discrepancy observed in the budgets.

Alternatively, there is potential for greater atmospheric input to have occurred in the run-up to the cruise or, as a large area was covered, during the cruise. Backward air mass trajectory analysis for the region, using the HYSPLIT model and based on an arrival height of 100 m, suggests that air masses that had passed directly over Iceland

reached the Iceland Basin in the week prior to the first sampling and in between the two periods of sampling within that basin (11th – 15th July and 3rd – 7th August 2010).

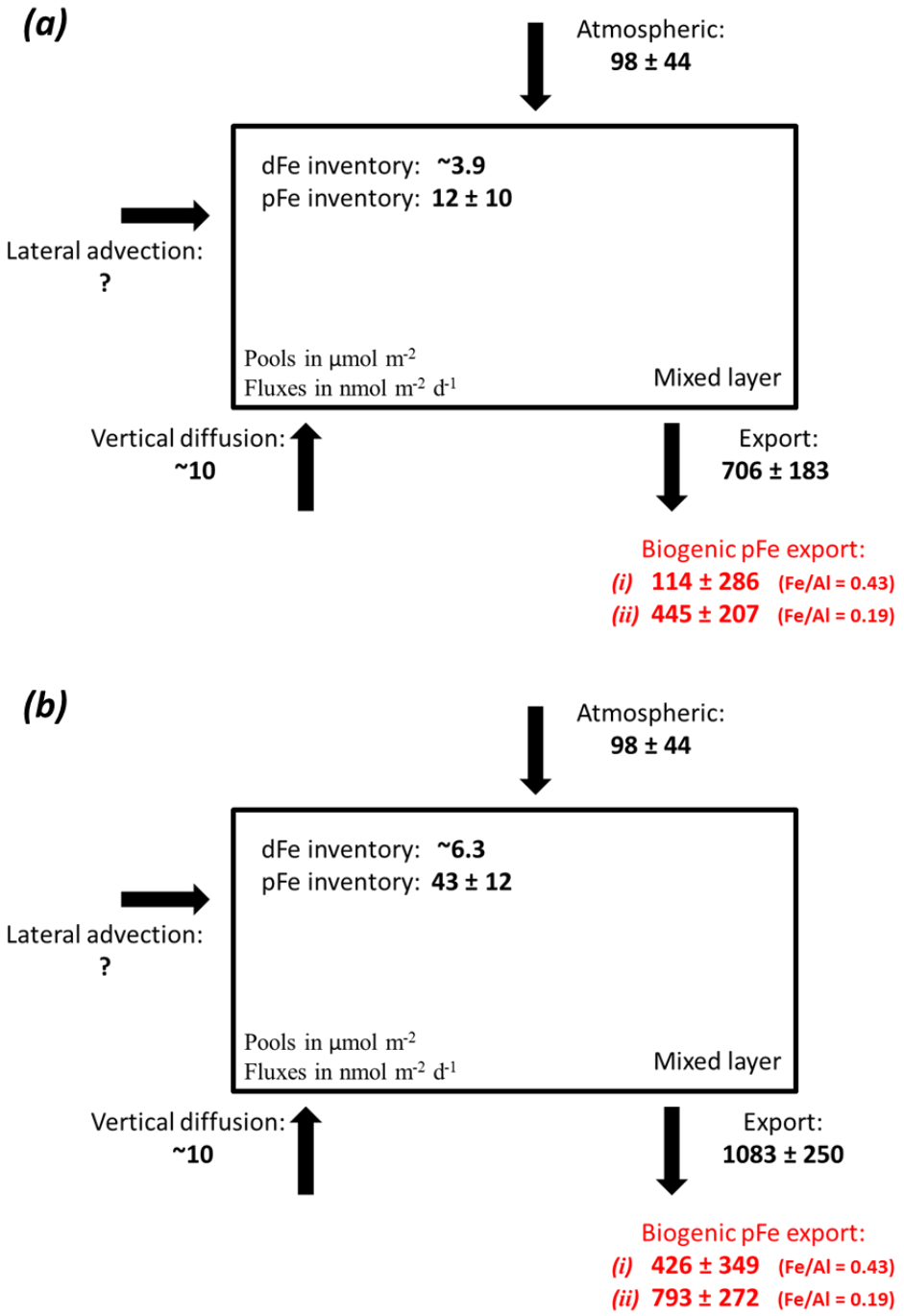

Figure 5.2: Partial biogeochemical iron budgets for *(a)* the Irminger Basin and *(b)* the Iceland Basin during D354, with pools in µmol m^{-2} and fluxes in nmol m^{-2} d^{-1}. Atmospheric Fe input (shown as mean and standard deviation) is averaged over both basins during the entire cruise period, as is vertical diffusion of dFe. Inventory values for pFe are mean and standard deviation of multiple stations, while dFe values are provisional estimates. Export values are sinking pFe flux measured for each basin by one PELAGRA trap at 80 m depth (with propagated uncertainty). Biogenic pFe export (in red) is calculated by applying Fe/Al ratios of *(i)* 0.43 and *(ii)* 0.19 to pAl fluxes measured by the same trap.

The region can receive sporadic atmospheric input from proglacial dust storms originating in Iceland, though the summer months are typically a time of low dust concentrations (Prospero *et al.*, 2012). For the Irminger Basin, there is less evidence of locally-derived atmospheric inputs during the period of interest: the model suggests that air masses affecting most of the basin in the run up to the sampling period had not passed over land for at least three days prior. Parts of the region did receive significant inputs of volcanic ash during the Eyjafjallajökull eruption in spring 2010, which could therefore be a candidate for the high inputs of Fe prior to D354 sampling needed to account for the observed discrepancy between inputs and outputs.

5.4.2.2 D350 iron budget: volcanic influence on the HLNA Fe cycle

The budget shown in Figure 5.3 was constructed to summarise the known Fe biogeochemical data for the area influenced by the Eyjafjallajökull eruption only, thought to include stations D350-7 and D350-8. As there were no sediment traps available to directly measure sinking flux during D350, the SAPS-derived pFe fluxes were used. No measurements were made of the vertical turbulent diffusivity during D350, though it is thought that such a term would represent a relatively minor input of Fe to the surface mixed layer.

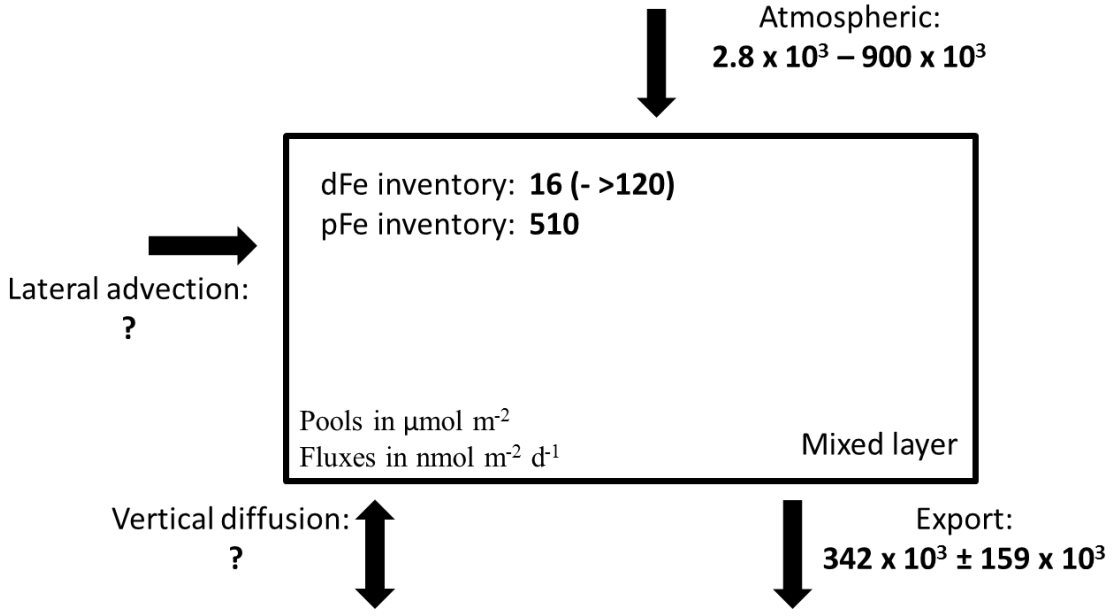

Figure 5.3: Partial biogeochemical iron budget for the region of the Iceland Basin influenced by heavy volcanic ash deposition. Fluxes shown are in nmol pFe m^{-2} d^{-1} and inventories in μmol m^{-2}. Values shown were measured as described in the text.

The known values included in Figure 5.3 were all of a greater magnitude than their counterparts in the D354 budgets. The total mixed layer iron inventory was upwards of thirty times larger, while the calculated atmospheric input was 28 – 9000 times that measured during D354. The export flux of pFe shown in Figure 3, estimated from SAPS measurements, equates to between 140 and 960 times the values measured by PELAGRA during D354 (or 45 – 250 times the export flux estimated during D354 using SAPS data). Clearly the volcanic eruption and ash deposition had a large effect on the iron cycle in the region.

Unlike during the summer cruise, the calculated export term falls within the range of measurements for atmospheric input, consistent with a large input of volcanically-derived material that rapidly sank out of the mixed layer. Using the same approach of considering the export flux and mixed layer pFe inventory to calculate residence time of pFe, an estimate of just 1 – 3 days was calculated for the data shown in Figure 5.3, much shorter than that calculated for the Iceland Basin during D354. This rapid throughput of pFe is supported by sinking experiments carried out on ash samples collected during the cruise; results demonstrated that the volcanic material had a size-dependent residence time of 1 hour to 1 day, assuming a 30 m mixed layer (Achterberg *et al.* submitted).

This finding appears to rule out the possibility of volcanic ash inputs in the spring leading to a large inventory of surface mixed layer pFe that was gradually exported over the next 2-3 months; instead it appears to have largely passed quickly through the system. As a result, consideration of the D350 budget supports the argument for a lateral input of pFe to balance the budgets in Figure 5.2.

5.4.3 Comparison to previous budgets

Table 5.1 summarises the measurements made for the three iron budgets shown in Figures 5.2 and 5.3, alongside those made for the FeCycle, SAZ-Sense and CROZEX budgets. As outlined in Section 5.2, not all of the budgets were approached in the same way; no mixed layer measurements of pFe concentrations were made during the CROZEX study, while no consideration of biogenic pFe flux was made during SAZ-Sense. Measurements of export were made by drifting sediment traps during FeCycle, SAZ-Sense and during cruise D354, while *in-situ* pumps were used for the CROZEX study and during D350 (and also during D354 for comparative purposes – see Section 5.4.1). The table does however allow comparisons to be made between estimates made for different areas if the variations in approach are considered.

Table 5.1: Summary of measurements made for iron budgets in this and previous studies.

	FeCycle[1,2]	*SAZ-Sense 1*[3]	*SAZ-Sense 2*[3]	*SAZ-Sense 3*[3]	*CROZEX*[4,5,6]	*D354 Irminger*	*D354 Iceland*	*D350*
Mixed layer inventory								
pFe (μmol m^{-2})	31 ± 7	4 ± 1	6 ± 2	7 ± 5	n/a	12 ± 10	43 ± 12	~510
dFe (μmol m^{-2})	4 ± 1	14 ± 2	11 ± 1	31 ± 5	n/a	~3.9[a]	~6.3[a]	16 – 120+[a]
POC (mmol m^{-2})	n/a	152 ± 110	101 ± 18	575 ± 436	n/a	41 ± 34	69 ± 39	~72
pFe/POC (μmol mol^{-1})	42	40 ± 31	55 ± 14	32 ± 30	n/a	305 ± 225	613 ± 221	~7200
Fluxes (nmol m^{-2} d^{-1})								
Atmospheric	183 – 1650	488 ± 386	288 ± 180	354 ± 212	~890	98 ± 44	98 ± 44	2.8×10^3 – 900×10^3
Vertical diffusive dFe	15 ± 3	-2 ± 0	7 ± 1	-31 ± 5	34	~10[a]	~10[a]	n/a

Table 5.1 continued…

	FeCycle[1,2]	*SAZ-Sense 1*[3]	*SAZ-Sense 2*[3]	*SAZ-Sense 3*[3]	*CROZEX*[4,5,6]	*D354 Irminger*	*D354 Iceland*	*D350*
Fluxes (nmol m^{-2} d^{-1})								
Lateral advective dFe	0 ± 2	67 ± 22	24 ± 7	124 ± 53	228	n/a	n/a	n/a
pFe export	216 ± 27 – 548 ± 128	166 ± 89	69 ± 14	213 ± 51	(~40000)[b]	706 ± 183	1083 ± 250	(342×10^3 ± 159×10^3)[b]
Biogenic pFe export	139 ± 31 – 352 ± 123	n/a	n/a	n/a	(~12000)[b]	114 ± 286 – 445 ± 207	426 ± 349 – 793 ± 272	(54×10^3 – 203×10^3)[b]
Export pFe/POC (μmol mol^{-1})	218 ± 51	50 ± 38	33 ± 15	248 ± 125	n/a	~344	~248	(~50700)[b]
pFe residence time (days)	~100	~24	~87	~33	n/a	~17	~40	~1.5

"n/a" is data not available.
[a] Values are provisional.
[b] Values in brackets were measured using *in situ* pumps rather than sediment traps.
References: [1] (Boyd *et al.*, 2005), [2] (Frew *et al.*, 2006), [3] (Bowie *et al.*, 2009), [4,5,6] (Planquette *et al.*, 2007; 2009; 2011).

Comparison of the mixed layer inventory terms in Table 5.1 shows that the HLNA budgets shared with that of FeCycle a dominance of the total iron pool by particulate iron, unlike the SAZ-Sense sites which were relatively pFe poor. The most noticeable feature of the inventory terms, other than the much higher values for all Fe terms associated with the D350 budget, is the relatively low POC pool calculated in all three HLNA budgets. It is not known if this is a result of an under-estimation of POC concentrations in this study (see Section 4.4.2.2 for discussion). If so, it could be expected that the HLNA POC concentrations listed would be too low by a factor of three or four. The adjusted values would take them within the range of the SAZ-Sense values.

The mixed layer pFe pool estimated for the Irminger Basin was similar to that for the previous budgets, while that for the Iceland Basin was slightly higher than the FeCycle study. Combined with the low POC concentrations, these result in higher mixed layer Fe/C ratios than for the previous studies. Even with any correction to POC concentrations (and assuming that the same would not need to be made to pFe concentrations), the Iceland Basin Fe/C ratio would be 3 – 5 times higher than that for the previous budgets. The higher Fe/C in the HLNA therefore seems to be a combination of higher pFe concentrations (compared to SAZ-Sense sites) and lower POC concentrations (relative to FeCycle). The even higher Fe/C ratio observed in the D350 budget was evidently a result of the much greater pFe concentrations measured at that time.

The aerosol input measured during D354 was the lowest of such estimates for the budgets included in Table 5.1. This is not surprising as the SAZ-Sense cruise took place during the annual maximum of Australian aerosol supply (Bowie *et al.*, 2009), while the FeCycle value was derived from literature data rather than direct measurement. The atmospheric input data demonstrates that the high latitude North Atlantic, like the areas for which the previous budgets were prepared, is usually an area of relatively low dust deposition. The D350 measurements, by far the greatest in the dataset, highlight the perturbation to the system resulting from the plume of volcanic ash.

The vertical diffusive flux estimated for the HLNA region during D354 was within the range measured at the other sites, and this term represents a small contribution to the budget in all cases. Though no such flux was calculated during D350, it is not thought that it would vary significantly from the other values listed and would therefore only represent a minor contribution to the D350 budget. Unlike the previous budgets, no lateral advective dFe flux has yet been calculated for the HLNA. Estimates for the other sites suggest that it could represent a significant contribution to the budget. Not included in the table is the lateral advective flux of pFe estimated for the Crozet

Plateau, which was calculated (by difference) to be of the same order as the export pFe flux at that site, making it one of the largest terms in the CROZEX budget (Planquette *et al.*, 2011).

Export of pFe during D354 was ~3 to 16 times greater than at the SAZ-Sense sites and roughly twice the magnitude as during FeCycle, both of which studies used drifting sediment traps. POC export fluxes during D354 (2 – 4 mmol m^{-2} d^{-1}) were similar in magnitude to those during FeCycle (2.5 mmol m^{-2} d^{-1}) and those at SAZ-Sense 1 and 2 (2 – 3 mmol m^{-2} d^{-1}; SAZ-Sense 3 had a lower flux of 0.9 mmol m^{-2} d^{-1}). This is reflected in the relatively smaller Fe/C ratios in exported material at SAZ-Sense 1 and 2. Export of pFe during D350 was only comparable in magnitude to that of the CROZEX study (which it exceeded by nearly an order of magnitude), again highlighting the effect of the large Fe input upon the system.

Finally, the residence times calculated for each budget, based upon comparison of the sinking pFe flux to mixed layer pFe inventory, shows that the values calculated for the D354 HLNA budgets were within the range of estimates from previous similar studies. The D350 budget, by contrast, showed a much shorter residence time, as the large amount of particles introduced through deposition of volcanic ash quickly sank through the upper water column, meaning that the increased iron concentrations measured in the surface mixed layer would have been a transient feature that would have soon returned to normal levels following cessation of ash inputs.

5.5 Summary and conclusions

Data from PELAGRA and SAPS measurements of pFe have been used, along with aerosol data and provisional dFe measurements, to construct iron budgets for the Irminger and Iceland Basins during summer 2010, and for an area of the Iceland Basin under the influence of volcanic ash deposition during spring 2010. During D354, the mixed layer in the Irminger Basin was calculated to have a generally lower Fe inventory than the Iceland Basin, though the latter was possibly biased by the small number of stations sampled. Though pFe concentrations during D354 were similar to those in FeCycle (and in the Irminger Basin, to those in the SAZ-Sense study), Fe/C ratios ranged from 3.5 to 18 times greater, due to lower POC concentrations measured in this study and to specific stations with higher pFe levels. The pFe concentration at the one station sampled in the northern Iceland Basin during D350 was an order of magnitude greater than those from D354 and up to two orders of magnitude greater than those in previous studies.

Estimates of pFe export made during D354 using *in situ* pumps and consideration of ^{234}Th disequilibria were up to twenty times greater than those made using PELAGRA sediment traps, highlighting the caution that should be used when comparing results calculated by the two methods. Comparisons of SAPS-derived pFe export showed that in the summer of 2010 the HLNA had a lower pFe export flux than that observed on the Crozet Plateau, but that at the time of the Eyjafjallajökull eruption, areas of the Iceland Basin had a significantly higher flux than that measured near the Crozet Islands. This was a result of significant volcanic ash deposition to the surface ocean, which sank out of the mixed layer on a timescale of hours to a couple of days. Thus the impact of the volcanic eruption is thought to have been a transient one, with little effect upon measurements made during D354, two months later.

Unlike the FeCycle and SAZ-Sense budgets, the export flux of pFe estimated for each basin during D354 was not balanced by the measured inputs of iron into the mixed layer. In this way the area is thought to resemble the area studied during the CROZEX project, in that lateral advection of lithogenic pFe is thought necessary to account for the observed sinking pFe flux, though in this case the magnitude of advective flux is not required to be as large. An alternative explanation may be that, due to export flux being derived from only one 80 m depth sediment trap in each basin, an upward bias of the export flux would result from enhanced local flux in the locale of each trap. This would most likely have been an issue for the Iceland Basin trap, which was deployed just to the east of the Reykjanes Ridge (see Chapter 3).

Biogenic pFe fluxes calculated for the Irminger Basin based on two possible Fe/Al ratios of source lithogenic material fell either side of those made during FeCycle, suggesting a similar biogenic pFe flux at the two locations, while the corresponding fluxes for the Iceland Basin were slightly higher (by a factor of 1.5 to 6) than FeCycle.

Chapter 6: Conclusions and future work

The major aims of this project were to gain fresh insights into processes that control the strength and efficiency of the biological carbon pump and to further our understanding of the role of particulate material in the upper ocean biogeochemical cycle of iron. Events conspired to also provide the opportunity to study the effect of substantial volcanic ash deposition upon stocks and fluxes of particulate trace metals in the upper ocean. The main findings of the work are summarised below, followed by suggestions for future research that have emerged from this study.

6.1 Conclusions and major findings

6.1.1 Fluxes of POC, PON and biominerals

Due to the known challenges inherent with measurements of sinking particle fluxes at mesopelagic depths using traditional sediment traps, the data presented here of POC, PON and biomineral fluxes in the North Atlantic represent an important contribution to the very limited global dataset of multiple-depth measurements made using free-drifting traps. Along with studies at the VERTIGO stations in the north central Pacific and northwest Pacific subarctic gyre (Lamborg *et al.*, 2008b), these measurements from the PAP site and the high latitude North Atlantic represent the only known investigations in which such traps have been successfully deployed at three depths simultaneously. The five-trap deployment at the PAP site was the first time that neutrally buoyant traps have been used to determine sinking particle fluxes with such depth resolution.

POC and biomineral fluxes measured at the PAP site were within the range observed there by previous measurements using surface-tethered traps and bottom-moored deep-sea traps (Martin *et al.*, 1993; Salter *et al.*, 2010), while those in the Iceland Basin were of a similar magnitude to fluxes previously observed in the same region during the early stages of a spring diatom bloom, but significantly lower than fluxes measured during the latter part of the same bloom (Martin *et al.*, 2011). Correlations between POC and PON were observed in trap samples at both the PAP site and in the HLNA, demonstrating their similar fate of remineralisation with depth after sinking out of the surface mixed layer, but a statistically significant (P <0.05) increase in the C/N

ratio with depth at the PAP site also revealed a more rapid remineralisation of PON with depth compared to POC.

Neither opal nor calcite showed a correlation with POC at either site, indicating that the biominerals did not experience the same attenuation of flux whilst sinking. At the PAP site (and to a lesser extent, the HLNA), there was a general trend of stronger bSi flux at depth. This is ascribed to the bSi flux constituting small slowly sinking fragments of opal left over from the peak of an earlier diatom bloom, with the greater part of the material having already sunk through the depths sampled before traps were deployed. This conclusion was supported (at the PAP site) by the presence in some of the deeper traps of the remains of plankton that had not been detected in surface waters in the region since two months prior to the cruise (J. Riley, *pers. comm.*). Further evidence for the slow sinking nature of the opal was given by particle settling experiments carried out on material sampled by the Marine Snow Catcher, which differentiated between slow and fast sinking components of particle flux at the PAP site (Riley *et al.*, 2012).

The multiple-depth measurements of POC (and PON) flux were used with the Martin equation to estimate the flux attenuation coefficient, *b*, for POC (and PON) at the PAP site and for the Irminger and Iceland Basins. All three produced *b* values are in between those measured at the two contrasting Pacific Ocean sites sampled during VERTIGO (Buesseler *et al.*, 2008), and falling either side of the "open ocean composite" value of 0.86 suggested by Martin *et al.* (1987). Scatter plots were produced from the small dataset of mesopelagic-depth neutrally-buoyant sediment trap measurements (this study and VERTIGO), with calculated *b* plotted against various parameters to determine the main control(s) on the remineralisation of POC in the mesopelagic. The outstanding candidate was temperature of the upper water column, no doubt due to its effect on rates of microbial respiration (Rivkin and Legendre, 2001).

Such a finding implies that the main control on POC flux attenuation in the mesopelagic (or at least, the upper mesopelagic) is akin to one of the factors (*i.e.*, temperature) identified as a major control on the ratio of POC export to primary production in the surface ocean (Dunne *et al.*, 2007). The fact that deep sea traps show a correlation between POC and biomineral fluxes suggests that the latter may influence POC flux attenuation, or rather its persistence (Armstrong *et al.*, 2002; Klaas and Archer, 2002), but the results of this study suggest that any such relationship is not an important factor in the upper mesopelagic. This finding leads to the question: to what depth does the water temperature represent the main control on POC flux attenuation (*i.e.*, does it have a large influence to depths where the remaining POC would be considered sequestered)? A caveat of this finding is the very small dataset considered in this case, which makes the observed results susceptible to bias by distinctive individual data.

6.1.2 PELAGRA measurements of particulate trace metal fluxes

The traps were also used to measure trace metal fluxes, with one of the major achievements of this work being to confirm that, with due care, PELAGRA can be used for this purpose. Process blanks carried out during D354, by leaving one sample cup unopened throughout a deployment, yielded trace metal values as low as those measured using a similar strategy for NBST samples (Lamborg *et al.*, 2008a). These blank values were low relative to sample concentrations and provided us with confidence in the measurements. The results for both the PAP site and HLNA fell within the range of the small literature dataset to which they can be compared. The variations in particulate iron flux with depth did not show a common trend, being somewhat confused by multiple sampling over a four week period at the PAP site, and showing minor and major increases with depth in the Irminger and Iceland Basins respectively. Given the ratios of Fe to Al and Mn measured, the much larger flux measured by the deepest trap in the Iceland Basin is thought to show evidence of material being transported from the nearby Reykjanes Ridge, though a hydrothermal influence cannot be ruled out.

Efforts were made to estimate the contribution of "biogenic" iron to the total pFe, based upon corrections for the lithogenic contribution, but without an Fe/Al ratio of a definite source material, this proved rather speculative. While the HLNA data showed a strong correlation between pFe and pAl (and also pMn), signifying a strong influence of lithogenic material on the total pFe, the same was not true for the PAP site, where a decrease in Fe/Al with depth suggested that a significant biogenic pFe fraction was being remineralised. The Fe/C ratios in trap material showed an increase with depth in both regions, presumably due to more significant remineralisation of POC with depth and/or readsorption of iron onto particles following remineralisation. The increase observed in the HLNA was greater than at the PAP site, which could be explained by the additional factor of an increase in pFe concentrations with depth through advection of material from the continental shelf/Reykjanes Ridge.

6.1.3 SAPS findings and conclusions

The use of SAPS pumps during the HLNA research cruises was intended to provide information about spatial and temporal variations of particulate trace metal (and POC and PON) concentrations, with a particular focus on iron. The TM-SAPS pumps were

deployed concurrently with Th-SAPS in order to allow an independent estimate of pFe flux, while the comparison of Fe/C and Fe/N ratios in the surface mixed layer to those in the subsurface ocean was intended to yield information regarding the relative cycling of those elements in the upper ocean. The biological fraction of pFe was estimated through consideration of pAl concentrations and a weak leach was used to estimate what fraction of pFe was readily accessible.

Consideration of pAl concentrations showed that lithogenic material generally contributed <5 % of the total SPM mass, though this increased to 12 % at D354-2, thought to be influenced by lateral advection of material from the Iceland Shelf, and up to 30 % at stations that showed evidence of influence from the volcanic ash plume of the Eyjafjallajökull eruption. Throughout the study, the elemental ratios of Fe, Al and Ti in the material collected by SAPS showed a strong correlation, indicating a strong lithogenic influence upon pFe concentrations. The relative ratios of these elements resembled that of volcanic ash collected from Iceland during the eruption (Gislason *et al.*, 2011) and heavily ash-influenced aerosol samples collected at sea.

The contrasting lack of correlation between pFe and POC datasets showed the differing fates of the two elements in material exported from the surface layer, which also led to a trend of increasing Fe/C with depth. Whereas POC contribution to SPM decreased with depth due to continuing remineralisation, any remineralised biogenic iron was at least partially readsorbed back on to particulate material (demonstrated by an increased proportion of leachable pFe in deeper samples) while lithogenic iron remained largely in particulate form. Consideration of only surface mixed layer samples from D354, however, did show a correlation between POC and pFe, indicating a significant biogenic component to those samples. Multiple linear regression analysis revealed that, overall, mixed layer refractory pFe concentrations could generally be accounted for by a combination of lithogenic material with an Fe/Al ratio of 0.42 mol mol^{-1}, and a biogenic contribution with an average Fe/C ratio of 159 μmol mol^{-1}.

A similar relationship was not found for material collected during D350 or D351 (though very few mixed layer samples were collected during those cruises), or for material collected below the surface mixed layer during D354. Furthermore, the increase in the relative contribution of biogenic iron to pFe documented for sinking material below the mixed layer relative to SPM in the mixed layer, as observed in subantarctic waters during FeCycle (Frew *et al.*, 2006) was not observed for the HLNA when >53 μm material was used as a proxy for the sinking fraction of material. This suggests a significant difference in the biogeochemical cycling of iron in the HLNA compared to the FeCycle site. Whereas the latter was hypothesised to demonstrate a conversion of lithogenic pFe to biological iron during a ~100 day mixed layer residence time, prior to loss of biogenic iron by export to the mesopelagic, the HLNA data imply

that material sinking out of the mixed layer was relatively poor in biogenic Fe, presumably due to rapid recycling of this fraction of pFe within the mixed layer.

6.1.4 Synthesis of iron budgets for the HLNA

The data collected from SAPS and PELAGRA deployments in the high latitude North Atlantic were used, along with aerosol data and preliminary dissolved iron data, to construct iron budgets for the surface mixed layer for both the Irminger and Iceland Basins during summer 2010, and for the area of the Iceland Basin influenced by the ash cloud from the Eyjafjallajökull eruption during D350 in spring 2010.

These were compared to other iron budgets composed in a similar manner. The HLNA budgets from summer 2010 were largely similar to those from FeCycle and SAZ-Sense studies (Boyd *et al.*, 2005; Bowie *et al.*, 2009), with the exception that our calculated export fluxes were not balanced by iron inputs, in part due to the relatively low atmospheric flux measured during the cruise. The implication was that a lateral advective flux of pFe (not measured) may be needed to balance the budgets, a feature that they would share with the budget constructed for the Crozet region (Planquette *et al.*, 2011).

The budget composed for D350 was distinctive in that an atmospheric Fe input much higher than that for any of the other budgets was matched by an export flux that was equally distinctive in its comparative magnitude. Despite the significantly higher mixed layer pFe concentrations measured, the calculated residence time for pFe was much lower (~1.5 days) than for any of the other budgets prepared, indicating that the majority of the volcanic ash will have quickly passed through the mixed layer with little long-term perturbation to the iron biogeochemistry in the region.

6.2 Future directions

The two main focuses of this thesis were the variability of mesopelagic POC flux attenuation and its controls, and the role of particles in the biogeochemistry of iron. Both are complex problems which cannot be fully explained by a study of this size. The information collected here should therefore be regarded as components of a bigger picture, and as stepping stones to elucidate further avenues of research, in order to gain a deeper understanding of the two study areas and their mutual relevance. In addition to this, certain technical aspects of the work carried out would

benefit from being revisited in order to improve the robustness of the approach for application in future work (*e.g.*, the methodology of SAPS sample processing), while the current data-set could be added to in the hope of providing a more comprehensive understanding of the findings.

One of the main outcomes of the thesis was the deduction of a link between water temperature in the upper ocean and the attenuation of POC flux at mesopelagic depths, represented by the coefficient, *b*. As such this link was based upon the very small available dataset of POC flux measurements made by neutrally-buoyant sediment traps, consisting of results from this study and those from the VERTIGO project. The influences of other factors, such as biomineral content of the material, were ruled out using the same small data-set. To strengthen the argument made, further multiple-depth measurements of POC flux by such traps are needed. Specifically, determination of POC flux attenuation in regions with water temperatures intermediate between those of the PAP site and station ALOHA, or lower than those in the Irminger Basin would be useful, in order to fill in the gaps between the current data points. It may be that in expanding the data-set by targeting such areas, the argument for the influence of temperature may be strengthened, and/or the influence of other variables may become more apparent.

The two data-sets compared in the study of controls on *b* (this work and the VERTIGO data) were collected using two different trap designs; variations on the neutrally-buoyant sediment trap concept. There have been numerous intercomparison exercises carried out in the past for differing sediment trap designs, but none as yet comparing these two relatively new platforms; the NBST and PELAGRA traps. In a carefully planned experiment, simultaneous deployments of the traps, along with traditional surface-tethered sediment traps would be a useful exercise in determining any biases associated with either trap design, and hopefully justify the comparison between them.

In terms of measuring the flux of trace metals with sediment traps, the effect of solubilisation within the sample cups should always be considered. Previous studies have shown that iron flux values are not greatly affected by the loss of material through solubilisation between material collection and sample processing, but for other elements, such as manganese, this can lead to a significant underestimation of the flux. Following processing of the PELAGRA trace metal splits, the filtered brine was saved for subsequent analysis of dissolved trace metals, along with aliquots of unused brine. Although time constraints did not allow for analysis of these at the time, doing so would allow a more complete interpretation of the trace metal results and provide a more robust set of flux measurements of several biologically important trace metals at the PAP site and in the high latitude North Atlantic.

The protocol used here in processing SAPS samples has largely been employed before, yet certain aspects of the procedure were not entirely satisfactory. The difficulty in measuring the mass remaining on the large filters, after rinsing the collected material onto smaller filters, left questions about the percentage recovery, as did the comparison of POC concentrations to those measured by the Th-SAPS. Ideally, the issue of rinsing material onto more manageable filters could be addressed by development of a system that allows for collection of sufficient material on a smaller filter at the same time as bulk sample collection, such as the "mini-MULVFS" adaptation (Planquette and Sherrell, 2012). The issue of the method of subsampling for POC could be addressed by experiment; the contrasting relationships between TM-SAPS POC and Th-SAPS POC observed in this work and during the CROZEX study could be examined by collecting a number of SAPS samples, cutting the filters into two and performing a different POC sub-sampling method (scraping material from the smaller filter as done during CROZEX, or using a syringe filter as was done here) on each.

Additionally, in future studies, it would be useful to determine biomineral concentrations of collected material, as well as trace metals and POC and PON. For this the larger filters may actually be an advantage, as sub-samples could be cut away from the filter for the different analyses. From a broader perspective, the procedure described here (from sample collection and treatment through to analysis by leach and acid digest) is one of many variations used for collection and analysis of SPM for trace metal analysis. The recent efforts made by the GEOTRACES intercalibration programme to compare different approaches and suggest standardised methods show the way forward in terms of verifying the effectiveness of the component aspects of a method.

The key finding of the SAPS-based study of pFe in this work was the lack of evidence found in the high latitude North Atlantic for the relative increase in the biogenic fraction of pFe between surface mixed layer and subsurface ocean, documented for subantarctic waters during the FeCycle study (Frew *et al.*, 2006). This finding invites a study to determine how this characteristic varies with location, and which of the two findings is most representative of the cycling of iron in the upper ocean.

Finally, the budgets prepared for iron in the Irminger and Iceland Basins can be modified by the inclusion of additional data. Finalised dFe data will be included when ready, along with the revised vertical diffusive flux data, though both are likely to involve small changes. Consideration of finalised dFe and total dissolvable Fe (and aluminium) profiles will also help in further interpretation of some of the features of the SAPS data. Due to the suspected influence of lateral advection upon the Fe budgets for the region, it would be useful to try and estimate these fluxes by modelling studies; work on this is currently being conducted at Liverpool as part of the larger project.

Appendix A: Collection of sinking particulate material using the PELAGRA sediment trap

A.1 PELAGRA trap components

The overall design of the PELAGRA trap is shown in Figure A.1. Around the Autonomous Profiling Explorer (APEX) float are arranged four collecting funnels, manufactured from glass fibre reinforced polyester and with a smooth finish on their inner surface to facilitate the passage of sinking particles down through the funnel. Each funnel has a collecting area of 0.115 m^2, giving a total collecting area of 0.46 m^2.

At the base of the trap, each funnel leads to a closable, removable sample pot. The configuration used for this sampling work consisted of a polypropylene lid secured by nylon screws to the trap, to which a 675 mL straight-sided polypropylene sample pot was attached. Unlike in some early deployments of PELAGRA (Salter *et al.*, 2007; Lampitt *et al.*, 2008), the trap can now be programmed so that the sample cups remain closed during deployment, as well as being closed prior to surfacing and recovery.

As well as collecting CTD data from the APEX float every few minutes (which is used to help maintain the desired depth; see Section 2.3.1), the trap is fitted with an Idronaut Ocean Seven 304 CTD data logger, which records oceanographic data twice every minute for the duration of the deployment. The Idronaut is removable and is secured prior to deployment to a chassis, manufactured from polypropylene, which also serves to protect the sample pots and provide a stable base for the trap while it is stood on deck. In addition, a titanium lifting frame is attached to the top of the trap.

The extra mass given to the trap (*i.e.*, over and above that of the float) needs to be offset in order for the float to still be able to control its buoyancy. To achieve this, additional buoyancy is provided to the trap by the inclusion of six semi-toroids which are manufactured from aluminium alloy tubes and which surround the four sample funnels, thus also providing protection to them.

A.2 Operation of PELAGRA

PELAGRA maintains its position at the specified depth in the water column through adjustments to the oil bladder of the APEX float, which are controlled according to any changes in sigma-theta detected by the float's sensor. The bladder is able to provide ±118 cm^3 of buoyancy adjustment, which is equivalent to ±115 g in weight. Consequently it is very important that the initial weight of the trap is known accurately, and each trap is weighed on land before each cruise, with stainless steel ballast added gradually until the trap is deemed to be neutrally buoyant.

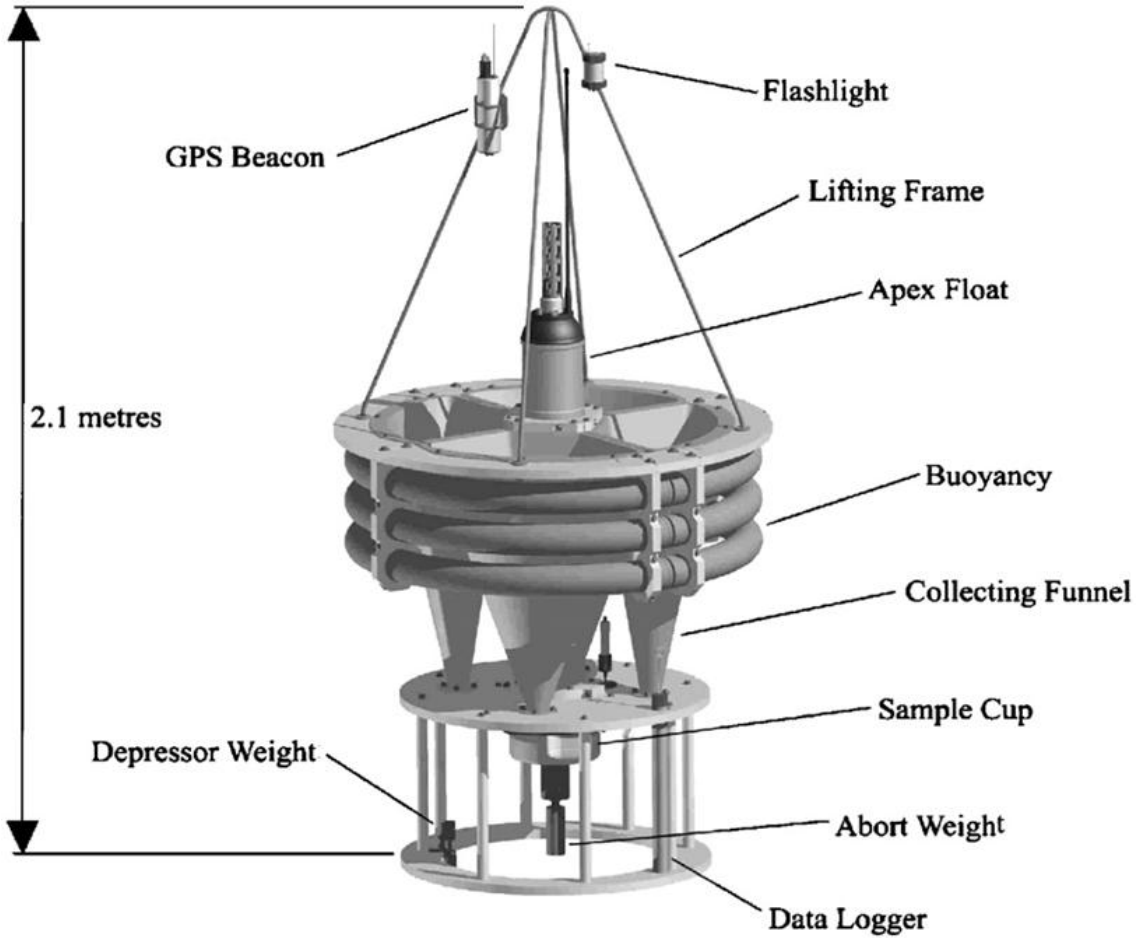

Figure A.1: Schematic of the PELAGRA sediment trap.

Prior to each deployment, a CTD profile is carried out at the deployment location and the potential density at the trap's target depth is calculated and programmed into the APEX float. Additional pre-weighed stainless steel nuts may be added in order to ballast the trap for the specific density at its deployment depth. At this time the trap is also programmed for the length of deployment (ranging from a few hours for test deployments up to around six days), and the opening and closing times for the sample cups. In this work each trap was given 18 – 24 hours to stabilise at the target depth before the sample cups opened.

In the run-up to deployment the trap is moved to its launch location and mounted in a wooden cradle. Covers that are kept over the sample funnels in between deployments are removed and the funnels are wiped down with a sponge and detergent as a precautionary measure. The polypropylene lids to which sample cups will be attached are also cleaned in this way to remove any particles, and the funnels and lids are then thoroughly rinsed with MQ water. The sample cups (see Section 2.2 for cleaning details) are attached immediately prior to deployment.

The trap is deployed following confirmation that the oil bladder is deflated to its "park position", and after checking that the APEX float is transmitting Argos satellite data. Following deployment, the trap sinks to the specified density surface. When deployed to depths >200 m, this is assisted by the addition to the trap of a small (< 0.5 kg) depressor weight, which is attached to a "burn-wire" and jettisoned as the trap descends past 200 m. Following a period of time determined by the target depth and expected sink-rate, the APEX float begins to monitor the local sigma-theta at ten minute intervals. If any two consecutive measurements fall outside of the ±0.01 sigma-theta target range, the oil bladder is adjusted to slightly change the buoyancy of the trap. During this period, the trap moves in a near-Lagrangian manner.

Unlike early configurations of PELAGRA (Salter *et al.*, 2007; Lampitt *et al.*, 2008), for this work the traps were set up so that during deployment the sample cups were "parked" away from the base of the sample funnels, sealing them off and preventing possible contamination from material falling into the funnels from the ship during deployment. Throughout this work, each trap was programmed to allow 18 – 24 hours for reaching the required depth and stabilising before the sample cups were rotated into position underneath the collection funnels to start collecting sinking material.

At the end of the pre-programmed sampling time, the sample cups are again moved away from the base of the sampling funnels and the oil bladder inflates fully, providing extra buoyancy to make the trap float to the surface. Each trap is also fitted with a 2 kg abort weight, attached before deployment to a timer-activated anodic "burn-wire" release. This is programmed so that it is also jettisoned at the end of the sampling period, providing enhanced buoyancy and increasing the trap's ascent rate to the

surface. The abort weight release also incorporates a pressure switch which bypasses the timer and can drop the abort weight if the trap at any point descends below its safe working depth.

Once the trap reaches the surface, Argos satellite transmissions commence, and continue for up to 255 hours. Since early 2010, iridium positioning has also been used on the traps to aid location and recovery. The trap is also fitted with a Gonio transmitter, strobe light and a brightly coloured flag, to aid precise location once the ship is within close enough range of the trap.

A.3 Brine preparation

As mentioned in Section 1.3.2.1 some of the issues associated with the use of sediment traps include *in situ* microbial remineralisation of the collected material and feeding upon the material by zooplankton "swimmers" (Buesseler *et al.*, 2007). To tackle these issues, the use of poisons or preservatives is commonplace, and these are typically added to the sample cups before deployment as part of a brine solution to reduce the possibility of the poison/preservative being washed out.

Salinity of the brine used in traps varies from ~5 salinity units above that of ambient seawater (JGOFS protocols, *e.g.*, Lampitt *et al.*, 2008) to hypersaline solutions with salinity of > 70 (Valdes and Price, 2000; Lamborg *et al.*, 2008b). Brine preparation is most commonly done through addition of sodium chloride (NaCl) to particle-free seawater (either filtered or collected from several hundred metres depth), but can also be done through freeze-concentrating filtered seawater (Lamborg *et al.*, 2008b).

The most commonly used poisons and preservatives for sediment trap studies are formaldehyde, mercuric chloride, sodium azide and chloroform. While some studies have been carried out to compare the effectiveness of these options (Knauer *et al.*, 1984; Lee *et al.*, 1992), no one choice is decisively superior to the others and the additive selected is typically done based on the specific requirements of a project. The US GOFS 1989 planning report on sediment trap sampling lists some advantages and disadvantages of the various options (U.S.GOFS, 1989).

For this work, it was decided to prepare brine for use in the PELAGRA traps by freeze-concentrating seawater, rather than by addition of NaCl. This was done to reduce any addition to the seawater used of trace elements present as impurities in the NaCl. To prepare the brine, seawater from 400 m depth was collected in trace metal clean 10 L OTE (Ocean Technology Equipment) sampling bottles with external springs, deployed on a titanium-framed CTD rosette, either during the same research cruise or on an

earlier cruise. Sample bottles were transferred to a class-1000 clean laboratory van on the back deck, where the collected water was filtered under slight positive pressure (0.2 bar, oxygen-free N_2) through a 0.2 µm pore-size filter cartridge (Sartobran 300 MF, Sartorius) into an acid-cleaned 20 L carboy. Typically, two sample bottles deployed at the same depth were drained into each carboy in this way to give a final volume of ~15 L filtered trace metal clean seawater.

Carboys were placed in a -20 ˚C chest freezer to partially freeze the collected seawater, forming a brine solution which was then drained into another trace metal clean 20 L carboy. In this way three or four carboys of trace metal clean seawater were combined to produce batches of ~ 20 L of brine with the required salinity. Brine was kept cool (~ 4 ˚C) and in the dark until needed and was refiltered through a fresh filter cartridge in the hours prior to use.

For cruise D341 to the Porcupine Abyssal Plain, chloroform ($CHCl_3$) was used as the poison for PELAGRA sampling. Chloroform (Fisher Scientific; 99.9+ % PrimaR grade) was added to the brine to give a saturated, 0.5 % solution (100 mL $CHCl_3$ in 20 L brine). For the high latitude North Atlantic cruise in summer 2010 (D354), formalin was added to the brine as a poison/preservative. Formalin (Formaldehyde, 36 % w/v; VWR AnalaR NORMAPUR) was first cleaned over Chelex-100 resin. To this, di-sodium tetraborate ($Na_2B_4O_7.10H_2O$; Merck Suprapur) was added at 5 g/1 L of concentrated formalin, and the mixture shaken and left overnight. The resulting borate-buffered formalin was added to brine (before re-filtering) at a ratio of 1 L formalin / 19 L of brine (*i.e.*, a 5 % solution) and mixed thoroughly.

Prior to deployment of PELAGRA traps, the appropriate number of sample pots were filled with the poisoned brine solution inside the clean van and bagged up until installation on the traps <30 minutes before deployment. Sample cups (Nalgene, polypropylene straight-sided wide-mouth jars) were rigorously cleaned before initial use, following the procedures described in Section 2.2.

A.4 Process blanks

During D354, the PELAGRA traps were set up so that one sample cup on each trap remained closed for the duration of each deployment. These cups were filled with the same poisoned brine before deployment, and processed in the same way after recovery, so the only difference between them and the sample cups was the fact that they were never moved into position under a sample funnel to collect sinking material. In this way, such cups provided a process blank of the PELAGRA sampling methodology.

A.5 Initial sample processing

Following recovery of each PELAGRA trap, the sample pots were carefully unscrewed from their positions and immediately capped with their own individual lids, then placed upright in a sealable plastic bag and transferred to the clean van for processing. The trap was rinsed with fresh water and the cover replaced over the collection funnels before it was secured until the next deployment.

Each trap sample was used to make measurements of various properties of the sinking particle flux and sample processing was designed to provide equal sub-samples with enough material for each analysis. To this end, the contents of the sample pots on each trap (typically two pots during D341, three pots during D354) were combined and then split into eight or more fractions. Sample pots designated as process blanks (one per sediment trap during D354) were not combined with the sample pots but processed individually. These pots were processed before the sample pots, and were otherwise treated in the same manner.

A.5.1 Sample splitting

For each PELAGRA sample, two or three sample pots were first combined by being poured through an acid-washed 350 µm nylon mesh (Nitex; Sefar), held in place across a filter funnel, into an acid-washed 4 L bottle. Each pot was rinsed with a small amount of the same poisoned brine. Acid-washed plastic tweezers were then used to transfer any swimmers from the mesh to a labelled glass vial (to which a small volume of poisoned brine was then added), before any remaining material was rinsed off the mesh into the 4 L bottle with a small volume of poisoned brine.

Each sample was initially split into eight subsamples using a custom-built rotary splitter of the type described by Lamborg *et al.* (2008b). The splitter was assembled, complete with eight acid-washed LDPE bottles (500 mL) and the 4 L bottle suspended above it, connected to the top of the splitter by acid-washed tubing (see Figure A.2). With the splitter switched on and an in-line stopcock opened, the water/particle mixture drained into the top of the splitter as it rotated and was diverted to each of the eight sample bottles in sequence. Once the mixture had drained, a small amount of poisoned brine was used to rinse the 4 L bottle and the rinse-water drained in the same way.

Figure A.2: Set-up used to split PELAGRA samples, showing the 4 L bottle into which cups were combined (inverted in photo) and the rotary splitter, loaded with 500 mL bottles.

During D354, more than eight splits were sometimes required from a sample (to provide replicate samples for some measurements). In these cases, three or four of the initial eight splits were recombined in the 4 L bottle and the above procedure repeated into fresh 500 mL LDPE sample bottles.

The design of rotary splitter used has previously been described as providing splits within <1 % of each other in fluid mass (Lamborg *et al.*, 2008b). However, in this work it quickly became apparent that there was a variation between split volumes of around 7 % (D341; difference between splits during D354 was typically <5 %). To improve the accuracy of calculations, the volume of each split was measured by comparison with a bottle with external calibration marks, and these absolute values used (see Equation A.1).

In between each sample, all plastic ware used in the sample processing, including those parts of the splitter that came into direct contact with the water/particle mixture, were rinsed with MQ water. These same parts of the splitter were cleaned with 10 % HCl and rinsed thoroughly with MQ water in between trap deployments. The 350 µm

nylon mesh was soaked in 2 % Decon 90 detergent solution in between deployments to remove any residual organic material, then rinsed thoroughly with MQ water and stored in a plastic bag.

A.6 Calculation of fluxes

The purpose of collecting material using sediment traps is to measure the flux of that material. To do this, the property measured has to be related to both the area and duration over which it was collected. Following analysis of each property of the collected material in individual splits, the calculated value was first converted into the total amount of that property collected by the trap. This could be as simple as multiplying by the number of splits to which the sample was divided, but in this case the split volume and total sample volume were used (see above), as shown in Equation A.1:

$$\text{Total (mg)} = \left(\frac{\text{material measured in split A (mg)}}{\text{volume of split A (mL)}}\right) \text{ x total volume (mL)} \qquad \text{(Eqtn. A.1)}$$

Next, the trap total calculated in Equation A.1 was divided by the collection area of the sediment trap and by the sampling time, in days, to give the flux, as shown in Equation A.2:

$$\text{Flux (mg m}^{-2}\text{ day}^{-1}\text{)} = \text{Total material (mg) x } \frac{1}{\text{area}}\ (\text{m}^{-2}) \text{ x } \frac{1}{\text{time}}\ (\text{day}^{-1}) \qquad \text{(Eqtn. A.2)}$$

Appendix B: Sampling using Stand Alone Pumping Systems (SAPS)

B.1 Overview of SAPS

The Challenger Oceanic Stand Alone Pump System (SAPS) consists of a magnetically coupled centrifugal pump mounted on the end of an anodised aluminium pressure tube, which contains the motor, rechargeable batteries and a magnetically activated programmable timer card that controls sampling. A mechanical displacement flow meter (accurate to ±2 %) is located between the pump and the inlet section, which can be set up to hold different filter types and sizes. Plumbing used to link the components is made from polyvinylchloride. The whole system is attached to a titanium mooring bar, by which it is clamped to the wire used for deployments.

For the purposes of this study, 293 mm filters were used with SAPS. These filters were loaded in a polypropylene filter housing, containing baffle grids. The inlet and outlet sections were secured together by an external stainless steel circular V-clamp. For most deployments, a second size fraction filter was loaded, which required the inclusion in the filter housing of a "pre-filter" insert, secured by a second stainless steel V-clamp.

B.2 Preparation

Two types of filter were used for this work: nylon and polycarbonate. Nylon filters were cut to size and shape from a roll of monofilament open mesh Nitex (Sefar) fabric. Two different mesh sizes – 53 µm and 1 µm – were used. All nylon filters were cleaned in advance by soaking for a week in a 1 % v/v detergent solution (Decon 90), followed by an overnight soak in 10 % v/v HCl (Fisher Scientific AR Grade), with thorough MQ water rinses after each step. Polycarbonate membranes (1 µm; Sterlitech) were cleaned in advance by soaking in 10 % v/v HCl for 1 week, with a thorough MQ rinse before and after. After rinsing, all filters were dried under a laminar flow-hood and individually stored in re-sealable plastic bags.

When at sea, the plastic components of the filter housing were soaked for a couple of days in detergent solution (2 % v/v Decon 90) prior to their first use, then rinsed thoroughly with MQ water. Filters were loaded inside a class-100 trace metal clean container laboratory, using acid-cleaned plastic forceps. Where the filter housing was set up to sample two size fractions, the 53 µm mesh was loaded onto the pre-filter insert and the 1 µm filter loaded onto the main filter support plate. In the case of 1 µm polycarbonate membranes, an additional piece of 53 µm Nitex was used between the membrane and the filter plate to provide extra support for the thin material and to make handling easier.

B.3 Deployment

After securing filter housings to the SAPS units, MQ water was used to prime the units immediately prior to deployment. Deployments were typically made with multiple SAPS on one line. The samples were often collected in tandem with samples for POC and ^{234}Th measurements, in which case the trace metal SAPS would be attached to the line directly above the C/Th SAPS. The majority of samples were collected at depths approximately 10 m below the mixed layer depth (determined by a CTD deployment before the SAPS deployment) and another 100 m below that. Some samples were also collected within the mixed layer, while occasional samples were taken at depths down to 400 m.

Pumps were programmed to operate for between 90 minutes and 2 hours, though where particle loading was high it is believed that the pumps stopped before this time. The volume of seawater sampled ranged from <150 L for some surface mixed layer depth deployments to >2000 L for pumps deployed at 150 m and deeper.

B.4 Sample processing

Following recovery of the SAPS units, the filter housings were transferred to the trace metal clean container, where excess seawater in the inlet assembly was drawn off using a small vacuum pump connected to the outlet assembly. The inlet section was then removed and any plankton swimmers visible on the top (53 µm) filter were removed using clean plastic tweezers. The filters were then folded into quarters, bagged and transferred immediately to a freezer (-20 ˚C) to minimise chemical changes before further processing could be carried out back in the laboratory.

It was decided to rinse particulate material off the large diameter SAPS filters onto smaller polycarbonate filters, following the reasons outlined by Planquette *et al.* (2009), namely:

- The size of the SAPS filters makes them difficult to handle and to process using the leach/digest protocol, described in Appendix C.
- Rinsing the material off allows the removal of sea-salt.
- Previous work involving the digestion of nylon filters has reported high blanks (Weinstein and Moran, 2004).

Each SAPS filter was unfolded onto a Teflon sheet (acid-cleaned), using clean plastic tweezers. An acid-cleaned, pre-weighed 47 mm polycarbonate membrane (0.4 µm; Whatman Nuclepore) was loaded onto a perfluoroalkoxy (PFA) Teflon filter rig (Savillex; acid-cleaned as described in Section 2.2). Material was then rinsed off the SAPS filter into the filter rig tower using MQ water adjusted to pH 8.3 with ammonium hydroxide solution (Romil, UpA grade). The material was then filtered under vacuum. Where necessary, more than one 47 mm polycarbonate membrane was used to collect the material

Sub-samples were also collected for POC and PON analysis after rinsing the material from the SAPS filters, by removing 10 – 50 ml of the rinse mixture from the filter tower by syringe and discharging this through a pre-combusted, pre-weighed 25 mm glass microfibre filter (Whatman GF/F; 0.7 µm). Used polycarbonate membranes and GF/F filters were all dried and re-weighed, as described in Section 2.5.1, prior to analysis.

Appendix C: Analytical method for the determination of trace metals in particulate material

C.1 Sample collection and processing

Samples were collected using PELAGRA sediment traps and SAPS as described in Appendices A and B respectively. At sea, trace metal splits of PELAGRA samples were stored in a refrigerator (4 ˚C) until filtered, which was done within 60 hours of trap recovery (and usually within 48 hours) through pre-weighed, acid-cleaned 47 mm polycarbonate membranes (Whatman Nuclepore; 0.4 µm during D341, 1.0 µm during D354). Filtration was carried out under vacuum under a laminar flow hood in the trace metal clean container laboratory, using an acid-cleaned PFA filtration rig (Savillex). Where necessary due to high particle loading, more than one filter was used for a single split. Following filtration, samples were rinsed with a small amount of poisoned brine, and during D354, with a few millilitres of pH-adjusted (pH 8.3) MQ water.

Some unused filters were kept during each cruise to use as filter blanks. Brine blanks were also taken during D354 by filtering 100 mL of poisoned brine through filters. These filtrations, along with those of process blanks carried out on trap deployments (see Appendix A) were carried out before samples in order to reduce the risk of cross-contamination. In between each filtration the filter rig was rinsed thoroughly with MQ water: between PELAGRA deployments the rig was soaked in detergent (2 % v/v Decon 90) and then 10 % HCl (Fisher Scientific AR Grade) for at least a day each, with MQ rinsing after each step.

All used filters were stored frozen (-20 ˚C) in individual Petri dishes until return to the laboratory, where they were dried in a desiccator and then weighed on a Sartorius ME-5 microbalance to the nearest ±1 µg. The polycarbonate filters (0.4 µm) used to collect material rinsed off the large SAPS filters were also stored frozen, and also dried and re-weighed prior to the leach/digest treatment. Filter blanks were clean filters that had been loaded onto the PFA filter rig and rinsed with a small amount of pH-adjusted MQ water, but otherwise unused.

C.2 Leach and digest procedures

All work was carried out in a class-100 clean laboratory. The two-step leach/digest process was carried out in PFA Teflon vials (Savillex), which were acid-cleaned before use, following the steps laid out in Section 2.2. Samples, including filter blanks, were processed in batches of twenty filters. With each batch, a reagent blank was carried out, in which the same leach and digest procedures were followed but with no filter in the sample pot. All pots were cleaned in between batches by being soaked first in a beaker of 50 % HCl on a hotplate (150 ˚C) overnight, then in a beaker of 50 % HNO_3 (150 ˚C, overnight), with thorough MQ rinsing before and after each step. The vials were then dried in a drying cabinet in the clean laboratory before their next use.

C.2.1 Acetic acid leach

The 25 % v/v acetic acid (HAc) solution was prepared using Romil acetic acid (SpA grade) and MQ water. 2 % HNO_3 solution was prepared from concentrated HNO_3 (sub-boiling distilled) and MQ water and contained internal standards for later sample analysis (see Section C.3.1).

Each filter was folded with clean plastic tweezers, particle side inward, and placed in the bottom of a 30 mL Teflon vial, to which 4 mL of 25 % v/v HAc was then added by auto-pipette – enough to completely cover the filter.

Vials were capped, and the samples left in the leach solution for 2 hours at room temperature, then centrifuged (15 minutes at 3000 rpm) to drive any material loosened from the filter to the bottom of the vial.

The leachates was transferred by auto-pipette to clean 15 mL Teflon vials, taking care not to transfer any particles, then each acidified with 100 µL concentrated HNO_3 (sub-boiling distilled) before being taken to dryness on a hotplate (100 ˚C).

The resulting residues were each redissolved in 2 mL of 2 % v/v HNO_3 and transferred to pre-weighed, acid-washed 30 mL LDPE bottles. Initial sample dilution with further 2 % HNO_3 was carried out to give volumes of approximately 12 mL, and the bottles were then reweighed, to accurately determine the mass of acid added.

C.2.2 Mixed acid total digest

Acids used were sub-boiling distilled HNO_3 (prepared in a designated PFA still) and Romil SpA grade hydrofluoric acid (HF). The 2 % HNO_3 was prepared as above.

Following the sample leach and transfer of the leachate to a fresh vial, clean plastic tweezers were used to unfold the membrane and spread it on the interior wall of the 30 mL Teflon vial, particle-side exposed.

Next, 2.5 mL of concentrated HNO_3 was added to the vial, followed by 0.5 mL of concentrated HF. Vials were sealed and placed on a hotplate at 130 ˚C for 4 hours, then uncapped and taken to dryness on the same hotplate.

A second digest step was then carried out using 1.5 mL concentrated HNO_3 only, with samples heated for 2 hours at 130 ˚C, and the solutions again dried down. As the vials approached dryness, the polycarbonate filters were removed with clean plastic tweezers.

At this point the filters were checked for any visible remaining material. For a couple of samples with particularly heavy loading it was found that some material did still remain, in which case the digest procedure was repeated.

Sample residues were redissolved in 5 mL of 2 % v/v HNO_3 and transferred to pre-weighed, acid-washed 30 mL LDPE bottles. Initial sample dilution with additional 2 % HNO_3 was carried out to give volumes of 15 – 20 mL, and the bottles then reweighed to accurately determine the mass of acid added.

C.3 Sample analysis

Solutions of leach and digest products, redissolved in 2 % HNO_3, were analysed on a Thermo Fisher Scientific Element 2 XR HR-ICP-MS (Bremen, Germany) for Li, Al, P, Ti, V, Cr, Mn, Fe, Co, Ni, Cu, Zn, Ga, As, Rb, Sr, Cd, Sn, Cs, Ba, Pb, Th and U. Samples were introduced via an Elemental Scientific Inc. autosampler (ESI SC2; Omaha, USA) using a pumped micro nebuliser (ESI PFA-ST) into a peltier cooled PFA cyclonic spray chamber (ESI PC3). Low-resolution (LRM, m/Δm = 300), medium-resolution (MRM, m/Δm = 3000) and high-resolution (HRM, m/Δm = 7500) modes were utilised to avoid spectral interferences. Additional argon (Ar) “add” gas was ported into the spray chamber to improve sensitivity and signal stability. The instrument used the standard torch, sapphire injector and guard electrode, along with adjusting ion lens settings to

maximise sensitivity, and was tuned to achieve sensitivity of around 1.4 x 10^6 counts per second in low resolution mode for 1ng g^{-1} ^{115}In. Oxide formation was monitored using the $^{238}U^{16}O^+/^{238}U^+$ ratio, which was minimised as part of the tuning procedure. Further settings are given in Table C.1.

Table C.1: Operating parameters used during ICP-MS analysis.

RF power (W)	*1200*
Sample uptake rate (mL min^{-1})	*0.15, pumped*
Argon gas flow rates (L min^{-1})	
Cooling	15.0
Auxiliary	0.95
Nebuliser	0.7 (via nebuliser)
Add gas	0.3 (ported into spray chamber)
Acquisition mode	E-scan, Mode 1, 3 runs x 3 passes per resolution
Mass window (%)	20 (LRM), 125 (MRM and HRM)
Search window (%)	0 (LRM), 60 (MRM and HRM)
Integration window (%)	20 (LRM), 60 (MRM and HRM)
No. of samples per peak	100 (LRM), 25 (MRM and HRM)

C.3.1 Internal standards

Due to the large number of samples analysed on the instrument during each run, and the length of time for which the instrument is in operation (it is not uncommon for sample runs to take >20 hours), it is important to correct for instrumental drift during analysis by ICP-MS. This is done by adding a known amount to each standard and sample of one or more elements that are known to be otherwise absent or present in negligible concentrations. The variations in measured signal intensity for these elements, due to instrumental drift, can then be used to correct the data for other elements.

In this work, three elements – beryllium (Be), indium (In) and rhenium (Re) – were used as internal standards. These were selected because they span a large range in atomic

mass from low (^{9}Be) to high (^{185}Re), thus allowing more accurate drift correction for the range of elements to be measured.

All solutions analysed on the ICP-MS were thus prepared such that they contained concentrations of 20 ppb Be and 10 ppb In and Re. In early sample batches, this was done by spiking sample solutions with a standard solution containing the three elements. However, this approach was replaced by the more efficient method of including additions of Be, In and Re while preparing the 2 % HNO_3 solution used for redissolving residues and making standards. Thus, each batch of the 2 % HNO_3 prepared contained 10 ppb In and Re and 20 ppb Be.

C.3.2 ICP-MS run details

Samples were run alongside blanks (2 % HNO_3 containing internal standards) and a series of multi-element standards, which were prepared using Romil PrimAg-xtra and Inorganic Ventures single element reference solutions and gravimetrically diluted as required using the same 2 % HNO_3. A small volume (~4 mL) of each blank/standard/sample was poured into acid-cleaned sample vials (polypropylene Omni-vials; Cole-Parmer) for analysis on the ICP-MS. Each run on the instrument was set up with two or three blanks, followed by a series of multi-element standards, then another two or three blanks. Following this, the samples were always arranged such that any reagent blanks were run first, followed by filter blanks, then brine and process blanks, and then the samples themselves.

After every twenty samples a sequence of one blank, one standard, one blank was included, with the same standard being repeated throughout the run (but varying between runs). At the end of the samples, another couple of blanks were run, followed by a truncated selection of the initial standard range, to double check for instrument drift. Sample runs were segregated into leach samples or digest samples.

The instrument had a 60 second uptake time for each sample, followed by a four minute wash time (2 % HNO_3). Each sample underwent three runs (each the average of three sweeps), with a % RSD value given for each element for each sample. The RSD values varied with element, sample and run, but for Fe and Al were typically <2 %.

After studying data from a trial run, sample solutions were further diluted with 2 % HNO_3 (with internal standard) before analysis to try and keep measurements within the standard range for each element (see Table C.2). These dilutions were based on the mass of material on the filter and ranged from no further dilution through to a factor of 20 for leach samples, 150 for digest samples and 300 for CRMs.

Instrument detection limits, based on three times the standard deviation of replicate acid blanks (2 % HNO_3 with internal standard; n = 11) were element and run specific, but typically <0.1 ppb.

Table C.2: Range of standard concentrations used for ICP-MS analysis. All concentrations are in ppb.

Elements	*Concentration range*
Al, P, Sr, Fe	0.5 - 500
Zn	0.25 – 250
Ba, Ti	0.050 – 50
Zn	0.025 – 25
Mn, Cu, As, Pb, Cd, Cr	0.010 – 10
Li, V, Ga, Rb	0.005 – 5
Sn	0.002 – 2
Co, Cs, Th, U	0.001 – 1

C.3.3 Measured blank values

The values obtained for reagent blanks and for filter blanks during SAPS, D341 PELAGRA and D354 PELAGRA studies are summarised in Table C.3 (leach values) and Table C.4 (total digest values). All values are given in ng, as the final solution volumes varied between blanks and so calculated concentrations (in ng g^{-1}) were multiplied by the mass of acid used to make them comparable. Multiple blanks were analysed for each, and so the value is given as a mean and standard deviation of the mean, with the number of blanks in each case shown in the column titles.

Table C.3: Mean reagent blank and filter blank values for 25 % HAc leaches (±1σ). All values are in ng.

Element	*Reagent blank (n=17)*	*SAPS filter blank (n=11)*	*D341 PELAGRA filter blank (n=7)*	*D354 PELAGRA filter blank (n=7)*
Li	0.18 ± 0.17	0.20 ± 0.16	0.03 ± 0.02	0.08 ± 0.06
Al	6.6 ± 4.2	8.5 ± 3.4	33.3 ± 12.9	20.4 ± 6.7
P	10.2 ± 7.6	14.7 ± 6.1	18.4 ± 5.6	7.3 ± 1.0
Ti	0.08 ± 0.09	0.08 ± 0.04	0.25 ± 0.17	0.15 ± 0.14
V	0.004 ± 0.005	0.01 ± 0.01	0.03 ± 0.01	0.03 ± 0.01
Cr	0.08 ± 0.12	8.3 ± 3.0	2.9 ± 0.4	3.4 ± 0.4
Mn	0.05 ± 0.02	0.17 ± 0.06	0.16 ± 0.05	0.09 ± 0.02
Fe	1.4 ± 0.9	2.7 ± 1.7	2.6 ± 0.9	1.4 ± 0.3
Co	0.004 ± 0.004	0.008 ± 0.005	0.002 ± 0.002	0.013 ± 0.003
Ni	0.18 ± 0.36	0.42 ± 0.39	0.26 ± 0.17	0.00 ± 0.18
Cu	1.0 ± 0.6	1.9 ± 0.3	1.0 ± 0.3	0.8 ± 0.1
Zn	2.0 ± 1.3	13.1 ± 3.2	14.0 ± 4.9	3.4 ± 1.5
Ga	0.013 ± 0.016	0.02 ± 0.01	0.000 ± 0.004	0.010 ± 0.019
As	0.021 ± 0.014	0.020 ± 0.015	0.040 ± 0.023	0.015 ± 0.011
Rb	0.03 ± 0.03	0.06 ± 0.03	0.04 ± 0.01	0.00 ± 0.01
Sr	1.0 ± 0.8	4.3 ± 2.6	3.0 ± 1.4	0.7 ± 0.1
Cd	0.01 ± 0.01	0.06 ± 0.05	0.04 ± 0.03	0.02 ± 0.00
Sn	0.7 ± 0.2	0.9 ± 0.4	1.1 ± 0.2	1.2 ± 0.3
Cs	0.002 ± 0.003	0.004 ± 0.002	0.004 ± 0.001	0.000 ± 0.001
Ba	0.1 ± 0.1	2.0 ± 0.7	0.5 ± 0.2	0.2 ± 0.2
Pb	0.06 ± 0.02	0.16 ± 0.04	0.17 ± 0.06	0.11 ± 0.04
Th	0.008 ± 0.006	0.006 ± 0.001	0.000 ± 0.001	0.002 ± 0.000
U	0.002 ± 0.001	0.003 ± 0.002	0.018 ± 0.001	0.006 ± 0.002

Table C.4: Mean reagent blank and filter blank values for total acid digestions (±1σ). All values are in ng.

Element	*Reagent blank (n=17)*	*SAPS filter blank (n=11)*	*D341 PELAGRA filter blank (n=7)*	*D354 PELAGRA filter blank (n=6)*
Li	0.03 ± 0.03	0.07 ± 0.02	0.06 ± 0.01	0.06 ± 0.02
Al	7 ± 4	28 ± 16	72 ± 49	75 ± 36
P	15 ± 8	27 ± 6	28 ± 7	64 ± 9
Ti	4 ± 1	31 ± 37	19 ± 13	26 ± 19
V	0.01 ± 0.01	0.05 ± 0.01	0.08 ± 0.04	0.08 ± 0.04
Cr	0.4 ± 0.3	36 ± 22	12 ± 1	20 ± 2
Mn	0.07 ± 0.04	0.3 ± 0.1	0.4 ± 0.1	0.5 ± 0.1
Fe	3 ± 1	18 ± 5	18 ± 10	14 ± 3
Co	0.01 ± 0.01	0.03 ± 0.01	0.01 ± 0.01	0.03 ± 0.01
Ni	0.4 ± 0.3	4.0 ± 2.4	2.3 ± 0.9	3.1 ± 0. 8
Cu	1.4 ± 0.9	1.1 ± 0.4	0.8 ± 0.2	1.4 ± 0.3
Zn	6 ± 4	13 ± 5	10 ± 2	11 ± 3
Ga	0.00 ± 0.01	0.01 ± 0.01	0.03 ± 0.02	0.01 ± 0.02
As	0.40 ± 0.10	0.31 ± 0.16	0.23 ± 0.16	0.32 ± 0.02
Rb	0.06 ± 0.06	0.11 ± 0.11	0.14 ± 0.08	0.06 ± 0.02
Sr	0.9 ± 0.6	2.9 ± 0.8	3.8 ± 1.8	1.6 ± 0.4
Cd	0.01 ± 0.01	0.03 ± 0.02	0.04 ± 0.05	0.03 ± 0.01
Sn	0.97 ± 0.22	1.41 ± 0.33	1.35 ± 0.42	0.91 ± 0.06
Cs	0.003 ± 0.001	0.003 ± 0.001	0.011 ± 0.008	0.007 ± 0.001
Ba	0.3 ± 0.2	8.3 ± 3.7	0.9 ± 0.2	0.8 ± 0.7
Pb	0.06 ± 0.03	0.20 ± 0.07	0.19 ± 0.06	0.17 ± 0.05
Th	0.314 ± 0.344	0.316 ± 0.476	0.015 ± 0.010	0.010 ± 0.009
U	0.001 ± 0.001	0.006 ± 0.003	0.009 ± 0.004	0.011 ± 0.005

Appendix D: PELAGRA sampling details

This section contains details regarding deployment and recovery times and locations for all PELAGRA deployments during D341 and D354. Also shown are depth profiles for each trap deployment, showing the depth of the trap as a function of time.

Table D.1: Deployment details for D341 (depths in brackets represent average depth during stable period if not stable for entire sampling time).

	Deployment date/time	*Deployment location*	*Pots open*	*Sampling time*	*Mean sampling depth ± 1σ*	*Surfacing date/time*	*Surfacing location*
PAP1 P2	14/07/09 12:30	49°02.1′ N 16°30.0′ W	15/07/09 06:30	48 h	156 ± 37 m (143 ± 10 m)	17/07/09 07:08	49°04.4′ N 16°19.9′ W
PAP1 P4	14/07/09 12:55	49°02.3′ N 16°30.0′ W	15/07/09 06:55	----	----	----	----
PAP1 P5	14/07/09 13:20	49°02.3′ N 16°30.0′ W	15/07/09 07:20	48 h	287 ± 28 m (278 ± 5 m)	17/07/09 08:08	49°01.4′ N 16°45.3′ W
PAP1 P6	14/07/09 13:45	49°02.4′ N 16°30.0′ W	15/07/09 07:45	----	----	----	----
PAP1 P7	14/07/09 14:10	49°02.6′ N 16°30.0′ W	15/07/09 08:10	48 h	669 ± 65 m (638 ± 6 m)	17/07/09 09:33	49°01.1′ N 16°40.1′ W
PAP2 P2	19/07/09 19:00	49°01.2′ N 16°30.9′ W	20/07/09 13:00	132 h	68 ± 55 m (52 ± 5 m)	26/07/09 02:03	49°53.0′ N 15°54.1′ W
PAP2 P4	19/07/09 19:25	49°01.1′ N 16°31.0′ W	20/07/09 13:25	----	----	----	----
PAP2 P5	19/07/09 19:50	49°01.1′ N 16°31.1′ W	20/07/09 13:50	132 h	312 ± 17 m	26/07/09 03:07	48°45.3′ N 16°41.6′ W
PAP2 P6	19/07/09 20:15	49°00.7′ N 16°31.1′ W	20/07/09 14:15	132 h	449 ± 7 m	26/07/09 03:35	48°38.5′ N 16°28.0′ W
PAP2 P7	19/07/09 20:40	49°00.3′ N 16°31.9′ W	20/07/09 14:40	132 h	565 ± 15 m	26/07/09 04:17	48°21.9′ N 16°36.6′ W

Table D.1 continued…

Trap	*Deployment date/time*	*Deployment location*	*Pots open*	*Sampling time*	*Mean sampling depth ± 1σ*	*Surfacing date/time*	*Surfacing location*
PAP3 P2	28/07/09 21:00	49°01.4′ N 16°50.2′ W	29/07/09 21:00	76 h	49 ± 8 m	02/08/09 01:42	49°06.8′ N 16°45.5′ W
PAP3 P4	28/07/09 21:25	49°01.4′ N 16°50.1′ W	29/07/09 21:25	76 h	171 ± 82 m (222 ± 6 m)	02/08/09 02:18	48°55.2′ N 17°09.9′ W
PAP3 P5	28/07/09 21:50	49°01.1′ N 16°50.0′ W	29/07/09 21:50	76 h	48 ± 8 m	02/08/09 01:50	48°48.0′ N 17°05.2′ W
PAP3 P6	28/07/09 22:15	49°01.1′ N 16°50.0′ W	29/07/09 22:15	----	----	----	----
PAP3 P7	28/07/09 22:40	49°00.9′ N 16°50.4′ W	29/07/09 22:40	76 h	198 ± 29 m (205 ± 7 m)	02/08/09 03:33	49°08.5′ N 16°37.5′ W
PAP4 P2	03/08/09 12:00	48°55.2′ N 16°23.3′ W	04/08/09 12:00	48 h	51 ± 5 m	06/08/09 12:30	48°46.3′ N 17°00.6′ W
PAP4 P4	03/08/09 12:25	48°55.1′ N 16°23.3′ W	04/08/09 12:25	48 h	184 ± 9 m	06/08/09 13:05	48°47.8′ N 16°57.8′ W
PAP4 P5	03/08/09 12:50	48°54.9′ N 16°23.2′ W	04/08/09 12:50	48 h	312 ± 9 m	06/08/09 13:44	48°46.9′ N 17°01.0′ W
PAP4 P6	03/08/09 13:15	48°54.8′ N 16°23.3′ W	04/08/09 13:15	48 h	446 ± 6 m	06/08/09 14:23	48°47.5′ N 17°01.8′ W
PAP4 P7	03/08/09 13:40	48°54.8′ N 16°23.4′ W	04/08/09 13:40	48 h	589 ± 8 m	06/08/09 14:58	48°49.0′ N 17°04.7′ W

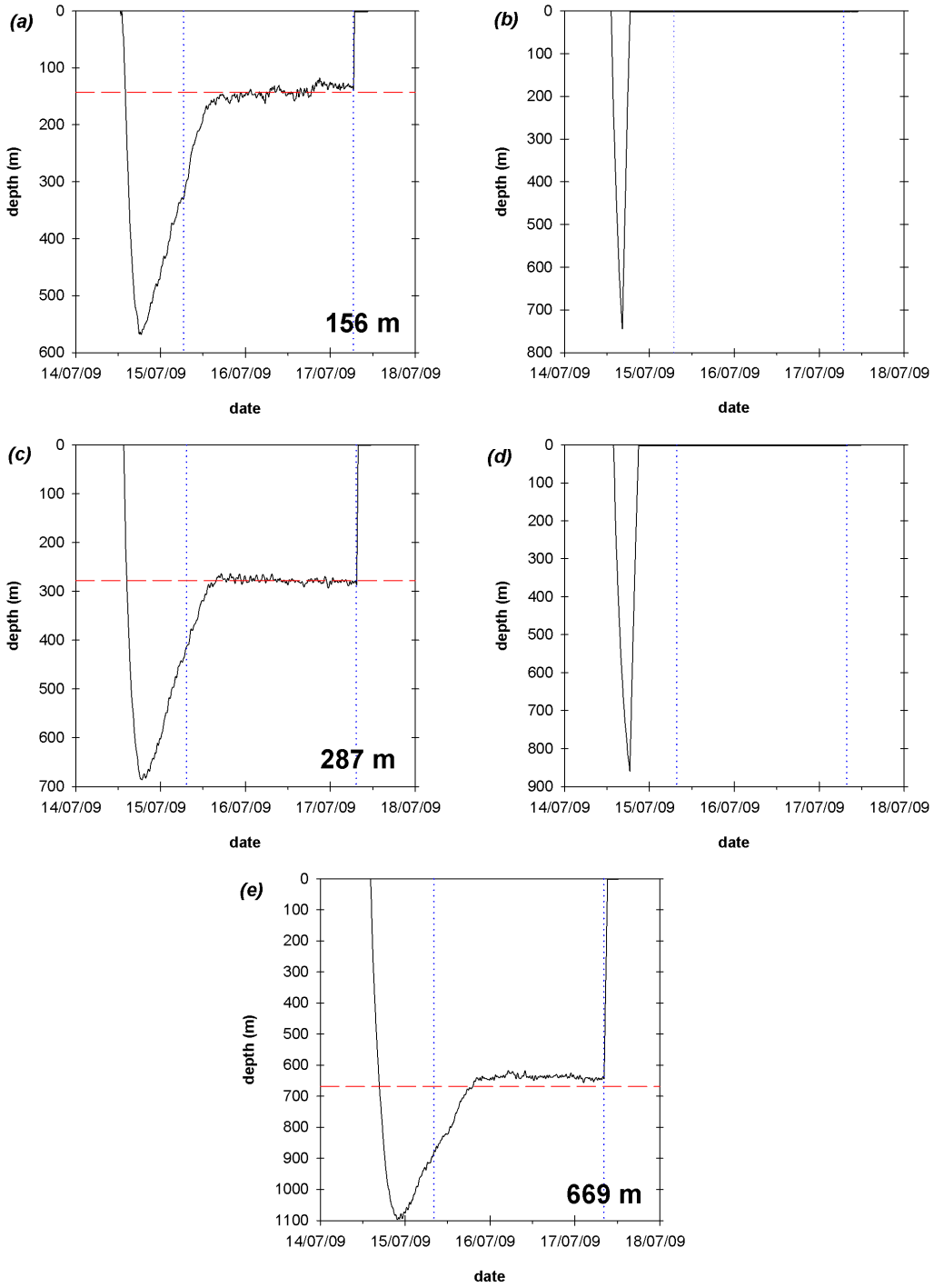

Figure D.1: PAP1 deployment profiles for *(a)* P2, *(b)* P4, *(c)* P5, *(d)* P6 and *(e)* P7. Blue vertical dotted lines represent pot opening/closing times; red horizontal dashed line represents average trap depth over entire sampling period (shown in bottom corner). Note that vertical axis scales differ between plots.

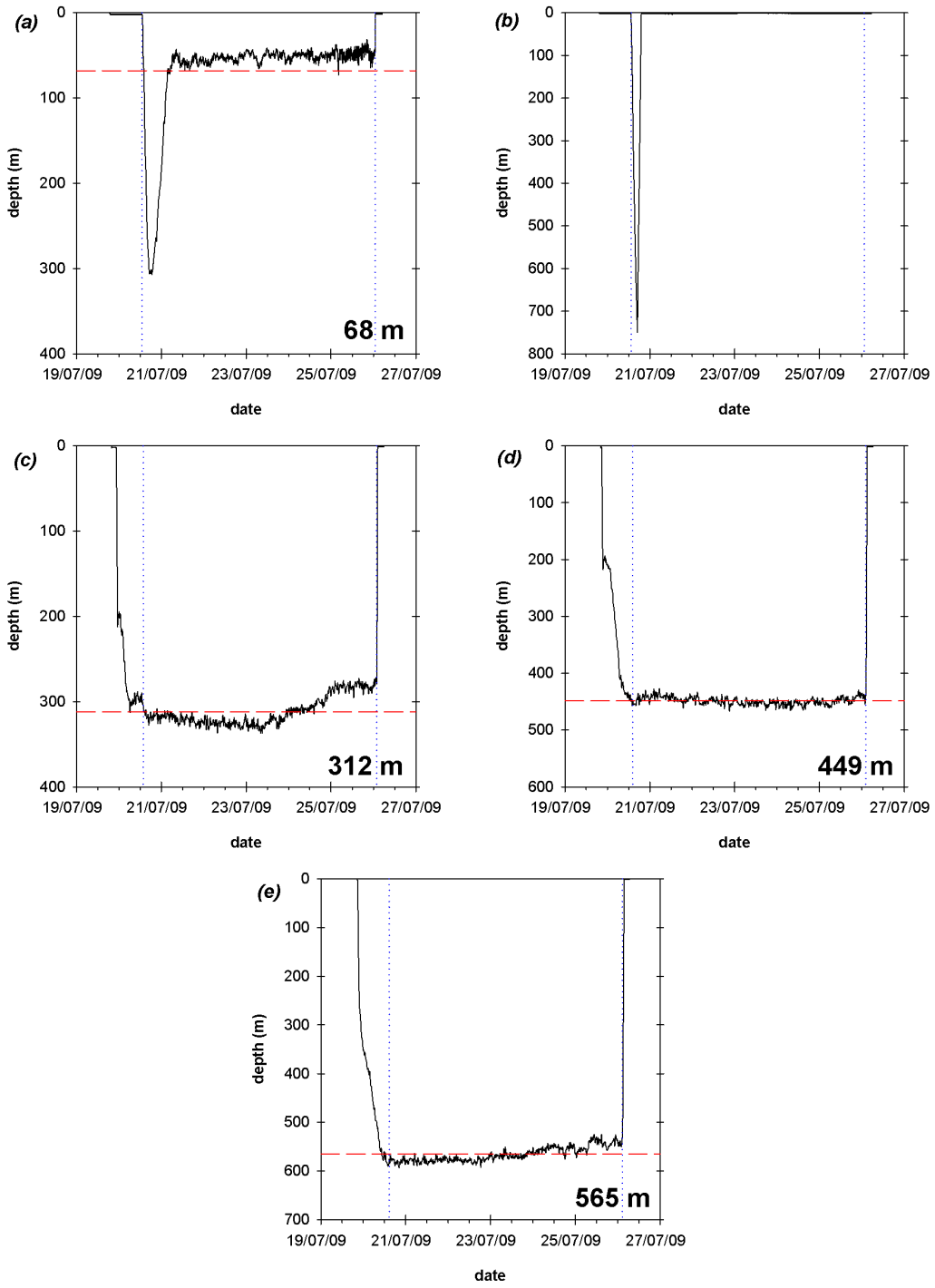

Figure D.2: PAP2 deployment profiles for *(a)* P2, *(b)* P4, *(c)* P5, *(d)* P6 and *(e)* P7. Details are as for Figure D.1.

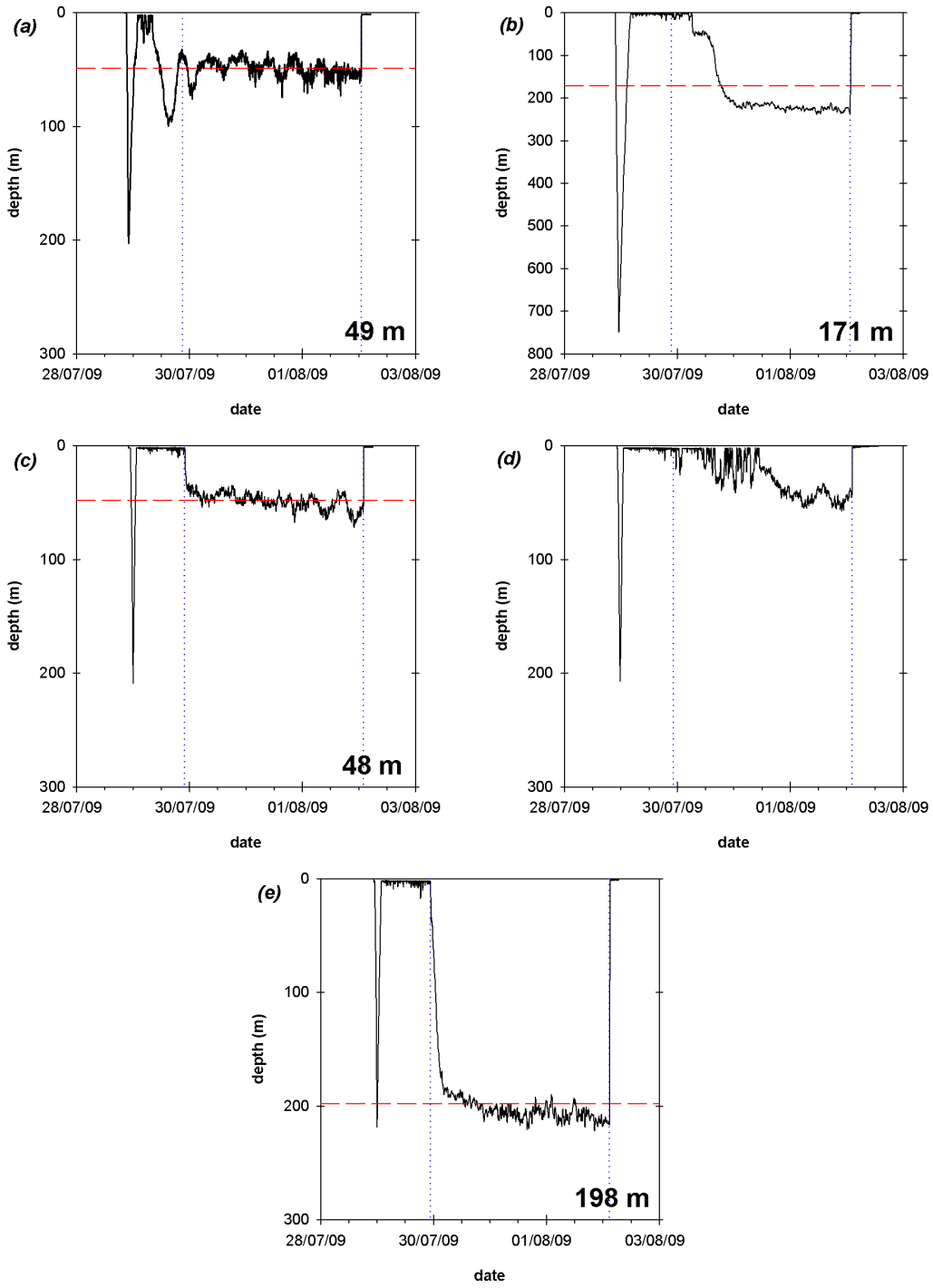

Figure D.3: PAP3 deployment profiles for *(a)* P2, *(b)* P4, *(c)* P5, *(d)* P6 and *(e)* P7. Details are as for Figure D.1.

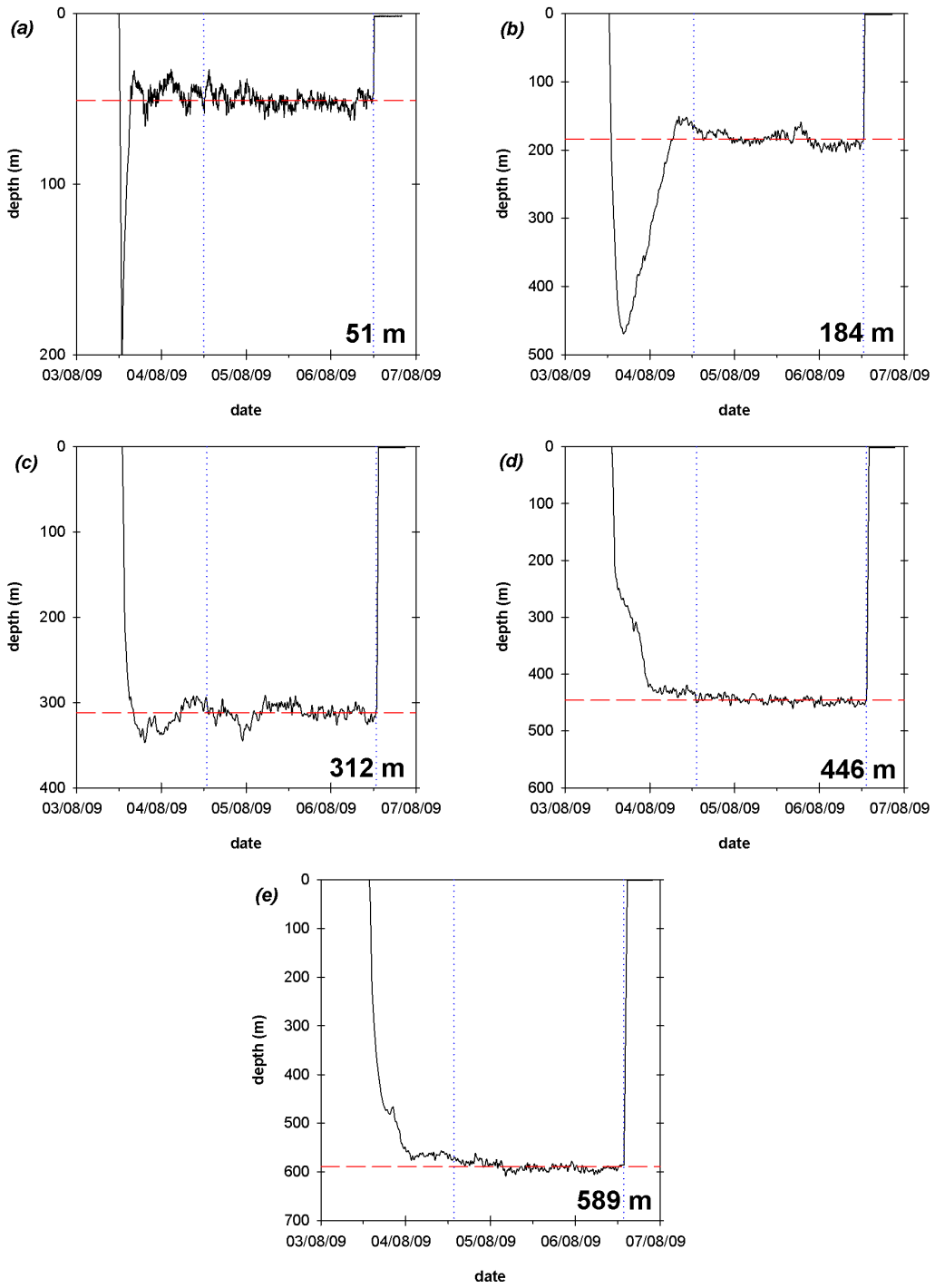

Figure D.4: PAP4 deployment profiles for *(a)* P2, *(b)* P4, *(c)* P5, *(d)* P6 and *(e)* P7. Details are as for Figure D.1.

Table D.2: Deployment details for D354 (depth in brackets represents average depth during stable period, as trap was not stable for entire sampling time).

	Deployment date/time	*Deployment location*	*Pots open*	*Sampling time*	*Mean sampling depth ± 1σ*	*Surfacing date/time*	*Surfacing location*
IB1 P4	12/07/10 00:34	60°00.0′ N 19°59.8′ W	13/07/10 00:30	30 h	72 ± 27 m (83 ± 5 m)	14/07/10 03:43	60°05.4′ N 18°48.4′ W
IB1 P6	12/07/10 01:03	60°00.0′ N 19°59.7′ W	13/07/10 01:00	30 h	156 ± 5 m	14/07/10 07:22	60°07.9′ N 18°44.8′ W
IB2 P4[a]	18/07/10 01:05	60°03.0′ N 34°58.5′ W	19/07/10 01:00	----	----	----	----
IB2 P6	18/07/10 01:37	60°03.2′ N 34°58.0′ W	19/07/10 01:30	54 h	152 ± 6 m	21/07/10 08:54	60°05.6′ N 34°39.1′ W
IB3 P4	25/07/10 08:04	60°50.6′ N 31°35.8′ W	26/07/10 08:00	44 h	84 ± 5 m	28/07/10 06:53	60°37.9′ N 32°14.4′ W[b]
IB3 P6	25/07/10 08:36	60°50.3′ N 31°35.9′ W	26/07/10 08:30	50 h	154 ± 4 m	28/07/10 10:54	60°33.7′ N 31°47.3′ W
IB3 P7	25/07/10 07:39	60°50.9′ N 31°35.7′ W	26/07/10 07:30	44 h	402 ± 4 m	28/07/10 09:47	60°35.6′ N 31°54.4′ W

[a] **Pots malfunctioned – it is suspected that they did not open properly during the deployment.**
[b] **Surfacing location given is actually the recovery location of the trap. Recovery took place ~9 hours after surfacing.**

Table D.2 continued…

	Deployment date/time	*Deployment location*	*Pots open*	*Sampling time*	*Mean sampling depth ± 1σ*	*Surfacing date/time*	*Surfacing location*
IB4 P4	03/08/10 08:35	62˚08.7′ N 24˚23.4′ W	04/08/10 08:30	40 h	82 ± 5 m	06/08/10 03:32	62˚08.2′ N 25˚05.5′ W
IB4 P6	03/08/10 09:10	62˚08.7′ N 24˚24.2′ W	04/08/10 09:00	46 h	152 ± 5 m	06/08/10 07:23	61˚56.5′ N 25˚12.7′ W
IB4 P7	03/08/10 08:04	62˚08.7′ N 24˚24.2′ W	04/08/10 08:00	40 h	402 ± 6 m	06/08/10 06:21	62˚11.8′ N 24˚41.9′ W

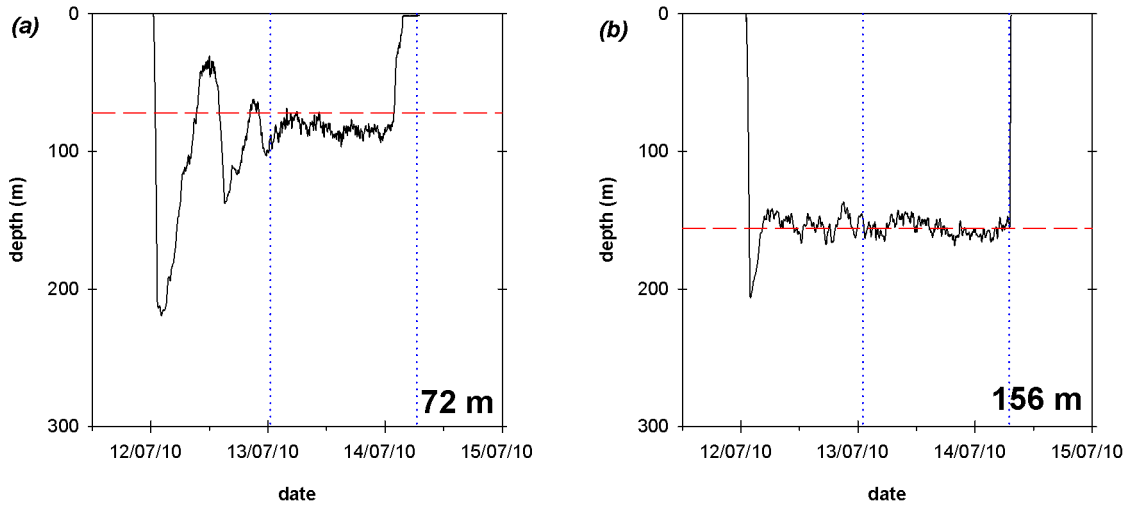

Figure D.5: IB1 deployment profiles for *(a)* P4 and *(b)* P6. Blue, vertical dotted lines represent pot opening/closing times; red horizontal dashed line represents average trap depth during sampling period (shown in bottom corner).

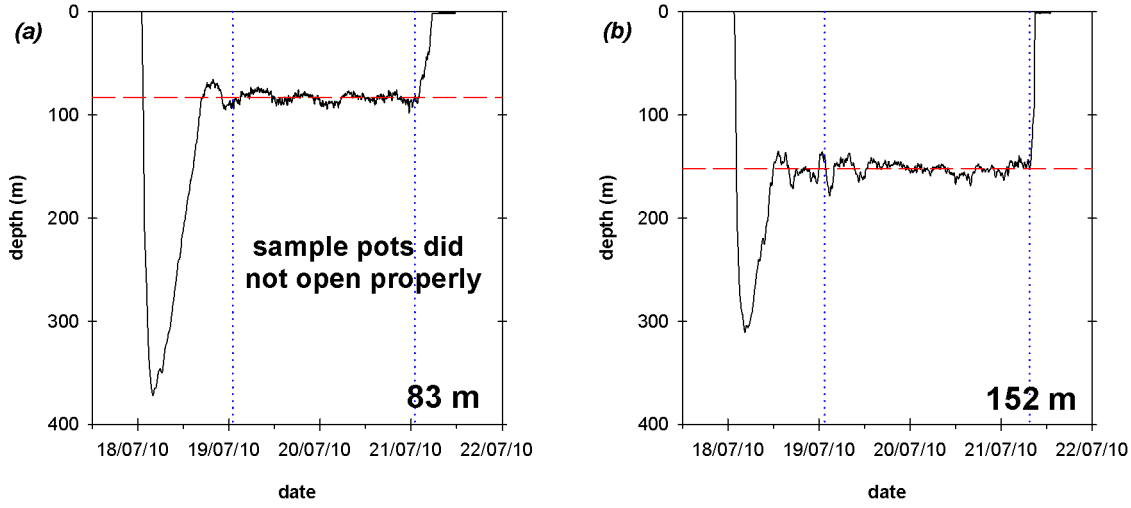

Figure D.6: IB2 deployment profiles for *(a)* P4 and *(b)* P6. Details are as for Figure D.5.

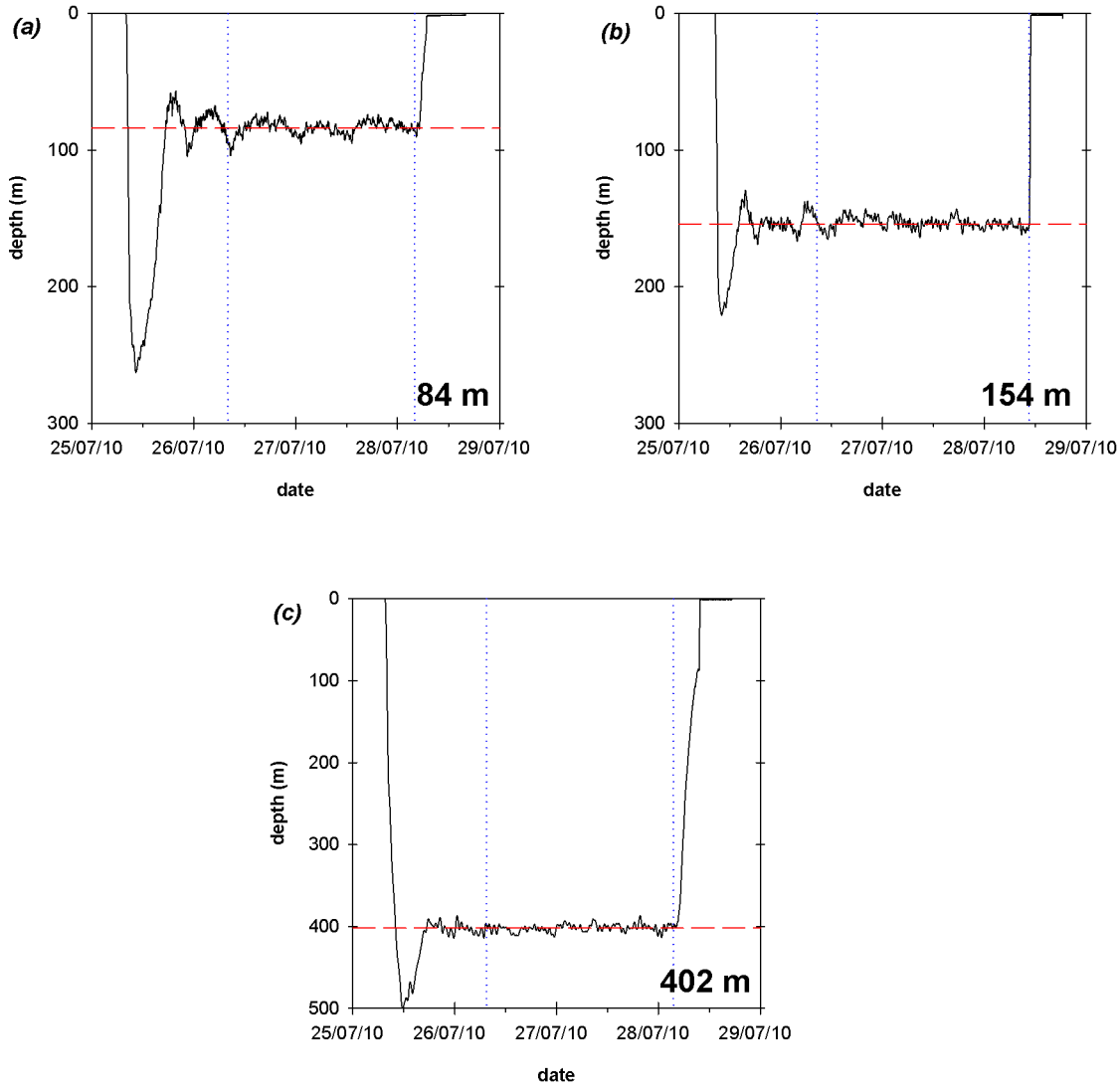

Figure D.7: IB3 deployment profiles for *(a)* P4, *(b)* P6 and *(c)* P7. Details are as for Figure D.5. Note change to vertical axis scale in *(c)*.

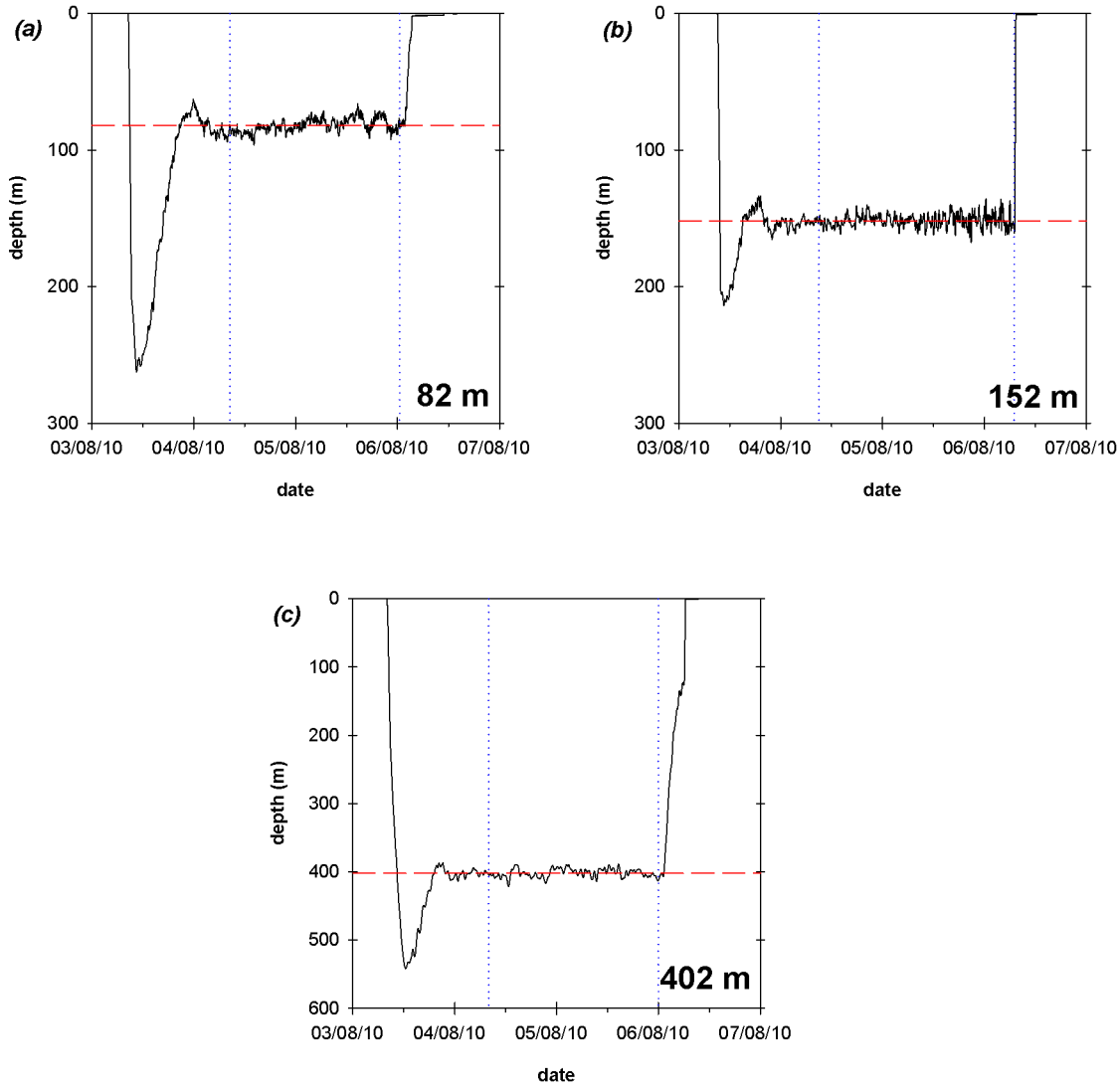

Figure D.8: IB4 deployment profiles for *(a)* P4, *(b)* P6 and *(c)* P7. Details are as for Figure D.5. Note change to vertical axis scale in *(c)*.

Appendix E: SAPS sampling details

Table E.1: Sample details for D350 SAPS deployments.

Station	*Date & Time (GMT)*	*Latitude (°N)*	*Longitude (°W)*	*Depth (m)*	*Volume filtered (L)*	*Size fraction*	*Mass collected[1] (mg)*
D350-1	01/05/10 10:19	60.962	34.908	50	772	>53 µm 1 – 53 µm	6.6 28.9
D350-2	02/05/10 04:35	60.005	34.988	50	527	>53 µm 1 – 53 µm	7.8 34.0
				150	890	>53 µm 1 – 53 µm	7.4 26.3
D350-3	03/05/10 08:56	59.99	31.96	60	467	>53 µm 1 – 53 µm	11.8 62.4
				160	1136	>53 µm 1 – 53 µm	6.1 48.2
D350-4	04/05/10 10:51	59.975	29.003	50	562	>53 µm 1 – 53 µm	9.6 120.3
				150	1346	>53 µm 1 – 53 µm	5.7 29.4
D350-5	05/05/10 08:48	59.927	26.087	50	773	>53 µm 1 – 53 µm	4.5 54.2
				150	1259	>53 µm 1 – 53 µm	4.6 52.6
D350-6	06/05/10 09:04	60.842	21.725	50	DNP[2]		
				150	1124	>53 µm 1 – 53 µm	3.4 43.8
D350-7	07/05/10 08:06	61.985	20.008	50	1227	>53 µm 1 – 53 µm	2.3 20.9
D350-8	08/05/10 07:04	63.108	19.893	15	407	>53 µm 1 – 53 µm	2.6 55.3
				50	996	>53 µm 1 – 53 µm	2.8 67.3
				150	DNP[2]		

[1] **Mass collected is the sum of mass of material rinsed on to filters for trace metal and POC analyses.**
[2] **Did not pump.**

Table E.2: Sample details for D351 SAPS deployments.

Station	*Date & Time (GMT)*	*Latitude (°N)*	*Longitude (°W)*	*Depth (m)*	*Volume filtered (L)*	*Size fraction*	*Mass collected[1] (mg)*
D351-1	13/05/10 16:27	61.997	20.052	25	415	>53 µm	24.4
						1 – 53 µm	99.0
				70	776	>53 µm	16.4
						1 – 53 µm	65.1
				170	1412	>53 µm	13.0
						1 – 53 µm	49.1
D351-2	16/05/10 06:10	59.997	20.018	60	458	>53 µm	4.8
						1 – 53 µm	35.6
				160	1306	>53 µm	14.8
						1 – 53 µm	44.5
D351-3	19/05/10 03:57	57.530	12.643	60	632	>53 µm	5.2
						1 – 53 µm	4.4
				160	1375	>53 µm	7.4
						1 – 53 µm	11.9

[1] **Mass collected is the sum of mass of material rinsed on to filters for trace metal and POC analyses.**

Table E.3: Sample details for D354 SAPS deployments.

Station	*Date & Time (GMT)*	*Latitude (°N)*	*Longitude (°W)*	*Depth (m)*	*Volume filtered (L)*	*Size fraction*	*Mass collected[1] (mg)*
				20		DNP[2]	
D354-1	11/07/10 20:22	60.005	19.985	50	1547	>53 µm 1 – 53 µm	11.5 14.0
				150	2313	>53 µm 1 – 53 µm	5.8 9.1
D354-2	13/07/10 09:41	61.795	21.077	20	1052	>53 µm 1 – 53 µm	64.9 19
				50	2047	>53 µm 1 – 53 µm	5.7 14.9
				150	2145	>53 µm 1 – 53 µm	3.7 10.7
D354-3	15/07/10 10:12	60.000	23.628	20	926	>53 µm 1 – 53 µm	38.8 13.6
				40	1996	>53 µm 1 – 53 µm	17.6 17.9
				140	1313	>53 µm 1 – 53 µm	2.7 7.3
D354-4	17/07/10 21:52	60.032	34.958	20	323	>53 µm 1 – 53 µm	7.3 10.6
				50	1793	>53 µm 1 – 53 µm	7.8 22.7
				150	2150	>53 µm 1 – 53 µm	2.9 5.1
D354-5	19/07/10 09:43	59.910	41.418	20	1606	>53 µm 1 – 53 µm	38.4 7.8
				50	2056	>53 µm 1 – 53 µm	19.3 18.6
				150	1180	>53 µm 1 – 53 µm	3.7 7.8
D354-6	21/07/10 01:58	59.973	34.960	20	506	>53 µm 1 – 53 µm	14.0 12.3
				50	1431	>53 µm 1 – 53 µm	13.2 20.9
				150	1023	>53 µm 1 – 53 µm	5.9 7.0
D354-7	22/07/10 12:35	62.995	34.973	20	1240	>53 µm 1 – 53 µm	22.6 11.3
				40	1899	>53 µm 1 – 53 µm	11.0 12.8
				140	950	>53 µm 1 – 53 µm	2.2 5.1

Table E.3 continued…

Station	*Date & Time (GMT)*	*Latitude (°N)*	*Longitude (°W)*	*Depth (m)*	*Volume filtered (L)*	*Size fraction*	*Mass collected[1] (mg)*
D354-8	24/07/10 09:44	62.983	29.867	20	972	>53 µm	16.3
						1 – 53 µm	9.0
				40	2054	>53 µm	17.1
						1 – 53 µm	12.0
				140	1968	>53 µm	15.1
						1 – 53 µm	14.0
D354-9 (a)	26/07/10 15:31	58.222	35.070	20	556	>53 µm	23.5
						1 – 53 µm	16.4
				50	1930	>53 µm	11.8
						1 – 53 µm	22.8
				150	2121	>53 µm	4.4
						1 – 53 µm	8.9
D354-9 (b)	26/07/10 22:44	58.207	35.200	300	2174	>53 µm	4.0
						1 – 53 µm	6.1
				400	2152	>53 µm	3.1
						1 – 53 µm	7.0
D354-10	30/07/10 06:44	63.833	35.055	20	1253	>53 µm	23.5
						1 – 53 µm	4.7
				50	613	>53 µm	3.1
						1 – 53 µm	4.8
				150	1884	>53 µm	4.0
						1 – 53 µm	8.6
				300	1745	>53 µm	1.6
						1 – 53 µm	6.1
				400	2112	>53 µm	2.7
						1 – 53 µm	8.8
D354-11	01/08/10 08:46	62.473	28.362	20	278	>53 µm	7.5
						1 – 53 µm	25.3
				40	DNP[2]		
				140	736	>53 µm	2.2
						1 – 53 µm	16.8
D354-12	03/08/10 12:59	62.112	24.345	20	596	>53 µm	9.7
						1 – 53 µm	5.5
				40	1274	>53 µm	9.8
						1 – 53 µm	7.2
				140	2318	>53 µm	8.7
						1 – 53 µm	14.9
D354-13	04/08/10 10:19	61.242	20.770	40	858	>53 µm	2.5
						1 – 53 µm	7.2
				140	2041	>53 µm	4.8
						1 – 53 µm	15.5

Table E.3 continued...

Station	*Date & Time (GMT)*	*Latitude (°N)*	*Longitude (°W)*	*Depth (m)*	*Volume filtered (L)*	*Size fraction*	*Mass collected[1] (mg)*
D354-14	05/08/10 19:04	61.987	26.643	20	378	>53 µm	4.3
						1 – 53 µm	17.4
				50	949	>53 µm	2.1
						1 – 53 µm	21.6
				150	680	>53 µm	1.3
						1 – 53 µm	16.6
D354-15	07/08/10 05:18	60.337	20.930	20	145	>53 µm	0.7
						1 – 53 µm	13.8
				50	664	>53 µm	2.1
						1 – 53 µm	18.1
				150	1248	>53 µm	2.6
						1 – 53 µm	19.6
				400	1241	>53 µm	1.5
						1 – 53 µm	10.0

[1] Mass collected is the sum of mass of material rinsed on to filters for trace metal and POC analyses.
[2] Did not pump.

References

Achterberg, E. P., Holland, T. W., Bowie, A. R., Mantoura, R. F. C. and Worsfold, P. J. (2001). Determination of iron in seawater. *Analytica Chimica Acta,* **442,** 1-14, doi:10.1016/S0003-2670(01)01091-1.

Aguilar-Islas, A. M., Wu, J., Rember, R., Johansen, A. M. and Shank, L. M. (2010). Dissolution of aerosol-derived iron in seawater: leach solution chemistry, aerosol type, and colloidal iron fraction. *Marine Chemistry,* **120,** 25-33, doi:10.1016/j.marchem.2009.01.011.

Alldredge, A. L. and Silver, M. W. (1988). Characteristics, dynamics and significance of marine snow. *Progress in Oceanography,* **20,** 41-82, doi:10.1016/0079-6611(88)90053-5.

Alldredge, A. L., Passow, U. and Logan, B. E. (1993). The abundance and significance of a class of large, transparent organic particles in the ocean. *Deep-Sea Research Part I: Oceanographic Research Papers,* **40,** 1131-1140, doi:10.1016/0967-0637(93)90129-Q.

Alonso-González, I. J., Arístegui, J., Lee, C., Sanchez-Vidal, A., Calafat, A., Fabrés, J., Sangrá, P., Masqué, P., Hernández-Guerra, A. and Benítez-Barrios, V. (2010). Role of slowly settling particles in the ocean carbon cycle. *Geophysical Research Letters,* **37,** Article No. L13608, doi:10.1029/2010gl043827.

Anderson, L. A. (1995). On the hydrogen and oxygen content of marine phytoplankton. *Deep-Sea Research Part I: Oceanographic Research Papers,* **42,** 1675-1680, doi:10.1016/0967-0637(95)00072-E.

Antia, A. N. (2005). Solubilization of particles in sediment traps: revising the stoichiometry of mixed layer export. *Biogeosciences,* **2,** 189-204, doi:10.5194/bg-2-189-2005.

Archer, D. E. and Johnson, K. (2000). A model of the iron cycle in the ocean. *Global Biogeochemical Cycles,* **14,** 269-279, doi:10.1029/1999GB900053.

Arimoto, R., Duce, R. A., Ray, B. J., Ellis Jr., W. G., Cullen, J. D. and Merrill, J. T. (1995). Trace elements in the atmosphere over the North Atlantic. *Journal of Geophysical Research-Atmospheres,* **100,** 1199-1213, doi:10.1029/94JD02618.

Armstrong, R. A., Lee, C., Hedges, J. I., Honjo, S. and Wakeham, S. G. (2002). A new, mechanistic model for organic carbon fluxes in the ocean based on the quantitative association of POC with ballast minerals. *Deep-Sea Research Part II: Topical Studies in Oceanography,* **49,** 219-236, doi:10.1016/S0967-0645(01)00101-1.

Arrigo, K. R. (2005). Marine microorganisms and global nutrient cycles. *Nature,* **437,** 349-355, doi:10.1038/Nature04159.

Asper, V. L. (1996). Particle flux in the ocean: oceanographic tools. *In:* V. Ittekkot, P. Schafer, S. Honjo & P. J. Depetris (eds.) *Particle Flux in the Ocean.* Chichester: John Wiley, *pp.* 71 - 84.

Azam, F., Fenchel, T., Field, J. G., Gray, J. S., Meyer-Reil, L. A. and Thingstad, F. (1983). The ecological role of water-column microbes in the sea. *Marine Ecology Progress Series,* **10,** 257-263, doi:10.3354/meps010257.

Bacon, M. P., Huh, C. A., Fleer, A. P. and Deuser, W. G. (1985). Seasonality in the flux of natural radionuclides and plutonium in the deep Sargasso Sea. *Deep-Sea Research Part A: Oceanographic Research Papers,* **32,** 273-286, doi:10.1016/0198-0149(85)90079-2.

Baker, A. R. and Jickells, T. D. (2006). Mineral particle size as a control on aerosol iron solubility. *Geophysical Research Letters,* **33,** Article No. L17608, doi:10.1029/2006gl026557.

Baker, A. R., Jickells, T. D., Witt, M. and Linge, K. L. (2006). Trends in the solubility of iron, aluminium, manganese and phosphorus in aerosol collected over the Atlantic Ocean. *Marine Chemistry,* **98,** 43-58, doi:10.1016/j.marchem.2005.06.004.

Barbeau, K., Rue, E. L., Bruland, K. W. and Butler, A. (2001). Photochemical cycling of iron in the surface ocean mediated by microbial iron(III)-binding ligands. *Nature,* **413,** 409-413, doi:10.1038/35096545.

Bennett, S. A., Achterberg, E. P., Connelly, D. P., Statham, P. J., Fones, G. R. and German, C. R. (2008). The distribution and stabilisation of dissolved Fe in deep-sea hydrothermal plumes. *Earth and Planetary Science Letters,* **270,** 157-167, doi:10.1016/j.epsl.2008.01.048.

Berelson, W. M. (2001). The flux of particulate organic carbon into the ocean interior: a comparison of four U.S. JGOFS regional studies. *Oceanography,* **14,** 59-67, doi:10.5670/oceanog.2001.07.

Berelson, W. M., McManus, J., Coale, K., Johnson, K., Burdige, D., Kilgore, T., Colodner, D., Chavez, F., Kudela, R. and Boucher, J. (2003). A time series of benthic flux measurements from Monterey Bay, CA. *Continental Shelf Research,* **23,** 457-481, doi:10.1016/s0278-4343(03)00009-8.

Berger, C. J. M., Lippiatt, S. M., Lawrence, M. G. and Bruland, K. W. (2008). Application of a chemical leach technique for estimating labile particulate aluminum, iron, and manganese in the Columbia River plume and coastal waters off Oregon and Washington. *Journal of Geophysical Research-Oceans,* **113,** Article No. C00B01, doi:10.1029/2007jc004703.

Billett, D. S. M. and Rice, A. L. (2001). The BENGAL programme: introduction and overview. *Progress in Oceanography,* **50,** 13-25, doi:10.1016/S0079-6611(01)00046-5.

Bishop, J. K. B. and Edmond, J. M. (1976). A new large volume filtration system for the sampling of oceanic particulate matter. *Journal of Marine Research,* **34,** 181-198.

Bishop, J. K. B., Edmond, J. M., Ketten, D. R., Bacon, M. P. and Silker, W. B. (1977). The chemistry, biology, and vertical flux of particulate matter from the upper 400 m of the equatorial Atlantic Ocean. *Deep-Sea Research,* **24,** 511-548, doi:10.1016/0146-6291(77)90526-4.

Bishop, J. K. B., Schupack, D., Sherrell, R. M. and Conte, M. H. (1985). A multiple-unit large-volume in situ filtration system for sampling oceanic particulate matter in mesoscale environments. *In:* A. Zirino (ed.) *Mapping Strategies in Chemical Oceanography.* Washington, D.C.: American Chemical Society, *pp.* 155 - 175.

Bishop, J. K. B. and Wood, T. J. (2009). Year-round observations of carbon biomass and flux variability in the Southern Ocean. *Global Biogeochemical Cycles,* **23,** Article No. GB2019, doi:10.1029/2008gb003206.

Bowie, A. R., Maldonado, M. T., Frew, R. D., Croot, P. L., Achterberg, E. P., Mantoura, R. F. C., Worsfold, P. J., Law, C. S. and Boyd, P. W. (2001). The fate of added iron during a mesoscale fertilisation experiment in the Southern Ocean. *Deep-Sea Research Part II: Topical Studies in Oceanography,* **48,** 2703-2743, doi:10.1016/S0967-0645(01)00015-7.

Bowie, A. R., Lannuzel, D., Remenyi, T. A., Wagener, T., Lam, P. J., Boyd, P. W., Guieu, C., Townsend, A. T. and Trull, T. W. (2009). Biogeochemical iron budgets of the Southern Ocean south of Australia: decoupling of iron and nutrient cycles in the subantarctic zone by the summertime supply. *Global Biogeochemical Cycles,* **23,** Article No. GB4034, doi:10.1029/2009gb003500.

Boyd, P. W., Watson, A. J., Law, C. S., Abraham, E. R., Trull, T., Murdoch, R., Bakker, D. C. E., Bowie, A. R., Buesseler, K. O., Chang, H., Charette, M., Croot, P., Downing, K., Frew, R., Gall, M., Hadfield, M., Hall, J., Harvey, M., Jameson, G., LaRoche, J., Liddicoat, M., Ling, R., Maldonado, M. T., McKay, R. M., Nodder, S., Pickmere, S., Pridmore, R., Rintoul, S., Safi, K., Sutton, P., Strzepek, R., Tanneberger, K., Turner, S., Waite, A. and Zeldis, J. (2000). A mesoscale phytoplankton bloom in the polar Southern Ocean stimulated by iron fertilization. *Nature,* **407,** 695-702, doi:10.1038/35037500.

Boyd, P. W., Law, C. S., Wong, C. S., Nojiri, Y., Tsuda, A., Levasseur, M., Takeda, S., Rivkin, R., Harrison, P. J., Strzepek, R., Gower, J., McKay, R. M., Abraham, E., Arychuk, M., Barwell-Clarke, J., Crawford, W., Crawford, D., Hale, M., Harada, K., Johnson, K., Kiyosawa, H., Kudo, I., Marchetti, A., Miller, W., Needoba, J., Nishioka, J., Ogawa, H., Page, J., Robert, M., Saito, H., Sastri, A., Sherry, N., Soutar, T., Sutherland, N., Taira, Y., Whitney, F., Wong, S. K. E. and Yoshimura, T. (2004). The decline and fate of an iron-induced subarctic phytoplankton bloom. *Nature,* **428,** 549-553, doi:10.1038/nature02437.

Boyd, P. W., Law, C. S., Hutchins, D. A., Abraham, E. R., Croot, P. L., Ellwood, M., Frew, R. D., Hadfield, M., Hall, J., Handy, S., Hare, C., Higgins, J., Hill, P., Hunter, K. A., LeBlanc, K., Maldonado, M. T., McKay, R. M., Mioni, C., Oliver, M., Pickmere, S., Pinkerton, M., Safi, K., Sander, S., Sañudo-Wilhelmy, S. A., Smith, M., Strzepek, R., Tovar-Sanchez, A. and Wilhelm, S. W. (2005). FeCycle: Attempting an iron biogeochemical budget from a mesoscale SF_6 tracer experiment in unperturbed low iron waters. *Global Biogeochemical Cycles,* **19,** Article No. GB4S20, doi:10.1029/2005gb002494.

Boyd, P. W. and Trull, T. W. (2007). Understanding the export of biogenic particles in oceanic waters: is there consensus? *Progress in Oceanography,* **72,** 276-312, doi:10.1016/j.pocean.2006.10.007.

Boyd, P. W. and Ellwood, M. J. (2010). The biogeochemical cycle of iron in the ocean. *Nature Geoscience,* **3,** 675-682, doi:10.1038/Ngeo964.

Boyd, P. W., Ibisanmi, E., Sander, S. G., Hunter, K. A. and Jackson, G. A. (2010). Remineralization of upper ocean particles: implications for iron biogeochemistry. *Limnology and Oceanography,* **55,** 1271-1288, doi:10.4319/lo.2010.55.3.1271.

Brewer, P. G., Spencer, D. W., Biscaye, P. E., Hanley, A., Sachs, P. L., Smith, C. L., Kadar, S. and Fredericks, J. (1976). The distribution of particulate matter in the Atlantic

Ocean. *Earth and Planetary Science Letters,* **32,** 393-402, doi:10.1016/0012-821X(76)90080-7.

Brewer, P. G., Nozaki, Y., Spencer, D. W. and Fleer, A. P. (1980). Sediment trap experiments in the deep North Atlantic: isotopic and elemental fluxes. *Journal of Marine Research,* **38,** 703-728.

Briggs, N., Perry, M. J., Cetinić, I., Lee, C., D'Asaro, E., Gray, A. M. and Rehm, E. (2011). High-resolution observations of aggregate flux during a sub-polar North Atlantic spring bloom. *Deep-Sea Research Part I: Oceanographic Research Papers,* **58,** 1031-1039, doi:10.1016/j.dsr.2011.07.007.

Brown, L., Sanders, R., Savidge, G. and Lucas, C. H. (2003). The uptake of silica during the spring bloom in the Northeast Atlantic Ocean. *Limnology and Oceanography,* **48,** 1831-1845, doi:10.4319/lo.2003.48.5.1831.

Brown, L., Sanders, R. and Savidge, G. (2006). Relative mineralisation of C and Si from biogenic particulate matter in the upper water column during the North East Atlantic diatom bloom in spring 2001. *Journal of Marine Systems,* **63,** 79-90, doi:10.1016/j.jmarsys.2006.03.001.

Buck, C. S., Landing, W. M., Resing, J. A. and Lebon, G. T. (2006). Aerosol iron and aluminum solubility in the northwest Pacific Ocean: results from the 2002 IOC cruise. *Geochemistry Geophysics Geosystems,* **7,** Article No. Q04M07, doi:10.1029/2005gc000977.

Buesseler, K. O. (1991). Do upper-ocean sediment traps provide an accurate record of particle flux? *Nature,* **353,** 420-423, doi:10.1038/353420a0.

Buesseler, K. O., Michaels, A. F., Siegel, D. A. and Knap, A. H. (1994). A three dimensional time-dependent approach to calibrating sediment trap fluxes. *Global Biogeochemical Cycles,* **8,** 179-193, doi:10.1029/94GB00207.

Buesseler, K. O. (1998). The decoupling of production and particulate export in the surface ocean. *Global Biogeochemical Cycles,* **12,** 297-310, doi:10.1029/97GB03366.

Buesseler, K. O., Steinberg, D. K., Michaels, A. F., Johnson, R. J., Andrews, J. E., Valdes, J. R. and Price, J. F. (2000). A comparison of the quantity and composition of material caught in a neutrally buoyant versus surface-tethered sediment trap. *Deep-Sea Research Part I: Oceanographic Research Papers,* **47,** 277-294, doi:10.1016/S0967-0637(99)00056-4.

Buesseler, K. O., Antia, A. N., Chen, M., Fowler, S. W., Gardner, W. D., Gustafsson, O., Harada, K., Michaels, A. F., Rutgers van der Loeff, M., Sarin, M., Steinberg, D. K. and Trull, T. (2007). An assessment of the use of sediment traps for estimating upper ocean particle fluxes. *Journal of Marine Research,* **65,** 345-416.

Buesseler, K. O., Trull, T. W., Steinberg, D. K., Silver, M. W., Siegel, D. A., Saitoh, S. I., Lamborg, C. H., Lam, P. J., Karl, D. M., Jiao, N. Z., Honda, M. C., Elskens, M., Dehairs, F., Brown, S. L., Boyd, P. W., Bishop, J. K. B. and Bidigare, R. R. (2008). VERTIGO (VERtical Transport In the Global Ocean): a study of particle sources and flux attenuation in the North Pacific. *Deep-Sea Research Part II: Topical Studies in Oceanography,* **55,** 1522-1539, doi:10.1016/j.dsr2.2008.04.024.

Buesseler, K. O. and Boyd, P. W. (2009). Shedding light on processes that control particle export and flux attenuation in the twilight zone of the open ocean. *Limnology and Oceanography,* **54,** 1210-1232, doi:10.4319/lo.2009.54.4.1210.

Burd, A. B., Hansell, D. A., Steinberg, D. K., Anderson, T. R., Arístegui, J., Baltar, F., Beaupré, S. R., Buesseler, K. O., DeHairs, F., Jackson, G. A., Kadko, D. C., Koppelmann, R., Lampitt, R. S., Nagata, T., Reinthaler, T., Robinson, C., Robison, B. H., Tamburini, C. and Tanaka, T. (2010). Assessing the apparent imbalance between geochemical and biochemical indicators of meso- and bathypelagic biological activity: What the @$#! is wrong with present calculations of carbon budgets? *Deep-Sea Research Part II: Topical Studies in Oceanography,* **57,** 1557-1571, doi:10.1016/j.dsr2.2010.02.022.

Chen, J. H., Edwards, R. L. and Wasserburg, G. J. (1986). ^{238}U, ^{234}U and ^{232}Th in seawater. *Earth and Planetary Science Letters,* **80,** 241-251, doi:10.1016/0012-821X(86)90108-1.

Chen, Y. and Siefert, R. L. (2004). Seasonal and spatial distributions and dry deposition fluxes of atmospheric total and labile iron over the tropical and subtropical North Atlantic Ocean. *Journal of Geophysical Research-Atmospheres,* **109,** Article No. D09305, doi:10.1029/2003jd003958.

Chester, R. and Hughes, M. J. (1967). A chemical technique for the separation of ferro-manganese minerals, carbonate minerals and adsorbed trace elements from pelagic sediments. *Chemical Geology,* **2,** 249-262, doi:10.1016/0009-2541 (67)90025-3.

Christian, J. R., Lewis, M. R. and Karl, D. M. (1997). Vertical fluxes of carbon, nitrogen, and phosphorus in the North Pacific Subtropical Gyre near Hawaii. *Journal of Geophysical Research-Oceans,* **102,** 15,667-15,677, doi:10.1029/97JC00369.

Coale, K. H., Johnson, K. S., Fitzwater, S. E., Gordon, R. M., Tanner, S., Chavez, F. P., Ferioli, L., Sakamoto, C., Rogers, P., Millero, F., Steinberg, P., Nightingale, P., Cooper, D., Cochlan, W. P., Landry, M. R., Constantinou, J., Rollwagen, G., Trasvina, A. and Kudela, R. (1996). A massive phytoplankton bloom induced by an ecosystem-scale iron fertilization experiment in the equatorial Pacific Ocean. *Nature,* **383,** 495-501, doi:10.1038/383495a0.

Collier, R. and Edmond, J. (1984). The trace element geochemistry of marine biogenic particulate matter. *Progress in Oceanography,* **13,** 113-199, doi:10.1016/0079-6611(84)90008-9.

Cullen, J. T., Field, M. P. and Sherrell, R. M. (2001). Determination of trace elements in filtered suspended marine particulate material by sector field HR-ICP-MS. *Journal of Analytical Atomic Spectrometry,* **16,** 1307-1312, doi:10.1039/B104398f.

de Baar, H. J. W., Farrington, J. W. and Wakeham, S. G. (1983). Vertical flux of fatty acids in the North Atlantic Ocean. *Journal of Marine Research,* **41,** 19-41, doi:10.1357/002224083788223009.

de Baar, H. J. W. and de Jong, J. T. M. (2001). Distributions, sources and sinks of iron in seawater. *In:* D. R. Turner & K. A. Hunter (eds.) *The Biogeochemistry of Iron in Seawater.* Chichester: John Wiley & Sons, *pp.* 123 - 254.

de Jong, M. F., van Aken, H. M., Våge, K. and Pickart, R. S. (2012). Convective mixing in the central Irminger Sea: 2002–2010. *Deep Sea Research Part I: Oceanographic Research Papers,* **63,** 36-51, doi:10.1016/j.dsr.2012.01.003.

De La Rocha, C. L. and Passow, U. (2007). Factors influencing the sinking of POC and the efficiency of the biological carbon pump. *Deep-Sea Research Part II: Topical Studies in Oceanography,* **54,** 639-658, doi:10.1016/j.dsr2.2007.01.004.

Dellino, P., Gudmundsson, M. T., Larsen, G., Mele, D., Stevenson, J. A., Thordarson, T. and Zimanowski, B. (2012). Ash from the Eyjafjallajökull eruption (Iceland): fragmentation processes and aerodynamic behavior. *Journal of Geophysical Research-Solid Earth,* **117,** Article No. B00C04, doi:10.1029/2011jb008726.

Devol, A. H. and Hartnett, H. E. (2001). Role of the oxygen-deficient zone in transfer of organic carbon to the deep ocean. *Limnology and Oceanography,* **46,** 1684-1690, doi:10.4319/lo.2001.46.7.1684.

Doney, S. C., Lindsay, K., Caldeira, K., Campin, J.-M., Drange, H., Dutay, J.-C., Follows, M., Gao, Y., Gnanadesikan, A., Gruber, N., Ishida, A., Joos, F., Madec, G., Maier-Reimer, E., Marshall, J. C., Matear, R. J., Monfray, P., Mouchet, A., Najjar, R., Orr, J. C., Plattner, G.-K., Sarmiento, J., Schlitzer, R., Slater, R., Totterdell, I. J., Weirig, M.-F., Yamanaka, Y. and Yool, A. (2004). Evaluating global ocean carbon models: the importance of realistic physics. *Global Biogeochemical Cycles,* **18,** Article No. GB3017, doi:10.1029/2003gb002150.

Doney, S. C., Fabry, V. J., Feely, R. A. and Kleypas, J. A. (2009). Ocean acidification: the other CO_2 problem. *Annual Review of Marine Science,* **1,** 169-192, doi:10.1146/annurev.marine.010908.163834.

Draxler, R. R. and Rolph, G. D. 2012. HYSPLIT (HYbrid Single-Particle Lagrangian Intergrated Trajectory) Model access via NOAA ARL READY. Available at: http://ready.arl.noaa.gov/HYSPLIT.php [Website], NOAA Air Resources Laboratory, Silver Spring, MD. [Accessed September 2012].

Duce, R. A., Liss, P. S., Merrill, J. T., Atlas, E. L., Buat-Menard, P., Hicks, B. B., Miller, J. M., Prospero, J. M., Arimoto, R., Church, T. M., Ellis, W., Galloway, J. N., Hansen, L., Jickells, T. D., Knap, A. H., Reinhardt, K. H., Schneider, B., Soudine, A., Tokos, J. J., Tsunogai, S., Wollast, R. and Zhou, M. (1991). The atmospheric input of trace species to the world ocean. *Global Biogeochemical Cycles,* **5,** 193-259, doi:10.1029/91GB01778.

Duce, R. A. and Tindale, N. W. (1991). Atmospheric transport of iron and its deposition in the ocean. *Limnology and Oceanography,* **36,** 1715-1726, doi:10.4319/lo.1991.36.8.1715.

Duggen, S., Olgun, N., Croot, P., Hoffmann, L., Dietze, H., Delmelle, P. and Teschner, C. (2010). The role of airborne volcanic ash for the surface ocean biogeochemical iron cycle: a review. *Biogeosciences,* **7,** 827-844, doi:10.5194/bg-7-827-2010.

Dunne, J. P., Sarmiento, J. L. and Gnanadesikan, A. (2007). A synthesis of global particle export from the surface ocean and cycling through the ocean interior and on the seafloor. *Global Biogeochemical Cycles,* **21,** Article No. GB4006, doi:10.1029/2006gb002907.

Ebersbach, F. and Trull, T. W. (2008). Sinking particle properties from polyacrylamide gels during the KErguelen Ocean and Plateau compared Study (KEOPS): zooplankton control of carbon export in an area of persistent natural iron inputs in the Southern Ocean. *Limnology and Oceanography,* **53,** 212-224, doi:10.4319/lo.2008.53.1.0212.

Ebersbach, F., Trull, T. W., Davies, D. M. and Bray, S. G. (2011). Controls on mesopelagic particle fluxes in the Sub-Antarctic and Polar Frontal Zones in the Southern Ocean south of Australia in summer - Perspectives from free-drifting sediment traps. *Deep-Sea Research Part II: Topical Studies in Oceanography,* **58,** 2260-2276, doi:10.1016/j.dsr2.2011.05.025.

Elrod, V. A., Berelson, W. M., Coale, K. H. and Johnson, K. S. (2004). The flux of iron from continental shelf sediments: a missing source for global budgets. *Geophysical Research Letters,* **31,** Article No. L12307, doi:10.1029/2004gl020216.

Eppley, R. W. and Peterson, B. J. (1979). Particulate organic matter flux and planktonic new production in the deep ocean. *Nature,* **282,** 677-680, doi:10.1038/282677a0.

Ernst, G. G. J., Cave, R. R., German, C. R., Palmer, M. R. and Sparks, R. S. J. (2000). Vertical and lateral splitting of a hydrothermal plume at Steinahóll, Reykjanes Ridge, Iceland. *Earth and Planetary Science Letters,* **179,** 529-537, doi:10.1016/s0012-821x(00)00140-0.

Falkowski, P. G., Barber, R. T. and Smetacek, V. (1998). Biogeochemical controls and feedbacks on ocean primary production. *Science,* **281,** 200-206, doi:10.1126/science.281.5374.200.

Feely, R. A., Sabine, C. L., Lee, K., Berelson, W., Kleypas, J., Fabry, V. J. and Millero, F. J. (2004). Impact of anthropogenic CO_2 on the $CaCO_3$ system in the oceans. *Science,* **305,** 362-366, doi:10.1126/science.1097329.

Fischer, G., Ratmeyer, V. and Wefer, G. (2000). Organic carbon fluxes in the Atlantic and the Southern Ocean: relationship to primary production compiled from satellite radiometer data. *Deep-Sea Research Part II: Topical Studies in Oceanography,* **47,** 1961-1997, doi:10.1016/S0967-0645(00)00013-8.

Fitzwater, S. E., Johnson, K. S., Elrod, V. A., Ryan, J. P., Coletti, L. J., Tanner, S. J., Gordon, R. M. and Chavez, F. P. (2003). Iron, nutrient and phytoplankton biomass relationships in upwelled waters of the California coastal system. *Continental Shelf Research,* **23,** 1523-1544, doi:10.1016/j.csr.2003.08.004.

Forryan, A., Martin, A. P., Srokosz, M. A., Popova, E. E., Painter, S. C. and Stinchcombe, M. C. (2012). Turbulent nutrient fluxes in the Iceland Basin. *Deep Sea Research Part I: Oceanographic Research Papers,* **63,** 20-35, doi:10.1016/j.dsr.2011.12.006.

Francois, R., Honjo, S., Krishfield, R. and Manganini, S. (2002). Factors controlling the flux of organic carbon to the bathypelagic zone of the ocean. *Global Biogeochemical Cycles,* **16,** Article No. 1087, doi:10.1029/2001gb001722.

Frankignoulle, M., Canon, C. and Gattuso, J.-P. (1994). Marine calcification as a source of carbon dioxide: positive feedback of increasing atmospheric CO_2. *Limnology and Oceanography,* **39,** 458-462, doi:10.4319/lo.1994.39.2.0458.

Frew, R. D., Hutchins, D. A., Nodder, S., Sañudo-Wilhelmy, S., Tovar-Sanchez, A., Leblanc, K., Hare, C. E. and Boyd, P. W. (2006). Particulate iron dynamics during FeCycle in subantarctic waters southeast of New Zealand. *Global Biogeochemical Cycles,* **20,** Article No. GB1S93, doi:10.1029/2005gb002558.

Fung, I. Y., Meyn, S. K., Tegen, I., Doney, S. C., John, J. G. and Bishop, J. K. B. (2000). Iron supply and demand in the upper ocean. *Global Biogeochemical Cycles,* **14,** 281-295, doi:10.1029/1999GB900059.

Gardner, W. D. (1977). Incomplete extraction of rapidly settling particles from water samplers. *Limnology and Oceanography,* **22,** 764-768.

Gardner, W. D. (2000). Sediment trap sampling in surface waters. *In:* R. B. Hanson, H. W. Ducklow & J. G. Field (eds.) *The Changing Ocean Carbon Cycle : a midterm*

synthesis of the Joint Global Ocean Flux Study. Cambridge: Cambridge University Press, *pp.* 240 - 284.

German, C. R., Briem, J., Chin, C., Danielsen, M., Holland, S., James, R., Jónsdóttir, A., Ludford, E., Moser, C., Ólafsson, J., Palmer, M. R. and Rudnicki, M. D. (1994). Hydrothermal activity on the Reykjanes Ridge: the Steinahóll vent-field at 63°06' N. *Earth and Planetary Science Letters,* **121,** 647-654, doi:10.1016/0012-821x(94)90098-1.

Gislason, S. R., Hassenkam, T., Nedel, S., Bovet, N., Eiriksdottir, E. S., Alfredsson, H. A., Hem, C. P., Balogh, Z. I., Dideriksen, K., Oskarsson, N., Sigfusson, B., Larsen, G. and Stipp, S. L. S. (2011). Characterization of Eyjafjallajökull volcanic ash particles and a protocol for rapid risk assessment. *Proceedings of the National Academy of Sciences of the United States of America,* **108,** 7307-7312, doi:10.1073/pnas.1015053108.

Gordon, R. M., Johnson, K. S. and Coale, K. H. (1998). The behaviour of iron and other trace elements during the IronEx-I and PlumEx experiments in the Equatorial Pacific. *Deep-Sea Research Part II: Topical Studies in Oceanography,* **45,** 995-1041, doi:10.1016/S0967-0645(98)00012-5.

Green, D. R. H., Cooper, M. J., German, C. R. and Wilson, P. A. (2003). Optimization of an inductively coupled plasma-optical emission spectrometry method for the rapid determination of high-precision Mg/Ca and Sr/Ca in foraminiferal calcite. *Geochemistry Geophysics Geosystems,* **4,** Article No. 8404, doi:10.1029/2002gc000488.

Grotti, M., Soggia, F., Abelmoschi, M. L., Rivaro, P., Magi, E. and Frache, R. (2001). Temporal distribution of trace metals in Antarctic coastal waters. *Marine Chemistry,* **76,** 189-209, doi:10.1016/S0304-4203(01)00063-9.

Guieu, C., Loÿe-Pilot, M. D., Ridame, C. and Thomas, C. (2002). Chemical characterization of the Saharan dust end-member: some biogeochemical implications for the western Mediterranean Sea. *Journal of Geophysical Research-Atmospheres,* **107,** Article No. 4258, doi:10.1029/2001jd000582.

Guieu, C., Bonnet, S., Wagener, T. and Loÿe-Pilot, M. D. (2005). Biomass burning as a source of dissolved iron to the open ocean? *Geophysical Research Letters,* **32,** Article No. L19608, doi:10.1029/2005gl022962.

Hartman, S. E., Larkin, K. E., Lampitt, R. S., Lankhorst, M. and Hydes, D. J. (2010). Seasonal and inter-annual biogeochemical variations in the Porcupine Abyssal Plain 2003-2005 associated with winter mixing and surface circulation. *Deep-Sea Research Part II: Topical Studies in Oceanography,* **57,** 1303-1312, doi:10.1016/j.dsr2.2010.01.007.

Hedges, J. I., Eglinton, G., Hatcher, P. G., Kirchman, D. L., Arnosti, C., Derenne, S., Evershed, R. P., Kögel-Knabner, I., de Leeuw, J. W., Littke, R., Michaelis, W. and Rullkötter, J. (2000). The molecularly-uncharacterized component of nonliving organic matter in natural environments. *Organic Geochemistry,* **31,** 945-958, doi:10.1016/S0146-6380(00)00096-6.

Helmers, E. (1996). Trace metals in suspended particulate matter of Atlantic Ocean surface water (40°N to 20°S). *Marine Chemistry,* **53,** 51-67, doi:10.1016/0304-4203(96)00012-6.

Henson, S. A., Sanders, R., Holeton, C. and Allen, J. T. (2006). Timing of nutrient depletion, diatom dominance and a lower-boundary estimate of export

production for Irminger Basin, North Atlantic. *Marine Ecology Progress Series,* **313,** 73-84, doi:10.3354/meps313073.

Henson, S. A., Sanders, R., Madsen, E., Morris, P. J., Le Moigne, F. and Quartly, G. D. (2011). A reduced estimate of the strength of the ocean's biological carbon pump. *Geophysical Research Letters,* **38,** Article No. L04606, doi:10.1029/2011gl046735.

Henson, S. A., Sanders, R. and Madsen, E. (2012). Global patterns in efficiency of particulate organic carbon export and transfer to the deep ocean. *Global Biogeochemical Cycles,* **26,** Article No. GB1028, doi:10.1029/2011gb004099.

Hilton, J., Lishman, J. P., Mackness, S. and Heaney, S. I. (1986). An automated method for the analysis of 'particulate' carbon and nitrogen in natural waters. *Hydrobiologia,* **141,** 269-271, doi:10.1007/BF00014221.

Ho, T. Y., Quigg, A., Finkel, Z. V., Milligan, A. J., Wyman, K., Falkowski, P. G. and Morel, F. M. M. (2003). The elemental composition of some marine phytoplankton. *Journal of Phycology,* **39,** 1145-1159, doi:10.1111/j.0022-3646.2003.03-090.x.

Ho, T. Y., Wen, L. S., You, C. F. and Lee, D. C. (2007). The trace-metal composition of size-fractionated plankton in the South China Sea: biotic versus abiotic sources. *Limnology and Oceanography,* **52,** 1776-1788, doi:10.4319/lo.2007.52.5.1776.

Ho, T. Y., Chou, W. C., Wei, C. L., Lin, F. J., Wong, G. T. F. and Lin, H. L. (2010). Trace metal cycling in the surface water of the South China Sea: vertical fluxes, composition, and sources. *Limnology and Oceanography,* **55,** 1807-1820, doi:10.4319/lo.2010.55.5.1807.

Ho, T. Y., Chou, W. C., Lin, H. L. and Sheu, D. D. (2011). Trace metal cycling in the deep water of the South China Sea: the composition, sources, and fluxes of sinking particles. *Limnology and Oceanography,* **56,** 1225-1243, doi:10.4319/lo.2011.56.4.1225.

Holliday, N. P., Waniek, J. J., Davidson, R., Wilson, D., Brown, L., Sanders, R., Pollard, R. T. and Allen, J. T. (2006). Large-scale physical controls on phytoplankton growth in the Irminger Sea Part I: hydrographic zones, mixing and stratification. *Journal of Marine Systems,* **59,** 201-218, doi:10.1016/j.jmarsys.2005.10.004.

Honjo, S., Manganini, S. J. and Cole, J. J. (1982). Sedimentation of biogenic matter in the deep ocean. *Deep-Sea Research Part A: Oceanographic Research Papers,* **29,** 609-625, doi:10.1016/0198-0149(82)90079-6.

Honjo, S., Spencer, D. W. and Gardner, W. D. (1992). A sediment trap intercomparison experiment in the Panama Basin, 1979. *Deep-Sea Research Part A: Oceanographic Research Papers,* **39,** 333-358, doi:10.1016/0198-0149(92)90112-7.

Honjo, S. (1996). Fluxes of particles to the interior of the open oceans. *In:* V. Ittekkot, P. Schäfer, S. Honjo & P. J. Depetris (eds.) *Particle Flux in the Ocean.* Chichester: John Wiley, *pp.* 91 - 154.

Honjo, S., Manganini, S. J., Krishfield, R. A. and Francois, R. (2008). Particulate organic carbon fluxes to the ocean interior and factors controlling the biological pump: a synthesis of global sediment trap programs since 1983. *Progress in Oceanography,* **76,** 217-285, doi:10.1016/j.pocean.2007.11.003.

Huang, S. and Conte, M. H. (2009). Source/process apportionment of major and trace elements in sinking particles in the Sargasso sea. *Geochimica et Cosmochimica Acta,* **73,** 65-90, doi:10.1016/j.gca.2008.08.023.

Hurst, M. P. and Bruland, K. W. (2007). An investigation into the exchange of iron and zinc between soluble, colloidal, and particulate size-fractions in shelf waters using low-abundance isotopes as tracers in shipboard incubation experiments. *Marine Chemistry,* **103,** 211-226, doi:10.1016/j.marchem.2006.07.001.

Hutchins, D. A., DiTullio, G. R. and Bruland, K. W. (1993). Iron and regenerated production: evidence for biological iron recycling in two marine environments. *Limnology and Oceanography,* **38,** 1242-1255, doi:10.4319/lo.1993.38.6.1242.

Hutchins, D. A., Witter, A. E., Butler, A. and Luther, G. W. (1999). Competition among marine phytoplankton for different chelated iron species. *Nature,* **400,** 858-861, doi:10.1038/23680.

Ittekkot, V. (1993). The abiotically driven biological pump in the ocean and short-term fluctuations in atmospheric CO_2 contents. *Global and Planetary Change,* **8,** 17-25, doi:10.1016/0921-8181(93)90060-2.

Jerlov, N. G. (1968). *Optical Oceanography,* Amsterdam, Elsevier.

Jickells, T. D., Deuser, W. G. and Knap, A. H. (1984). The sedimentation rates of trace elements in the Sargasso Sea measured by sediment trap. *Deep-Sea Research Part A: Oceanographic Research Papers,* **31,** 1169-1178, doi:10.1016/0198-0149(84)90056-6.

Jickells, T. D., Dorling, S., Deuser, W. G., Church, T. M., Arimoto, R. and Prospero, J. M. (1998). Air-borne dust fluxes to a deep water sediment trap in the Sargasso Sea. *Global Biogeochemical Cycles,* **12,** 311-320, doi:10.1029/97GB03368.

Jickells, T. D. and Spokes, L. J. (2001). Atmospheric iron inputs to the oceans. *In:* D. R. Turner & K. A. Hunter (eds.) *The Biogeochemistry of Iron in Seawater.* Chichester: John Wiley & Sons, *pp.* 85 - 122.

Jickells, T. D., An, Z. S., Andersen, K. K., Baker, A. R., Bergametti, G., Brooks, N., Cao, J. J., Boyd, P. W., Duce, R. A., Hunter, K. A., Kawahata, H., Kubilay, N., LaRoche, J., Liss, P. S., Mahowald, N., Prospero, J. M., Ridgwell, A. J., Tegen, I. and Torres, R. (2005). Global iron connections between desert dust, ocean biogeochemistry, and climate. *Science,* **308,** 67-71, doi:10.1126/science.1105959.

Johnson, K. S., Gordon, R. M. and Coale, K. H. (1997). What controls dissolved iron concentrations in the world ocean? *Marine Chemistry,* **57,** 137-161, doi:10.1016/S0304-4203(97)00043-1.

Johnson, W. K., Miller, L. A., Sutherland, N. E. and Wong, C. S. (2005). Iron transport by mesoscale Haida eddies in the Gulf of Alaska. *Deep-Sea Research Part II: Topical Studies in Oceanography,* **52,** 933-953, doi:10.1016/j.dsr2.2004.08.017.

Jouandet, M. P., Trull, T. W., Guidi, L., Picheral, M., Ebersbach, F., Stemmann, L. and Blain, S. (2011). Optical imaging of mesopelagic particles indicates deep carbon flux beneath a natural iron-fertilized bloom in the Southern Ocean. *Limnology and Oceanography,* **56,** 1130-1140, doi:10.4319/lo.2011.56.3.1130.

Keeling, R. F., Piper, S. C., Bollenbacher, A. F. and Walker, S. J. 2012. Atmospheric CO_2 concentrations (ppm) derived from in situ air measurements at Mauna Loa Observatory, Hawaii: latitude 19.5 °N, longitude 155.6 °W, elevation 3397 m.

Available at: http://scrippsco2.ucsd.edu [Website], Scripps Institution of Oceanography, La Jolla, CA. [Accessed October 2012].

King, A. L., Sañudo-Wilhelmy, S. A., Boyd, P. W., Twining, B. S., Wilhelm, S. W., Breene, C., Ellwood, M. J. and Hutchins, D. A. (2012). A comparison of biogenic iron quotas during a diatom spring bloom using multiple approaches. *Biogeosciences,* **9,** 667-687, doi:10.5194/bg-9-667-2012.

Kirchman, D. L. (1996). Microbial ferrous wheel. *Nature,* **383,** 303-304, doi:10.1038/383303a0.

Klaas, C. and Archer, D. E. (2002). Association of sinking organic matter with various types of mineral ballast in the deep sea: implications for the rain ratio. *Global Biogeochemical Cycles,* **16,** Article No. 1116, doi:10.1029/2001gb001765.

Knauer, G. A., Martin, J. H. and Bruland, K. W. (1979). Fluxes of particulate carbon, nitrogen, and phosphorus in the upper water column of the northeast Pacific. *Deep-Sea Research,* **26,** 97-108, doi:10.1016/0198-0149(79)90089-X.

Knauer, G. A., Karl, D. M., Martin, J. H. and Hunter, C. N. (1984). *In situ* effects of selected preservatives on total carbon, nitrogen and metals collected in sediment traps. *Journal of Marine Research,* **42,** 445-462, doi:10.1357/002224084788502710.

Kremling, K. and Streu, P. (1993). Saharan dust influenced trace element fluxes in deep North Atlantic subtropical waters. *Deep-Sea Research Part I: Oceanographic Research Papers,* **40,** 1155-1168, doi:10.1016/0967-0637(93)90131-L.

Krishnaswami, S. and Sarin, M. M. (1976). Atlantic surface particulates: composition, settling rates and dissolution in the deep sea. *Earth and Planetary Science Letters,* **32,** 430-440, doi:10.1016/0012-821X(76)90083-2.

Kuss, J. and Kremling, K. (1999a). Spatial variability of particle associated trace elements in near-surface waters of the North Atlantic (30°N/60°W to 60°N/2°W), derived by large volume sampling. *Marine Chemistry,* **68,** 71-86, doi:10.1016/S0304-4203(99)00066-3.

Kuss, J. and Kremling, K. (1999b). Particulate trace element fluxes in the deep northeast Atlantic Ocean. *Deep-Sea Research Part I: Oceanographic Research Papers,* **46,** 149-169, doi:10.1016/S0967-0637(98)00059-4.

Kuss, J., Waniek, J. J., Kremling, K. and Schulz-Bull, D. E. (2010). Seasonality of particle-associated trace element fluxes in the deep northeast Atlantic Ocean. *Deep-Sea Research Part I: Oceanographic Research Papers,* **57,** 785-796, doi:10.1016/j.dsr.2010.04.002.

Kustka, A. B., Sañudo-Wilhelmy, S. A., Carpenter, E. J., Capone, D., Burns, J. and Sunda, W. G. (2003). Iron requirements for dinitrogen- and ammonium-supported growth in cultures of *Trichodesmium* (IMS 101): comparison with nitrogen fixation rates and iron:carbon ratios of field populations. *Limnology and Oceanography,* **48,** 1869-1884, doi:10.4319/lo.2003.48.5.1869.

Kwon, E. Y., Primeau, F. and Sarmiento, J. L. (2009). The impact of remineralization depth on the air-sea carbon balance. *Nature Geoscience,* **2,** 630-635, doi:10.1038/Ngeo612.

Lam, P. J., Bishop, J. K. B., Henning, C. C., Marcus, M. A., Waychunas, G. A. and Fung, I. Y. (2006). Wintertime phytoplankton bloom in the subarctic Pacific supported

by continental margin iron. *Global Biogeochemical Cycles,* **20,** Article No. GB1006, doi:10.1029/2005gb002557.

Lam, P. J. and Bishop, J. K. B. (2007). High biomass, low export regimes in the Southern Ocean. *Deep-Sea Research Part II: Topical Studies in Oceanography,* **54,** 601-638, doi:10.1016/j.dsr2.2007.01.013.

Lam, P. J. and Bishop, J. K. B. (2008). The continental margin is a key source of iron to the HNLC North Pacific Ocean. *Geophysical Research Letters,* **35,** Article No. L07608, doi:10.1029/2008gl033294.

Lam, P. J., Doney, S. C. and Bishop, J. K. B. (2011). The dynamic ocean biological pump: insights from a global compilation of particulate organic carbon, $CaCO_3$, and opal concentration profiles from the mesopelagic. *Global Biogeochemical Cycles,* **25,** Article No. GB3009, doi:10.1029/2010gb003868.

Lamborg, C. H., Buesseler, K. O. and Lam, P. J. (2008a). Sinking fluxes of minor and trace elements in the North Pacific Ocean measured during the VERTIGO program. *Deep-Sea Research Part II: Topical Studies in Oceanography,* **55,** 1564-1577, doi:10.1016/j.dsr2.2008.04.012.

Lamborg, C. H., Buesseler, K. O., Valdes, J., Bertrand, C. H., Bidigare, R., Manganini, S., Pike, S., Steinberg, D., Trull, T. and Wilson, S. (2008b). The flux of bio- and lithogenic material associated with sinking particles in the mesopelagic "twilight zone" of the northwest and North Central Pacific Ocean. *Deep-Sea Research Part II: Topical Studies in Oceanography,* **55,** 1540-1563, doi:10.1016/j.dsr2.2008.04.011.

Lampitt, R. S. and Antia, A. N. (1997). Particle flux in deep seas: regional characteristics and temporal variability. *Deep-Sea Research Part I: Oceanographic Research Papers,* **44,** 2141-2141, doi:10.1016/S0967-0637(98)00004-1.

Lampitt, R. S., Bett, B. J., Kiriakoulakis, K., Popova, E. E., Ragueneau, O., Vangriesheim, A. and Wolff, G. A. (2001). Material supply to the abyssal seafloor in the Northeast Atlantic. *Progress in Oceanography,* **50,** 27-63, doi:10.1016/S0079-6611(01)00047-7.

Lampitt, R. S., Boorman, B., Brown, L., Lucas, M., Salter, I., Sanders, R., Saw, K., Seeyave, S., Thomalla, S. J. and Turnewitsch, R. (2008). Particle export from the euphotic zone: estimates using a novel drifting sediment trap, ^{234}Th and new production. *Deep-Sea Research Part I: Oceanographic Research Papers,* **55,** 1484-1502, doi:10.1016/j.dsr.2008.07.002.

Lampitt, R. S., Billett, D. S. M. and Martin, A. P. (2010). The sustained observatory over the Porcupine Abyssal Plain (PAP): insights from time series observations and process studies - Preface. *Deep-Sea Research Part II: Topical Studies in Oceanography,* **57,** 1267-1271, doi:10.1016/j.dsr2.2010.01.003.

Landing, W. M. and Bruland, K. W. (1987). The contrasting biogeochemistry of iron and manganese in the Pacific Ocean. *Geochimica et Cosmochimica Acta,* **51,** 29-43, doi:10.1016/0016-7037(87)90004-4.

Lee, C., Hedges, J. I., Wakeham, S. G. and Zhu, N. (1992). Effectiveness of various treatments in retarding microbial activity in sediment trap material and their effects on the collection of swimmers. *Limnology and Oceanography,* **37,** 117-130, doi:10.4319/lo.1992.37.1.0117.

Lee, C., Peterson, M. L., Wakeham, S. G., Armstrong, R. A., Cochran, J. K., Miquel, J. C., Fowler, S. W., Hirschberg, D., Beck, A. and Xue, J. H. (2009). Particulate organic matter and ballast fluxes measured using time-series and settling velocity sediment traps in the northwestern Mediterranean Sea. *Deep-Sea Research Part II: Topical Studies in Oceanography,* **56,** 1420-1436, doi:10.1016/j.dsr2.2008.11.029.

Lin, H., Rauschenberg, S., Hexel, C. R., Shaw, T. J. and Twining, B. S. (2011). Free-drifting icebergs as sources of iron to the Weddell Sea. *Deep-Sea Research Part II: Topical Studies in Oceanography,* **58,** 1392-1406, doi:10.1016/j.dsr2.2010.11.020.

Longhurst, A. (1998). *Ecological Geography of the Sea,* San Diego, CA, Academic Press.

Lowenstam, H. A. and Weiner, S. (1989). *On Biomineralization,* New York, Oxford University Press.

Lutz, M., Dunbar, R. and Caldeira, K. (2002). Regional variability in the vertical flux of particulate organic carbon in the ocean interior. *Global Biogeochemical Cycles,* **16,** Article No. 1037, doi:10.1029/2000gb001383.

Macrellis, H. M., Trick, C. G., Rue, E. L., Smith, G. and Bruland, K. W. (2001). Collection and detection of natural iron-binding ligands from seawater. *Marine Chemistry,* **76,** 175-187, doi:10.1016/S0304-4203(01)00061-5.

Mahowald, N. M., Baker, A. R., Bergametti, G., Brooks, N., Duce, R. A., Jickells, T. D., Kubilay, N., Prospero, J. M. and Tegen, I. (2005). Atmospheric global dust cycle and iron inputs to the ocean. *Global Biogeochemical Cycles,* **19,** Article No. GB4025, doi:10.1029/2004gb002402.

Maldonado, M. T. and Price, N. M. (2000). Nitrate regulation of Fe reduction and transport by Fe-limited *Thalassiosira oceanica*. *Limnology and Oceanography,* **45,** 814-826, doi:10.4319/lo.2000.45.4.0814.

Martin, J. H., Knauer, G. A., Karl, D. M. and Broenkow, W. W. (1987). VERTEX: carbon cycling in the northeast Pacific. *Deep-Sea Research Part A: Oceanographic Research Papers,* **34,** 267-285, doi:10.1016/0198-0149(87)90086-0.

Martin, J. H. and Fitzwater, S. E. (1988). Iron deficiency limits phytoplankton growth in the north-east Pacific subarctic. *Nature,* **331,** 341-343, doi:10.1038/331341a0.

Martin, J. H., Gordon, R. M., Fitzwater, S. and Broenkow, W. W. (1989). VERTEX: phytoplankton/iron studies in the Gulf of Alaska. *Deep-Sea Research Part A: Oceanographic Research Papers,* **36,** 649-680, doi:10.1016/0198-0149(89)90144-1.

Martin, J. H. (1990). Glacial-interglacial CO_2 change: the iron hypothesis. *Paleoceanography,* **5,** 1-13, doi:10.1029/PA005i001p00001.

Martin, J. H., Gordon, R. M. and Fitzwater, S. E. (1991). The case for iron. *Limnology and Oceanography,* **36,** 1793-1802, doi:10.4319/lo.1991.36.8.1793.

Martin, J. H., Fitzwater, S. E., Gordon, R. M., Hunter, C. N. and Tanner, S. J. (1993). Iron, primary production and carbon-nitrogen flux studies during the JGOFS North Atlantic Bloom Experiment. *Deep-Sea Research Part II: Topical Studies in Oceanography,* **40,** 115-134, doi:10.1016/0967-0645(93)90009-C.

Martin, P., Lampitt, R. S., Perry, M. J., Sanders, R., Lee, C. and D'Asaro, E. (2011). Export and mesopelagic particle flux during a North Atlantic spring diatom bloom.

Deep-Sea Research Part I: Oceanographic Research Papers, **58,** 338-349, doi:10.1016/j.dsr.2011.01.006.

Mayer, L. M. (1994). Surface area control of organic carbon accumulation in continental shelf sediments. *Geochimica et Cosmochimica Acta,* **58,** 1271-1284, doi:10.1016/0016-7037(94)90381-6.

McDonnell, A. M. P. and Buesseler, K. O. (2010). Variability in the average sinking velocity of marine particles. *Limnology and Oceanography,* **55,** 2085-2096, doi:10.4319/lo.2010.55.5.2085.

McGillicuddy, D. J., Anderson, L. A., Bates, N. R., Bibby, T., Buesseler, K. O., Carlson, C. A., Davis, C. S., Ewart, C., Falkowski, P. G., Goldthwait, S. A., Hansell, D. A., Jenkins, W. J., Johnson, R., Kosnyrev, V. K., Ledwell, J. R., Li, Q. P., Siegel, D. A. and Steinberg, D. K. (2007). Eddy/wind interactions stimulate extraordinary mid-ocean plankton blooms. *Science,* **316,** 1021-1026, doi:10.1126/science.1136256.

Michaels, A. F., Silver, M. W., Gowing, M. M. and Knauer, G. A. (1990). Cryptic zooplankton "swimmers" in upper ocean sediment traps. *Deep-Sea Research Part A: Oceanographic Research Papers,* **37,** 1285-1296, doi:10.1016/0198-0149(90)90043-U.

Middag, R., de Baar, H. J. W., Laan, P. and Bakker, K. (2009). Dissolved aluminium and the silicon cycle in the Arctic Ocean. *Marine Chemistry,* **115,** 176-195, doi:10.1016/j.marchem.2009.08.002.

Millero, F. J. (1998). Solubility of Fe(III) in seawater. *Earth and Planetary Science Letters,* **154,** 323-329, doi:10.1016/S0012-821X(97)00179-9.

Milliman, J. D., Troy, P. J., Balch, W. M., Adams, A. K., Li, Y. H. and Mackenzie, F. T. (1999). Biologically mediated dissolution of calcium carbonate above the chemical lysocline? *Deep-Sea Research Part I: Oceanographic Research Papers,* **46,** 1653-1669, doi:10.1016/S0967-0637(99)00034-5.

Mioni, C. E., Poorvin, L. and Wilhelm, S. W. (2005). Virus and siderophore-mediated transfer of available Fe between heterotrophic bacteria: characterization using an Fe-specific bioreporter. *Aquatic Microbial Ecology,* **41,** 233-245, doi:10.3354/ame041233.

Moffett, J. W. (2001). Transformations among different forms of iron in the ocean. *In:* D. R. Turner & K. A. Hunter (eds.) *The Biogeochemistry of Iron in Seawater.* Chichester: John Wiley & Sons, *pp.* 343 - 372.

Moore, C. M., Mills, M. M., Achterberg, E. P., Geider, R. J., LaRoche, J., Lucas, M. I., McDonagh, E. L., Pan, X., Poulton, A. J., Rijkenberg, M. J. A., Suggett, D. J., Ussher, S. J. and Woodward, E. M. S. (2009). Large-scale distribution of Atlantic nitrogen fixation controlled by iron availability. *Nature Geoscience,* **2,** 867-871, doi:10.1038/Ngeo667.

Moore, J. K., Doney, S. C., Glover, D. M. and Fung, I. Y. (2002). Iron cycling and nutrient-limitation patterns in surface waters of the World Ocean. *Deep-Sea Research Part II: Topical Studies in Oceanography,* **49,** 463-507, doi:10.1016/S0967-0645(01)00108-4.

Moore, J. K., Doney, S. C. and Lindsay, K. (2004). Upper ocean ecosystem dynamics and iron cycling in a global three-dimensional model. *Global Biogeochemical Cycles,* **18,** Artical No. GB4028, doi:10.1029/2004gb002220.

Morel, F. M. M., Hudson, R. J. M. and Price, N. M. (1991). Limitation of productivity by trace metals in the sea. *Limnology and Oceanography,* **36,** 1742-1755, doi:10.4319/lo.1991.36.8.1742.

Morel, F. M. M. and Price, N. M. (2003). The biogeochemical cycles of trace metals in the oceans. *Science,* **300,** 944-947, doi:10.1126/science.1083545.

Morel, F. M. M., Milligan, A. J. and Saito, M. A. (2004). Marine bioinorganic chemistry: the role of trace metals in the oceanic cycles of major nutrients. *In:* H. Elderfield (ed.) *Treatise on Geochemistry, Vol. 6: The Oceans and Marine Geochemistry.* Oxford: Elsevier-Pergamon, *pp.* 113 - 143.

Morris, P. J., Sanders, R., Turnewitsch, R. and Thomalla, S. (2007). ^{234}Th-derived particulate organic carbon export from an island-induced phytoplankton bloom in the Southern Ocean. *Deep-Sea Research Part II: Topical Studies in Oceanography,* **54,** 2208-2232, doi:10.1016/j.dsr2.2007.06.002.

Mortlock, R. A. and Froelich, P. N. (1989). A simple method for the rapid determination of biogenic opal in pelagic marine sediments. *Deep-Sea Research Part A: Oceanographic Research Papers,* **36,** 1415-1426, doi:10.1016/0198-0149(89)90092-7.

Murray, R. W. and Leinen, M. (1996). Scavenged excess aluminum and its relationship to bulk titanium in biogenic sediment from the central equatorial Pacific Ocean. *Geochimica et Cosmochimica Acta,* **60,** 3869-3878, doi:10.1016/0016-7037(96)00236-0.

Nameroff, T. J., Balistrieri, L. S. and Murray, J. W. (2002). Suboxic trace metal geochemistry in the eastern tropical North Pacific. *Geochimica et Cosmochimica Acta,* **66,** 1139-1158, doi:10.1016/S0016-7037(01)00843-2.

Nelson, D. M., Anderson, R. F., Barber, R. T., Brzezinski, M. A., Buesseler, K. O., Chase, Z., Collier, R. W., Dickson, M. L., François, R., Hiscock, M. R., Honjo, S., Marra, J., Martin, W. R., Sambrotto, R. N., Sayles, F. L. and Sigmon, D. E. (2002). Vertical budgets for organic carbon and biogenic silica in the Pacific sector of the Southern Ocean, 1996-1998. *Deep-Sea Research Part II: Topical Studies in Oceanography,* **49,** 1645-1674, doi:10.1016/S0967-0645(02)00005-X.

Neuer, S., Davenport, R., Freudenthal, T., Wefer, G., Llinás, O., Rueda, M. J., Steinberg, D. K. and Karl, D. M. (2002). Differences in the biological carbon pump at three subtropical ocean sites. *Geophysical Research Letters,* **29,** Article No. 1885, doi:10.1029/2002gl015393.

Nielsdóttir, M. C., Moore, C. M., Sanders, R., Hinz, D. J. and Achterberg, E. P. (2009). Iron limitation of the postbloom phytoplankton communities in the Iceland Basin. *Global Biogeochemical Cycles,* **23,** Article No. GB3001, doi:10.1029/2008gb003410.

Orians, K. J. and Bruland, K. W. (1986). The biogeochemistry of aluminum in the Pacific Ocean. *Earth and Planetary Science Letters,* **78,** 397-410, doi:10.1016/0012-821X(86)90006-3.

Passow, U. (2004). Switching perspectives: do mineral fluxes determine particulate organic carbon fluxes or vice versa? *Geochemistry Geophysics Geosystems,* **5,** Article No. Q04002, doi:10.1029/2003gc000670.

Peterson, M. L., Hernes, P. J., Thoreson, D. S., Hedges, J. I., Lee, C. and Wakeham, S. G. (1993). Field evaluation of a valved sediment trap. *Limnology and Oceanography,* **38,** 1741-1761, doi:10.4319/lo.1993.38.8.1741.

Peterson, M. L., Wakeham, S. G., Lee, C., Askea, M. A. and Miquel, J. C. (2005). Novel techniques for collection of sinking particles in the ocean and determining their settling rates. *Limnology and Oceanography: Methods,* **3,** 520-532, doi:10.4319/lom.2005.3.520.

Planquette, H., Statham, P. J., Fones, G. R., Charette, M. A., Moore, C. M., Salter, I., Nédélec, F. H., Taylor, S. L., French, M., Baker, A. R., Mahowald, N. and Jickells, T. D. (2007). Dissolved iron in the vicinity of the Crozet Islands, Southern Ocean. *Deep-Sea Research Part II: Topical Studies in Oceanography,* **54,** 1999-2019, doi:10.1016/j.dsr2.2007.06.019.

Planquette, H. (2008). *Iron Biogeochemistry in the Waters Surrounding the Crozet Islands, Southern Ocean.* Ph.D. thesis, University of Southampton.

Planquette, H., Fones, G. R., Statham, P. J. and Morris, P. J. (2009). Origin of iron and aluminium in large particles (> 53 μm) in the Crozet region, Southern Ocean. *Marine Chemistry,* **115,** 31-42, doi:10.1016/j.marchem.2009.06.002.

Planquette, H., Sanders, R. R., Statham, P. J., Morris, P. J. and Fones, G. R. (2011). Fluxes of particulate iron from the upper ocean around the Crozet Islands: a naturally iron-fertilized environment in the Southern Ocean. *Global Biogeochemical Cycles,* **25,** Article No. GB2011, doi:10.1029/2010gb003789.

Planquette, H. and Sherrell, R. M. (2012). Sampling for particulate trace element determination using water sampling bottles: methodology and comparison to in situ pumps. *Limnology and Oceanography-Methods,* **10,** 367-388, doi:10.4319/lom.2012.10.367.

Pohl, C., Löffler, A. and Hennings, U. (2004). A sediment trap flux study for trace metals under seasonal aspects in the stratified Baltic Sea (Gotland Basin; 57°19.20'N; 20°03.00'E). *Marine Chemistry,* **84,** 143-160, doi:10.1016/j.marchem.2003.07.002.

Poulton, A. J., Sanders, R., Holligan, P. M., Stinchcombe, M. C., Adey, T. R., Brown, L. and Chamberlain, K. (2006). Phytoplankton mineralization in the tropical and subtropical Atlantic Ocean. *Global Biogeochemical Cycles,* **20,** Article No. GB4002, doi:10.1029/2006gb002712.

Prego, R., Caetano, M., Vale, C. and Marmolejo-Rodríguez, J. (2009). Rare earth elements in sediments of the Vigo Ria, NW Iberian Peninsula. *Continental Shelf Research,* **29,** 896-902, doi:10.1016/j.csr.2009.01.009.

Price, N. M. (2005). The elemental stoichiometry and composition of an iron-limited diatom. *Limnology and Oceanography,* **50,** 1159-1171, doi:10.4319/lo.2005.50.4.1159.

Prospero, J. M., Bullard, J. E. and Hodgkins, R. (2012). High-latitude dust over the North Atlantic: inputs from Icelandic proglacial dust storms. *Science,* **335,** 1078-1082, doi:10.1126/science.1217447.

Quétel, C. R., Remoudaki, E., Davies, J. E., Miquel, J. C., Fowler, S. W., Lambert, C. E., Bergametti, G. and Buat-Ménard, P. (1993). Impact of atmospheric deposition on particulate iron flux and distribution in northwestern Mediterranean waters. *Deep-Sea Research Part I: Oceanographic Research Papers,* **40,** 989-1002, doi:10.1016/0967-0637(93)90085-H.

Ragueneau, O. and Tréguer, P. (1994). Determination of biogenic silica in coastal waters: applicability and limits of the alkaline digestion method. *Marine Chemistry,* **45,** 43-51, doi:10.1016/0304-4203(94)90090-6.

Ragueneau, O., Tréguer, P., Leynaert, A., Anderson, R. F., Brzezinski, M. A., DeMaster, D. J., Dugdale, R. C., Dymond, J., Fischer, G., François, R., Heinze, C., Maier-Reimer, E., Martin-Jézéquel, V., Nelson, D. M. and Quéguiner, B. (2000). A review of the Si cycle in the modern ocean: recent progress and missing gaps in the application of biogenic opal as a paleoproductivity proxy. *Global and Planetary Change,* **26,** 317-365, doi:10.1016/S0921-8181(00)00052-7.

Redfield, A. C., Ketchum, B. H. and Richards, F. H. (1963). The influence of organisms on the composition of seawater. *In:* M. N. Hill (ed.) *The Sea: Ideas and Observations on Progress in the Study of the Seas.* New York: John Wiley & Sons Ltd, *pp.* 26 - 77.

Rijkenberg, M. J. A., Fischer, A. C., Kroon, J. J., Gerringa, L. J. A., Timmermans, K. R., Wolterbeek, H. T. and de Baar, H. J. W. (2005). The influence of UV irradiation on the photoreduction of iron in the Southern Ocean. *Marine Chemistry,* **93,** 119-129, doi:10.1016/j.marchem.2004.03.021.

Riley, J. S., Sanders, R., Marsay, C., Le Moigne, F. A. C., Achterberg, E. P. and Poulton, A. J. (2012). The relative contribution of fast and slow sinking particles to ocean carbon export. *Global Biogeochemical Cycles,* **26,** Article No. GB1026, doi:10.1029/2011gb004085.

Rivkin, R. B. and Legendre, L. (2001). Biogenic carbon cycling in the upper ocean: effects of microbial respiration. *Science,* **291,** 2398-2400, doi:10.1126/science.291.5512.2398.

Rose, A. L. and Waite, T. D. (2002). Kinetic model for Fe(II) oxidation in seawater in the absence and presence of natural organic matter. *Environmental Science & Technology,* **36,** 433-444, doi:10.1021/es0109242.

Rue, E. L. and Bruland, K. W. (1995). Complexation of iron(III) by natural organic ligands in the central North Pacific as determined by a new competitive ligand equilibration/adsorptive cathodic stripping voltammetric method. *Marine Chemistry,* **50,** 117-138, doi:10.1016/0304-4203(95)00031-L.

Sabine, C. L., Feely, R. A., Gruber, N., Key, R. M., Lee, K., Bullister, J. L., Wanninkhof, R., Wong, C. S., Wallace, D. W. R., Tilbrook, B., Millero, F. J., Peng, T. H., Kozyr, A., Ono, T. and Rios, A. F. (2004). The oceanic sink for anthropogenic CO_2. *Science,* **305,** 367-371, doi:10.1126/science.1097403.

Salter, I. (2007). *Particle Fluxes in the North-East Atlantic and Southern Ocean.* Ph.D. thesis, University of Southampton.

Salter, I., Lampitt, R. S., Sanders, R., Poulton, A., Kemp, A. E. S., Boorman, B., Saw, K. and Pearce, R. (2007). Estimating carbon, silica and diatom export from a naturally fertilised phytoplankton bloom in the Southern Ocean using PELAGRA: a novel drifting sediment trap. *Deep-Sea Research Part II: Topical Studies in Oceanography,* **54,** 2233-2259, doi:10.1016/j.dsr2.2007.06.008.

Salter, I., Kemp, A. E. S., Lampitt, R. S. and Gledhill, M. (2010). The association between biogenic and inorganic minerals and the amino acid composition of settling particles. *Limnology and Oceanography,* **55,** 2207-2218, doi:10.4319/lo.2010.55.5.2207.

Sanders, R., Brown, L., Henson, S. and Lucas, M. (2005). New production in the Irminger Basin during 2002. *Journal of Marine Systems,* **55,** 291-310, doi:10.1016/j.jmarsys.2004.09.002.

Sanders, R., Morris, P. J., Poulton, A. J., Stinchcombe, M. C., Charalampopoulou, A., Lucas, M. I. and Thomalla, S. J. (2010). Does a ballast effect occur in the surface ocean? *Geophysical Research Letters,* **37,** Article No. L08602, doi:10.1029/2010gl042574.

Sarmiento, J. L. and Le Quéré, C. (1996). Oceanic carbon dioxide uptake in a model of century-scale global warming. *Science,* **274,** 1346-1350, doi:10.1126/science.274.5291.1346.

Sarthou, G., Vincent, D., Christaki, U., Obernosterer, I., Timmermans, K. R. and Brussaard, C. P. D. (2008). The fate of biogenic iron during a phytoplankton bloom induced by natural fertilisation: impact of copepod grazing. *Deep-Sea Research Part II: Topical Studies in Oceanography,* **55,** 734-751, doi:10.1016/j.dsr2.2007.12.033.

Saw, K. A., Boorman, B., Lampitt, R. S. and Sanders, R. (2004). PELAGRA: early development of an autonomous, neutrally buoyant sediment trap. *In: Advances in Technology for Underwater Vehicles, Conference Proceedings*, 16-17 March 2004. Advances in Technology for Underwater Vehicles, London, UK. Institute of Marine Engineering, Science and Technology, 165 - 175.

Schiebel, R. (2002). Planktic foraminiferal sedimentation and the marine calcite budget. *Global Biogeochemical Cycles,* **16,** Article No. 1065, doi:10.1029/2001gb001459.

Schilling, J. G., Zajac, M., Evans, R., Johnston, T., White, W., Devine, J. D. and Kingsley, R. (1983). Petrologic and geochemical variations along the Mid-Atlantic Ridge from 29 °N to 73 °N. *American Journal of Science,* **283,** 510-586, doi:10.2475/ajs.283.6.510.

Schneider, B., Schlitzer, R., Fischer, G. and Nöthig, E. M. (2003). Depth-dependent elemental compositions of particulate organic matter (POM) in the ocean. *Global Biogeochemical Cycles,* **17,** Article No. 1032, doi:10.1029/2002gb001871.

Scholten, J. C., Fietzke, J., Vogler, S., Rutgers van der Loeff, M., Mangini, A., Koeve, W., Waniek, J., Stoffers, P., Antia, A. and Kuss, J. (2001). Trapping efficiencies of sediment traps from the deep Eastern North Atlantic: the ^{230}Th calibration. *Deep-Sea Research Part II: Topical Studies in Oceanography,* **48,** 2383-2408, doi:10.1016/S0967-0645(00)00176-4.

Sedwick, P. N. and DiTullio, G. R. (1997). Regulation of algal blooms in Antarctic shelf waters by the release of iron from melting sea ice. *Geophysical Research Letters,* **24,** 2515-2518, doi:10.1029/97GL02596.

Shaffer, G., Bendtsen, J. and Ulloa, O. (1999). Fractionation during remineralization of organic matter in the ocean. *Deep-Sea Research Part I: Oceanographic Research Papers,* **46,** 185-204, doi:10.1016/S0967-0637(98)00061-2.

Sheridan, C. C., Lee, C., Wakeham, S. G. and Bishop, J. K. B. (2002). Suspended particle organic composition and cycling in surface and midwaters of the equatorial Pacific Ocean. *Deep-Sea Research Part I: Oceanographic Research Papers,* **49,** 1983-2008, doi:10.1016/S0967-0637(02)00118-8.

Sherman, A. D., Hobson, B. W., McGill, P. R., Davis, R. E., McClune, M. C. and Smith, K. L. (2011). Lagrangian sediment traps for sampling at discrete depths beneath

free-drifting icebergs. *Deep-Sea Research Part II: Topical Studies in Oceanography,* **58,** 1327-1335, doi:10.1016/j.dsr2.2010.11.008.

Sherrell, R. M. and Boyle, E. A. (1992). The trace metal composition of suspended particles in the oceanic water column near Bermuda. *Earth and Planetary Science Letters,* **111,** 155-174, doi:10.1016/0012-821X(92)90176-V.

Sholkovitz, E. R. (1976). Flocculation of dissolved organic and inorganic matter during the mixing of river water and seawater. *Geochimica et Cosmochimica Acta,* **40,** 831-845, doi:10.1016/0016-7037(76)90035-1.

Sholkovitz, E. R., Sedwick, P. N. and Church, T. M. (2009). Influence of anthropogenic combustion emissions on the deposition of soluble aerosol iron to the ocean: empirical estimates for island sites in the North Atlantic. *Geochimica et Cosmochimica Acta,* **73,** 3981-4003, doi:10.1016/j.gca.2009.04.029.

Sigman, D. M. and Boyle, E. A. (2000). Glacial/interglacial variations in atmospheric carbon dioxide. *Nature,* **407,** 859-869, doi:10.1038/35038000.

Smith, K. L., Sherman, A. D., Shaw, T. J., Murray, A. E., Vernet, M. and Cefarelli, A. O. (2011). Carbon export associated with free-drifting icebergs in the Southern Ocean. *Deep-Sea Research Part II: Topical Studies in Oceanography,* **58,** 1485-1496, doi:10.1016/j.dsr2.2010.11.027.

Stanley, R. H. R., Buesseler, K. O., Manganini, S. J., Steinberg, D. K. and Valdes, J. R. (2004). A comparison of major and minor elemental fluxes collected in neutrally buoyant and surface-tethered sediment traps. *Deep-Sea Research Part I: Oceanographic Research Papers,* **51,** 1387-1395, doi:10.1016/j.dsr.2004.05.010.

Statham, P. J., German, C. R. and Connelly, D. P. (2005). Iron(II) distribution and oxidation kinetics in hydrothermal plumes at the Kairei and Edmond vent sites, Indian Ocean. *Earth and Planetary Science Letters,* **236,** 588-596, doi:10.1016/j.epsl.2005.03.008.

Stavn, R. H., Rick, H. J. and Falster, A. V. (2009). Correcting the errors from variable sea salt retention and water of hydration in loss on ignition analysis: implications for studies of estuarine and coastal waters. *Estuarine, Coastal and Shelf Science,* **81,** 575-582, doi:10.1016/j.ecss.2008.12.017.

Strzepek, R. F., Maldonado, M. T., Higgins, J. L., Hall, J., Safi, K., Wilhelm, S. W. and Boyd, P. W. (2005). Spinning the "Ferrous Wheel": the importance of the microbial community in an iron budget during the FeCycle experiment. *Global Biogeochemical Cycles,* **19,** Article No. GB4S26, doi:10.1029/2005gb002490.

Suess, E. (1980). Particulate organic carbon flux in the oceans: surface productivity and oxygen utilization. *Nature,* **288,** 260-263, doi:10.1038/288260a0.

Sunda, W. G. and Huntsman, S. A. (1995). Iron uptake and growth limitation in oceanic and coastal phytoplankton. *Marine Chemistry,* **50,** 189-206, doi:10.1016/0304-4203(95)00035-P.

Taylor, S. R. (1964). Abundance of chemical elements in the continental crust: a new table. *Geochimica et Cosmochimica Acta,* **28,** 1273-1285, doi:10.1016/0016-7037(64)90129-2.

Taylor, S. R. and McLennan, S. M. (1995). The geochemical evolution of the continental crust. *Reviews of Geophysics,* **33,** 241-265, doi:10.1029/95RG00262.

Tovar-Sanchez, A., Sañudo-Wilhelmy, S. A., Garcia-Vargas, M., Weaver, R. S., Popels, L. C. and Hutchins, D. A. (2003). A trace metal clean reagent to remove surface-bound iron from marine phytoplankton. *Marine Chemistry,* **82,** 91-99, doi:10.1016/s0304-4203(03)00054-9.

Tréguer, P., Nelson, D. M., van Bennekom, A. J., DeMaster, D. J., Leynaert, A. and Quéguiner, B. (1995). The silica balance in the world ocean: a reestimate. *Science,* **268,** 375-379, doi:10.1126/science.268.5209.375.

Trull, T. W., Bray, S. G., Buesseler, K. O., Lamborg, C. H., Manganini, S., Moy, C. and Valdes, J. (2008). *In situ* measurement of mesopelagic particle sinking rates and the control of carbon transfer to the ocean interior during the Vertical Flux in the Global Ocean (VERTIGO) voyages in the North Pacific. *Deep-Sea Research Part II: Topical Studies in Oceanography,* **55,** 1684-1695, doi:10.1016/j.dsr2.2008.04.021.

Turner, J. T. (2002). Zooplankton fecal pellets, marine snow and sinking phytoplankton blooms. *Aquatic Microbial Ecology,* **27,** 57-102, doi:10.3354/ame027057.

Twining, B. S., Baines, S. B., Fisher, N. S. and Landry, M. R. (2004). Cellular iron contents of plankton during the Southern Ocean Iron Experiment (SOFeX). *Deep-Sea Research Part I: Oceanographic Research Papers,* **51,** 1827-1850, doi:10.1016/j.dsr.2004.08.007.

Twining, B. S., Nuñez-Milland, D., Vogt, S., Johnson, R. S. and Sedwick, P. N. (2010). Variations in *Synechococcus* cell quotas of phosphorus, sulfur, manganese, iron, nickel, and zinc within mesoscale eddies in the Sargasso Sea. *Limnology and Oceanography,* **55,** 492-506, doi:10.4319/lo.2009.55.2.0492.

U.S.GOFS (1989). Sediment Trap Technology and Sampling: Report of the U.S. GOFS Working Group on Sediment Trap Technology and Sampling, November 1988. *U.S. GOFS planning report No. 10*, U.S. GOFS Planning and Coordination Office, Woods Hole Oceanographic Institution, MA.

U.S.JGOFS (2001). *A New Wave of Ocean Science: U.S. JGOFS Brochure*. U.S. JGOFS Planning and Data Management Office, Woods Hole.

Ussher, S. J., Achterberg, E. P. and Worsfold, P. J. (2004). Marine biogeochemistry of iron. *Environmental Chemistry,* **1,** 67-80, doi:10.1071/En04053.

Valdes, J. R. and Price, J. F. (2000). A neutrally buoyant, upper ocean sediment trap. *Journal of Atmospheric and Oceanic Technology,* **17,** 62-68, doi:10.1175/1520-0426(2000)017<0062:ANBUOS>2.0.CO;2.

Van Cappellen, P., Dixit, S. and van Beusekom, J. (2002). Biogenic silica dissolution in the oceans: reconciling experimental and field-based dissolution rates. *Global Biogeochemical Cycles,* **16,** Article No. 1075, doi:10.1029/2001gb001431.

van den Berg, C. M. G. (1995). Evidence for organic complexation of iron in seawater. *Marine Chemistry,* **50,** 139-157, doi:10.1016/0304-4203(95)00032-M.

Verardo, D. J., Froelich, P. N. and McIntyre, A. (1990). Determination of organic carbon and nitrogen in marine sediments using the Carlo Erba NA-1500 Analyzer. *Deep-Sea Research Part A: Oceanographic Research Papers,* **37,** 157-165, doi:10.1016/0198-0149(90)90034-S.

Verdeny, E., Masqué, P., Maiti, K., Garcia-Orellana, J., Brauch, J. M., Mahaffey, C. and Benitez-Nelson, C. R. (2008). Particle export within cyclonic Hawaiian lee eddies

derived from ^{210}Pb-^{210}Po disequilibrium. *Deep-Sea Research Part II: Topical Studies in Oceanography,* **55,** 1461-1472, doi:10.1016/j.dsr2.2008.02.009.

Verdeny, E., Masqué, P., Garcia-Orellana, J., Hanfland, C., Cochran, J. K. and Stewart, G. M. (2009). POC export from ocean surface waters by means of ^{234}Th/^{238}U and ^{210}Po/^{210}Pb disequilibria: a review of the use of two radiotracer pairs. *Deep-Sea Research Part II: Topical Studies in Oceanography,* **56,** 1502-1518, doi:10.1016/j.dsr2.2008.12.018.

Volk, T. and Hoffert, M. I. (1985). Ocean carbon pumps: analysis of relative strengths and efficiencies in ocean-driven atmospheric CO_2 changes. *In:* E. T. Sundquist & W. S. Broecker (eds.) *The Carbon Cycle and Atmospheric CO_2 : Natural Variations Archean to Present.* Washington, DC: American Geophysical Union, *pp.* 99 - 110.

Watson, A. J. (2001). Iron limitation in the oceans. *In:* D. R. Turner & K. A. Hunter (eds.) *The Biogeochemistry of Iron in Seawater.* Chichester: John Wiley & Sons, *pp.* 9 - 40.

Wedepohl, K. H. (1995). The composition of the continental crust. *Geochimica et Cosmochimica Acta,* **59,** 1217-1232, doi:10.1016/0016-7037(95)00038-2.

Wefer, G. (1989). Particle flux in the ocean: effects of episodic production. *In:* W. H. Berger, V. S. Smetacek & G. Wefer (eds.) *Productivity of the Ocean: Present and Past. .* Chichester: John Wiley & Sons Ltd, *pp.* 139 - 153.

Weinstein, S. E. and Moran, S. B. (2004). Distribution of size-fractionated particulate trace metals collected by bottles and in-situ pumps in the Gulf of Maine-Scotian Shelf and Labrador Sea. *Marine Chemistry,* **87,** 121-135, doi:10.1016/j.marchem.2004.02.004.

Weinstein, S. E. and Moran, S. B. (2005). Vertical flux of particulate Al, Fe, Pb, and Ba from the upper ocean estimated from ^{234}Th/^{238}U disequilibria. *Deep-Sea Research Part I: Oceanographic Research Papers,* **52,** 1477-1488, doi:10.1016/j.dsr.2005.03.008.

Wells, M. L., Price, N. M. and Bruland, K. W. (1995). Iron chemistry in seawater and its relationship to phytoplankton: a workshop report. *Marine Chemistry,* **48,** 157-182, doi:10.1016/0304-4203(94)00055-I.

Wells, M. L., Smith, G. J. and Bruland, K. W. (2000). The distribution of colloidal and particulate bioactive metals in Narragansett Bay, RI. *Marine Chemistry,* **71,** 143-163, doi:10.1016/S0304-4203(00)00046-3.

Wu, J. F. and Luther, G. W. (1995). Complexation of Fe(III) by natural organic ligands in the northwest Atlantic Ocean by a competitive ligand equilibration method and a kinetic approach. *Marine Chemistry,* **50,** 159-177, doi:10.1016/0304-4203(95)00033-N.

Yu, E. F., Francois, R., Bacon, M. P., Honjo, S., Fleer, A. P., Manganini, S. J., Rutgers van der Loeff, M. and Ittekot, V. (2001). Trapping efficiency of bottom-tethered sediment traps estimated from the intercepted fluxes of ^{230}Th and ^{231}Pa. *Deep-Sea Research Part I: Oceanographic Research Papers,* **48,** 865-889, doi:10.1016/S0967-0637(00)00067-4.